Review Article

Machine tool calibration: Measurement, modeling, and compensation of machine tool errors

Wei Gao [a,*], Soichi Ibaraki [b], M. Alkan Donmez [c], Daisuke Kono [d], J.R.R. Mayer [e], Yuan-Liu Chen [f], Károly Szipka [g], Andreas Archenti [g], Jean-Marc Linares [h], Norikazu Suzuki [i]

[a] *Tohoku University, Japan*
[b] *Hiroshima University, Japan*
[c] *National Institute of Standards and Technology (NIST), USA*
[d] *Kyoto University, Japan*
[e] *Polytechnique Montreal, Canada*
[f] *Zhejiang University, China*
[g] *KTH Royal Institute of Technology, Sweden*
[h] *Aix-Marseille Université, France*
[i] *Chuo University, Japan*

Keywords:
Machine tool
Calibration
Measurement
Uncertainty
Self-calibration
Machine learning

A B S T R A C T

Advanced technologies for the calibration of machine tools are presented. Kinematic errors independently of their causes are classified into errors within one-axis as intra-axis errors, errors between axes as inter-axis errors, and as volumetric errors. As the major technological elements of machine tool calibration, the measurement methods, modeling theories, and compensation strategies of the machine tool errors are addressed. The criteria for selecting a combination of the technological elements for machine tool calibration from the point of view of accuracy, complexity, and cost are provided. Recent applications of artificial intelligence and machine learning in machine tool calibration are introduced. Remarks are also made on future trends in machine tool calibration.

1. Introduction

Machine tool calibration is a process periodically carried out over the lifetime of a machine tool for the purposes of performance verification and characterization, maintenance, and performance improvement (via mechanical adjustment or error compensation). Measurement and modeling are the major technological elements of machine tool calibration. The calibration process starts with a set of measurement operations to quantify the undesired motion of machine positioning axes and how they change with changes in the machine thermal status (thermal errors), static load (elastic errors), dynamic loading (dynamic errors), as well as motion control errors. Then the measurement data are used directly or input to a mathematical model based on the machine structural loop, to quantify the resultant volumetric errors in the machine work volume or the internal error sources. Machine tool calibration is often associated with error compensation, either on-line or off-line, which is implemented based on the predicted machining errors through modifying the machining parameters, including the tool path either within the machine numerical controllers or externally with reprogrammed numerical control code (e.g., in the computer-aided manufacturing software). Another application of machine tool calibration is to predict whether a machine is capable to manufacture a workpiece to specified tolerances, e.g., through virtual machining simulation.

A number of review papers, which are related to machine tool calibration, were published in the past years. Schwenke et al. and Ibaraki et al. reviewed measurement of quasi-static kinematic errors in 2008 [1] and 2012 [2], respectively. Ramesh et al. and Li et al. reviewed thermal error measurement and compensation in 2000 [3], 2003 [4], and 2015 [5]. Munoa et al. reviewed chatter suppression techniques in 2016 [6]. This paper reviews the state-of-the-art of the measurement methods, mathematical models and compensation strategies for machine tool calibration as an update to the previous review papers. Taking into consideration that each of the previous review papers mainly focused on

* Corresponding author.
E-mail address: i.ko.c2@tohoku.ac.jp (W. Gao).

a specific aspect of machine tool errors, such as quasi-static kinematic errors, a more comprehensive overview is made in this paper to cover all aspects of machine tool errors, from kinematic errors, thermal errors to elastic and dynamic errors. Recent achievements and cutting-edge technologies in measurement and compensation of these errors are highlighted. More importantly, the paper aims to provide machine tool builders and users clear criteria for selecting a proper combination of the technological elements for calibration of a specific machine tool from the point of view of accuracy, machine downtime, complexity, and cost. Meanwhile, recent applications of artificial intelligence and machine learning in machine tool calibration are introduced. Future trends of the technological elements of machine tool calibration will also be addressed as a guidance for further research and development.

The International Vocabulary of Metrology (VIM) [7] defines that calibration is "an operation that, under specified conditions, in a first step, establishes a relation between the quantity values with measurement uncertainties provided by measurement standards and corresponding indications with associated measurement uncertainties, and, in a second step, uses this information to establish a relation for obtaining a measurement result from an indication". Some calibration studies reviewed in this paper neither strictly establish traceability to measurement standards nor include all calibration phases, i.e., modeling, measurement, identification, and implementation. As the "machine calibration" is a popularly used term both in academia and industry, this paper adopts it for a wider class of works.

2. Classifications of error sources

This section covers errors within one axis as intra-axis errors, errors between axes as inter-axis errors and finally the resulting volumetric errors defined as the difference between the actual position and orientation of the tool relative to the workpiece and its nominal (desired) value. Such volumetric errors may potentially result in manufacturing or measuring errors depending on the specific interaction between a cutting or measuring tool and a workpiece. Intra-axis kinematic errors, inter-axis kinematic errors, and the resulting volumetric errors, are induced by multiple causes [8] such as: 1) the imperfect geometry of machine components and of their assembly under a defined initial thermal status and no load conditions, 2) thermo-elastic-geometric deviations, or simply thermal errors, from internal heat generation under normal operations and external heat sources from ambient conditions, 3) elastic-geometric deviations, or simply load-induced errors, from process load and the weight of machine components and workpiece causing deflection not compensated by mechanical design, 4) trajectory generation and individual axis controls, 5) structural dynamics, 6) friction forces, 7) rolling elements [9], and 8) other disturbances.

2.1. Kinematic errors

The term "kinematic error" has not been clearly defined in the literature, including ISO. Some use this term as quasi-static errors, and others use it with broader definitions. In this paper, the term "kinematic error" is defined as follows: the undesired motion of bodies without consideration, but not without the presence, of the causes. This undesired motion can be 1) that of a single linear axis, as intra-axis kinematic errors, e.g., the *X*-axis that moves in a nominally straight line, 2) the motion of an axis with respect to one or more other axes, as inter-axis kinematic errors, e.g., out-of-squareness or 3) a tool, or functional point, motion that should reach a desired position and orientation relative to the workpiece through specified command position of any number of mechanical axes, as volumetric errors. Whenever appropriate the particular cause being considered can be specified such as "thermally-induced kinematic errors'' to refer to the undesired motion due to changes in the thermal status of the machine.

The term "geometric errors" is commonly used in the literature to refer to kinematic errors. However, in Ref. [10] [11] [12,13] the causal relation between geometric errors of machine components, such as guideways and bearing elements, and their impact on kinematic errors was demonstrated. In Ref. [14] a clear distinction is also made between the kinematic errors of the machine tool and the resulting geometric errors of the machined workpiece. It remains, however, that an imposing number of published research and relevant machine tool standards use the term "geometric errors" for quasi-static kinematic errors.

2.1.1. Intra-axis kinematic errors

Intra-axis kinematic errors [15] are also known in the literature and standards as error motions [16], motion errors [17], geometric errors (of a single axis) [18], position dependent geometric errors (PDGE) [19] [20] [21], component errors [22], and joint kinematic errors [13]. They are unwanted linear and angular displacements that occur when moving one machine axis. For a linear axis these are the positioning error in the direction of nominal axis motion, straightness errors in two orthogonal planes, and roll, pitch, and yaw error motions [23]. For a rotary axis these are the difference between the actual and commanded axis rotation, as well as axial, radial, and tilt error motions in the position and orientation of the axis of rotation [24].

The nomenclature for the six error components, based on [16,25], is $E_{X?}$, $E_{Y?}$, $E_{Z?}$, $E_{A?}$, $E_{B?}$, $E_{C?}$ where *X*, *Y*, *Z*, *A*, *B*, and *C* are the nature of the error, i.e., a translation in *X*, *Y*, or *Z* or a rotation around *X*, *Y*, or *Z*, respectively. "?" is replaced by the symbol for the nominal motion axis having the error, i.e., typically one of *X*, *Y*, *Z*, *A*, *B*, *C*, and *C*1. The definition of a reference is necessary to quantify these errors as the same error motion may lead to different values as for the quantification of the straightness error of a linear axis with respect to a different reference line or the definition of an axis average line for the errors of a rotary axis [16]. Fig. 1 illustrates the intra-axis errors nomenclature for a linear and for a rotary axis. However, researchers have used various notations for the error terms deviating from the symbols indicated in this figure. Therefore, to better reflect the original research efforts found in literature, this paper does not use uniform set of notations.

In the presence of angular errors, linear (translational) error motions may have different values depending on the selection of the functional point or position on the moving body where the error is measured. This is due to rotational errors causing translational effects at a distance that

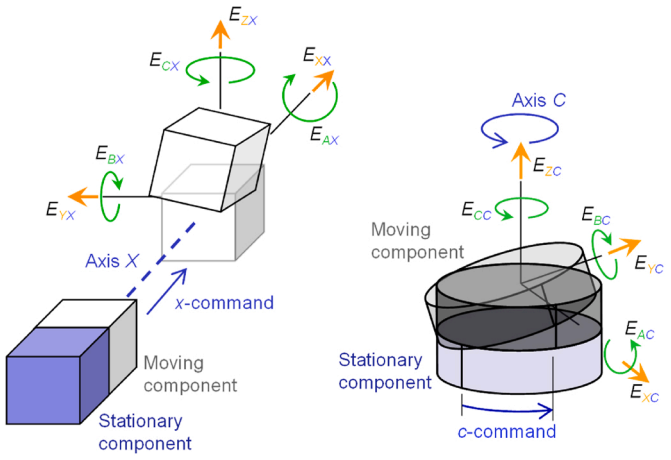

Fig. 1. A linear and a rotary axis with their translational and rotational intra-axis kinematic errors [15] [16] [25]. (a) Intra-axis errors for a linear axis (*X*). E_{XX}, E_{YX}, and E_{ZX} represent translational error motions in the *X*-, *Y*-, and *Z*-directions, respectively. E_{AX}, E_{BX}, and E_{CX} represent angular error motions around the *X*-, *Y*-, and *Z*-axes, respectively. (b) intra-axis errors for a rotary axis (*C*-axis). E_{XC}, E_{YC}, and E_{ZC} represent translational error motions in *X*-, *Y*-, and *Z*-directions, respectively. E_{AC}, E_{BC}, and E_{CC} represent angular error motions around *X*-, *Y*-, and *Z*-axes, respectively.

may change with the selection of the functional point. These geometric effects have led to the definition of the Abbe and Bryan principles to reduce or eliminate them [26] [12]. Guideways straightness, alignment, sliding block compliance, defects of rolling components [9], and position feedback systems are found to be contributors to intra-axis kinematic errors of linear axes [13] [11] [27] [28].

2.1.2. Inter-axis kinematic errors

Inter-axis kinematic errors [25] [15] are deviations from the nominal position and orientation of one axis of motion relative to one or more other axes of motion. They are also defined as the alignment errors between multiple axes of machine tools [16]. In practice due to the presence of intra-axis kinematic errors, an axis of motion average line [25] is defined using pre-defined criteria to quantify inter-axis kinematic errors. The axis average line of a rotary axis is defined in Ref. [24] as "a straight line segment located with respect to the reference coordinate axes representing the mean location of the axis of rotation." The inter-axis kinematic errors of a rotary axis represent the position and orientation errors of its axis average line with respect to the specified reference axes. For a linear axis, the inter-axis kinematic errors typically represent the relative orientation errors of its reference straight line, which is "the associated straight line fitting the measured trajectory of a functional point in accordance with specified conventions" as defined in Ref. [16].

Inter-axis kinematic errors are also known as position independent geometric error parameters (PIGEP), as appeared in Ref. [19] [29] and re-appeared in Refs. [30,31] without the word parameters (the last P in the acronym), which specifically refer to variables used to quantify the deviations. The word position refers to an axis position along its nominal motion. The term "position independent geometric errors" are commonly used today in the scientific literature [32] [33]. They are position-independent because they represent the translational and rotational errors of the axis average line of a rotary axis or the reference straight line of a linear axis. Fig. 2 shows four inter-axis kinematic errors for a *C*-axis as well as a constant positioning error named *C0C* [1]. In Ref. [16] the four errors are called axis alignment errors and their symbols start with an "*E*" . They are classified as geometric errors in Refs. [18,34]. Fig. 3 shows a possible set of eight inter-axis errors for the axes of a five-axis machine tool with two additional translational errors added for the spindle (for completeness the spindle should also have two rotational inter-axis kinematic errors). The nomenclature used in Figs. 2 and 3 does not specify the reference axis [15].

The nomenclature, based on [16,25], was extended in Ref. [24] to make explicit the machine axis used as the reference axis. Such nomenclature and its necessity for a complete definition of inter-axis errors is shown in Fig. 4.

The published literature focuses on the measurement and compensation of such errors as opposed to their physical causes.

2.1.3. Volumetric errors

The term "volumetric error" appeared in Ref. [25] and in Ref. [37]. Both the workpiece and cutting tool may experience deviations from their desired position and orientation under the effect of all types of machine errors. The volumetric error is the relative deviation of the tool functional point with respect to the workpiece. This can be quantified by three translational and three rotational components. In Ref. [16], for the assumed purpose of quantifying a particular machine's performance, the volumetric accuracy is defined as the maximum value of each such error component over the entire workspace of a three-axis machine. In this paper, volumetric errors refer to any quantity used to describe the relative deviation of the tool functional point with respect to the workpiece and it may be accompanied by a suitable descriptor, whenever appropriate, to refer to one or more cause being considered.

2.1.4. Quasi-static kinematic errors

In Ref. [34] quasi-static errors are described as errors slowly varying in time and related to the machine structure and specifically include errors due to geometric departure from the design intent, deflection under the machine's own weight, over-constrained slides, and workpiece weight. In Ref. [16] quasi-static behavior is simply defined as behavior in the absence of dynamic influence and servo limitations but

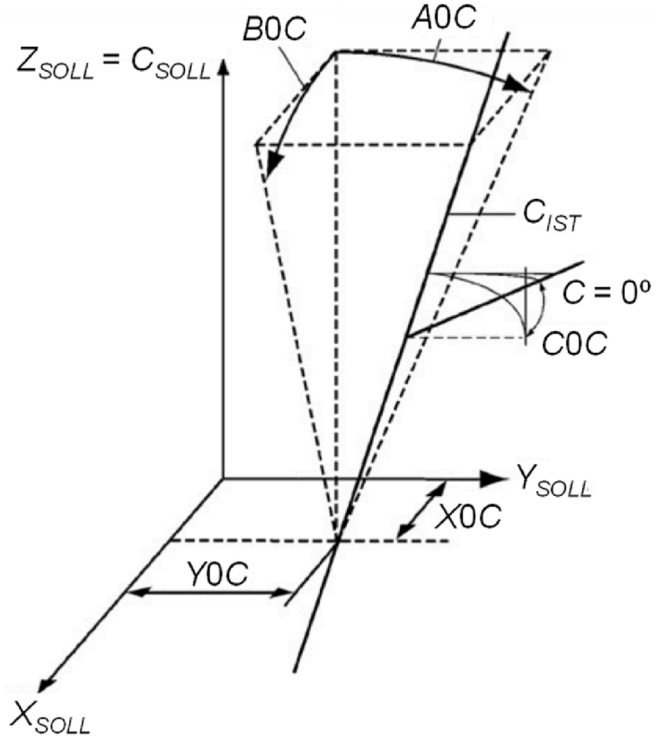

Fig. 2. Inter-axis errors of rotary axis *C* of a machine tool [1]. Rotary axes have a maximum of four inter-axis errors to fully describe their position and orientation with respect one or more other axes of the machine. *X0C* and *Y0C* represent the position errors in the *X*- and *Y*-directions of the *C*-axis average line, respectively. *A0C* and *B0C* represent its orientation errors around the *X*- and *Y*-axes, respectively. *C0C* is a CNC angular positioning offset.

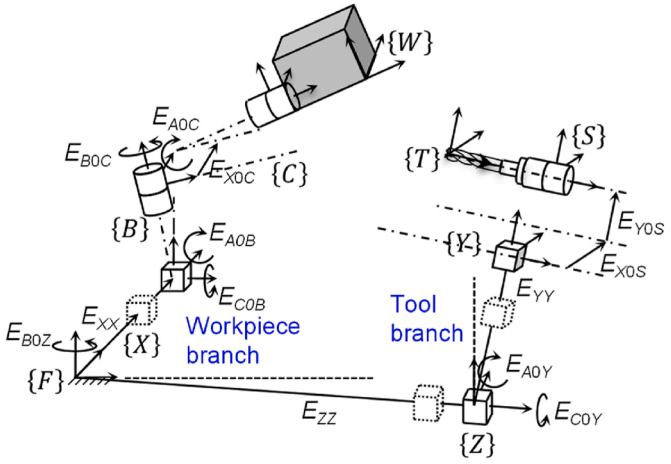

Fig. 3. Some inter-axis errors of a five-axis machine tool using the *X*- and *Z*-axes as primary and secondary axes, respectively [35]. It shows the eight axis alignment errors of the main five axes and two (the translational errors) of the four alignment errors of the spindle axis. This machine's kinematic chain is denoted by the designation [*w C′ B′ X′ b Z Y* (*C1*) *t*] [36] with *S* replacing *C1*. The position and orientation of the tool coordinate system, denoted by {*T*}, with respect to the workpiece coordinate system, denoted by {*W*} is the resulting volumetric error.

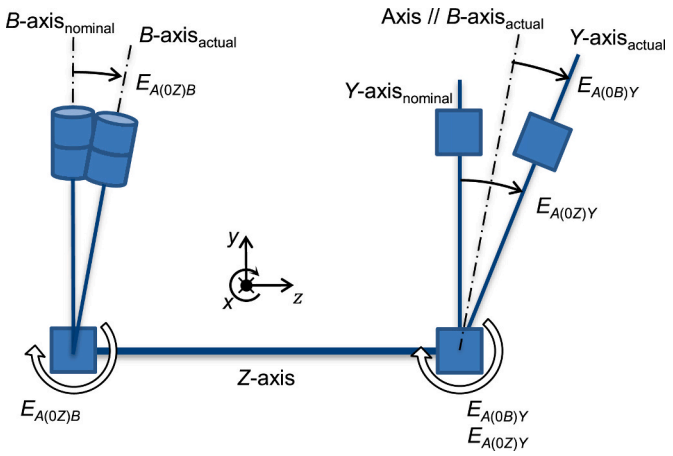

Fig. 4. Inter-axis errors with the reference axis specified. In this example the *Y*-axis orientation error can be measured either with respect to the *B*-axis as a parallelism error around *x*, $E_{A(0B)Y}$, or with respect to the *Z*-axis as a perpendicularity around *x*, $E_{A(0Z)Y}$. Because the *B*-axis may have an out-of-squareness error $E_{A(0Z)B}$ with respect to *Z* around *x* the values of $E_{A(0B)Y}$ and $E_{A(0Z)Y}$ may differ and are related by the algebraic relation $E_{A(0Z)Y} = E_{A(0Z)B} + E_{A(0B)Y}$.

load and thermal status are specified separately.

A review of accuracy degradation, in terms of changes in kinematic errors, over long-term machine tool use can be found in Ref. [38] but will not be addressed here.

2.2. Thermally-induced kinematic and volumetric errors

Thermally-induced errors are the result of thermo-elastic deformations of the machine tools and workpieces caused by various internal heat sources related to the machine and machining process and external heat sources from the environment. They are considered as the primary factors influencing the accuracy of machine tools [39] [3]. In-depth research of thermal errors can be traced back to the 1960s by J. Bryan [40] [41] who pioneered this topic, which remains an active research topic today.

Fig. 5 summarizes the heat sources, classified as internal and external, and the mechanisms by which they cause thermal errors [42]. The internal heat sources are typically ball screws, bearings, gears, motors, and hydraulic oils related to the moving axes and spindle of a machine tool and the machining process, as well as cutting fluid that would warm up the tool, toolholder, workpiece, and the clamping device [43][44][45]. The external heat sources come from variations in environmental temperature, the effect of people and the thermal memory from any previous environment [46][47]. Heat is transferred by conduction, convection, and radiation and consequently leads to geometric errors of the machine tool through thermo-elastic deformations of the workpiece, tool, and machine elements. It is recognized that thermal errors could contribute 40%–70% of the overall geometric errors of machined workpieces [41][40].

2.3. Static load-induced elastic errors

Machine tool structures deform when load is induced on any machine component. When the load is constant, it can be regarded as static. The load can be regarded as quasi-static when the load is slowly varying with deflections having frequency components higher than 0 Hz and lower than approximately 10% of the first eigenfrequency of the machine [48] [16]. This means that no dynamic influence can be observed. In practice, loads are due to the weight of the workpiece, fixturing, and work table on the workpiece side, tool holder, tool, and other accessories on the tool side and finally to quasi-static process related forces.

The resulting deformation is quantified through static compliance or

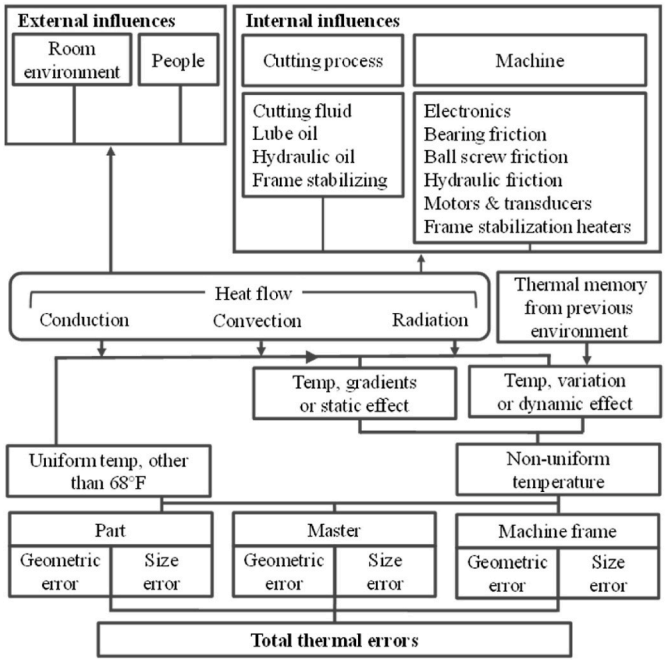

Fig. 5. Heat sources of machine tools and their effect on thermal errors [40]. The sources of thermal errors of the machine tool are divided into two categories, namely, the influence of uniform temperature other than 20 °C (68 °F) and the effect of uneven temperature, and the geometric error and dimensional error of the machine tool. The main sources of errors include external influences and internal influences. External influences include environmental temperature changes and human interference. Internal interferences include machining process and internal heat source interference of machine tool.

static stiffness, which is the reciprocal of static compliance. ISO 230–1 [16], defines static compliance as a "linear (or angular) displacement per unit static force (or moment) between two objects, specified with respect to the structural loop, the location and direction of the applied forces, and the location and direction of the displacement of interest'". The term "cross compliance" is used when displacement and force are not in the same direction. As the definition suggests, the compliance values are dependent on the position of the machine tool axes and the direction and position of the applied static force. The field of study related to static load-induced deformation, from a machine calibration viewpoint, is limited to elastic deformations. Elastic deformations are temporary changes in the machines' geometric shape that reverse after the withdrawal of the applied load. This implies an upper limit on the load to avoid permanent deformations by staying within the so-called elastic limit. Nevertheless, hysteresis may still occur. ISO 230–1 [16] defines hysteresis as linear (or angular) displacement between two objects resulting from the sequential application and removal of equal forces (or moments) in opposite directions [16].

2.4. Dynamically induced errors

Dynamic errors are undesirable response of the machine tool to dynamic forces, which vary with time, as opposed to quasistatic forces. The nature of this response is determined by the coupled dynamics of mechanical and control systems (Fig. 6). Dynamic forces include machining process forces generated at the tool/workpiece interface, which has non-negligible stiffness and damping characteristics. Although vibrations caused by periodic forces are typical dynamic errors, non-periodic tracking error such as the one caused by the response difference between different feed drives are also included in the dynamic error [49].

Dynamic errors can be classified into two cases. One case is the error caused by dynamic disturbances. The response difference between the tool and workpiece positions leads to relative displacements between

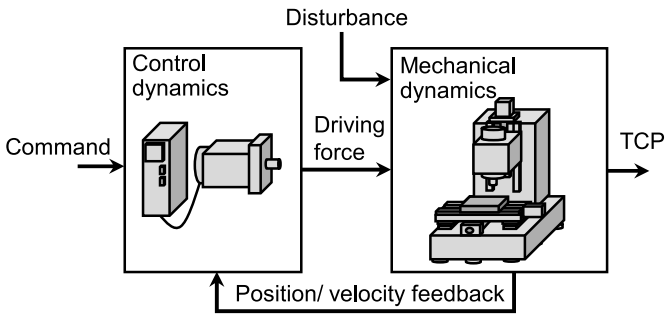

Fig. 6. Coupled dynamics of mechanical and control systems (TCP: tool center point). The response to the command and disturbance is determined by the coupled system. The interaction between the mechanical and control systems is caused by the feedback control.

them. Typical dynamic forces are the cutting force [50] and forces in the feed drive system such as the inertial force [51] [52] [53] and friction force [54] [55]. External disturbances such as the seismic vibration transmitted from neighboring systems may also result in dynamic errors [56] [57].

The other case covers errors caused by the undesirable response of a machine tool to the position commands. The response of the mechanical system is generally not considered in command generation [58] [59]. The feedback control cannot suppress the dynamic error effectively because the tool-workpiece relative position is not directly measured and fed back in most machine tools. The response of the control system is also often lower than the bandwidth of the dynamic error.

Contributors to machine tool dynamics exist in both mechanical and control systems. The dynamic response of the mechanical system is determined by the mass, stiffness and damping in its mechanical structure. These parameters depend on the design of each mechanical component and on the machine's structural configuration. The stiffness and damping are significantly influenced by the joints or interfaces such as preloaded joints [60] [61], guideways [62], and bearings [63]. Because the characteristics of these interfaces are affected by preload dependency, individual machines with the same design, and structure could have different dynamic characteristics.

Dynamic performance of machine tools may also strongly depend on the placement of the machine tool structure on the factory's foundation [57]. Two of the major reasons for the effect of the foundation on the dynamics of machine tools are the added stiffness and the increased mass from the installation site's foundation. A change of these characteristics greatly affects the dynamic characteristics of the overall machine tool and therefore also the machining dynamics. The machine tool foundation and interface with the machine also play a major role in the transmission of seismic vibrations.

In the servo controller, cascaded feedback loops for the position, velocity, and motor current are adopted. Many commercial servo controllers employ a proportional and proportional-integral (P-PI) controller scheme that uses proportional control for the position loop and proportional–integral control for the velocity loop. The gain for these control loops dominates the response and bandwidth of the control system. Because the controller gain is limited by vibrations in the mechanical system, the response of the mechanical system is also important to develop a high-response servo system.

3. Measurement instruments and methods

3.1. Quasi-static kinematic errors

Machine tool quasi-static kinematic error motions can either be directly measured for each machine axis or they can be measured indirectly using calibrated artifacts, machined workpieces, or other methods that involve coordinated motion of more than one machine axis [16].

3.1.1. Direct measurement of quasi-static error motions

3.1.1.1. Linear axis error motions. Linear axis error motions are intra-axis errors comprising the positioning (translational) error along the nominal direction of motion of the linear axis, two translation errors orthogonal to the nominal direction of motion, which are called straightness errors, as well as three rotational errors around three orthogonal coordinate axes, which are usually called roll, pitch, and yaw. The direct measurement methods for each of these errors are well established in international standards. Since ultimately the relative errors between the cutting tool location and the workpiece location limit the accuracy of the machined workpiece, the error measurements should reflect this relationship. Therefore, for machine calibration and error assessment purposes, the international standard for checking geometric accuracy of machine tools introduces the concept of "functional point," and requires that the error measurements are conducted to reflect the errors at its location in the machine work volume [16]. First introduced in Ref. [12], the functional point, in the context of machine tools, is defined as the point where the cutting tool and the workpiece interacts. [64] summarizes many instruments used for measurements of linear axis error motions. The selection of instruments appropriate for a particular measurement depends on the acceptable levels of measurement uncertainty, which includes the influence of environment on the measuring device or the method.

Table 1 shows examples of the state-of-the-art commercial measuring instruments for direct measurement of the linear-axis error motions illustrated Fig. 1. Some cutting-edge measurement technologies are also listed in the table. Although there are multiple methods and instruments to measure linear positioning error motion, which are summarized in Ref. [64], the most common method uses a heterodyne laser Michelson interferometer, where the wavelength of laser light provides the traceable length reference. It is important to note that, to minimize setup-induced uncertainties in such measurements, the laser beam should be aligned parallel to the direction of motion of the component. Furthermore, the interferometer optics should be mounted on the stationary component (cutting tool side or workpiece side) while the laser beam reflector is moving with the moving component for linear positioning error motion. As shown in Table 1, a state-of-the-art commercial laser interferometer can measure linear positioning error motion over an axis travel distance up to 80 m with a resolution of 1 nm. The measurement accuracy is in the order of ±0.5 ppm (parts per million) with environmental compensation.

Straightness error motion measurements involve measuring small displacements in orthogonal directions relative to a straightness reference representing the ideal linear motion of the component under test. The straightness reference can be a physical artifact (straightedge, taut wire, or straightness reflector mirror on a laser interferometer system), the laser light beam of an alignment laser system, or the optical axis of an alignment telescope. For long range travels a taut wire/microscope system is a practical alternative for measuring straightness error motions. However, wire profile errors and gravitational sag as well as inefficient data acquisition (via microscope) create difficulties implementing this method. To automate such measurements and eliminate wire related errors, Borisov et al. developed a system with low-cost sensing head consisting of an optical emitter and a receiver [80]. For a short range of travel less than 3 or 4 m, using a straightedge as the straightness reference is the most practical method to measure straightness error motions where a cost-effective straightedge of steel is often selected. However, for high-precision machine tools, form errors of the straightedge and gravitational sag for the measurements in the vertical direction must be taken into account. The form error of a steel straightedge increases significantly with the increase of its length. The Japanese Industrial Standards (JIS) B 7514 regulates the form errors for the rank-A steel straightedges of 0.25 m, 1 m, 2 m, and 3 m long to be less than 3 μm, 6 μm, 11 μm, and 14 μm, respectively. As recent

Table 1
State-of-the-art measuring instruments for direct measurement of the linear-axis error motions illustrated in Fig. 1.

		Laser interferometer [65]	Artifact method (Straightedge + linear displacement sensor)	Autocollimator [66]	Electronic level [67]
Axial distance range L		Linear measurement: up to 80 m Straightness measurement: 0.1 m–4 m (short distance range), 1 m–30 m (long distance range) Angular measurement: up to 15 m	Length of straightedge Up to 3 m for steel [68] Up to 4 m for ceramics [69] Up to 1 m for Zerodur [70]	Up to 20 m	No limitation
Translational errors	Positioning error E_{XX}	With length optics Resolution: 1 nm Accuracy: ±0.5 ppm (with environmental compensation)	Measurable with a step gauge	Not applicable	Not applicable
	Horizontal straightness E_{YX} Vertical straightness E_{ZX}	With straightness optics (Short travel range L) Resolution: 10 nm Accuracy: $\pm 0.005A \pm 0.5 \pm 0.15L^2$ μm (Long travel range L) Resolution: 100 nm Accuracy: $\pm 0.025A \pm 5 \pm 0.015L^2$ μm A: measured displacement, L: travel range in meters	LVDT [71]/capacitive sensor [72] Resolution: 0.1 μm/1 nm Range: ±400 μm/±100 μm Linearity: 0.5%/0.2% of range Form accuracy of straightedge Steel: $\left(2+\frac{L}{0.25}\right)$ μm [68] Ceramics: 2 μm [69] Zerodur: 25 nm [70]		
Rotational errors	Pitch E_{BX} Yaw E_{CX}	With angular optics Resolution: 0.01" (0.1 μm/m) Accuracy: $\pm 0.002A \pm 0.5 \pm 0.1L$ μrad Range: ±10° A: measured displacement, L: travel range in meters	Not applicable	Resolution: 0.001″ Accuracy: 0.25″ Range: ±1000"	Resolution: 0.36″ Accuracy: 3.6″ Range: ±15° Not applicable
	Roll E_{AX}	Not applicable		Not applicable	Resolution: 0.36″ Accuracy: 3.6″ Range: ±15°
Measurement speed or sensor bandwidth		4 m/s	LVDT [71]/capacitive sensor [72] 20 Hz/5 kHz	25 Hz	1 Hz
Complexity of setup and alignment		One setup only for one axis measurement Careful alignment required for axes of laser beams and optics	Careful alignment required for parallelism between straightedge and axis of motion, and gap between straight edge and sensor	Simple setup and fast alignment	Simple setup and fast alignment
Robustness to environmental disturbances		Sensitive to temperature, humidity and pressure variations	Sensitive to mechanical vibration	Sensitive to air flow	Sensitive to temperature variation and mechanical vibration
Estimated cost (may vary with manufacturer, system configuration, purchasing area, and time)		Laser head with environmental compensation: 30k US$ Length optics: 4k US$ Straightness optics: 10k US$ Angular optics: 5k US$	stainless steel straightedge: 1 m long 2k US$ 3 m long 6k US$ LVDT/capacitive sensor 2k US$/10k US$	45k US$	1k US$
Cutting-edge technology		Six degrees of freedom (DOF) simultaneous measurement [73] with roll measurement [74]	Roll measurement with a straightedge and two capacitive sensors [75] Self-calibration of straightedge form error [**Section 3.1.3**]	Photodiode-based high-speed laser autocollimator [76] Grating reflector-based three-axis autocollimator [77]	Differential roll-measurement by two inclinometers [78] Liquid surface-based three-axis inclinometer [79]

advances, ceramic straightedges and Zerodur straightedges with better form accuracies are commercially available. A 4 m long ceramic straightedge with a form error less than 2 μm and a 1 m long Zerodur straightedge with a form error less than 25 nm are listed in Table 1 as examples. In general, a reversal method can remove the straightedge profile errors from straightness measurements in horizontal directions. Removing the effects of gravitational sag is more difficult [81]. **Section 3.1.3** will present self-calibration schemes to remove the geometric error of a straightness reference artifact. On the other hand, linear variable differential transformers (LVDT) and capacitance-type displacement sensors (also called capacitive sensors or capacitive probes) are the most well used linear displacement sensors in the straightedge-based method. The former is cost-effective and is suitable for micrometric straightness measurement while the latter is more expensive and is suitable for nanometric straightness measurement. As a cutting-edge technology, precision roll measurement in the order of 0.1 arcsecond was achieved by using a combination of a straightedge and two capacitive sensors [75]. It should be noted that when a capacitive sensor is used with a ceramic or Zerodur straightedge, it is necessary to coat a layer of metal on the straightedge surface since a capacitive sensor basically can only detect a conductive surface.

Interferometer-based straightness error motion measurements typically split a laser beam to generate two diverging beams via a Wollaston prism [82] or holographic grating [83] that are reflected back by a V-shaped reflector or roof prism. In such instruments, precise alignment between the straightness reflector and interferometer is required. To relax this requirement [84] developed a modified version of this method using two right-angle prisms in place of the straightness reflector and a retroreflector attached to the Wollaston prism. Alignment lasers use the laser beam as the straightness reference and measure the lateral displacements of the moving component with respect to the laser beam by photodetectors. A variation of this principle is used to simultaneously measure straightness in the vertical and horizontal directions [85]. This system uses a simple retroreflector mounted on the moving component and a camera to capture the return beam spot to measure lateral motions in the horizontal and vertical directions. As shown in Fig. 7, Gao et al. has demonstrated that a moving-reflector arrangement of the straightness measurement kit in a laser interferometer-based system suffers from

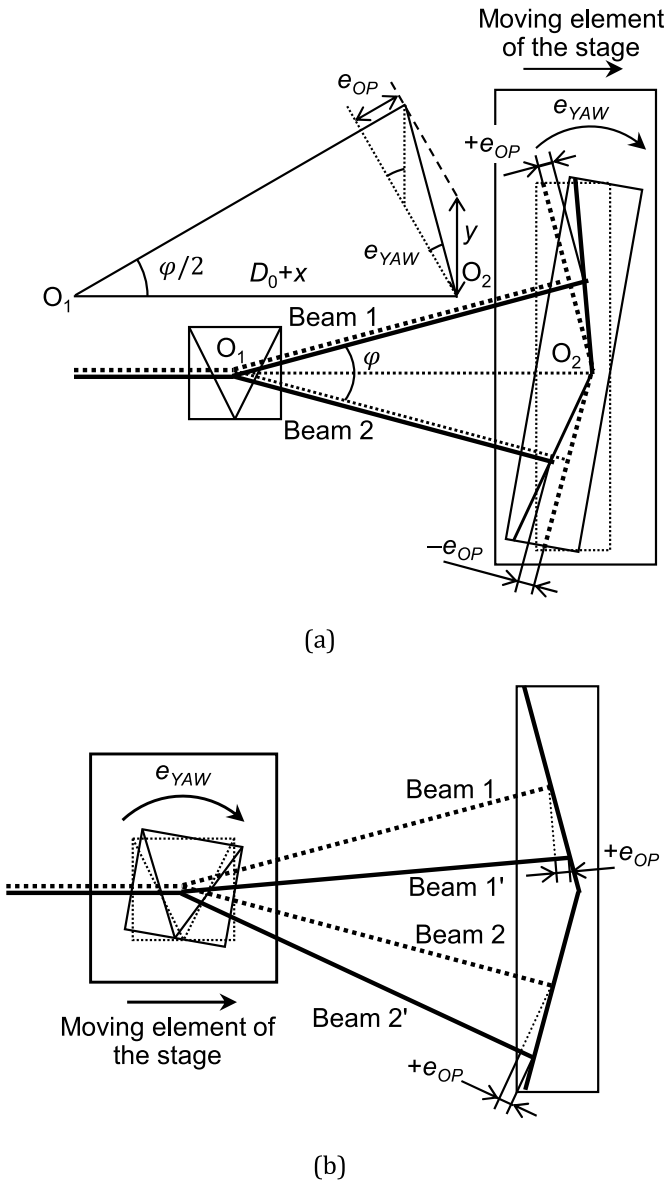

Fig. 7. Influence of the yaw error (or pitch error) on laser interferometric straightness measurement [75]. (a) A yaw error $e_{yaw}(x)$ of the moving reflector generates an optical path change $e_{OP}(x)$ in Beam 1 and $-e_{OP}(x)$ in Beam 2, causing a measurement error $(D_0 + x)e_{yaw}(x)$of straightness error motion in a moving reflector arrangement, where D_0 is the distance between the center of the prism (O1) and that of the reflector (O2) at the starting position of the moving element of the stage. (b)A yaw error $e_{yaw}(x)$of a moving prism/receiver assembly generates an equal optical path change $e_{OP}(x)$ in Beams 1 and Beam 2, which are canceled in the measurement of straightness error motion for a moving prism/receiver assembly arrangement.

the yaw or pitch error (Fig. 7a) [75]. To avoid the influence of yaw or pitch errors, it is necessary to mount the moving prism/receiver assembly on the moving component of the linear axis (Fig. 7b) [75]. It should be noted that the laser-interferometer-based systems are sensitive to external turbulences. The measurement resolution of straightness is also much lower than that of linear position (displacement).

Angular error motions of a linear axes are intra-axis errors comprising rotational errors around the three orthogonal axes. Their direct measurements are carried out using, most commonly, laser angle interferometers, but also precision levels (inclinometers) and autocollimators. Both autocollimators and laser interferometers with angular optics can measure pitch and yaw errors but not roll error. Inclinometers can measure pitch and roll errors for the horizontal axes, and pitch and yaw errors for the vertical axis. Interferometric angle measurements use two parallel laser beams, generated with a beam splitter and 90° beam bender, reflected by two retroreflectors that are separated by a known distance [86]. The path length difference between the two laser beams is measured as the indication of an angular error motion. Rotational errors around the two axes orthogonal to the axis of motion of the component, which are typically called pitch and yaw errors, can be easily measured by changing the orientation of the instrument optics. As shown in Table 1, a laser angle interferometer can typically reach a high resolution of 0.001 arcsecond over a wide range of ±10° for separated pitch and yaw measurements.

Autocollimators use a collimated light beam projected on a mirror mounted on a moving component and detect the position of the beam, reflected along the same collimated optical path, on a photodetector to determine the angle of the mirror with respect to the emitted beam. The angular error motions around two orthogonal axes (pitch and yaw) can be measured simultaneously with a charge-coupled device (CCD) area image sensor [87]. As shown in Table 1, a commercial CCD-based autocollimator can reach a high resolution of 0.001 arcsecond over a wide range of ±1000 arcseconds for simultaneous pitch and yaw measurements. However, the measurement speed of the CCD-based autocollimator is limited on 25 Hz due to the limited sampling rate of CCD image sensor. As a cutting-edge technology, Shimizu et al. developed a photodiode-based laser autocollimator that can reach a measurement speed of 1 kHz with the same resolution of 0.001 arcsecond [76].

However, such laser angle interferometers and autocollimators cannot measure the angular error motion around the axis of motion (roll error). Conventionally, two parallel sets of straightness measurements separated by a known distance are used to calculate the roll angular error motion [16]. As a cutting-edge technology, a three-axis autocollimator was recently developed utilizing two detectors separated by a known distance and a grating reflector, capable of measuring angular error motions around three orthogonal axes with a resolution of 0.01 arcsecond (see Fig. 8) [77]. A new roll measurement method using diffraction gratings and heterodyne interferometer with a measurement resolution of 0.002 arcsecond is described in Ref. [88].

For roll error motion around horizontal axes of motion, using electronic levels (inclinometers) is a traditional method. As shown in Table 1, a commercial inclinometer can reach a resolution of 3.6 arcseconds over a range of ±15°. An inclinometer detects the absolute angle with respect to the direction of gravitational vector. Due to this reason, the output of an inclinometer includes not only the roll error motion of a linear stage but also external inclinations such as tilt angle of the table where the stage is mounted. As a cutting-edge technology, Shimizu et al. developed a differential-type roll measurement system where two inclinometers are mounted on the stage and the table, respectively. The influence of the stage inclination can then be removed by taking the difference of the outputs of inclinometers [78]. A new three-axis inclinometer [79] was recently developed for making simultaneous measurement of three-axis rotational error motions (pitch, yaw, roll) by combining a three-axis autocollimator [77] with a floating grating reflector. This sensor can be employed for rotational error measurements of not only horizontal axis of motion but also vertical axes of motion.

Recent advances were also achieved in simultaneous measurement of six-DOF error motions. In a commercially available system [73], a light source unit consisting of a Helium–Neon laser source and a light-emitting diode (LED) source, and a receiver unit consisting of retroreflectors and photodetectors for the LED beam, are used for the measurement. Four laser beams and one LED beam are output from the launch unit. The three laser beams are employed for simultaneous measurement of linear, pitch, and yaw errors based on laser interferometry, whose specifications are similar to those of the conventional-type laser interferometer system shown in Table 1. The LED beam is employed for simultaneous measurement of straightness

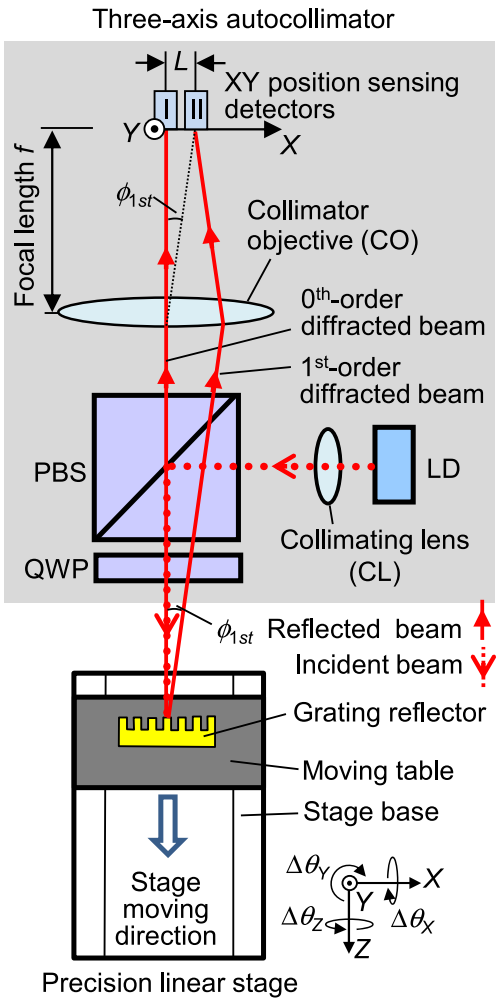

Fig. 8. Principle of a three-axis angular measuring autocollimator (LD – laser diode, PBS – polarized beam splitter, QWP – Quarter wave plate) [77]. A collimated laser beam from a laser diode is projected onto a grating reflector mounted on a linear stage. The reflected 0th-order diffracted beam is received by an autocollimation unit, which consists of a collimator objective and a quadrant photodiode, for detecting the pitch and yaw errors. The reflected 1st-order diffracted beam is received by another autocollimation unit for detecting the roll error.

and roll error motions. In the straightness measurement, a light spot position-sensing detector (PSD) is employed to detect the lateral shift of the LED beam from a corner cube mirror, which is associated with the straightness error motion, with a resolution of 250 nm over a range of ±250 μm. For the roll measurement, the LED beam is passed through a stationary reference polarizer and a measurement polarizer where the beam is polarized into vertical and horizontal components. When the measurement polarizer rotates about the axis of the source beam, the intensities of the polarized components change accordingly. The roll angle of the measurement polarizer relative to the light source can then be measured from the changes of the light intensities with a resolution of 0.12 μrad (0.02 arcsecond) and ±500 μrad (±103 arcseconds). Similar roll measurement technique can be seen in Ref. [74]. Meanwhile, Zheng et al. developed a six-DOF system in which only the positioning error is measured by laser interferometry and other error motions are measured based on laser collimation [89].

3.1.1.2. Rotary axis error motions. Rotary axis error motions include axis of rotation error motions as well as angular positioning error motion in the direction of the nominal axis motion. Measurements of axis of rotation error motions require a reference artifact representing the axis of rotation, which is attached to the rotating component. Displacement sensors attached to the opposite side of the machine tool (tool or workpiece side) are used to measure deviations in the relative location of the artifact in the sensitive direction(s) of interest as a function of the angular position of the rotating component [24]. The sensitive direction is the direction perpendicular to the workpiece surface at the tool-workpiece interface [24]. The reference artifact could be a precision mandrel, or two precision spheres separated by a known distance. A sensor nest with three or five displacement sensors is needed to measure radial, axial, and tilt error motions of the axis of rotation. Depending on the function of the rotary axis, fixed sensitive or rotating sensitive directions are of interest. For fixed-sensitive direction measurements, only three sensors (two in the radial directions of interests and one in axial direction) are used. Early studies identifying and measuring axis of rotation errors are found in Refs. [90–92]. Although a precision artifact is used for these measurements, its accuracy may not be sufficient for measuring ultraprecision machine tool spindles and axes. **Section 3.1.3** provides details of self-calibration techniques for such applications. The specifications of a commercial five-sensor test system (spindle error analyzer) are listed in Table 2 [93]. A reference artifact with two 25.4 mm diameter master spheres made of stainless steel is employed. The distance between the centers of the two spheres are designed to be 76.2 mm. When using a capacitive sensor with a resolution of 1 nm, the resolution of tilt error measurement is calculated to be approximately 0.003 arcseconds.

As a cutting-edge technology, Gao et al. presented a multi-probe method for multi-DOF (MDOF) spindle error measurement by using two-dimensional (2D) surface slope sensors [99]. Each sensor detects the 2D local slopes of a point on a cylindrical artifact, along the tangential and the axial directions, respectively. The radial and tilt error motions can be simultaneously measured from the 2D outputs of the sensor, respectively. The four-DOF radial and tilt error motions can be simultaneously measured by using two 2D slope sensors with a 90° angular spacing. Other cutting-edge technologies on spindle error measurement are summarized in Ref. [101].

Axis of rotation error motions of rotary tables and spindle heads are also critical machine kinematic errors, which need to be measured. The direct measurements of these error motions use the same principles and instruments used for spindle measurements.

The angular positioning errors of rotary tables and rotating spindle heads can be significant sources of inaccuracies in workpieces. Several methods of direct measurements are listed in Ref. [16], including using a polygon mirror with an autocollimator, a reference angle encoder, and a reference indexing table with a laser angle interferometer. Table 2 shows examples of state-of-the-art measuring instruments for direct measurement of the rotary-axis error motions illustrated in Fig. 1. The combination of a polygon mirror and an autocollimator is the most traditional method and it is still well used by national measurement institutes where polygon mirrors are used as angular transfer standards. However, it is not often used in machine tool calibration due to its limited measurable angular positions. For calibration of low-speed rotary tables of machine tools, the combination of a reference indexing table with a laser angle interferometer can be selected. One of the most significant advantages of such a system, compared with the reference angle encoder and the combination of a polygon mirror and an autocollimator, is its large tolerance against the centering alignment error of the reference indexing table with respect to the rotary axis for measurement. For the system listed in Table 2, the tolerance for centering the reference indexing table is approximately ±1 mm, which makes the centering alignment easy. For calibration of higher speed rotary tables of machine tools, a reference angle encoder would be a better choice. For the reference angle encoder listed in Table 2, the maximum measurable rotational speed is 1000 rpm. As a cutting-edge technology, Lou et al. presented a multi-head rotary encoder that can measure radial error motions of a rotary axis [97] where the radial error motions along the *Y*- and *X*-axis can be obtained from the pair of scanning heads A, B, and that

Table 2
State-of-the-art measuring instruments for direct measurement of the rotary-axis error motions illustrated in Fig. 1.

	Reference indexing table with laser angle interferometer [94]	Reference angle encoder [95]	Polygon mirror [96] with Autocollimator [66]	Five-sensor test system (spindle error analyzer) [93])
Angular positioning error E_{CC}	Resolution: 0.1″ Accuracy: ±1″ Range: 360°	Resolution: 0.02″ Accuracy: ±1″ Range: 360°	Autocollimator Resolution: 0.001″ Accuracy: 0.1″ Polygon mirror Accuracy: 2″ Measurement interval: 30° (12 faced polygon) Range: 360°	Not applicable
Radial E_{XC}, E_{YC}, and axial E_{ZC} error motions	Not applicable			Capacitive sensors Resolution: 1 nm Range: ±100 μm Linearity: 0.2% of range Precision spheres Sphere diameter: 25.4 mm Material: stainless steel Roundness: 50 nm
Tilt error motions E_{AC}, E_{BC}				Resolution: 0.003″ Range: ±270″ Linearity: 0.2% of range Dual-sphere target Sphere distance: 76.2 mm
Measurement speed or sensor bandwidth/	10 rpm	1000 rpm	25 Hz (autocollimator)	50 kHz
Complexity of setup and alignment	Complicated setup but no strict requirements on centering alignment of the reference indexing table	Simple setup but strict requirements on centering alignment of the reference rotary encoder	Simple setup but strict requirements on centering alignment of the polygon mirror	Complicated setup and strict requirements on alignment of the gaps between the artifact and the sensors
Robustness to environmental disturbances	Sensitive to temperature, humidity and pressure variations	Robust to environmental disturbances	Sensitive to air flow	Sensitive to mechanical vibrations
Estimated cost (may vary with manufacturer, system configuration, purchasing area and time)	70k US$ (including laser angle interferometer)	10k US$	Polygon mirror (12 faces): 12k US$ Autocollimator: 40k US$	70k US$
Cutting-edge technology	Auto-calibration [94], Self-calibration of indexing table [**Section 3.1.3**]	Multi-head rotary encoder for radial error measurement [97] Absolute angle encoder based on time grating [98] Self-calibration of angle encoder [**Section 3.1.3**]	Self-calibration of polygon mirror [**Section 3.1.3**]	Spindle error measurement by using angle sensor unit [99] [100] Self-calibration of ball roundness [**Section 3.1.3**]

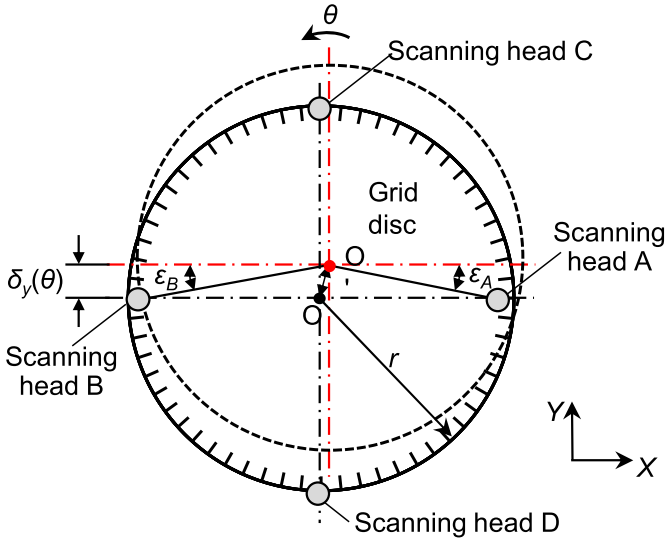

Fig. 9. Measurement of radial error motions of the grid disc of a rotary encoder by using four scanning heads [97]. In addition to the rotary position θ, the radial error motion components along the *X*- and *Y*-directions can be obtained from the four scanning heads A, B, C, D.$\varepsilon_A(\theta)$, *and* $\varepsilon_A(\theta)$are the rotary position measurement errors in scanning heads A and B, respectively, caused by the *Y*-directional radial error motion $\delta_y(\theta)$. (Figure courtesy of Dr. Yindi Cai).

of scanning heads C, D, respectively (Fig. 9). Liu et al. proposed a new type of absolute angle encoder [98] based on the principle of time gating using capacitive sensors [102] [103]. The sensor utilizes an orthogonally alternating electric field to build a reference system with high uniform velocity, connecting space displacement and time reference. This makes the sensor to achieve a high resolution of position with a sub-millimetric scale line spacing, which significantly reduces the requirement on the manufacturing precision and cost. Meanwhile, self-calibration methods shown in **Section 3.1.3** can be employed to calibrate the rotary encoder errors.

On the other hand, due to the relatively large sizes of the instruments listed in Table 2 and the workspace limitations of a machine tool, they are difficult to use, especially in the case of measuring rotary spindle heads. Therefore, indirect methods described in the following sections are more common to quantify such error motions [104]. provides a detailed analysis of a method using a reference indexing table and laser interferometer applied to off-axis measurements involving coordinated motions of linear and rotary axes, where the actual axis of rotation is difficult to access such as the case of rotary spindle heads.

3.1.2. Indirect measurement of quasi-static error motions

3.1.2.1. General formulation of indirect measurement. As described in **Section 2.1.1**, every axis can have six intra-axis kinematic errors (error motions). Their direct measurement, reviewed in **Section 3.1.1**, can be time-consuming, and requires multiple measuring instruments, as well

as an experienced operator. Typically, direct measurement of individual error motions is essential for accuracy check or mechanical adjustment during machine assembly. To diagnose error sources for a fully assembled machine, or to perform numerical compensation, indirect measurement can be a practical option [105].

When the functional point is positioned at an arbitrary position, all the error motions of the axes can influence its position. This relationship of quasi-static error motions to errors in the tool center point (TCP) position can be formulated by the quasi-static kinematic model in **Section 4.1**. By "best-fitting" the model's prediction to the measured positions, error sources included in the model can be estimated. Such a model-based identification of error motions is called "indirect measurement" by Schwenke et al. [1].

Error identification by indirect measurements can be generally formulated as follows. Suppose that the k-th TCP position in the workpiece coordinate system (CS) is given by $p(k)\in\Re^3$ (see **Section 4.1** for the term "workpiece CS"). Denote the measurable projection of the TCP position by $\Phi(p(k))$: $\Re^3\rightarrow\Re^d$, where d represents the dimension of the measurement (the number of axes involved) (d = 1, 2 or 3). Many measuring instruments only measure the projection of the TCP position onto a line or a plane. **Example 1:** By probing a sphere at the pre-calibrated position (see Fig. 10a and b), the three-dimensional (3D) positioning error of the TCP can be directly measured, and thus $\Phi(p(k)) = p(k)$. **Example 2:** In the circular test by using the telescoping ball bar (see **Section 3.1.2.2**), only its projection in the radial direction of the TCP circular trajectory can be measured, and thus $\Phi(p(k)) = p(k)\cdot v(k)\in\Re$, where $v(k)\in\Re^3$ represents a unit direction vector of the telescoping ball bar. **Example 3:** In the flank milling of a face (see Fig. 10e and f), the geometry of the finished face is determined by $\Phi(p(k)) = p(k)\cdot v(k)\in\Re$, where $v(k)\in\Re^3$ represents a unit vector normal to the machined face.

Suppose that X represents a set of all the error sources to be identified. **Example 1:** X contains eight inter-axis errors of two rotary axes (see Figs. 2 and 3) in a five-axis machine tool. **Example 2**: X contains the linear positioning error motion of a linear axis. The error motion, an intra-axis error, is position-dependent (see **Section 2.1.1**) and can be represented by a lookup table with the prescribed set of command positions as input. The table can also be direction-dependent to represent the bidirectional linear positioning error motion. Then X is given by:

$$X = [E_{XX}(x_1, +1), \ldots, E_{XX}(x_N, +1), E_{XX}(x_1, -1), \ldots, E_{XX}(x_N, -1)] \quad (1)$$

where x_i represents the nominal axis position and "+1" and "-1" indicate the direction of axis motion.

Denote the model, f, describing the relationship of a k-th set of the command positions of all the axes, $q^*(k) \in\Re^N$, where N represents the number of axes involved, and the error sources, X, to the TCP position, $\hat{p}(k) \in R^3$, by:

$$\hat{p}(k) = f(q^*(k), X) \quad (2)$$

When $\varphi(k)\in\Re^d$ represents the measured values, X can be identified by solving:

$$\min_X \sum_{k=1}^{N} \|\Phi(\hat{p}(k)) - \varphi(k)\| \quad (3)$$

Numerous research works on indirect measurements can be categorized by 1) measuring schemes, which determine Φ, and 2) the error sources to be identified, X.

3.1.2.2. Linear axis error motions.

I) Cirular test

The circular test, typically performed with a telescoping ball bar, is probably the most widely accepted indirect measurement by machine tool builders and users. It was first presented by Bryan [106] and is described in ISO 230–4:2005 [107]. Other instruments can also be used. For example, for small-radius and high-speed tests, a two-dimensional digital scale is preferable [108].

As a simple example, the squareness error of two orthogonal linear axes makes the contour error profile elliptic and tilted by 45° [107]. In other words, the squareness error can be identified by best-fitting an ellipse to the measured contour error profile or by adjusting the out-of-squareness parameter in the error model so that the model prediction fits the measurement data. This illustrates a simplest form of indirect measurement [2]. Typically, the circular test is not sufficient to uniquely determine all the error motions of linear axes by numerical best-fitting as shown in **Eq. (3)** [109]. Instead, the influence of typical error motions on the circular test can be simulated [110] [111] [107]. With a good understanding of the machine kinematics, a user can estimate dominant error causes.

II) 3D or 2D position measurement by artifact

To measure the 3D position of the TCP, in other words, to measure $\Phi(p(k)) = p(k)$ in **Eq. (3)**, an established method is the measurement of calibrated artifacts by the machine using a suitable probing system mounted in the spindle. Artifact-based verification is well established for coordinate measuring machines (CMMs) [112] [113]. When a one-dimensional single ball array artifact is aligned to a linear axis, the linear positioning and straightness error motions can be directly measured [114] [115]. When it is measured at multiple positions and/or orientations over the entire workspace, all the errors can be measured in an indirect manner [116] [117]. This principle was extended to a 2D ball array or 2D hole plates [118] [119] or 3D ball plates [120] [121] (see Fig. 10a), Various design variants, such as spheres on diagonal stairs [122] (see Fig. 10b), or a set of cubic artifacts [123], have been presented. A good review on various artifacts for CMMs and machine tools is in Ref. [124].

The 2D digital scale (Fig. 10c) uses a 2D grid as a reference [131]. Recent works have studied vision-based 2D measurement using a grid [132] [133] [134]. Vision-based 3D measurement has been also studied [135] but ensuring measurement accuracy sufficient for machine tool calibration is a research challenge.

Artifact-based measurements have the following common issues: 1) the machine's position can be measured only at the reference points on the artifact, which typically requires a large artifact to evaluate large workspaces; 2) the artifact's geometric accuracy significantly influences the measurement accuracy. A self-calibration using reversal techniques can potentially reduce the uncertainty due to the artifact's geometric errors, excluding overall scale (see **Section 3.1.3**). For example, self-calibration for a 2D digital scale is presented in Ref. [136].

III) Distance measurement

When the TCP positions are nominally constrained on a line, the projection of the 3D positioning error along the line can be measured using a length measuring instrument, typically a laser interferometer. In other words, $\Phi(p(k)) = p(k)\cdot v_n \in\Re$, where $v_n\in\Re^3$ represents the unit direction vector of the laser beam, fixed at the n-th location. By properly designing multiple lines measured over the workspace, all the error motions of linear axes can be identified indirectly [137] [138] [139] [140].

The diagonal test, described in ISO 230–6:2002 [141], and the step-diagonal test [142], can be seen as variants of such distance measurement schemes with fixed laser lines. The diagonal test can assess the squareness errors between linear axes but no other error motion can be separately quantified [143] [82] [144]. The step-diagonal test can additionally quantify the linear positioning and straightness error motions of linear axes [142] [145] [146] but it fails when a linear axis has excessive angular error motions [147] [148]. An attempt has been reported in Ref. [149] to quantify angular error motions by increasing the

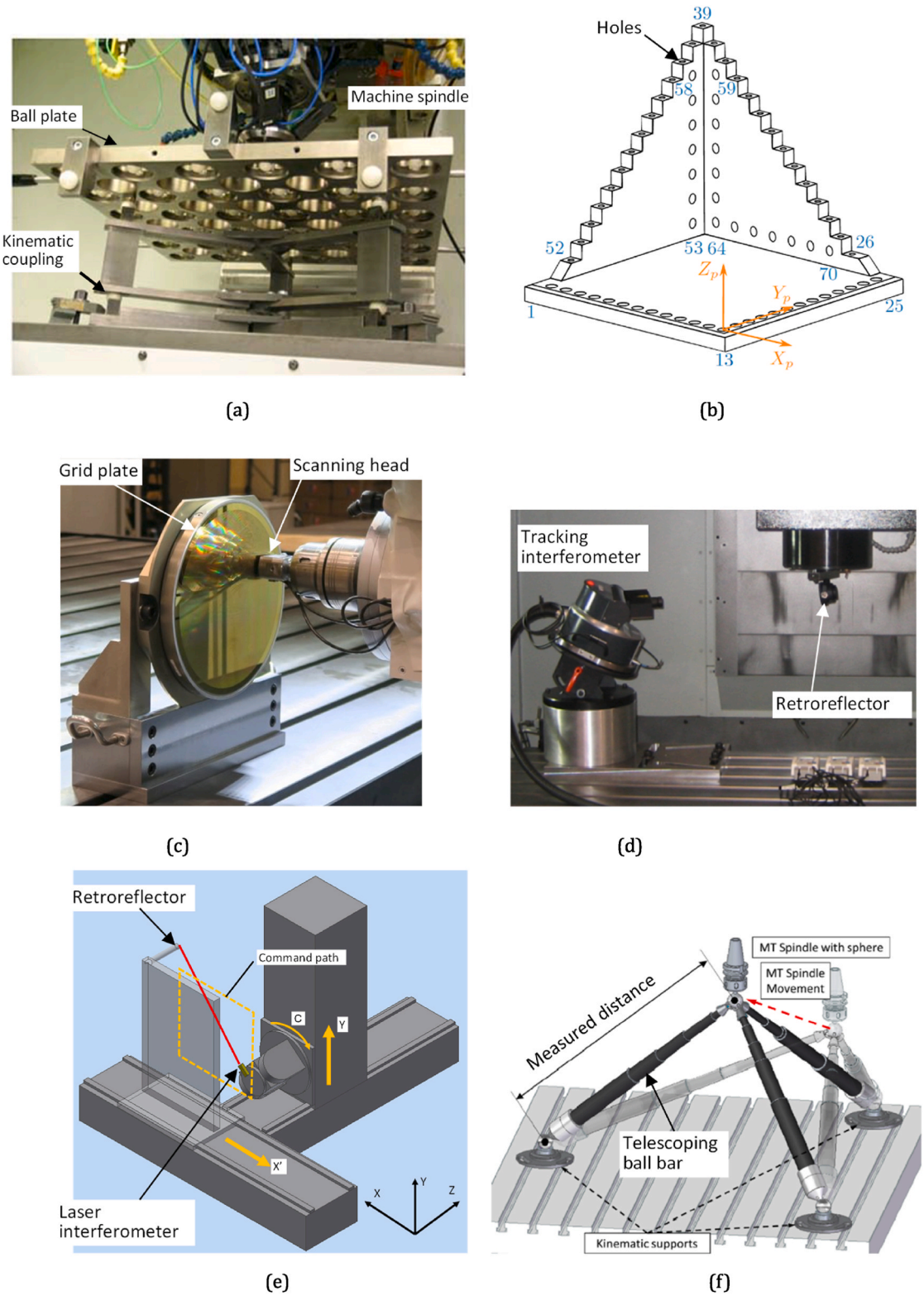

Fig. 10. Measuring instruments for indirect measurement of linear axis error motions. (a) 3D ball plate in Ref. [120]. The balls of the pre-calibrated 3D position are probed. The vertical position of the ball plate can be changed with a kinematic coupling. (b) diagonal hole artifact in Ref. [122]. The holes of the pre-calibrated position are aligned along face diagonals, such that 3D error motions of three linear axes can be identified. (c) 2D digital scale [125]. The 2D position of an optical detector can be measured by scanning orthogonally aligned gratings. (d) tracking interferometer [126] [127] [128]. It is a laser interferometer with a steering mechanism so that the laser beam automatically follows the target retroreflector. (e) multilateration by a laser interferometer attached to a spindle-side rotary axis in Ref. [129]. The rotary axes are indexed such that the laser beam is nominally directed to the target retroreflector. (f) multilateration by a telescoping ball bar of longer range [130]. The telescoping bar lengths are measured for the multilateration.

number of measured lines.

A tracking interferometer (the term in ISO 230–1 [16]) continuously measures the distance (displacement) to a retroreflector moving in space by automatically regulating the laser beam direction to it. It can be applied to the indirect measurement of all the linear axis error motions [150] [151] [152] [153] based on the multilateration principle [16]. A commercial tracking interferometer with this indirect measurement algorithm is available [126] [127] [128] (Fig. 10d). Its measurement can be written as:

$$\Phi(p(k)) = p(k)\cdot(p(k) - P_n) \,/\, \|p(k) - P_n\| \tag{4}$$

where $P_n \in \Re^3$ denotes the n-th position of the tracking interferometer. The uncertainty of the multilateration-based indirect measurement heavily depends on the measurement procedure, particularly target command positions and tracking interferometer positions, and many researchers presented numerical uncertainty assessments, as well as experimental investigations [154] [155] [134] [156].

Table 3 summarizes indirect measurement methods for linear axis error motions. The measurement schemes can be categorized by 1) the model DOF in X (two or three axes) and 2) the measurement DOF in Φ (1D: distance measurement over a line, 2D: 2D position measurement over a plane, 3D: 3D position measurement).

As a recent achievement, less expensive alternative schemes have been developed to perform the multilateration. The schemes include, 1) Tracking in "open-loop" manner: The multilateration can be performed by changing the laser beam direction based on the known target command position given a priori (Fig. 10e [129]). The laser beam orientation error, due to the machine tool's positioning error, would not cause significant uncertainty in the length measurement [157] [158] [129]. 2): Tracking by a physically connected link (Fig. 10f): a telescoping laser ball bar connects two spheres, one at the TCP and the other on the work table, by a link and measures the distance between them by a laser interferometer. The telescoping ball bar of a longer measurable range is not restricted to a circular path, and can be applied to arbitrary paths within its measurable range [159][160] [161]. By having three ball bars, or by three successive measurements with different positions of the reference sphere, the TCP 3D position can be measured [130], by using the multilateration. Six measurements enable the estimation of both position and orientation errors [162]. To further increase the measurable range, some researchers [52][163] combined two links with a rotary joint to measure the distance from the angle between them. More complex passive multi-axis mechanisms are also possible for 3D position measurement [164]. For such multiple-link mechanisms, attention should be paid to the uncertainty due to the kinematic errors in the measuring mechanism itself.

Recently, extension to non-rigid body influences has also been achieved. The majority of past works assume the rigid-body kinematics model (see Section 4.1) to describe and evaluate the error motions of each axis. Particularly on large-sized machine tools, error motions that do not satisfy this rigid-body assumption may have a significant impact on the machine's overall volumetric accuracy (see Fig. 39 in Section 4.1). The indirect measurement based on Eq. (3) is not restricted to a rigid-body kinematics. The model containing non-rigid body motions, as will be discussed in Section 4.1, can be adopted for the model, f, in Eq. (2) [165].

Table 3
Summary of indirect measurement schemes for linear axis error motions. A: artifact-based (including linear encoders), O: optical.

		Measurement DOF in Φ		
		1D (distance measurement)	2D	3D
Model DOF in *X*	2D	A: Telescoping ball bar	A: 2D digital scale (Fig. 10c) A: 2D machining test pieces	
	3D (X, Y, and Z-axes)	A:/O: Multilateration (Fig. 10d, e, f) O: Multi-line distance measurement (including diagonal and step-diagonal tests)	A: 2D ball grid (Fig. 10a)	A: 3D artifact (Fig. 10a and b) A: 3D test piece

3.1.2.3. Rotary axis error motions. When a tool or a work table is orientated by a rotary axis (axes), rotary axis intra- or inter-axis errors can be included in the kinematic model f in **Eq. (2)**, and thus their indirect measurement can be represented in the same formulation of **Eq. (3)**. The measured displacements, $\varphi(k)$, can be in the workpiece CS or the machine CS, depending on the measuring instrument setup.

I) Single-point tests

When the TCP is nominally constrained to a fixed point in the workpiece CS, the actual displacement of a precision sphere at the TCP can be measured by one or more linear displacement sensor, with a small measuring range, fixed on the work table. During the indexing of the rotary axis (axes) at a given set of angular positions, the nominally fixed TCP in the workpiece CS is achieved by positioning linear axes accordingly. For rotary axes on the tool side, this test is essentially the same as the single point articulation test for the verification of a robotic articulated arm described in ISO 10360–12:2016 [166]. Bringmann et al. [22] called it the "chase-the-ball test" for rotary axes on the workpiece side (rotating work table).

The application of the telescoping ball bar to this test has been reported since the 1990s [167] [168] [169] [20] [30] [44], where it is used simply as a linear displacement sensor for a precision sphere nominally fixed in the workpiece CS (Fig. 11a). The same test can be done by any linear displacement sensors, for example, a dial gauge. Due to the wide acceptance of the telescoping ball bar in the machine tool industry, its application to rotary axis indirect measurement has been reported by numerous researchers even lately [170] [171] [172]. By using a nest of three linear displacement sensors, the precision sphere's 3D small displacements can be measured. The application of a sensor nest to measure the error motions of a spindle has a long history [24] [173]. A comprehensive approach to its application to measure the intra- and inter-axis kinematic errors of rotary axes was first presented by Weikert et al. as the R-Test (Fig. 11b) [174] [22]. The single-point tests, performed either by the telescoping ball bar, a linear displacement sensor, or the R-Test, are adopted in ISO 10791–6:2014 [36]. While many works employed contact linear displacement sensors for the R-Test (Fig. 11b), some works presented an R-Test instrument with non-contact displacement sensors, including capacitive sensors [175], eddy current sensors [176], refraction-based laser displacement sensors [177], and triangulation-based laser displacement sensors [178] [179]. A commercially available non-contact R-Test instrument is shown in Fig. 11c [115].

The single-point test can also be conducted using a touch-trigger probe, which is available on many machining centers in today's market. When a user places a precision sphere on a machine table and measures its position using the machine probe, the sphere's position can be probed at various rotary axis angular positions in an automated manner [184] [185].

When a rotary axis rotates, the measured position of a sphere attached to it forms a nominally circular (arc) trajectory. The center position and orientation of the trajectory are determined by the position and orientation of the rotary axis average line in the machine CS (inter-axis errors) whereas its shape is determined by the position-dependent error motions of the rotary axis. This is the principle for their indirect measurement. The contribution of position-dependent error motions can

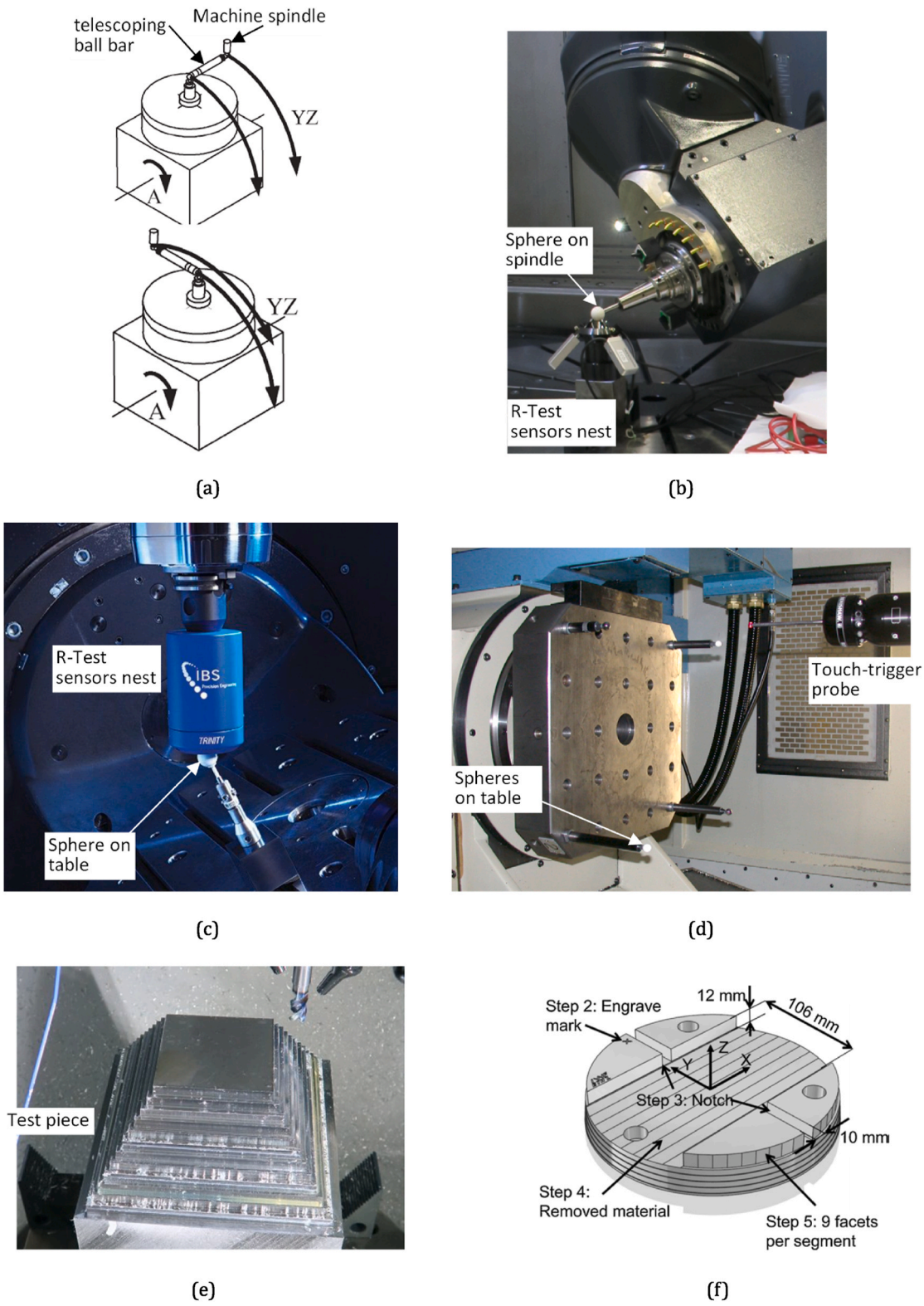

Fig. 11. Indirect tests for rotary axis error motions. (a) telescoping ball bar setups for *A*-axis in Ref. [30]. With the *A*-axis rotation, linear axes are regulated such that the telescoping ball bar is nominally in the axial or tangential direction of *A*-axis. It measures the radial and angular positioning error motions of *A*-axis, assuming that linear axis error motions are negligibly small. (b) an R-Test setup. Similar to a), with the rotation of rotary axes, linear axes are regulated such that the sphere is nominally not displaced with respect to the work table. Three displacement sensors measure the sphere's actual 3D displacement. (c) a commercially available R-test device [115]. It has non-contact displacement sensors. (d) a set of spheres to be probed on a five-axis horizontal machine in Ref. [180]. As rotary axes are indexed, the spheres are probed to observe not only linear error motions but also angular error motions of rotary axes. (e) the pyramid machining test piece in Ref. [181] [182]. Each step is machined at different angular positions of rotary axes. Linear and angular error motions of rotary axes are copied to the geometric errors of the finished test piece. (f) the machining test piece in Ref. [183] [182]. Thermal influence on position and orientation errors of a rotary axis can be observed from the geometric errors of the finished test piece.

be determined by removing the reference circle (e.g., least square circle) and analyzing the residuals. However, to separate linear and angular position-dependent error motions, the repeated single point tests need to be carried out with multiple spheres or artifacts with different geometries. The application of the R-Test to measure rotary axis error motions (intra-axis errors) is presented in Ref. [186] [187] [188]. Analogous measurements are possible with other measuring instruments, for example, the telescoping ball bar [170], but the efficiency of the 3D measurement is a strong advantage of the R-Test.

The heat generated by a rotating spindle can cause machine kinematic errors. The tests reviewed above should be performed in a thermal condition as close as possible to actual machining conditions, typically by sufficient machine warm-up. The machine kinematic errors during machining operations should be ideally identified with a rotating spindle, but the tests reviewed above can be performed only when the machine spindle stops. This typically causes a rapid initial thermal drift that can be challenging for indirect methods to estimate kinematic errors. Ibaraki et al. [189] [190] used a non-contact laser barrier tool measurement system to perform essentially the same single-point test by measuring the position of a rotating tool. The machining tests, reviewed below, can observe machine geometric errors as the spindle continuously generates heat.

II) **Measurement of the position and orientations of the axis of rotation**

A machine probe can measure multiple points at each stationary position of the rotary axes. This information can be used to estimate static orientations of the axis of rotation and static angular and linear error motions of rotary axes. Multiple blocks [191] and a rectangular block [192] [193] can be used as targets. Mayer et al. [180] [35] [194] used a set of spheres fixed on a machine table at uncalibrated positions (Fig. 11d).

By machining a workpiece using different stationary positions of the rotary axes, the effect of the position and orientation of the rotary axis with respect to the machine CS can be observed from the finished workpiece's geometry. Ibaraki et al. [181] showed that rotary axis inter- and intra-axis errors can be indirectly identified from the geometry of any finished test pieces, but the sensitivity of each error depends on the test piece geometry. For the indirect measurement, the test piece geometry should be designed to maximize the sensitivity and distinguishability of the errors to be identified.

A set of simple machining tests is presented in Ref. [14] [195] to quantify the rotary axis inter-axis errors. Similar machining tests, performed at different angular positions of the rotary axis, are integrated into the pyramid test piece [181] [192] [196] [189] [197] (Fig. 11e). Various machining tests were presented for different types of machine tools. Morimoto et al. [198] presented a machining test using a non-rotating tool. Ibaraki et al. [199] presented a machining test for turning operations with the angular indexing of a test piece. Arizmendi et al. [200] analyzed five-axis machined elliptical dimples. Huang et al. [201] presented a machining test such that the influence of the rotary axis inter-axis errors is visually quantifiable. ISO 230–12:2022 [23] presents many machining tests that can be applied to the indirect measurement of intra- and inter-axis errors.

By repeatedly performing the same machining operation, one may observe a change in the geometry of the finished test pieces, which is typically caused by thermal effects. The machining test proposed by Wiessner et al. [183], and the one in Ref. [181], are adopted as thermal machining tests in ISO 10791–10:2022 [182].

The test pieces for indirect measurement are typically machined with rotary axes fixed at the prescribed angular positions. However, ISO 10791–7:2020 [202] proposes the cone frustum and the *S*-curve test pieces, which are machined by dynamic, simultaneous five-axis motions. Researchers showed that it is not possible to separately quantify all the rotary inter-axis errors from the finished cone frustum test piece [203] [31] and the *S*-curve test piece [204]. In other words, these tests are not suitable for indirect measurement. The *S*-curve test shows the influence of dynamic errors of each axis [205].

III) Separation of linear and rotary axis error motions

All the tests reviewed here somehow measure the relative displacement between the tool-holding and workpiece-holding components. Thus, they involve the positioning not only by rotary axes but also by linear axes. This is a common potential challenge when error motions of a rotary axis are indirectly identified. Many previous studies assume negligibly small linear axis error motions. Bringmann et al. [206] [207] discussed the influence of linear axis error motions on the uncertainty in the estimation of rotary axis inter-axis errors. They established an assessment methodology of the uncertainty propagation from the linear axis error motions based on the Monte Carlo simulation [208]. They showed that linear axis error motions can be a major uncertainty contributor and stated that "you have to pay for bad axes twice" [206]. Analogous uncertainty assessment was presented in many other works, e.g., Ref. [191] [189].

When the measured artifact, e.g., a precision sphere, is placed nominally on the axis of rotation, rotary axis error motions can be measured without linear axis motions. This setup is equivalent to the direct measurement method in **Section 3.1.1**. This test can be done by e.g., the R-Test (ISO 230–7:2015 [24] and ISO/DIS 10791–2:2022 [209]) or the telescoping ball bar [210]. This test may not be applicable to every rotary axis; for example, it is difficult to apply to a table-side swivel axis having its centerline below the table surface, or a tool-side swivel axis having its centerline at a distance from the TCP. Multilateration can be used to measure the rotary axis error motions without moving linear axes [127].

Indirect "best-fitting" approaches to the identification of linear or rotary axis kinematic errors are well matured, and thus fewer researchers have adopted machine learning approaches to this problem. Rooker et al. [211] applied a pattern recognition approach, based on the Convolutional Neural Network (CNN), to the measured trajectories in the single-point test, for fault monitoring in the five-axis kinematics. The authors of [211] stated that "the approach, presented in this paper, is not intended as an improved alternative to the mature methods of the field … The general pattern recognition model could provide high-level fault detection, the ability to detect non-kinematic faults and robustness against trajectories influenced by machine-specific signatures." Fault monitoring through the observation of a change in linear or rotary axis quasi-static kinematic errors, by applying machine learning approaches, have been presented in Ref. [212] [194] [213].

Self-calibration schemes, reviewed in **Section 3.1.3**, can be an approach to the separation of linear and rotary axis error motions. This will be reviewed in **Section 3.1.3.3.**

Table 4 summarizes indirect measurement schemes for rotary axis error motions. Indirect tests can be categorized based on whether they involve linear axes, or rotary axis (axes) only, and whether they measure

Table 4
Summary of indirect measurement schemes for rotary axis error motions. A: artifact-based (including linear encoders), O: optical.

Schemes	Measurement of positions (single point tests)	Measurement of positions and orientations
Tests involving rotary and linear axes	A: Telescoping ball bar (Fig. 11a) A: R-Test (Fig. 11b and c) A: Probing of sphere	A: Probing of artifact with orientations, e.g., multiple spheres (Fig. 11d) A: Machining tests (Fig. 11e and f)
Tests involving rotary axis (axes) only	A: Same as above, with sphere located on the axis of rotation O: Multilateration	O: Multilateration (with multiple targets)

target positions, or both positions and orientations.

3.1.3. Self-calibration methods

In precision or ultraprecision machining, high motion accuracies are required for each of the machine axes [214]. As presented in **Sections 3.1.1**, artifacts such as straightedges and spheres, as well as angular scales such as polygon mirrors, indexing tables, and angle encoders are employed as the references in direct measurement of the error motions. Similar artifacts and measuring instruments are also employed in indirect measurement of error motions as shown in **Section 3.1.2**. However, for precision machines, the magnitudes of the machine error motions may be comparable to those of the form errors of the reference artifacts or the measurement errors of the measuring instruments. It is also desired to measure machine error motions under loaded conditions, where the actual workpiece is mounted on the machine. A precision drum lathe is such an example, where a roll (cylindrical) workpiece with a mass up to several thousands of kilograms is mounted on the spindle. In such cases, it is effective to employ an error-separation method for self-calibration of the reference artifact, in which a set of simultaneous equations are established from the displacement probe outputs for estimating both solving the motion error and the artifact form error mathematically [215] [216] [99] [217]. Evans et al. [216] provided a comprehensive overview of self-calibration methods over wide areas of dimensional metrology in 1996. In the following, advances in self-calibration of artifact form errors for direct measurement of slide and spindle errors are focused in responding to the significant achievements over this field. Recent progress in self-calibration of angular scales for direct measurement of angular positioning errors as well as self-calibration methods for indirect measurement are also presented briefly.

3.1.3.1. Self-calibration for direct measurement of slide and spindle errors. As summarized in Tables 5–7, based on how the simultaneous equations are established for slide and spindle error measurements, conventional self-calibration techniques can be classified into 1) the multi-step approach including the reversal method [218] [219] and the multi-position method) [220], 2) the multi-probe approach [221] [222] [223] [224] [225] [226] [227] [228], and 3) the hybrid approach of combining the multi-probe and the multi-step approaches [229]. In a multi-step approach, the equations are established from the outputs of a probe acquired in multi-step scan operations over the artifact surface. In each step, the positions of the artifact, the probe, and spindle/slide are changed with respect to each other. It should be noted that in practical implementation of the reversal method [230] [231], two probes are often employed so that the reversal operation of the probe can be removed. In a multi-probe approach, multiple probes are placed at different positions against the artifact. The equations are established by using the outputs of the probes acquired in one scan operation over the artifact surface. Although specified for measurement of carriage slide errors of precision drum lathes, the hybrid approach that combines the multi-probe configuration with multi-step measurements is also available more broadly [229]. The following provides and overview of the three types of approaches are explained in details.

Table 5
Summary of multi-step self-calibration techniques.

Category	Method	Configuration/tips	
		Spindle error measurement	Slide error measurement
Multi-step approach: - Multiple scans - Constant harmonic sensitivity - Can only measure repeatable error motion components - Can only measure slide out-of-straightness but not slide misalignment angle	Reversal method	1 displacement probe +1 reversal operation of workpiece and probe [218] [232] [219] - Reversal operation of probe can be replaced by adding one more displacement probe [233] - Spindle reversal method available for large roll lathe [233]	- Accurate positioning of workpiece necessary in reversal operation
- Major uncertainty source: repeatability of motions, probe calibration and stability error	Multi-position method	1 displacement probe + N rotary indexing operations - Time-consuming indexing process	Not applicable.

Table 6
Summary of multi-probe self-calibration techniques.

Category	Method	Configuration/tips	
		Spindle error measurement	Slide error measurement
Multi-probe approach - Single scan - Inconstant harmonic sensitivity - Short measurement time - Can measure both repeatable and non-repeatable motion error components - Can only measure slide out-of-straightness but not slide misalignment angle - Major uncertainty sources: loss of specific harmonic components, probe calibration error, zero-adjustment error in straightness measurement	Multi-displacement probe method	3 displacement probes [215] [221] [222] [228] [234] [235] - Asymmetric probe setup necessary for reducing harmonic loss	3 displacement probes [236] [237] [238], 2 displacement probes + 1 external autocollimator [239] - Asymmetric probe setup necessary for reducing harmonic loss, accurate probe zero-adjustment necessary for reducing parabolic calculation error in three-probe configuration - Simplified two-probe configuration possible [240] [241] [242]
	Muti-slope probe method - Only for mirror surface	Three slope probes [100] - Asymmetric probe setup necessary for reducing harmonic loss	Two slope probes [243] [244] - Accurate zero-adjustment necessary for reducing parabolic calculation error - Configurations of 1 slope probe+1 external autocollimator, 1 slope probe + pentaprism available
	Mixed method - Use both slope and displacement probes	2 displacement probes+1 slope probe [245] [246], or, 1 displacement probe +2 slope probes [99] - 1 displacement probe+1 slope probe (orthogonal mixed method) available [241]	- Accurate probe zero-adjustment necessary for reducing parabolic calculation error

I) The multi-step approach

Straightedge reversal is the most traditional multi-step method [250] [81]. It has been standardized for slide straightness error motion

Table 7
Summary of hybrid self-calibration techniques.

Category	Method	Configuration/tips	
		Spindle error measurement	Slide error measurement
Hybrid approach - Combines multi-probe and multi-step approaches - Only for slide error measurement - Can measure both repeatable and non-repeatable motion error components - Can measure both slide straightness error motion and slide alignment angle error - Major uncertainty source: probe calibration error	Reversal three-probe method - Only for slide out-of-straightness	Not applicable	Two sets of three-probe units +1 workpiece reversal operation [238] - Self-calibration capability of probe zero-adjustment error
	Rotating roll hybrid method - For both slide out-of-straightness and slide misalignment angle - Constant harmonic sensitivity - Simple configuration - No influence of probe zero-adjustment error		2 displacement probes + rotating roll workpiece [247] - For horizontal slide error 4 displacement probes + rotating roll workpiece [248] - For both horizontal and vertical slide errors 1 displacement probe + rotating self-cut roll workpiece [249] - Very simple configuration

measurement of precision machines [16]. Fig. 12 shows the implementation of the straightedge reversal method for accurate measurement of the horizontal straightness error motion $e_Z(x)$ of a V–V bearing X-slide and the form error $f_Z(x)$ of a 150 mm long Zerodur straightedge on a T-based diamond turning machine [232]. The straightedge is sandwiched by two capacitive probes (Probes 1 and 2) along the Z-direction. The fixture mounting the probes is placed and kept stationary on the workpiece spindle of the machine. From the probe outputs before and after a reversal operation of the straightedge about the X-axis, the peak-to-valley (PV) values of $e_Z(x)$ and $f_Z(x)$ were measured to be approximately 80 nm and 15 nm, respectively, over a travel of 80 mm.

The straightedge reversal method has also been applied to vertical out-of-straightness measurement [75] [251]. However, in such a measurement, the deflection of straightedge caused by the gravity force can be an uncertainty source for slides with a long stroke where a long straightedge is needed.

The reversal method was applied by Donaldson in 1972 for separating the spindle error motion from the roundness error of a precision sphere artifact [218]. Compared with the straightedge reversal operation in straightness and slide error measurement, the reversal operation to separate sphere roundness and spindle error from combined measurement is much easier in most cases. On the other hand, it is sometimes expected to measure the spindle error under loaded conditions where an actual workpiece is mounted on the spindle, i.e., the workpiece is employed as the artifact for measurement instead of a test sphere. This is especially important for large drum lathes. Commercially available drum lathes have a cylindrical workpiece capacity of up to 500 mm (diameter) × 2000 mm (length) [233]. The mass of such a roll workpiece can reach 3000 kg. Due to the heavy mass, it is difficult to make the reversal operation of the workpiece with respect to the spindle angular position. Lee et al. proposed a spindle reversal technique for solving this problem [233]. In this method, after the first scan of the workpiece by two displacement probes along the θ-direction, the workpiece is lifted up in order for rotating the headstock and the tailstock of the drum lathe by 180° with respect to the workpiece, followed by the second scan by the two probes. Fig. 13 shows a picture of lifting up the workpiece by using a crane for the spindle reversal operation.

It should be noted that the slide error or the spindle error is required to be repeatable in the two scans before and after the reversal operation. Horikawa et al. proposed an improved reversal method shown in Fig. 14 to solve this problem [236]. In this method, an additional probe (Probe B) is employed to detect the change $\Delta e_r(\theta)$ between the spindle radial error motions ($e_{r1}(\theta)$ and $e_{r2}(\theta)$) before and after the reversal operation, based on which the separation of $e_{r1}(\theta)$ or $e_{r2}(\theta)$ and the workpiece roundness error $r(\theta)$ can be made accurately without the influence of $\Delta e_r(\theta)$. It should be noted that this method is still influenced by the change of the spindle tilt error motion between the two scans before and after the reversal operation.

The multi-orientation or multi-position method is another type of multi-step method. In this method, N sets of measurements are carried out where the artifact angular positions are changed from 0 to (1-1/N) *2π with N equal intervals [220]. The spindle error can be evaluated

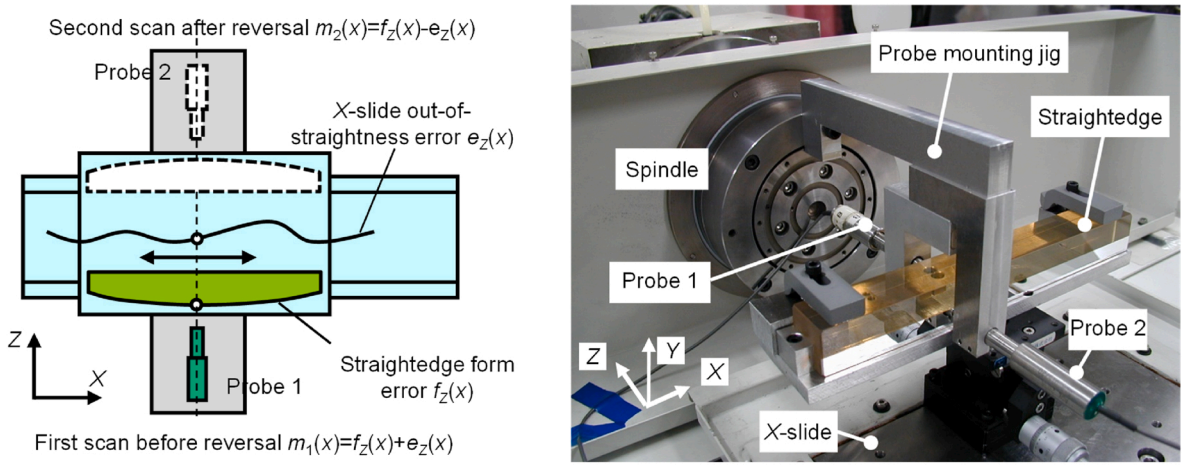

Fig. 12. Implementation of the straightedge reversal method on a diamond turning machine [232]. (a) Schematic of the straightedge reversal method; After the straightedge is scanned by Probe 1, the straightedge is reversed and the probe is set to the position of Probe 2 for the second scan by Probe 2. (b) Reversal setup on a diamond turning machine; two capacitance probes (Probes 1 and 2) are mounted on a fixture, which is placed and kept stationary on the workpiece spindle of the machine.

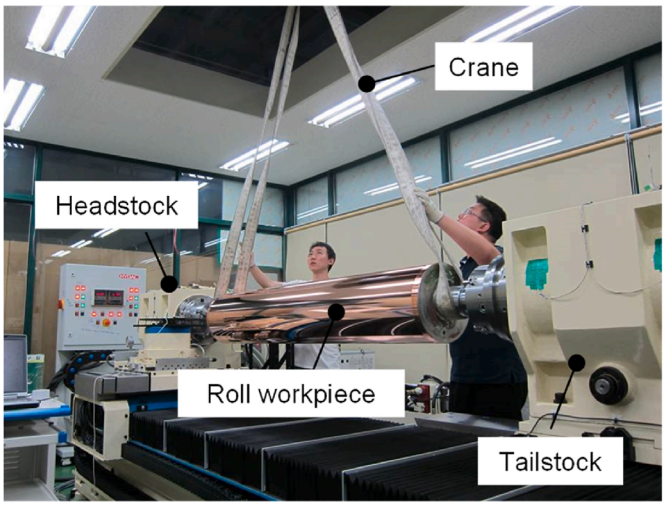

Fig. 13. Lift-up of workpiece by a crane for spindle reversal on a large drum lathe. After a scan of the workpiece along the θ-direction with two probes through rotating the workpiece by the spindle, the workpiece is lifted up in order to rotate the headstock and the tailstock of the drum lathe by 180° (spindle reversal). The workpiece is then mounted on the spindle again for the second scan after the spindle reversal [233].

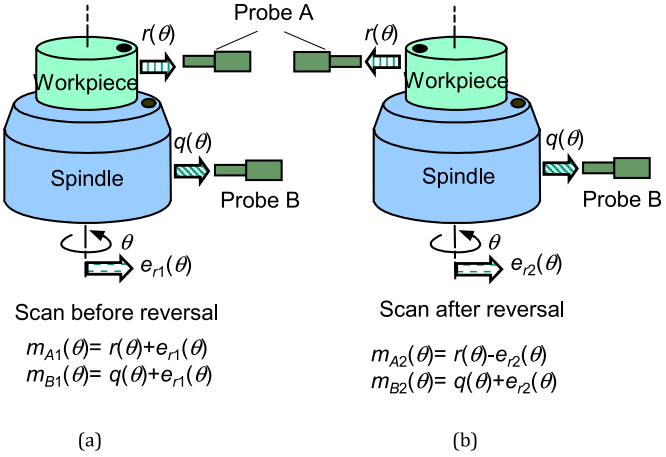

Fig. 14. The improved reversal method for spindle radial error measurement for reducing the influence of the non-repeatability of the spindle error (modified from Ref. [236]). (a) Scan before reversal. Probe A and B are employed to scan the workpiece surface with a roundness error $r(\theta)$) and the spindle surface with a roundness error $q(\theta)$, respectively, under the existence of a spindle error $e_{r1}(\theta)$. (b) Scan after reversal. After Probe A and the workpiece are reversed, the second scan is carried out under the existence of a spindle error $e_{r2}(\theta)$.

from the mean value of the N sets of measurements based on the fact that the mean value of the artifact roundness error over one rotation equals to zero. Compared with the reversal method, it takes more time for the measurement. A rotary indexing table is also required to change the angular position of the artifact. For these reasons, the multi-orientation method is often used in spindle error measurement of roundness measuring machines [252] but seldom used for the measurement of machine tool spindles. It should be noted that depending on the evaluation the Nth harmonic can appear in both the spindle error and artifact roundness error, or can be eliminated in both (in software they can be made zero).

II) The multi-probe methods

The concept of the three-probe method, as the first multi-probe method, was proposed by Aoki and Ozono in 1966 as an alternative to the traditional V-block method for roundness measurement [221]. The possibility of the three-probe method for spindle error measurement was demonstrated by Mitsui in 1972 through the radial error motion measurement results of the spindles of a lathe and a surface grinding machine [234]. It was then applied by Shinno et al. for the measurement of ultraprecision spindles at the nanometric level in 1987 [253].

In the three-probe method, three displacement probes are arranged around a cylindrical artifact being rotated by a spindle with its axis of rotation along the Z-axis. The run-outs of the artifact surface at the probe positions are scanned by the probes over one rotation. Three unknowns are included in each probe output: the artifact roundness error $r(\theta)$, and the X- and Y-directional spindle radial error motions $e_{rX}(\theta)$ and $e_{rY}(\theta)$, where θ is from 0 to 2π. As shown in Fig. 15, the probe outputs $m_A(\theta)$, $m_B(\theta)$, and $m_C(\theta)$ are employed to obtain a differential output $\Delta m_3(\theta)$ in which the spindle error components are removed and only the roundness error $r(\theta)$ is included [235]. Assume the Fourier transforms of $\Delta m_3(\theta)$ and $r(\theta)$ are denoted by $\Delta M_3(n)$ and $R(n)$, where n is the harmonic number (the spatial frequency showing the number of undulations per revolution). Since $\Delta M_3(n)$ is the product of $R(n)$ and $H_3(n)$, where $H_3(n)$ is referred to as the transfer function of the three-probe method, which is determined by the angular intervals of the probes [215], $R(n)$ can be obtained from $\Delta M_3(n)$ and $H_3(n)$. The roundness error $r(\theta)$ can then be obtained from the inverse Fourier transfer of $R(n)$, based on which the spindle radial error motions $e_{rX}(\theta)$ and $e_{rY}(\theta)$ can be evaluated.

Gao et al. expanded the three-probe method for multi-degree-of-freedom (MDOF) spindle error measurement by using 2D slope probes, which are based on 2D laser autocollimation, as shown in Fig. 16 [100]. A 2D slope probe can detect the 2D local slopes. In this case, error separation is carried out by using the angular outputs $\mu_i(\theta)$, $(i = A, B, C)$, of the slope probes in the horizontal plane for measurement of the artifact roundness error $r_r'(\theta)$, and the X- and Y-directional spindle radial error motions $e_{rX}(\theta)$ and $e_{rY}(\theta)$, which is the same as for the three-displacement probe methods. Meanwhile, error separation is also carried out by using the angular outputs $\upsilon_i(\theta)$, $(i = A, B, C)$ of the slope probes in the vertical plane for measurement of the artifact surface slope error $r_z'(\theta)$ along generatrix, and the spindle tilt error motions $e_{TX}(\theta)$ and $e_{TY}(\theta)$ about the X- and Y-axes.

The harmonic-loss problem is the most significant challenge for conventional multi-probe methods in which only displacement probes or only slope probes are employed. The transfer function $H_3(n)$ shown in Fig. 15 represents the harmonic sensitivity of the three-probe method [99]. There are some frequencies at which the amplitude of $H_3(n)$, i.e., the harmonic sensitivity, becomes zero. The frequency of the first zero-sensitivity position can be increased by selecting an asymmetric probe arrangement as shown in the figure. Similar phenomena are observed in the harmonic sensitivity of the three-slope probe method.

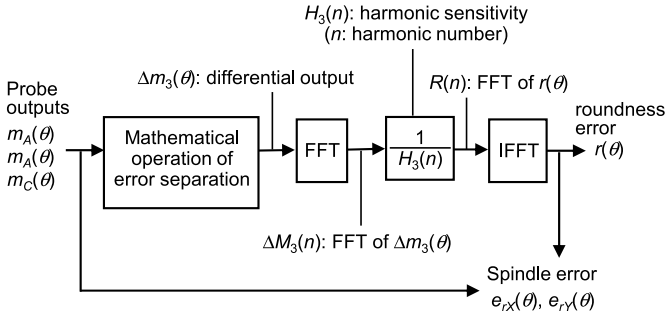

Fig. 15. Data processing in the three-probe method for separation of spindle error and workpiece roundness error. The probe outputs $m_A(\theta)$, $m_B(\theta)$, and $m_C(\theta)$ are treated as the inputs of the system. The workpiece roundness error $r(\theta)$ and the X- and Y-directional spindle error components $e_{rX}(\theta)$, $e_{rY}(\theta)$ are treated as the outputs of the system.

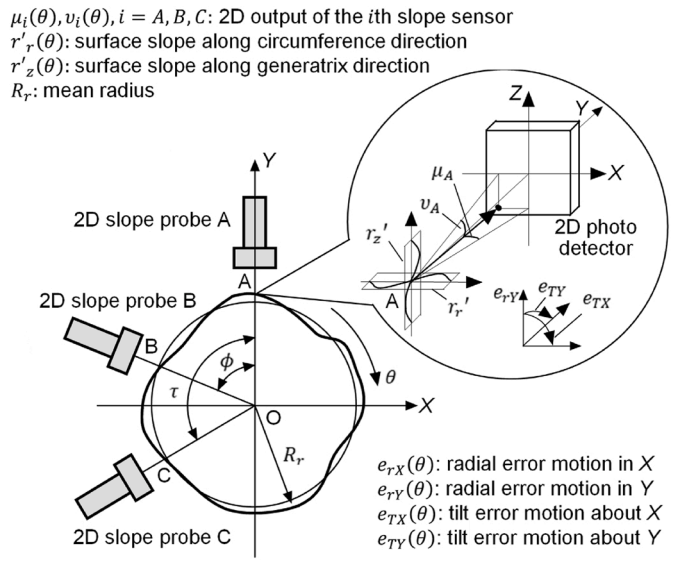

Fig. 16. The three 2D slope probe method for MDOF spindle error measurement [100]. Three 2D angle sensors A, B, and C are placed around a cylindrical workpiece. The workpiece is mounted in the spindle to be tested. Each sensor detects the two-dimensional local slopes $r'_z(\theta)$, $r'_r(\theta)$ of a point on the workpiece surface and the four spindle error components $e_{rX}(\theta)$, $e_{rY}(\theta)$, $e_{TX}(\theta)$, $e_{TY}(\theta)$.

This means that the corresponding harmonic components of the roundness error and the spindle error will be lost in the error-separation operation of the three-probe method, which is referred to as the harmonic-loss problem. It should be noted that this harmonic-loss problem exists in all kinds of multi-probe methods, including the four-probe method [223], where only displacement probes or only slope probes are used.

The harmonic-loss problem can be completely solved by using the mixed method that uses both displacement and slope probes [224]. The mixed method can be achieved by using the combination of two displacement probes and a slope probe (the 2D1S mixed method) [224], or the combination of a displacement probe and two slope probes (the 1D2S method) [99]. The simplest probe combination can be realized in the orthogonal mixed method [254] where a displacement probe and a slope probe are set with an angular interval of 90° as shown in Fig. 17a. The harmonic sensitivity $H_{om}(n)$ of the orthogonal mixed method is shown in Fig. 17b. The workpiece roundness error and the spindle radial error motion can be obtained accurately by using this method without any loss of harmonic components.

The multi-probe method has been employed for measurement of the straightness error motion. Fig. 18 shows a schematic of the measurement system with three displacement probes. Three unknowns included in each probe output are the workpiece straightness error $f(x)$, the Z-directional slide straightness error motion $e_Z(x)$, and the slide angular error motion $e_{yaw}(x)$ about the Y-axis. Basically, the same Fourier transform-based error separation operation shown in Fig. 15 can be applied for solving the unknowns from the three probe outputs, except for the parabolic straightness error components included in $f(x)$ and $e_Z(x)$. This is because the parabolic component will generate a constant term in the differential output and cannot be treated by Fourier transform. Instead, it is necessary to carry out a double integral operation of the constant term in the differential output with respect to the scan length to obtain the parabolic straightness error component. On the other hand, the differences in the zero outputs of the probes will cause a change in the constant term of the differential output of the three-probe method, which is referred to as the zero-adjustment error [255]. A parabolic measurement error will therefore be introduced in $f(x)$ and $e_Z(x)$ by the double integral operation of the differential output. The magnitude of the parabolic error in the straightness of artifact or slide is proportional to the square of the scan length, a significant parabolic calculation error will occur when the scan length increases as shown in Fig. 18. This is the greatest uncertainty source in the three-displacement probe method, as well as other types of multi-probe methods such as the four-displacement probe method [237], the two-slope probe method [243] [244], and the mixed method of using both displacement and slope probes [245] [246] for straightness measurement.

One way to avoid the influence of the zero-adjustment error is to employ the two-displacement probe method together with an autocollimator. In this case, the slide angular error motion $e_{yaw}(x)$ about the Y-axis is measured using an autocollimator. The Z-directional slide straightness error motion $e_Z(x)$ and the workpiece straightness error $f(x)$ are separated from each other by using the outputs from the two displacement probes. The zero-adjustment error between the two probes only causes a linear component in the calculated out-of-straightness result and will therefore not influence the measurement. If $e_{yaw}(x)$ is small enough to be omitted, only the two displacement probes are needed for error separation [240] [241] [242].

III) The hybrid approach

Fig. 19 shows another method that can compensate for the zero-adjustment error inherent in the three-probe method [238]. A reversal operation of the workpiece is added to the three-probe method for self-calibration of the zero-adjustment error. In this hybrid method combining the three-probe method with a reversal operation of the workpiece, the zero-adjustment errors of two three-probe units can be evaluated without using any accurate reference flat surfaces. The two probe units of the three-probe method are mounted on the slide to scan a workpiece simultaneously. The zero-difference between probes in each probe-unit can be obtained from the probe outputs of scanning the

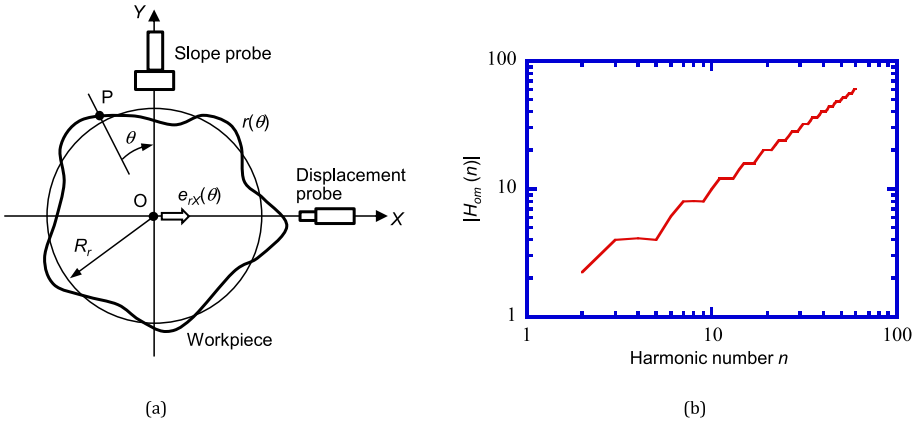

(a) (b)

Fig. 17. Configuration and harmonic sensitivities of the orthogonal mixed method [254]. (a) The probe configuration. A displacement probe and a slope probe are set in the X- and Y-direction to scan the workpiece being rotated by a spindle. The workpiece roundness error $r(\theta)$ and the spindle error component $e_{rX}(\theta)$ can be measured from the two probe outputs. (b) The magnitudes of the harmonic sensitivity. No zero values exist for the harmonic sensitivity of the mixed method, demonstrating the capability of the method for detecting all harmonic components without the harmonic-loss problem.

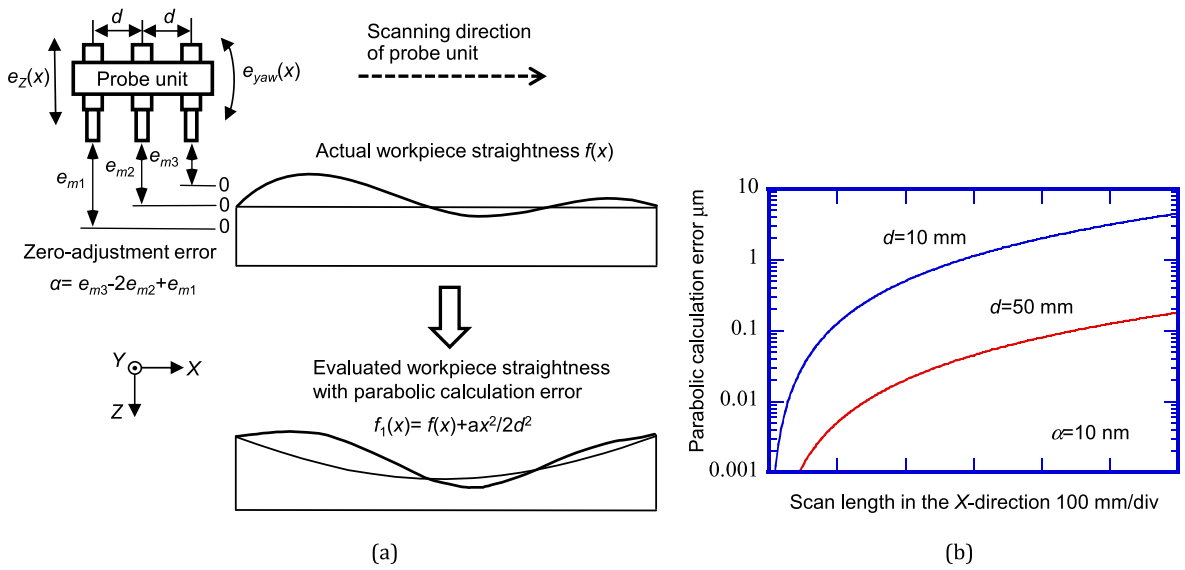

Fig. 18. Parabolic calculation error caused by the zero-adjustment error of probes in the three-probe method for straightness measurement [99]. (a) The influence of zero-adjustment error α. α, which is related to relative differences of zero-values e_{m1}, e_{m2}, e_{m2} between the probes, causes a parabolic error component (evaluation error) in the evaluated workpiece straightness $f_1(x)$. (b) Simulation results. A 10 nm zero-adjustment error causes the evaluation errors of 4.5 μm and 0.18 μm when the probe interval d is set to be 10 and 50 mm, respectively.

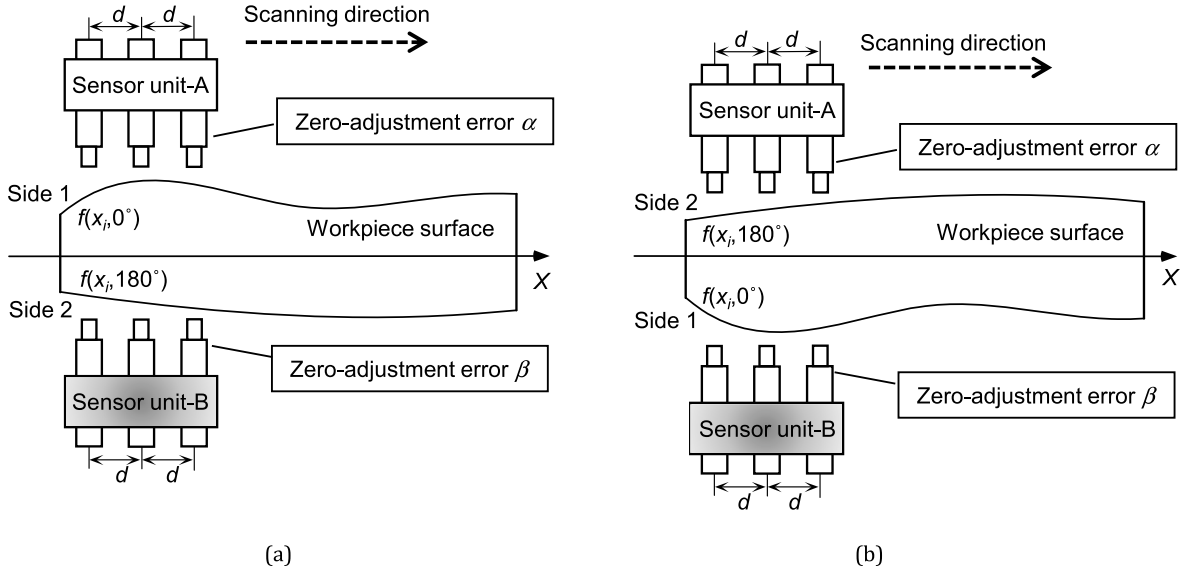

Fig. 19. A hybrid method combining the three-probe method with a reversal operation of the workpiece for self-calibration of zero-adjustment errors of three-probe units [238]. (a) The first scan before workpiece rotation. Two probe-units A and B with zero-adjustment errors α and β are placed on the two sides of the cylinder to simultaneously scan the two straightness profiles $f(x, 0^\circ)$ and $f(x, 180^\circ)$, respectively. (b) The second scan after workpiece rotation. The two straightness profiles $f(x, 180^\circ)$ and $f(x, 0^\circ)$ are scanned by the probe-units A and B, respectively.

cylinder surface along the X-direction before and after a 180° reversal/rotation of the workpiece. Although a reversal operation of the cylinder surface is used for self-calibration of the zero-adjustment error, the repeatability of the slide errors before and after the reversal operation is not required in this method. The variation of the zero-adjustment error caused by thermal drift can also be compensated by scanning a rotating cylindrical workpiece [238].

The hybrid method was further simplified for measurement of the carriage slide total error of a precision lathe in the horizontal XZ-plane by combining a two-probe unit with a rotating cylindrical workpiece. As shown in Fig. 20, the carriage slide total error $e_{slide}(z)$ in the horizontal plane at a position z is composed of the straightness error component $e_s(z)$ and the axis misalignment error component α^* z in the horizontal plane where α is the slide axis misalignment angle with respect to the axis average line of the spindle [247]. In this hybrid two-probe method, two displacement probes are placed on the two sides of a cylindrical workpiece. The probes are first moved by the carriage slide to scan the stationary workpiece from the starting position to the end position of the carriage before and after a 180° rotation of the workpiece about the axis of rotation of the spindle. The slide straightness error motion $e_s(z)$ can be accurately evaluated by removing the influence of the workpiece straightness form error $g(z)$ based on the reversal method. The two probes are then kept stationary at the start position and the end position of the carriage slide travel range, respectively, to scan the rotating workpiece over multiple rotations. The slide axis misalignment angle error α can be evaluated from an averaging operation of the probe

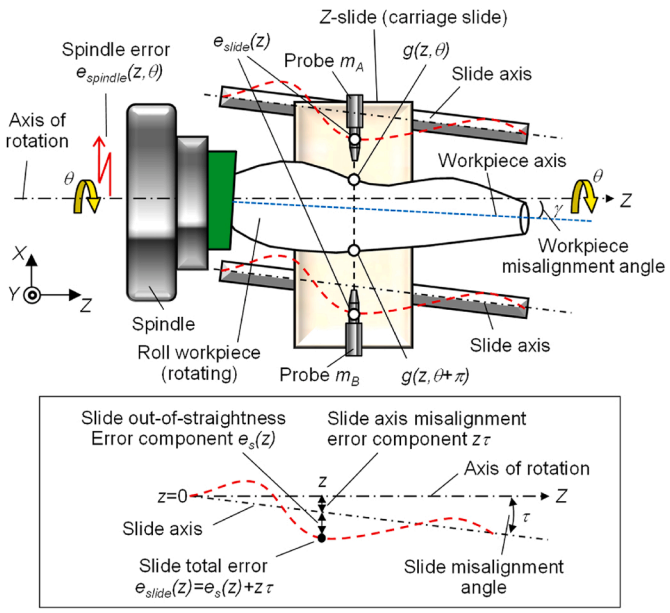

Fig. 20. A hybrid two-probe method for measurement of slide total error in the horizontal plane. The two probes are first moved by the *Z*-slide to scan the roll workpiece before and after a 180° rotation of the workpiece about the spindle axis for measurement of the slide straightness error motion $e_s(z)$ based on the reversal method. The two probes are then kept stationary at the start position and the end position of the carriage slide travel range, respectively, to scan the rotating workpiece over multiple rotations for measurement of the slide axis misalignment angle error α from an averaging operation of the probe outputs over one rotation or multiple rotations.

outputs over one rotation or multiple rotations. The influences of the workpiece out-of-roundness form error, the spindle motion error and the workpiece misalignment angle can be removed by this method. The hybrid two-probe method was extended to a hybrid four-probe method shown in Fig. 21 for measurement of the total slide errors of a large drum lathe in both the horizontal plane and the vertical plane [248].

A hybrid method which combines a single displacement probe and

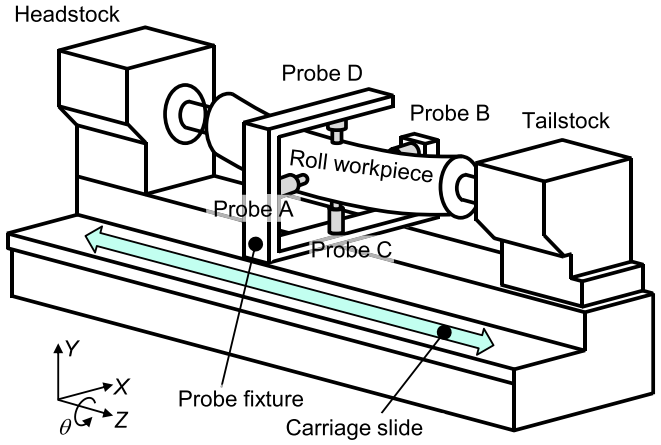

Fig. 21. A hybrid four-probe method with a rotating cylindrical workpiece for measurement of slide total errors in both the horizontal plane and the vertical plane [238]. For probes mounted on the tool post of the machine through a probe fixture are moved along the *Z*-slide to scan the roll workpiece. Based on the reversal method, the vertical straightness motion error with respect to the deformed axis of the roll workpiece and the horizontal straightness motion error are synchronously evaluated. The slide axis misalignment angle errors in both the *XZ*- and *YZ*-planes are evaluated by using the algorithm shown in Fig. 20.

diamond tool turning operation on a cylindrical workpiece is presented in Ref. [249]. The displacement probe is mounted on the opposite position of the workpiece with respect to the cutting tool. In this method, the cylindrical workpiece is first turned on the precision drum lathe and the measurement is carried out without removing the workpiece from the spindle. The slide total error, including both the slide straightness error component $e_s(z)$ and misalignment error component α^*z can be evaluated from the averaged value of half of the probe outputs over one rotation or multiple rotations. Because the surface form of the cylindrical workpiece is a replication of the tool motion, which is a combination of the slide motion and the spindle motion, the workpiece misalignment angle γ in Fig. 20 does not appear in the probe output. It should be noted that the techniques in the hybrid approach shown above are basically specified for a precision lathe or a precision grinding machine.

In addition to the techniques shown above, self-calibration is also effective for removing the influence of planar grating errors. Recently, surface encoders and planar encoders are widely used for planar motion measurement [256]. 2D error separation techniques have been developed for self-calibrating the *XY* position, excluding scale [257] [258]. In *XYZ* three-axis measurement [259], the out-of-flatness of the planar scale is another critical uncertainty factor in addition to the *X*- and *Y*-directional deviations of pitch spacing [260]. A fast and accurate self-calibration technique based on Fizeau interferometer measurements was developed for evaluating the *X*- and *Y*-directional deviations of pitch spacing, excluding scale as well as the *Z*-directional out-of-flatness error of a planar grating scale [261]. This method can also be applied to a variable-line-spacing (VLS) planar grating [262] [263], which is used as the scale of an absolute surface encoder [264].

3.1.3.2. Self-calibration for direct measurement of angular positioning errors. Polygon mirrors, indexing tables, and angle encoders are employed as the reference angular scales for angular positioning error measurement. All of these angular scales are realized by subdividing a circle into a certain number of equally-spaced angle intervals which are referred to as circular divisions. However, the actual angle intervals are not perfectly equal but having certain division errors (angular scale errors), which are the deviations from the nominal angle interval due to manufacturing errors. Based on the fact of circle closure, a summation of all the division errors over 2π will be zero, or a summation of all the angular intervals over 2π will be zero. This principle has long been employed for self-calibration of angular scale errors. Similar to the methods for self-calibration of roundness errors, the self-calibration of angular scale errors can be implemented by the multi-step method and the multi-head method, which are well summarized in Ref. [265] [266] [267] [268].

On the other hand, most of such self-calibration practices are made in a stand-alone self-calibration system, rather than on a machine tool. A unique method was proposed by Lu and Trumper for self-calibration of on-axis rotary encoder [269]. In this method, the rising and falling edges of the pair of the encoder quadrature signals are treated as spatial sampling events that mark the spindle rotary positions. These events are numbered with reference to rising edge of the encoder index signal. Under certain approximations on the free-response dynamics of an air-spindle, the angular scale errors can be obtained from applying the circle closure principle to two sets of pulse temporal widths captured from the spindle free responses. Although this method is limited to spindles with aerostatic bearings, it can be applied to calibrate the angular positioning error of such a spindle without using any additional references.

3.1.3.3. Self-calibration for indirect measurement. In the multilateration (see Fig. 10d), reviewed in **Section 3.1.2.2,** to indirectly measure linear or rotary axis error motions, both target retroreflector and tracking interferometer positions are unknown. When tracking interferometer

positions are known, three distance measurements are sufficient (trilateration). By using one or more additional distance measurements, a self-calibration method is applied to identify both target retroreflector and tracking interferometer positions [126] [127].

Interesting and new applications of a self-calibration method to indirect measurements include the separation of linear and rotary axis error motions. As reviewed in **Section 3.1.2.3,** many indirect measurement schemes for rotary axes also involves linear axes, in e.g., single point tests, and thus linear axis error motions can be a major uncertainty contributor. Zimmermann et al. [270] [271] applied a self-calibration scheme in a probing-based test with a nominally circular test piece. The test scheme can be seen as a classical multi-step approach to the roundness measurement, but it is applied to separate the influence of linear axis error motions from rotary axis error motions.

Self-calibration methods are, in principle, limited to the measurement of 1) the roundness of a nominally circular part, 2) the straightness of a nominally straight surface, and 3) the position of 2D grid points. This is because self-calibration methods require the probed points being in a closed set, as the workpiece is rotated or translated. Onishi et al. [272] extended their applications to arbitrary 2D geometries, by assuming that the machine's positioning error is in accordance with the rigid-body kinematic model reviewed in **Section 4.1**. The linear axis error motions are unknown variables to be identified, and they are in a closed set, as the object rotates. The application of self-calibration methods to indirect measurements is worthy for further study.

3.2. Thermal errors

Measurement of thermal errors can be classified as direct and indirect methods. The direct method is the measurement of changes in relative position or orientation by using appropriate measuring methods [273] [156] [274]. Indirect measurement is the estimation of thermal distortion of the machine tool based on models and measured temperatures [275] [276] [277].

ISO 230–3: 2020 [278] provides testing methods for systematic analysis of thermal behavior of machine tools, including tests for the environmental temperature variation error (ETVE), thermal distortion caused by rotating spindles, thermal distortion caused by moving linear axes, and thermal distortion caused by moving rotary axes. Fig. 22 shows a typical measurement setup for a milling machine with a vertical spindle. It measures thermal changes in the radial, axial and tilt of the spindle relative to the table, in the same way presented in Table 2. For thermal errors caused by rotating the spindle, the temperature close to the spindle bearing and the ambient air temperature are monitored with temperature sensors as shown in figure. A similar measurement setup can be applied to most machine tool configurations. For the thermal distortion caused by moving linear axes, an example of measurement setup is shown in Fig. 23. The measurement setup consists of one sensor fixture with seven displacement sensors mounted on the spindle and two target blocks located at positions close to the end points of travel of the moving axis. Based on such a setup, the change in traveled distance along the moving axis can be estimated, as well as changes in the two orthogonal linear deviations and three angular deviations at each target position. The displacement sensors can be laser interferometers [279] [280], capacitive [281] [282], inductive [283] [284] or contacting probes [285] [286]**.** The temperature measurements can be obtained by thermocouple, resistance or thermistor sensor, as well as, infrared cameras [287] [288] [289]. As pointed out by Mayr [39], the measurement for thermal deformation should meet the following requirements: a) measure all relevant geometric error parameters (intra- and inter-axis kinematic error parameters and volumetric errors), b) include the relevant work volume, c) achieve with sufficiently low measurement uncertainty, and d) last a short time so that the effect of changing temperatures can be monitored by the measurement system

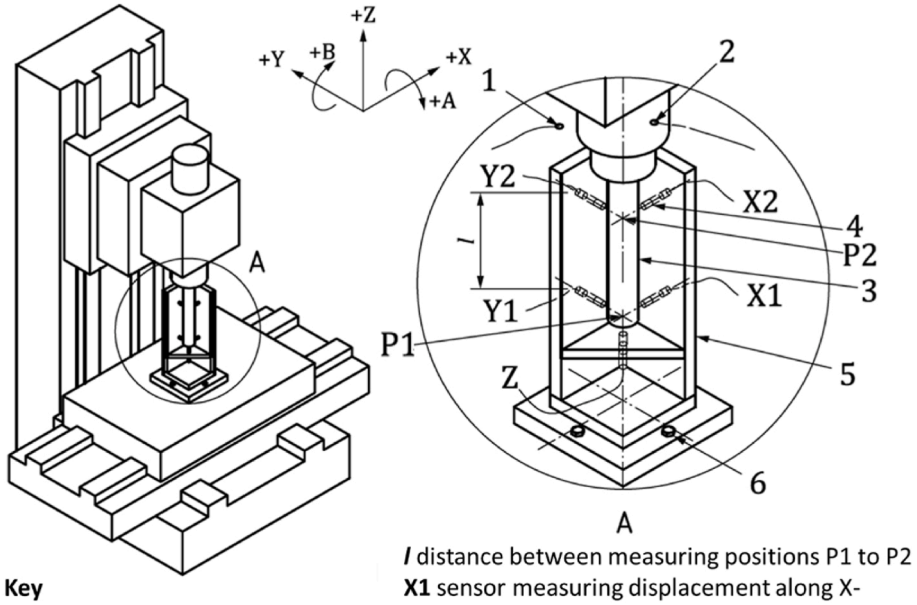

Fig. 22. Typical setup for tests of ETVE thermal distortion caused by rotating the spindle, and thermal distortion caused by moving linear axis on a vertical machining center [278]. The device in the figure is used to measure the thermal error of the vertical spindle machining center. The fixture for installing the linear displacement sensor shall be firmly fixed on the non-rotating workpiece fixture or tool fixture assembly of the machine tool for measurement. The relative displacement between the parts holding the tool and the parts holding the workpiece along the three orthogonal axes parallel to the travel axis of the machine tool, and the accurate position of the measuring device are recorded together with the test results.

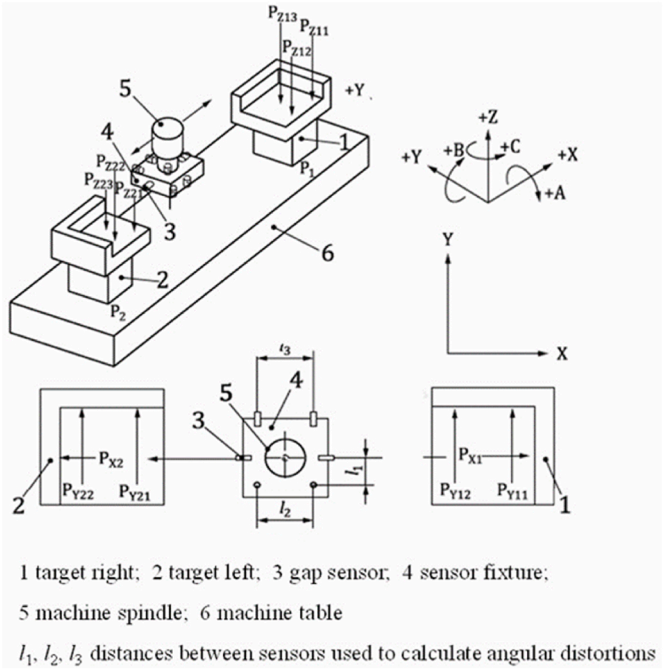

Fig. 23. Alternative setup for measurement of thermal distortion caused by moving the *X*-axis slide of a machining center [278]. The illustrated device includes a fixture with seven displacement sensors and two target blocks. In this device, the sensor holder is installed on the main shaft. Install two target blocks at each end of the stroke. This setting allows simultaneous measurement of six thermal deformation components, one in the direction of travel and two in the orthogonal direction and three angular components around three linear axes.

with sufficient temporal resolution. Table 8 summarizes the performance parameters of some measuring instruments used for thermal error measurement.

It should be noted that since the method proposed in ISO 230–3 only measures the tool displacement at one or two positions, it is difficult to obtain the change in volumetric error due to thermal deformation [278]. Multilateration using tracking interferometers is a standard method for volumetric error measurement [16]. However, its traditional operation is quite time-consuming and thus limits its usefulness to measure thermally induced volumetric error which requires measurement conducted within a short time. Ibaraki et al. propose a scheme to evaluate thermal influence on two-dimensional motion trajectory of a five-axis machine tool by a single-setup tracking interferometer and rotational motion of a table [294]. This method is further improved by Mori et al. to reduce the measurement uncertainty [295]. The application of a tracking interferometer to thermal tests is also explored in Refs. [296,297]. Brecher et al. [298] proposes a new system for measurement of thermal errors of a machine tool by using a position sensing detector (PSD) and a thermally-stable laser frame, from which changes in 13 of 21 kinematic errors of a three-axis machine tool can be obtained (Fig. 24).

The measurement efficiency is important in thermal induced error measurement [299] [4] [298]. Measuring thermal error by machine learning (ML) based methods is promising to effectively reduce the necessary measurement points and increase the measurement efficiency [300]. Zhu proposed a ML method based on random forest to predict thermal errors. By selecting key temperature points and iteratively eliminating the least important features to eliminate redundant features, the ML method has a prediction accuracy of more than 90% and effectively reduces the number of temperature points to be measured [301]. Recent advances of thermal error measurement deal with development of machine-integrated compact measuring devices integrated in the machine tool structure or designed as modules stored in the tool changing unit [298] [302]. Machine-integrated measurement setups enable an efficient measurement during machine idle time. Nabil Ouerhani predicted the thermal error by data-driven method [303]. The paper compared four ML methods: Linear regression, Decision tree regressor, Multi-Layer Perceptron regressor and ElasticNet. The average absolute error of three of the four ML algorithms is lower than 1 μm. The correlation coefficient is higher than 90%. Even the classical linear regression model can have high prediction accuracy. ML method has a good application prospect for the prediction of machine tool thermal error.

For the indirect measurement, the Finite Element Method (FEM), which enables in-depth analysis of thermal behavior of machine tools, is usually adopted to predict thermal errors [304] [305]. The indirect measurement of thermal errors must be based on an accurate modeling of thermal phenomena taking place in the machine tools [306]. The modeling methodology is reviewed in **Section 4.2.**

3.3. Static load-induced elastic deformation

Elastic load-induced deformations in machine tools and industrial robots have a significant impact on system performance and are linked to the compliance of the structural members and joints [307]. The compliance is the reciprocal of the stiffness that is defined as the ability to resist deformation when loads are applied [308] [309]. In machining systems (machine tool, cutting process, workpiece, and their interactions) loads (inertia, gravitational, and cutting process) directly affect the machined part dimensional and geometric accuracy [310]. Deflections can either be measured under static conditions, i.e., at discretized static configurations along trajectories or at quasi-static conditions, i.e., measured under motion along the same trajectories [311].

A standardized way to evaluate machine tool compliances, by applying a static load between the table and spindle, is described in ISO 230–1 [16]. The test provides a simplified method to quantify the

Table 8
Measuring instruments for measuring thermal errors.

	Thermocouple or other temperature sensors [290]	Infrared camera [291]	Laser tracking interferometer [292]	Capacitive sensor [72]	Inductive probe [293]
Resolution	16-bit resolution: 0.0078 °C (1 LSB)	≤0.05 °C (50 mK) at 30 °C target temperature	0.001 μm	0.05 nm@1 kHz	0.02 μm
Measuring range	−55 °C–150 °C	−40 °C to+1200 °C, high temperature option: up to 2000 °C	0.2 m–20 m (Larger machine size is covered by measuring stitching)	200 μm	±5 mm
Measuring accuracy	±0.3 °C (maximum) from −55 °C to 150 °C	±1.5 °C or ±1.5%	Uncertainty (95%) = 0.2 μm + 0.3 μm/m	Probe Maximum Drift: 0.02 % F.S./°C	700 nm
Other parameters	power consumption: 3.5 μA, 1 Hz conversion cycle; 150 nA shutdown current	spatial resolution: 0.6 mrad Image resolution (pixels): 2048 × 1536	Horizontal angle range: −225°–225° Vertical angle range: −35°–85°	Capacitive sensor module bandwidth: Selectable: 1, 10, 15, 50 kHz	Temperature drift ≤ ±10% Communication protocol IO-Link

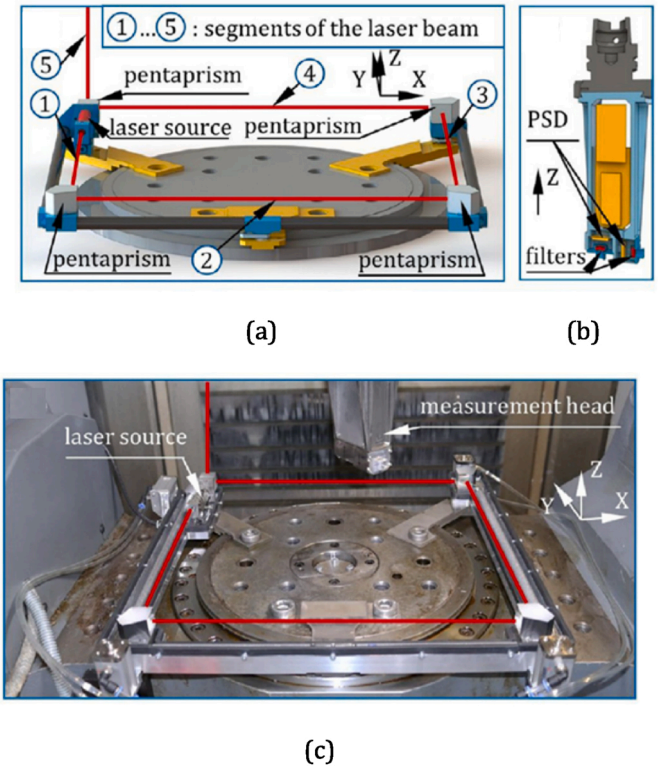

Fig. 24. Setup for measuring thermal changes in kinematic errors of a three-axis machine tool. (a) Laser beam and frame. The laser beam path is divided into five beam segments by four pentaprisms, and the four pentaprisms reorient the beam along the machine axis. (b) Measurement head. For the measuring PSD in the measuring head installed on the main shaft, move it to the discrete measuring points in each beam section in turn. By rotating the spindle, the vertical PSD is placed perpendicular to the laser beam segments 1 to 4. The horizontal PSD is used to measure the fifth segment. During the crossing process of each segment, only one feed axis is moved to produce two measuring straightness perpendicular to the feed direction. (c) Measurement setup including housing parts in a machine [298]. The laser frame is installed on the workbench with an invar adapter, and the measuring head is connected to the I/O data acquisition equipment by cable.

machine's static compliance in a single axis direction using a linear screw actuator to apply a load that is measured using a load cell, while monitoring deformations using a displacement sensor. Measurements are made close to the center of the machine workspace for each linear axis directions separately. Examples of the test setup for translational and rotary axs are shown in Fig. 25.

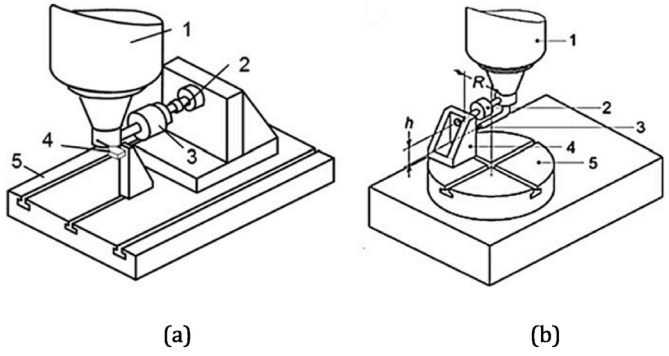

Fig. 25. The setup proposed by ISO 230–1 for machine static compliance and hysteresis by externally applied force. (a) Using a load cell 3, differential screw 2, and a probe 4 mounted on a table 5 to measure the deflections at the spindle 1. (b) Using a load cell 2, a displacement sensor with a special fixture 4 mounted on the rotary table 5 [16].

Following a similar approach, researchers have evaluated machine tools' static stiffness and compliance of a machine tool in 3D Cartesian space utilizing force actuators (hydraulic, electromechanical), pressure and force sensors, dynamometers, and displacement sensors.

The Elastically Linked Systems (ELS) was introduced to relate the machine tool positional and static and quasi-static accuracy to the machined part's dimensional and form deviations [312]. A practical implementation of the ELS concept is the telescoping Loaded Double Ball Bar (LDBB). It combines the circular test (described in ISO 230–4) methodology for evaluating the contouring accuracy of machine tools with the ability to apply variable loads during measurement [313]. The measurement system enables the evaluation of the machine tool equivalent stiffness in the circular trajectory by capturing the aggregated deformation of the machine tool including tool holder due to the quasi-static errors and load-induced deviations. The instrument and measurement method were further developed by introducing a metrology frame enabling separation between the force and measurement loops and it is used to quantify the full quasi-static translational stiffness matrix (Fig. 26) [314]. The rotation angle and clamping condition of a rotary axis influences the tool-workpiece compliance [315]. A comparison study shows that the rotational static stiffness is greater than the quasi-static rotational stiffness. The static measurement is direct, i.e., inducing a load to the machine tool table, while the quasi-static measurement is indirect, i.e., inducing a load between the tool and the table. Thus, the apparent lower stiffness can be a result of the longer force loop. i.e., with more components and that are affected by the applied load [316].

Different measurement instrument, sensors and actuators are used for machine tool compliance measurement. One study investigated how a pneumatic piston for loading the structure can be combined with measurements of force/torque and deflection, see Fig. 27a [317]. It highlighted that in order to have results with low uncertainty it is important to consider the accuracy of both the force and deflection measurement device.

A stiffness workspace system (SWS) was developed to evaluate the machine displacements and force values at the functional point [318]. It has the capability to load the structure, in three orthogonal directions while measuring, machine compliance. Fig. 27b shows the apparatus with its 12 displacement sensors mounted on a machine tool.

One study investigates the improvement of stiffness caused by force sensor integration into the machine tool axes [319]. The results were evaluated in comparison to compliances of other components, such as the kinematic joints, and to stiffness changes resulting from sensor-integration into the TCP or the application of a commercial force/torque sensor at the TCP. In conclusion, the study supports the approach of structure-integrated force measurement for machines with parallel kinematics, as their stiffness is relatively small in many cases.

3.4. Dynamic errors

3.4.1. Tracking errors

Contour tracking errors during synchronous motions of several axes are often evaluated because the difference in the dynamic response results in contour errors. Position detectors, such as rotary and linear encoders are used to measure the error in the servo system. Fig. 28 shows an example of the contour tracking error during circular motions measured by the rotary encoder in the servo motor [49]. The contour distortion observed in diagonal is directions caused by the mismatch of controller gains. Quadrant glitches caused by the response delay due to the friction force are also seen at the location of axis motion reversals. Even when no external load acts on the machine, internal disturbances such as the friction force cause dynamic errors. Fig. 29 shows the amplitude of the periodic positional deviation at a constant feed speed motion caused by such internal disturbances [320]. The contribution of disturbances in mechanical and control systems were separated by

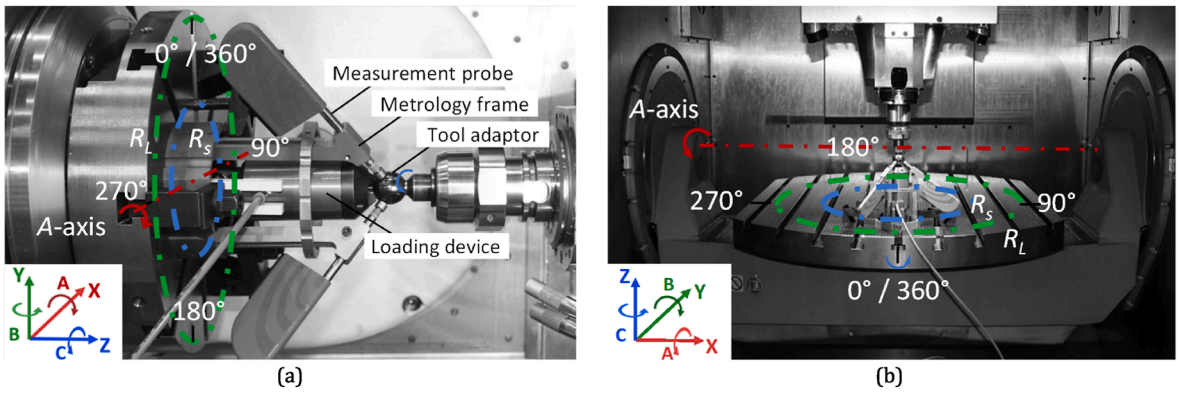

Fig. 26. Experimental setup for the measurement of the Cartesian translational stiffness matrix of 5-axis machining centers. The figures show two circular trajectories at different radii, R_S (*Radius Short*) in blue, and R_L (*Radius Long*) in green applied for two machines with different kinematic chain [314,316]. (a) A metrology frame , is used to separate the metrology loop from the force loop in a machine with kinematic configuration [*wC'A'bYXZ(C)t*]. (b) Experimental setup for the measurement of static and quasi-static rotational stiffness in a machine with kinematic configuration [*wB'A'YbXZ(C)t*] . (For interpretation of the references to color in this figure legend, the reader is referred to the Web version of this article.)

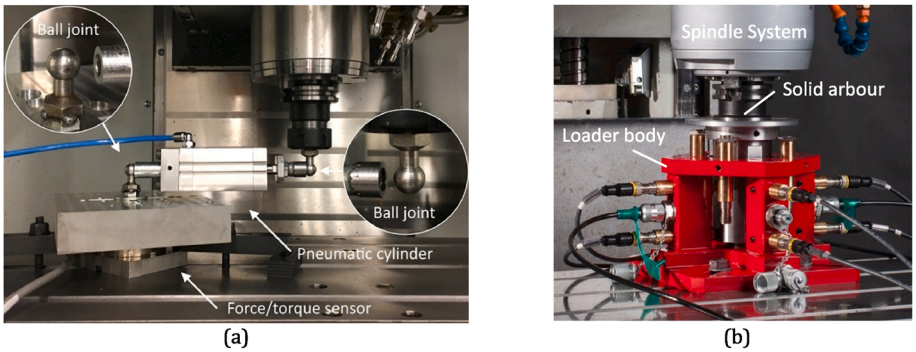

Fig. 27. (a) General test setup with pneumatic cylinder and force/torque sensor [317]. The two ends of the pneumatic cylinder are attached to the force/torque sensor and the spindle under test through ball joints, respectively. (b) Mechanical part of SWS — the prototype of the system [318]. The SWS is used to evaluate the machine displacements and force values at the functional point.

combining measurements from the linear and rotary encoders. In this case, one of the disturbances in the mechanical system was the result of the geometric imperfections in the ball screw. This disturbance seems to be static because the spatial period of the disturbance is constant. However, the frequency of the disturbance changes depending on the feed speed. Thus, this positional deviation is a dynamic error, and the resultant positional deviation is determined by the dynamic disturbance response of the servo system.

The measurement of TCP positioning error requires external sensors. The 2D digital scale (or grid encoder, see Fig. 10c) is a popular measuring instrument because it provides high-resolution, non-contact, and high-bandwidth measurement. Fig. 30 shows the contour error measured during circular motion with high feed speed and small radius [51]. The radius at the TCP trajectory is larger than that of the position feedback measured by the linear encoders. This radius of enlargement results from the dynamic deformation of the mechanical system due to the driving and counter forces in the feed drives. The error magnitude depends on the dynamic response of the mechanical system and frequency components of the driving force.

The measurement of the dynamic TCP positioning error in three dimensions remains challenging. A tracking interferometer can be used theoretically for the 3D measurement. However, the tracking system may not have the dynamic bandwidth required for high-speed contouring. Vision based measurements have good potential for 3D measurement. The contour tracking error at micrometer level in a 120 mm $\times$ 100 mm window can be detected using industrial video cameras with high resolution [135].

The presented measurement techniques are summarized in Table 9. As the emerging technology, the vision-based measurement can be focused on. Owing to the recent development in high-speed cameras and image processing algorithms, micrometer level resolution can be achieved at a frame rate of 1000 fps [321].

3.4.2. *Frequency response*

The frequency response of a machine tool is measured to understand the cause and mechanism of dynamic errors. The measured frequency response is used also in modeling and motion error compensation. The frequency response measurement requires an excitation with the target bandwidth. An impulse excitation using an instrumented hammer is the most popular excitation method because it is quick and easy to implement. White noise and sine sweep excitations using shakers are also applied [324]. Accelerometers, displacement sensors and laser-Doppler vibrometers are used to measure the response of the machine. Acoustic imaging can also be used for this purpose [325].

Driving force and cutting force excitations are common excitation methods for machine tools. The cause of dynamic errors such as shown in Fig. 30 can be investigated effectively by the driving force excitation method [51]. Many commercial computer numerical control (CNC) machines have the function of driving force excitation for servo parameter tuning. A white noise or sine sweep command is input to the feed drive as the excitation. The response difference is evaluated between the axis position detector and TCP position. In this case, TCP position is measured with the grid encoder or accelerometers as shown in Fig. 31. A surface encoder can also be employed for this measurement

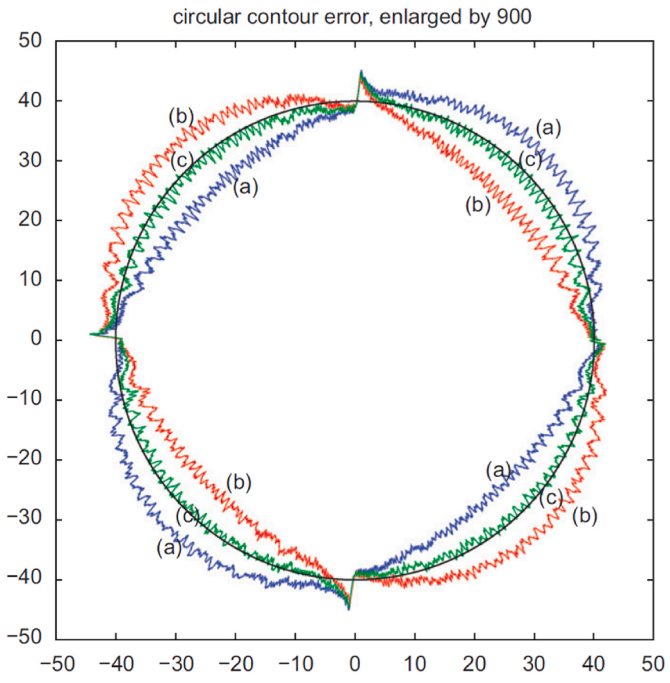

Fig. 28. Contour errors in circular motions for different servo gain combinations [49]. (a) Trajectory when the position loop gain for the X axis is larger. (b) Trajectory when the position loop gain for the Y axis is larger. (c) Trajectory when the same position loop gain is set for the X and Y axes. The unit for horizontal and vertical axes is millimeter. The radial deviation from the nominal circle is enlarged by 900 times. When the servo gain is different for two orthogonal feed drives, the circular trajectory by these feed drives is distorted in the diagonal direction.

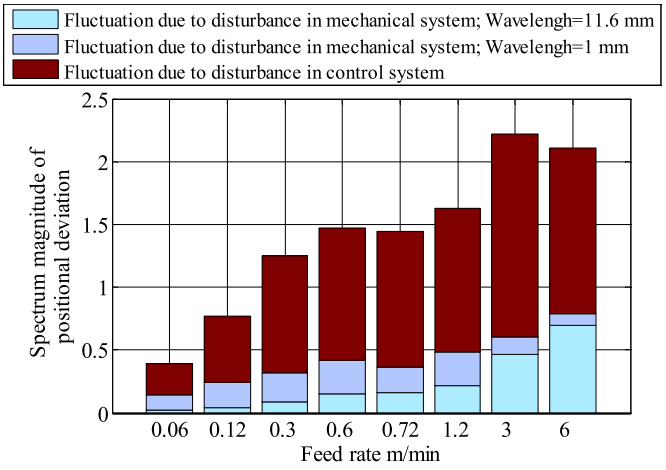

Fig. 29. Positional deviation caused by internal disturbances in feed drive systems [320]. Even when the spatial period of the disturbance is constant, the frequency of the disturbance changes depending on the feed speed. Thus, the resultant positional deviation caused by each disturbance is changed by the feed speed as shown in the figure.

[326]. A difficulty in driving force excitation is in measurement of the excitation force. Although the motor current feedback can be obtained from the CNC, data acquisition synchronized with other measurement signals is often difficult. To solve this problem, a data acquisition system was developed to synchronously record the data from the CNC and external sensors [327].

The cutting force excitation is effective to evaluate the machine's response to practical machining conditions. An instantaneous cutting of a small step is used for the impulse excitation [50]. A periodic cutting force from intermittent cutting is also used for excitation. However, the cutting force generally contains only frequency components with the tool passing frequency and its harmonics. A variable spindle speed technique was used to conduct excitation with a wider bandwidth in face milling [328] and turning [329]. The bandwidth of the cutting force measurement is also limited because the measured force is filtered by the dynamic response of the force measurement system. Although 3-axis dynamometers with a high natural frequency are used to measure the cutting force, their measurement bandwidth is often decreased to less than 1 kHz by the mass of the tool and the workpiece. The influence of the dynamic response of the force measurement system can be compensated by the inverse transfer function method. In this compensation, the increased noise can significantly increase the uncertainty at the anti-resonance frequency.

Special dynamic loading devices for machine tools were developed in several studies to emulate the cutting force and achieve a more flexible excitation. While the force loading devices in **Section 3.3** (see Figs. 25 and 26) are designed mainly for static loads, electromagnetic loading devices were developed to evaluate the dynamic response of the spindle (Fig. 32) [330] [331] [332]. These non-contact loading devices enable excitation during spindle rotation. Thus, the variation of the dynamic response depending on the spindle speed and temperature can be evaluated. A small and high bandwidth loading device was developed using piezoelectric devices, but it is a contact excitation system [315]. The direction dependent variation of the dynamic response in three dimensions was evaluated by the combination of this excitation system shown in Fig. 33 and interpolation of the frequency response. Fig. 34 shows a map of the compliance for a tilting-table type five-axis machine tool. The magnitude of the compliance is represented by a color map. The color map in three quadrants shows the compliance in the *XY*, *YZ*, and *ZX* planes. The direction dependency of the compliance owing to the machine tool structure can be visualized by this method. The comparison between Fig. 34 (a) and **(b)** indicate the compliance variation due to the posture of the tilting table. Such dynamic response variation depending on the direction, position, and posture has been studied because demands for ensuring the dynamic stability in the entire workspace are increasing [333] [334] [335] [336].

The estimation of dynamic response variation is a challenging work. A machine learning technique is used to estimate the position dependent dynamic response variation [336]. Although the real time estimation of the dynamic response variation during the process may be ideal, it has not been established well in current studies. A data assimilation technique such as Kalman filter [337] is a promising approach to develop the real time estimation system.

The introduced excitation methods are summarized in Table 10. Although the principle of excitation is traditional nowadays, the current focus is on their application in the in-process and on-machine measurements. The driving force and cutting force excitation can be used in the frequency response measurement in operational conditions. Owing to the development in battery and wireless communication technologies, even loading devices have potentials in on machine measurement [338]. These measurements provide important data to update the simulation model in development of digital twin of machining system..

3.5. *Error measurement result and uncertainty evaluation*

The accuracy of measurement results for machine tool errors is affected by various influence. These factors include deviations from performed under various predefined conditions for the measurements. In the case of reporting the result of a measurement of machine tool errors and physical quantities, the quality of the result shall be provided by a quantitative indication in terms of measurement uncertainty. There has been a historic confusion about error and uncertainty (budgets) in the field of machine tool metrology, where machine tool errors (and their repeatability) are the measurand, and measurement errors occur in their assessment. When these measurement errors are not identified and

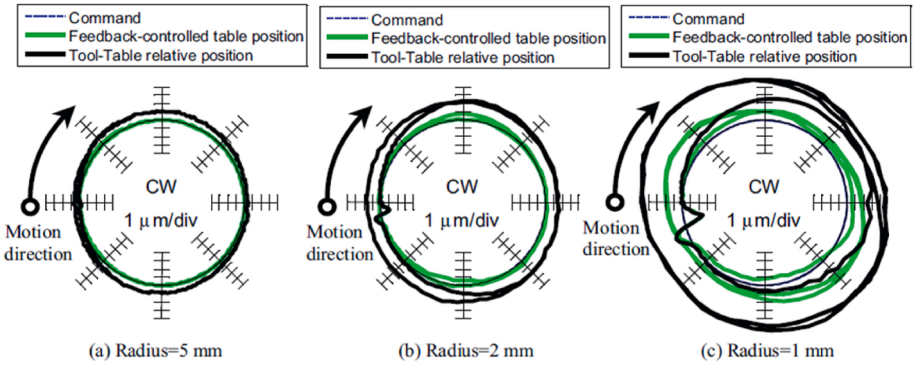

Fig. 30. Contour errors in circular motions measured using linear and grid encoders [51]. (a) Radius = 5 mm. (b) Radius = 2 mm. (c) Radius = 1 mm. The radius at the TCP trajectory is enlarged due to the dynamic deformation of the mechanical system even when the position feedback measured by the linear encoders is still similar to the commanded trajectory.

Table 9
Summary of dynamic error measurement. * low, *** high.

Category	Method	Measurement object	Accuracy	Setup cost	Degree of freedom	Cutting-edge technology
Internal measuring instruments	Rotary encoder [49]	Servo error in each feed drive	***	* no cost	1D	
	Linear encoder [51,320]		***	* no cost	1D	
External measuring instruments	Grid encoder [51]	Tool center point error	***	***	2D	
	Tracking interferometer		**	***	3D	
	Vision based measuring instrument [135]		*	**	3D	Measurement of dynamic errors and vibration [322,321,323]

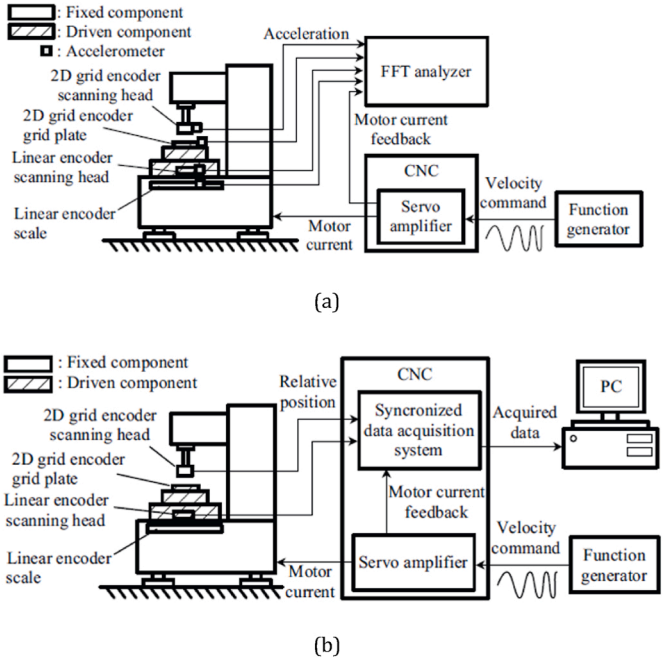

Fig. 31. Experimental setup for frequency response measurement with driving force excitation [51]. (a) Four-accelerometers method. (b) Two-encoders method. The white noise or sine sweep command is input to the feed drive to excite the machine. The response of the tool center point (TCP) position is measured using accelerometers and surface encoders to evaluate the response difference between the position detector and TCP position.

compensated, the quality of the measurements values for the machine errors is affected, which contributes to their uncertainty. Uncertainty of measurement shall be considered, both for establishing tolerance or compliance limit specification, as well as for conformance assessment. ISO/IEC Guide 98–3 [344] contains general procedures for the expression and the evaluation of measurement uncertainty, which are internationally accepted. ISO 14253–2 [345] introduces the Procedure for Uncertainty Management (PUMA), a generic procedure for the practical implementation of uncertainty evaluation. ISO/TR 230–9 [346] provides the estimation of measurement uncertainty specifically for machine tool tests performed according to the ISO 230 series. The ISO 230 series further discusses the main contributors of measurement uncertainty as well as the main assumptions. The uncertainty assessment of machine tool measurements is challenged by the inherent physical characteristics of the mechanics and control of machines affecting the repeatability of measurements. All measurement should be repeated if possible. If the variation of the measurement results is significant, the causes should be identified in either the method, the measuring instrument, the environment or the machine tool and its thermal state.

The coupling between machine performance and measurement uncertainty was discussed by researchers. Bringmann et al. [206] discussed how machine tool geometric calibration is affected by the test uncertainty and its dependence on machine tool performance. The problem of error interdependencies leading to a worse test uncertainty is explained and the occurrence of such effects is shown with example results for the measurement of geometric errors under unloaded test conditions (see also **Section 3.1.2.3**). A proposed method for estimating the overall test uncertainty is introduced that addresses indirect measurements. Ref. [347] describes how measurement uncertainty is associated with the performance of the machine tool under quasi-static loaded test conditions. The effect of variation of the static compliance of machine tools, hysteresis, play, and their interdependency are investigated with respect to the measurement uncertainty. A measurement methodology, using the telescoping loaded double ball bar (LDBB) is proposed to describe and demonstrate the variation of the contributing uncertainties associated with repeatability of the machine tool (see **Section 3.3** for its detailed description).

Knapp [348] published important fundamentals for measurement uncertainty in machine tool testing, which also served as a basis for future standard development particularly for unloaded geometric testing. The introduced concepts are further detailed in Ref. [349]

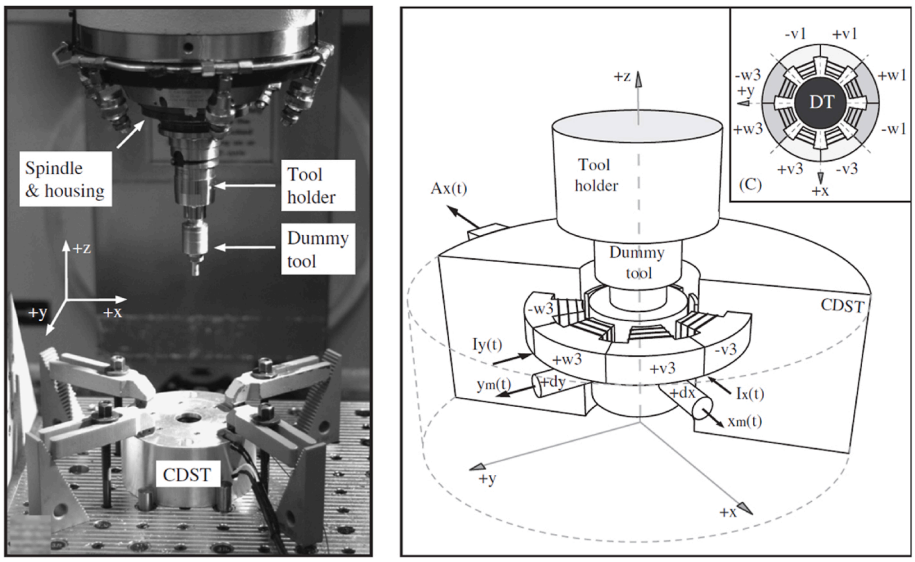

Fig. 32. Electromagnetic loading device for excitation of spindle [331]. (a) Appearance of device. (b) Schematic of device configuration. The non-contact system enables the excitation in the two-dimensional direction during spindle rotation.

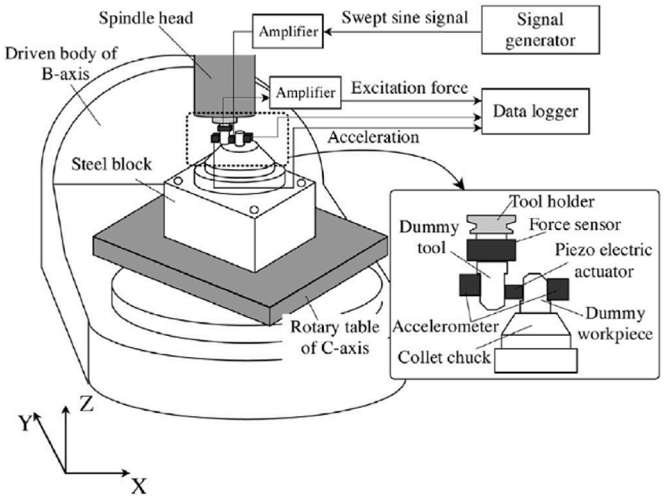

Fig. 33. Piezoelectric loading device for evaluating the direction dependency of the machine's response [315]. Three-dimensional tool-workpiece compliance matrix is measured by three orthogonal excitations. The color map representing the direction dependent compliance variation is obtained as shown in Fig. 34 by the interpolation of the frequency response.

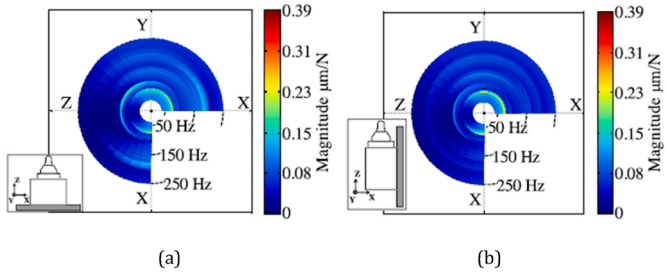

Fig. 34. Colormap of compliance in different directions at different frequencies [315]. (a)With horizontal tilt table. (b) With vertical tilt table. The color map in three quadrants shows the compliance in the *XY*, *YZ*, and *ZX* planes. The radial position in the map represents the frequency. The difference in (a) and (b) shows the influence of the tilt table attitude on the tool-workpiece compliance in a five-axis machine tool. (For interpretation of the references to color in this figure legend, the reader is referred to the Web version of this article.)

focusing on straightness measurements for long large travels. Ref. [350] introduced a laser calibration system that can evaluate the positioning accuracy of a numerically controlled axis of a machine tool or coordinate measuring machine (CMM) under dynamic conditions. To assess the measurement uncertainty of this calibration, an analysis of the uncertainty components that make up the uncertainty budget was carried out. Ref. [351] introduced uncertainty analysis for angle calibrations using circle closure, including two types of full-circle angle calibrations: a simple closure in which a single set of unknown angular segments is sequentially compared with an unknown reference angle, and a dual closure in which two divided circles are simultaneously calibrated by intercomparison. In each case, the constraint of circle closure provides auxiliary information that (1) enables a complete calibration process without reference to separately calibrated reference artifacts, and (2) serves to reduce measurement uncertainty. Ref. [352] introduced a measurement method and uncertainty analysis for position-independent quasi-static kinematic errors of a rotary axis using a telescoping double ball-bar. The standard uncertainty for the proposed method is analyzed to quantify the confidence interval of the measurement result. Errors of two trajectories are measured to estimate the position-independent quasi-static kinematic errors, including two offset errors and two squareness errors of a rotary axis. An error synthesis model was developed that uses homogenous transformation matrices and a telescoping ball bar equation to represent the relation between the positions of the two spheres and the measured distance between them. Setup errors, which are inevitable during the installation of the spheres, are modeled as constants and added to the nominal position of the spheres. Their effects on the measurement result are investigated in detail. The proposed method is validated using simulation and is applied to the rotary axis located on a five-axis machine tool.

For the estimation of uncertainties in the case of indirect measurements, the measurement uncertainties are propagated by the model during the best-fit. Generally, an estimation of the uncertainties of the movement or position/orientation errors is carried out by the best-fit method (least square method). By using the pseudo-inverse method [353], it is possible to propagate measurement uncertainties on the

Table 10
Summary of excitation methods in frequency response measurement. * low, *** high.

Excitation method		Controllability of force	Measurement possibility under operational condition	Setup cost	Cutting-edge technology
Hammering		*	*	*	
Driving force [51]		**	**	**	In process parameter identification [329, 339–342]
Cutting force [50,328,329]		**	***	**	
Loading device	Contact type [315]	***	*	**	Loading device for on machine measurement [338,343]
	Non-contact type [330–332]	***	**	***	

movement or position/orientation errors of machine tool. To reduce the uncertainty of the estimation of movement and position/orientation errors during the best-fit, the condition number must be satisfied. The choice of good measurement setup (range of measurements for example) and the increase in the number of measurements makes it possible to reduce the condition number thus to reduce the uncertainty on the estimation of the machine tool errors. For example, the uncertainty in direct measurement of thermal errors can be calculated directly from the measurement uncertainty budget including the uncertainty sources, such as the measurement accuracy and the thermal drift of each individual sensor itself, the arrangement of the sensors, the external influences such as room environment and human operation, etc. The uncertainty in indirect measurement of thermal errors comes from the accuracy and applicability of the thermal error model. Artificial intelligence (AI) and machine learning (ML) are data-driven thermal error estimation methods, which explore the internal characteristics of process data, establish the relationship between temperature and thermal error. The input data sets, the lag effect, redundant data, accuracy and robustness of the models are the main sources of uncertainty in AI and machine learning measurement methods.

4. Modeling theories

4.1. Quasi-static kinematic models

For the indirect measurements reviewed in **Section 3.1.2.1**, the error sources, X, are related to the actual TCP position, $\hat{p}(k) \in R^3$, by the kinematic model, f, in **Eq. (1)**. The kinematic model, f, clearly plays an essential role in determining errors in the TCP position and the respective uncertainty. The majority of past studies on indirect measurements, reviewed in **Section 3.1.2**, or numerical compensation, reviewed in **Section 5.1**, are based on essentially the same model assuming the rigid-body motion of axes. This model is reviewed in this subsection.

One example is the five-axis machine tool configuration shown in Fig. 35. When the X-, Y-, and Z-axes are positioned at an arbitrary command position (x, y, z), the position errors at the TCP in the X-, Y- and Z-directions are formulated as:

$$e_x(x,y,z) = E_{XX}(x) + E_{XY}(y) + E_{XZ}(z) - \left(E_{C(0X)Y} + E_{CX}(x)\right)y + \left(E_{B(0X)Z} + E_{BX}(x) + E_{BY}(y)\right)z \quad (5)$$

$$e_y(x,y,z) = E_{YX}(x) + E_{YY}(y) + E_{YZ}(z) + \left(E_{A(0Y)Z} + E_{AX}(x) + E_{AY}(y)\right)z \quad (6)$$

$$e_z(x,y,z) = E_{ZX}(x) + E_{ZY}(y) + E_{ZZ}(z) + E_{AX}(x)y \quad (7)$$

This model assumes no offset in the TCP from the point where the error motions are defined. This model formulates the influence of angular error motions on the TCP position [2]. As an example, when the Y-axis has a pitch error motion, $E_{AY}(y)$, as is illustrated in Fig. 36, it changes the motion direction of the Z-axis, mounted on the Y-axis, which results in a position error at the TCP in the Y-direction. This influence is in the 6th term of **Eq. (6)**.

A classical, well-developed way to derive this model is based on coordinate system (CS) transformation. Fig. 37 shows an illustrative example. With respect to the fixed reference CS, called the machine CS,

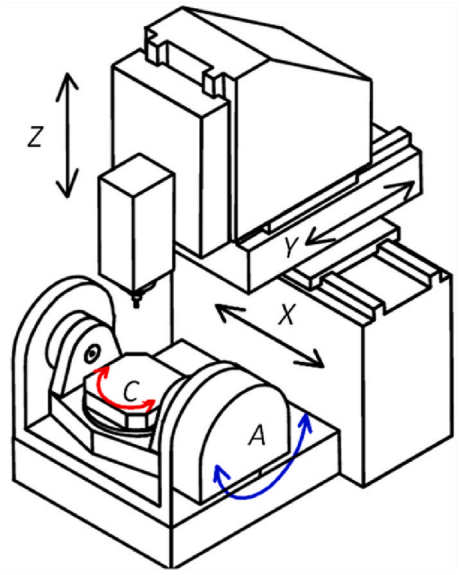

Fig. 35. Example of a five-axis machine tool configuration. Suppose that the X-axis has quasi-axis intra-axis error motions, described in **Section 2.1.1**, namely, linear error motions in the X, Y, and Z directions, denoted by $E_{XX}(x)$, $E_{YX}(x)$, and $E_{ZX}(x)$, and angular error motions around the X-, Y-, and Z-axes, denoted by $E_{AX}(x)$, $E_{BX}(x)$, and $E_{CX}(x)$, for the command position, $x \in \Re$. Error motions of the Y- and Z-axes are denoted similarly. $E_{C(0X)Y}$, $E_{B(0X)Z}$, $E_{A(0Y)Z}$ respectively represent the squareness errors of Y- to X-axis, of Z-to X-axis, and of Z-to Y-axis (see **Section 2.1.2**).

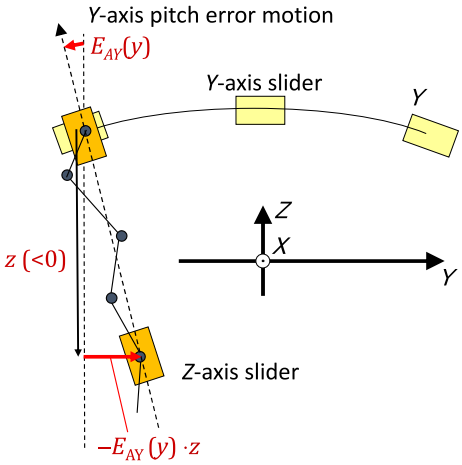

Fig. 36. Influence of the pitch error motion of Y-axis, $E_{AY}(y)$, on the TCP position error. Since the Z-axis is mounted on Y-axis, $E_{AY}(y)$ changes the direction of the Z-axis motion, which results in the positioning error at the TCP in Y-direction by $-E_{AY}(y)z$.

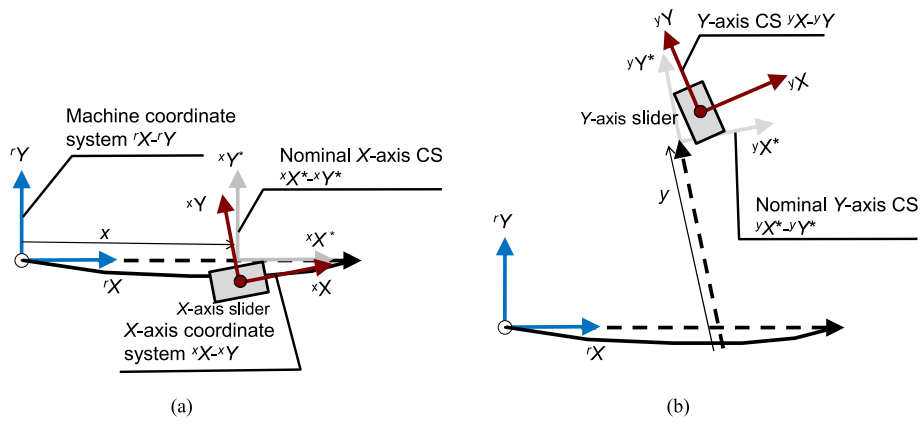

Fig. 37. a) Definition of the *X*-axis CS, ${}^{x}X\text{-}{}^{x}Y$, with respect to the machine CS, ${}^{r}X\text{-}{}^{r}Y$. For simplicity, the diagram depicts the influence of $E_{YX}(x)$ and $E_{CX}(x)$ only. The *X*-axis CS is a local CS attached to the *X*-axis slider. b) Definition of the *Y*-axis CS, ${}^{y}X\text{-}{}^{y}Y$, with respect to the *X*-axis CS. The *Y*-axis error motions determine the position and orientation of the *Y*-axis CS with respect to the X-axis CS.

suppose that the *X*-axis slider moves to the command position, *x*, with all the six error motions mentioned above. Define the *X*-axis CS attached to the *X*-axis slider, as depicted in Fig. 37 a. Then, define:

$${}^{r}T_{x} = D_{x}(x)D_{x}(E_{XX}(x))D_{y}(E_{YX}(x))D_{z}(E_{ZX}(x))D_{a}(E_{AX}(x))D_{b}(E_{BX}(x))D_{c}(E_{CX}(x)) \tag{8}$$

where $D^{*}(*)\in\Re^{4\times4}$ denotes the homogeneous transformation matrix (HTM) representing either translation in *X*, *Y*, or *Z*, or rotation around *X*, *Y*, or *Z*. See, for example [354], for their formulation. ${}^{r}T_{x}$ represents the position and orientation of the *X*-axis CS (denoted in the right-side subscript) in the machine CS (denoted in the left-side superscript). At the same time, it converts a vector in the *X*-axis CS to a vector in the machine CS, as will be shown in **Eq. (9)**. This notation of the CS transformation matrix, ${}^{r}T_{x}$, is adopted in many works, e.g. Ref. [20] [355] [354] [356], although many other analogous notations are available.

Similarly, a set of homogenous transformations is used to define the position and orientation of the *Y*-axis CS with respect to the *X*-axis CS (see Fig. 37 b). Its CS transformation is represented by ${}^{x}T_{y}$, formulated similarly as **Eq. (8)**. The origin of the *Z*-axis CS is here defined at the TCP. Then, the position of the TCP in the machine CS, denoted by ${}^{r}p\in\Re^{3}$ (the left-hand side superscript, *r*, represents a vector in the machine CS), is formulated by converting the origin of the *Z*-axis CS to the machine CS:

$$\begin{bmatrix} {}^{r}p \\ 1 \end{bmatrix} = {}^{r}T_{x}\cdot{}^{x}T_{y}\cdot{}^{y}T_{z}\begin{bmatrix} 0 \\ 0 \\ 0 \\ 1 \end{bmatrix} \tag{9}$$

Assuming all the error motions are sufficiently small, enabling ignoring the second- and higher-order terms, **Eq. (9)** gives **Eq. (5)** to **(7)**. More details in this derivation of the three-axis model are documented in earlier works such as [356]. It is important to note that the position and orientation of these CSs can be selected to accommodate practical considerations of error motion measurement procedures, based on rigid body assumptions.

This modeling can be straightforwardly applied to rotary axes. Consider the configuration of the *A*- and *C*-axes in Fig. 35 as an example. Define the machine CS with its origin at the nominal intersection of the *A*- and *C*-axes. The *A*-axis of rotation nominally coincides with the machine CS *X*-axis. The actual axis average line (see **Section 2.1.2**) can have arbitrary position and orientation errors. Define the *A*-axis CS, ${}^{a}X\text{-}{}^{a}Y\text{-}{}^{a}Z$, such that its *X*-axis coincides with the *A*-axis average line. This determines the position and orientation of the *A*-axis CS in the machine CS, except for 1) the position of its origin in the ${}^{a}X$-direction, and 2) the orientation around the ${}^{a}X$-axis. They can be set arbitrarily. One amongst reasonable choices is: 1) its origin is at ${}^{r}X = 0$, and 2) the projection of the ${}^{a}Y$-axis on the ${}^{r}Y\text{-}{}^{r}Z$ plane is parallel to the ${}^{r}Y$-axis. Fig. 38 illustrates this definition of the *A*-axis CS. Then, the position and orientation of the *A*-axis CS are formulated in the machine CS by:

$${}^{r}T_{a} = D_{b}(E_{B0A})D_{c}(E_{C0A})D_{y}(E_{Y0A})D_{z}(E_{Z0A})D_{a}(-a) \tag{10}$$

where $a\in\Re$ is the angular position of the *A*-axis, and E_{B0A}, E_{C0A}, E_{Y0A}, and E_{Z0A} represent the orientation and position errors of the A-axis average line (or inter-axis kinematic errors, see **Section 2.1.2**). Notice that D_{a} (E_{A0A}) and D_{x} (E_{X0A}) are missing because of the CS definition above. By similarly defining the workpiece CS, with its *Z*-axis aligned to the *C*-axis average line, and formulating ${}^{a}T_{w}$, the position and orientation of the workpiece CS in the machine CS are represented by:

$${}^{r}T_{w} = {}^{r}T_{a}\cdot{}^{a}T_{w} \tag{11}$$

This is a fundamental for various forms of the five-axis kinematic model. For example, when the TCP position in the machine CS is given

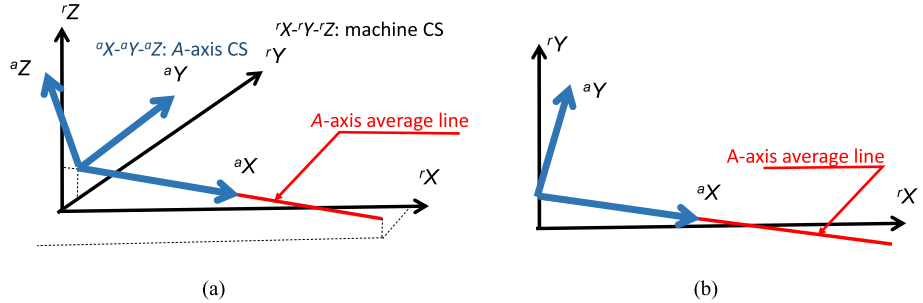

Fig. 38. Definition of the *A*-axis CS for an arbitrary position and the orientation of the *A*-axis average line in the machine CS, a) in 3D view, b) projected onto the ${}^{r}X\text{-}{}^{r}Y$ plane. Its ${}^{a}X$-axis is aligned to the *A*-axis average line. The origin is on the ${}^{r}Y\text{-}{}^{r}Z$ plane.

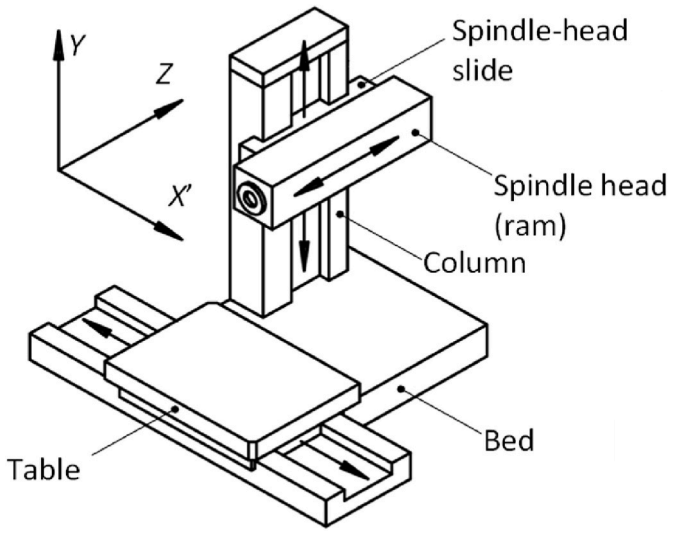

Fig. 39. An example of possible non-rigid body behavior of a *Y*-axis carrying a heavy *Z*-axis ram [357]. The angular error motion of the *Y*-axis, E_{AY}, may vary as a function of the position of the *Z*-axis.

by ${}^{r}p$ in **Eq. (9)**, its position in the workpiece CS, ${}^{w}p \in \Re^3$, is given by:

$$\begin{bmatrix} {}^{w}p \\ 1 \end{bmatrix} = \left({}^{r}T_{w}\right)^{-1} \begin{bmatrix} {}^{r}p \\ 1 \end{bmatrix} \tag{12}$$

Its possible application is the simulation of the geometry of the finished workpiece under the existence of rotary axis quasi-static kinematic errors. More details for this five-axis model are documented in earlier works such as [20] [358] [359]. Ibaraki et al. [354] showed that, when the nominal TCP position is given in the workpiece CS, its positioning error in the workpiece CS can be formulated as a linear function of rotary axis inter- and intra-axis errors, under the small error assumption. This formulation has been a basis for many indirect measurement methods [354] [189] [191] [192]. It was shown in Ref. [181] that the position and orientation of a workpiece feature, e. g. a face, machined with rotary axes fixed at arbitrary angular positions, can be formulated as a linear equation function of rotary axis quasi-static kinematic errors. The model of **Eq. (10)** contains the inter-axis position-independent errors only, but can be readily extended to include position-dependent error motions. Some researchers modeled the position-dependent error motions of linear or rotary axes as an analytical function such as a quadratic function [360] or Chebyshev polynomials [134], but many commercial machine tool controllers, for their numerical compensation, model them as a look-up table [357] (see **Section 5.1**).

The present kinematic model derivation, based on the CS transformation, was presented in the 1980s [355] [361]. It is essentially equivalent to the Denavit and Hartenberg (D-H) model [362], which has been a well-established basis for modeling robots [363] [364]. Many other modeling approaches have been presented, which yield essentially an equivalent model. The complete and parametrically continuous (CPC) model [365] and the product of exponentials (POE) model [366] have been proposed as alternatives to the D-H model. An HTM has 4×4 entries, whereas only 6 entries are needed to describe an arbitrary rigid-body motion. The unit dual quaternion (UDQ), which describes the rigid-body motion by an array with eight entries, can be more efficient computationally [367]. In the machine tool community, a considerable number of researchers have adopted the kinematic model derived from the screw theory [368] [369] [370] [371] [372] [373], which allows a global description of rigid body motion without constructing the local CSs.

The present models, **Eqs. (9) and (12)**, assume rigid-body motions, but can be extended to non-rigid body motions. ISO/TR 16907 [357] presents an example of non-rigid body behaviors, shown in Fig. 39. The angular error motion of the *Y*-axis (spindle-head slide), E_{AY}, may vary as a function of the position of the *Z*-axis (ram), due to the finite stiffness of the column, its connection to the bed, the bed itself, and its connection to the foundation. This example shows a case where the position of one linear axis influences error motions of another axis carrying it. Ibaraki et al. [165] presented the modeling of such a "cross-talk" influence for quasi-static error motions.

Okafor et al. presented quasi-static kinematic modeling for the derivation of machine tool error models and error compensation procedures for a three-axis vertical machining center using rigid body kinematics [356]. To improve machine tool volumetric positional accuracy cost-effectively, machine tool quasi-static kinematic errors as well as thermally induced errors were characterized and predicted for error compensation. The presented mathematical model is used to predict the resultant error vector at the tool–workpiece interface for error compensation. Lin et al. used a matrix summation approach for modeling five-axis machine tools [358]. The traditional approach of using a HTM relies on computationally expensive matrix multiplication. In this work, a matrix summation approach is developed and implemented for modeling the quasi-static kinematic errors of five-axis machine tools. This approach breaks down the kinematic equation into six components, each of which has clear physical meaning and reduces the computations substantially to make the five-axis kinematic model manageable and understandable. Suh et al. described a comprehensive procedure for error modeling and measurement of the rotary table of five-axis machine tools [359]. The introduced steps include geometric error model, error compensation method for the CNC controller, error measurement method, and verification of the error model and compensation algorithm. The developed procedure was verified by experiments, indicating that they can be used for multi-axis machine tools as a means of calibration and enhancement of the rotary table. Ferreira et al. introduced an analytical modeling approach using rigid body kinematics [360] that allows for the description of variation of errors along the machine's axes. The model relates the error vector at a point in the machine tool workspace to the coordinates of that point by the dimensional and form errors of the individual links and joints of the machine's kinematic scheme. Shape (inter-axis errors) and joint (intra-axis errors) transforms are developed for inaccurate machine elements. An expression is developed for the case where the individual joint errors vary linearly as well as the case of a quadratic relationship with the movement along the axis. A comparison made between the errors predicted by a model that allows for variation of individual errors and one that does not, indicates that the higher order terms of the expression make significant contributions to the predicted error. The presented research proposes a method for estimating the coefficients of the model from the errors of a workpiece.

4.2. Thermal models

Thermal models are built for studying the relationship between changes in temperature or heat sources, and thermally-induced errors as well as for compensation of thermal errors [374]. For temperature-based approaches, the model is fine-tuned based on precision measurement of temperatures and displacements at specific positions of the machine tool [39], which requires not only numerical simulation but also precise experimental data. Fig. 40 shows an example of measuring the temperature distribution of a machine tool fitted using a series of temperature sensors near the locations of heat sources like spindle box, guideway, motor, feed screw nut, etc [375].

Table 11 summarizes the modeling methods for thermal errors. The applicable machines and modeling accuracy are also compared and shown in the table. The FEM enables an in-depth analysis of thermally-induced errors of machines. A combination of FEM with the finite difference method (FDM), which is the so-called finite difference element method (FDEM), can produce an effective way for thermal modeling as

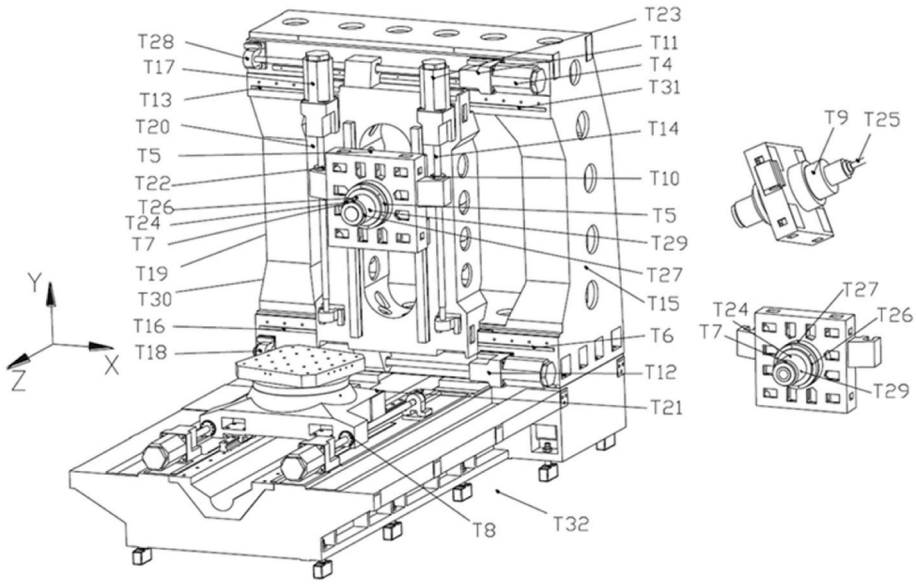

Fig. 40. Locations of temperature sensors on a four-axis milling machine [375]. Temperature measuring points are distributed on heat sources, such as headstock, feed nut, guide rail, motor, coupling, spindle cooling system, environment, etc.

shown in Fig. 41. The FDM is used first to compute the temperature distribution of the machine and FEM is used to compute the resulting thermally induced deformation of the machine [44] [376] [377]. The challenges in thermal modeling come from the complexity of machine tools and the thermal interaction between the various elements. The thermal boundary conditions are difficult to determine accurately. Fig. 41 shows the SATO system [378] for thermal behavior simulation and analysis for a spindle assembly based on FEM, FDM, and a series of procedures describing the boundary conditions. Other methods for thermal modeling such as the least square method, regression analysis, neural network, grey system method, etc. are reviewed in Ref. [5]. The advantages and disadvantages of the linear least squares regression, the back propagation network, and the radial basis function methods are compared in Ref. [375].

Based on the above-mentioned methods, a series of models describing the thermal behavior of rotary or linear axes of machine tools were developed. For example, Holkup et al. established a FEM based model of a high-speed spindle with ball bearings, emphasizing the accurate modeling of rolling elements loads as a function of spindle rotational speed and temperature distribution [379]. Brecher et al. proposed a model for spindle error compensation with model input consisting of spindle temperature, rotational speed, and motor current values [380]. Mayr et al. used the cooling power as input to model the location errors of rotary axes and spindle [381]. Gleich described an approach for modeling ball bearing screws in thermal finite element simulations. The thermal model of a machine is much more complicated than that of a single component due to the interactions among the various components and the environment. Gebhardt et al. established a grey-box model derived from measured data to predict the load-dependent behavior of a rotary axis of a five-axis machine tool [382]. More thermal modeling methods are reviewed in Ref. [39] [4] [47]. Building a physical model is a great challenge due to problems of establishing the boundary conditions and accurately obtaining the characteristics of heat transfer [383]. Recently, some artificial intelligent (AI) methodology are adopted in thermal modeling to bridge the trade-off between precision and profitability [384] [385] [386] [4] [387] [388]. Thermal modeling with self-learning and self-optimizing capabilities dealing with the case of changing boundary conditions in a machining process was developed by Zimmermann et al. [384] and Mayr [305], which increased the intelligence level in thermal modeling. Chiu et al. proposed a ML modeling method, which uses random forests and Gaussian process regression to model the thermal error of the spindle, with an accuracy of 90.49% [389].

4.3. Static load-induced deformation models

A matrix formulation of the kinematic and compliance model of a serial mechanism is used to generate a numerical Jacobian of the change in the telescoping loaded double ball bar (LDBB) length as a function of the machine joint compliances and the applied forces [390].

A modeling method for machine tool stiffness within the work volume is presented in Ref. [391]. A parametric model, considering six-directional static stiffness is established to predict machining errors under various loading situations considering practical machining positions and stress conditions. Experimental results are presented for a boring-milling machining center for the verification of the accuracy and efficiency of the proposed error prediction method by comparing the results from experimental data with those from finite element analysis. The proposed model is stated to be applicable in optimizing the machine tool design.

4.4. Dynamic models

To increase energy efficiency, recent machine tool designs are oriented toward low friction and weight reduction. These designs may simultaneously reduce the damping ability and the stiffness of the system, which has the effect of degrading the dynamic characteristics of the machine tool. This is a critical issue in the manufacturing industry because the dynamic motion accuracy of machine tools deteriorates as the dynamic stiffness of the machine tool deteriorates, which has a significant impact on machining quality, production efficiency, and manufacturing costs.

A comprehensive dynamic simulation of machine tool behaviors using coupled models of mechanical and control systems provides beneficial information in machine tool evaluation. The control system model is represented by a block diagram reflecting the control scheme and parameters in servo controllers. Traditionally, P-PI cascaded feedback loops are employed. The mechanical system is modeled by a mass-spring-damper model. The model for an entire machine tool structure is developed using a FEM or a multi body (MB) model.

A precise model considering higher order vibration modes can be developed using the FEM that can be obtained by meshing a 3D

Table 11
Summary of modeling methods for thermal errors.

Methods	Modeling steps	Characteristics	Applicable machines	Accuracy
The finite element method [5]	1. Simplifying the original geometric constructions and sending it to the software; 2. Meshing according to the structure of the parts; 3. Computing the power of heat sources; 4. Computing the convections; 5. Applying the thermal load and boundary conditions obtained before on the spindle; 6. Computing the steady/transient temperature field of the spindle by FEM; 7. Replacing thermal elements with structural elements to acquire the thermal deformation	- Determining the influence of free convection and forced convection on heat transfer coefficient (film coefficient) - Analyzing the thermal behavior of the machine tool under the influence of heat source in the machine tool structure and its surrounding environment. - Calculating static and dynamic machine characteristics	- Individual structural components, including those containing heat sources and those affected by external heat sources - The overall structure of machine tool	- Moderate accuracy, dependent on modeling constraints
The finite differences element method [39]	1. Using Finite Differences to compute the multidimensional temperature distribution of machine tools 2. Using Finite Elements to compute the thermally induced deformation of machine tools with a linear system of equations.	- Simulating the transient thermal behavior of machine tools. - Combining the advantages of FDM and FEM		- A serial simulation method with high accuracy and short calculation time
The linear least square regression [375]	1. Temperature and thermal deformation measurement 2. Thermal key point identification 3. Establish thermal error model according to different algorithms	- The prediction accuracy of the linear least square regression model is affected by measurement technology and thermal key points.	- Multi-axis machining center structure	- High prediction accuracy and low robustness
The back propagation network [375]		- the back propagation network model is more adaptive to the case of different feed rates, rotational speeds, and ambient temperatures and has certain versatility on machine tools of the same type, and not conducive for on-line thermal error compensation. - The fitting ability and the prediction ability of the back propagation network are limited by the number of hidden neurons.		- Good robustness for a long-term use and certain versatility on same type machine tools.
The radial basis function [375]		- The fitting accuracy and the prediction correctness usually vary according to the hidden neurons, thresholds, and weights and cannot achieve the peak performance simultaneously.		- The thermal error could be reduced to as less as 25% of the original thermal error with compensation using the radial basis function model under the machining conditions of various feed rates and rotational speeds. - The radial basis function model could improve the thermal precision by about 65% under the distinct environmental temperature conditions.
Grey system theory [5]	1. Temperature and thermal deformation measurement 2. Establish thermal error model according to the grey system theory 3. Describe the relationship between thermal drift of main shaft and temperature change through thermal error model	- Modeling based on the grey system theory is simpler, more convenient and does not depend on massive and complete data information as the modeling foundation. - The grey system theory model with AGO (accumulated generating operation) transformation can be used to describe the relationship between the temperature rise and thermal drift of the main shaft.	- Mainly used for thermal error modeling of machine tool spindle	- The online grey system theory model can compensate about 90% of the thermal error on average, while the offline pre-established grey system theory model can compensate about 75% of the error - The grey system theory model had good accuracy and robustness

computer-aided design (CAD) model. However, a large computation cost is required because of its high degrees of freedom (DOF). Additionally, because large motion is also not allowed in the FEM, the simulation of feed drive motions is limited. To solve these issues, a reduced order modeling based on the FEM [335] and a combination of FEM and MB model [392] were proposed.

The MB model is widely used in the comprehensive dynamic simulation of machine tool behavior [393] [394] [339]. Fig. 42 shows a MB model of a vertical machine tool. In the MB model, the structural components such as the bed and saddle are modeled as rigid bodies that are connected by springs and dampers. The MB model's DOF is sufficient in many cases because the important structural vibration affecting the machine's dynamic behavior is not the deformation of structural components themselves but the relative vibration between them.

In both the FEM and MB models, an important issue is the modeling and identification of non-linear characteristics that exist at mechanical interfaces. The friction behavior in the ball screw and guideway is a well-known non-linear effect [340] [396]. The preload dependent

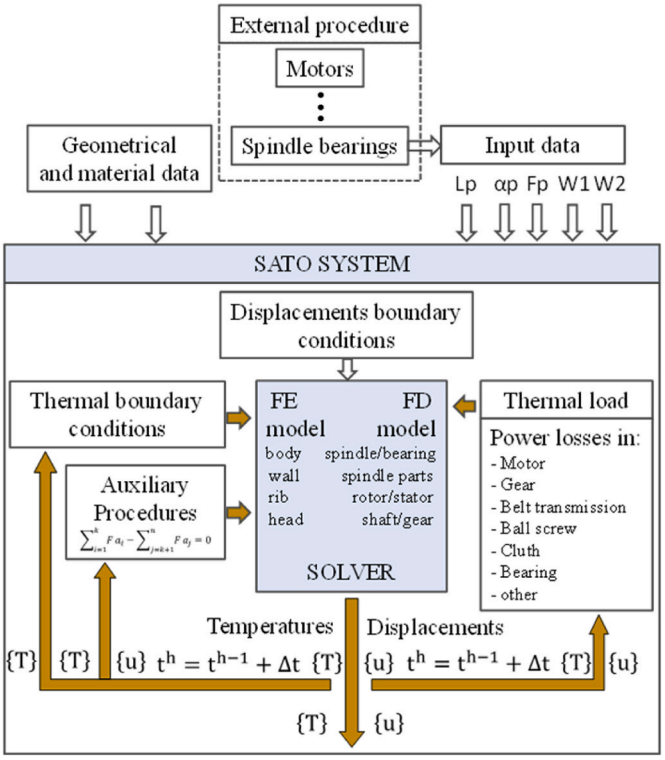

Fig. 41. Diagram of the SATO system for thermal modeling [378]. The system is used to simulate the thermal and static behavior of the machine tool, and combine the calculation of temperature and displacement distribution with the determination of power loss in the moving link of the drive system. The boundary conditions included in the system can ensure the modeling of thermal and elastic phenomena occurring in the structure and on the fixed and moving links between the machine tool units and components. Including: convection generated by radiation, natural convection and element movement, heat generated by coolant flow, contact conductivity and contact stiffness.

stiffness in guideways and bearings is also a non-linear effect that should be considered [397] [398]. In examples shown in Fig. 43, the difference in the frequency response due to different magnitude of the excitation forces is significant in the ball screw and linear motion guideway. These traditional approaches for non-linear modeling were combined with a data-driven model in recent years (Fig. 44) [399]. This combination is expected to improve estimation accuracy while yielding a model that is adaptive to variations in machine condition, such as preload change.

Another difficulty exists in modeling the supporting system of the machine and the foundation [402] [399] [57]. Although the support stiffness depends on the preload, the preload distribution for supports cannot be estimated easily when the number of supports is more than four. Developing a model that includes the foundation is still challenging because the material properties and structure of the floor can be different for each machine shop. An on-site parameter estimation of the floor [403] and parameter identification under an operational condition [339] are effective in such modeling.

The described modeling approaches are summarized in Table 12. The cutting-edge technology is in digital twin development of machine tools. However, the real time simulation of dynamic errors is still challenging because of its computation cost and short variation period. Only reduced order approaches such as the MB model can currently provide the real time solution. The utilization of a supercomputer is an interesting challenge to realize both high estimation accuracy and short computation time [404].

The machining process itself has a significant influence on the dynamic performance of a machine tool. The fluctuation of machining forces can cause vibration problems called “forced vibration” and self-excited vibrations, so called “chatter vibration”. Chatter vibration has been the focus of much research due to its importance for part quality and production efficiency [405] [6]. The mechanism by which the dynamic characteristics of the machine structure and the machining process interact with each other is well described in Ref. [406]. The process can be represented by the time-delay differential equation shown in **Eq. (13)**.

$$M\ddot{u} + C\dot{u} + Ku = F_n + A(u - u_t) \tag{13}$$

Where M, C, and K represent the modal parameters of the system. In other words, the dynamic characteristics of the machine structure that constitutes the machining system greatly affect the stability of the system.

The machine structure consists of the tool, tool holder, spindle, feed drive mechanism, machine tool structure, table, workpiece clamp, and workpiece. The structural components of the system are coupled in series, and the dynamic stiffness of the system is dependent on the properties of the least stiff structure and its joints [407]. In many cases, loop stiffness is calculated by simplifying the system to a MDOF vibration model of a mass-damper-spring system. The simplified model can accurately predict the machining results.

Examples of modeling for turning [400] and milling processes [401] are shown in Fig. 45. The dynamic characteristics of the machine structure are modeled and the effects of the relative displacement between the tool and workpiece on the cutting force fluctuations are modeled. As shown in Fig. 46, the structural dynamics and the machining process form a feedback loop so that the structural vibration

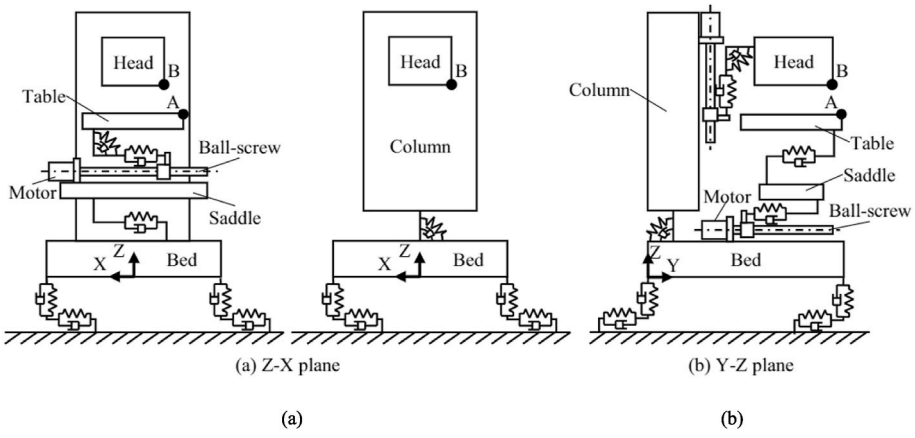

Fig. 42. Multi body model of vertical machine tool [395]. (a) *Z-X* Plane. (b) *Y-Z*-Plane. Major structural components are modeled as rigid bodies and connected by springs and dampers.

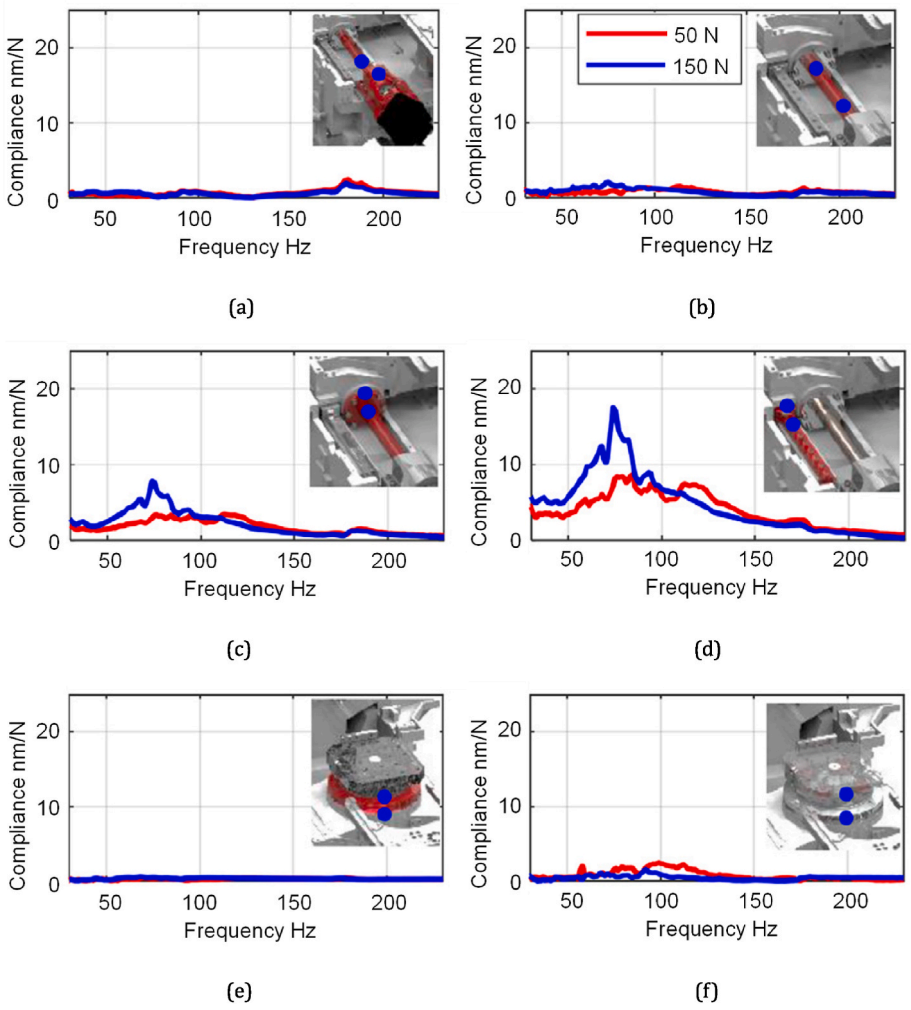

Fig. 43. Frequency response of different machine elements depending on excitation force [397]. (a) Support bearing. (b) Ball screw. (c) Ball screw/nut. (d) Linear motion (LM) guideway/carriage. (e) Table. (f) Table connection. The influence of the excitation force is larger in the ball screw and LM guideway because the stiffness and damping are changed by the preload in these rolling elements.

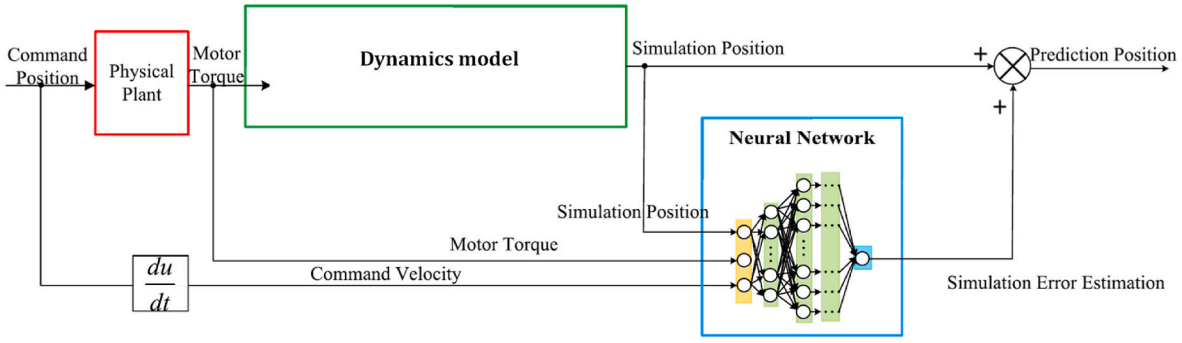

Fig. 44. Feed drive dynamics model combined with neural network [399]. The representation of "Dynamics model" bock was modified from the original figure. The simulation error of the dynamics model caused by complicated factors such as a position dependent friction variation is estimated by the neural network.

caused by the cutting force fluctuation generates further cutting force fluctuations. Chatter vibration will develop if the interaction between the dynamic behavior of the machine structure and the cutting process leads to system instability. Time-domain, frequency-domain, and semi-discrete-time-domain methods have been proposed for analyzing chatter vibration. The time-domain solution is widely used because it can estimate transient states of the system by directly solving ordinary differential equations in the time domain, and it is easy to implement nonlinear models. However, when large-amplitude vibration occurs under unstable conditions, the nonlinear behavior of the machine structure [397] and a phenomenon called process damping [408] [409], in which the tool flank face contacts the workpiece surface, must be considered to precisely simulate the phenomenon. These modeling studies are still in their developmental stages, and no reliable means has been established to quantitatively estimate the behavior under unstable conditions. Under stable conditions, the cutting force fluctuations

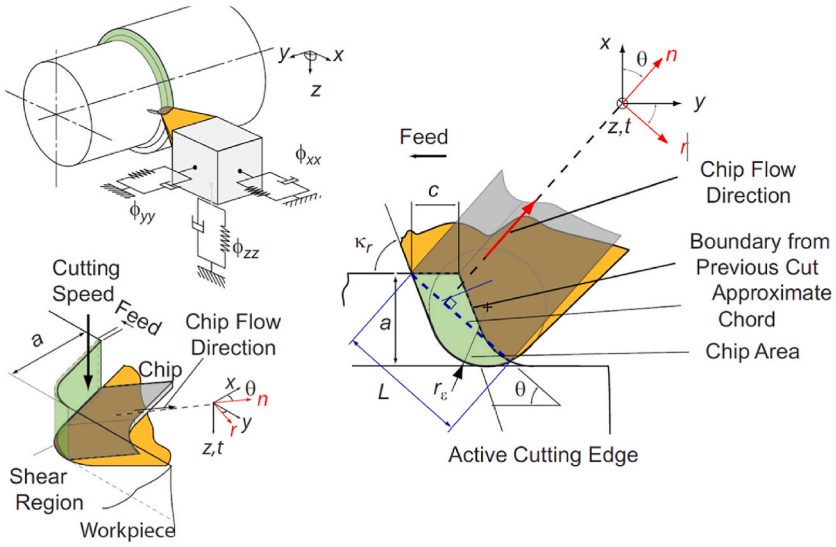

(a)

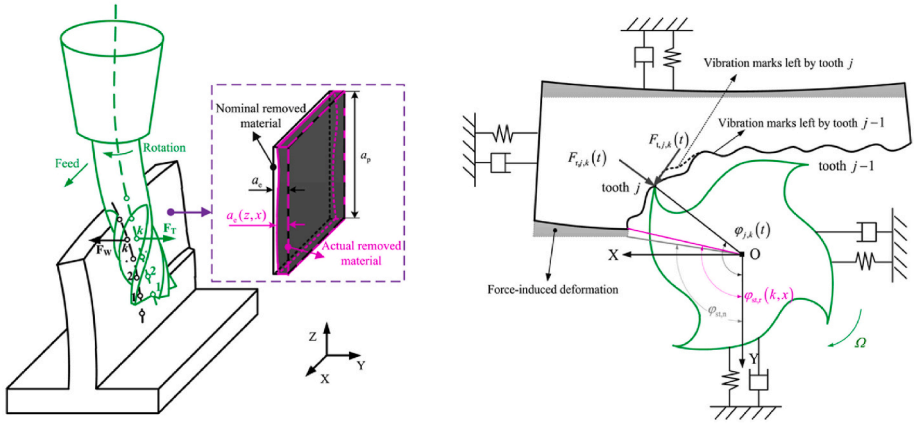

(b)

Fig. 45. Modeling of cutting processes. (a) Turning process [400]. The condition-dependent process force gain needs to be modeled. (b) Milling process [401]. Modeling of the motion kinematics, machine structural dynamics, and tool-workpiece engagement in a multi-DOF system is important.

Table 12
Summary of modeling approaches for machine tools.

Methods	Modeling cost	Computational cost	Estimation accuracy	Cutting-edge technology
Finite element method (FEM) [335]	*	***	***	Digital twin of machine tool and machining process [393, 394,404] In-process parameter identification [339–342]
Multi body method (MB) [393] [394] [339]	***	*	*	
Combination of FEM and MB [392]	**	**	**	

caused by chatter converge to zero in the steady state, hence the problem can be treated simply as a forced vibration problem. Therefore, in the analysis of chatter vibration, it is important to determine whether the system is stable or unstable. From this point of view, the frequency-domain approach is a computationally cost-effective method. Focusing on the dynamic characteristics of the mechanical structures as a filter, Budak and Altintas proposed a simple model called Zero-Order-Solution (ZOS) [410] that handles only the mean magnitude of the periodic cutting resistance coefficient matrix. Its excellent estimation performance has been well demonstrated experimentally, and hence it is widely used as a method to determine the stability and instability of a system. On the other hand, the ZOS is more likely to produce estimation errors in processes such as low immersion milling, where the periodicity of the machining process has a large influence. Under such conditions, estimation errors have been observed with the time-domain method [411]. The semi-discrete time-domain solution combines the advantages of the time-domain and frequency-domain methods to improve both higher estimation accuracy and relatively lower computational cost [412].

The accuracy of these vibration estimation methods depends on the accuracy of the model and model parameters. The model parameters comprise parameters such as specific cutting resistance, which is a coefficient used to estimate cutting forces, and modal parameters, which represent the dynamic characteristics of the machining system. Model parameters are generally identified through cutting experiments and impulse response methods [406]. Conventional methods based on off-line measurement cannot handle parameter identification that reflects changes in the system during machining. For this reason, the identification of cutting parameters [414] and modal parameters [415] [416] based on information obtained during actual operation has been

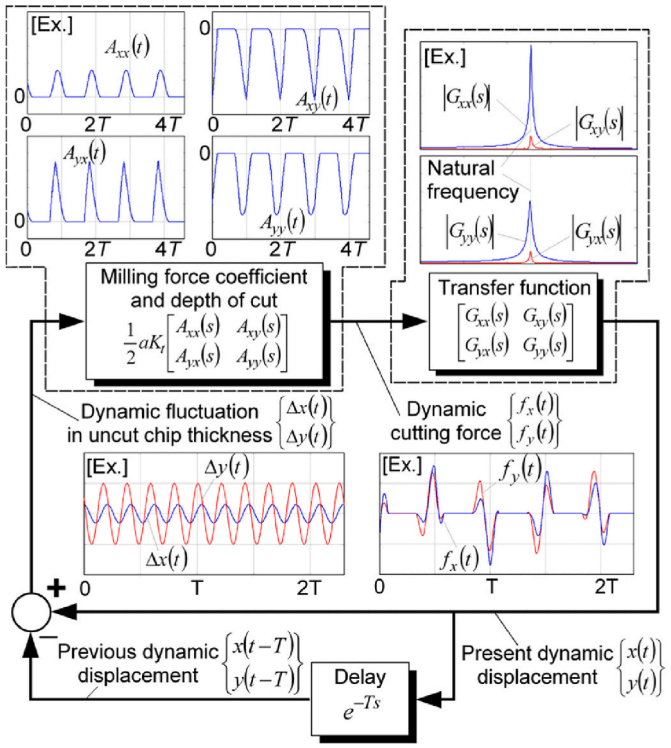

Fig. 46. Block diagram of the system consisting of the cutting process and machine dynamics [413]. The dynamic cutting force excites the machine structures, causing dynamic displacement, which triggers cutting force fluctuations with a regeneration effect. The diagram depicts a feedback Loop of the system consisting of the structural dynamics and the machining process.

proposed. Alternatively, simultaneous identification of all parameters using disturbance forces input to the feed system of a machine tool [341] [342] has been proposed. Fig. 47 shows an example of the parameter identification from transient fluctuations in the disturbance force that occur in a milling process with spindle speed variation. The identification techniques that use in-process information are useful for accurately estimating vibration phenomena caused by the machining process.

The described modeling approaches are summarized in Table 13. None of the methods proposed so far can guarantee sufficiently high accuracy in estimating the dynamic behavior of machine tools caused by dynamic processes. Further improvement of model accuracy and accurate identification of model parameters are essential to achieve highly accurate estimation using digital twins based on physical models. The consideration of nonlinearities in dynamic models of the machining processes [417] and the machine dynamics [418] is an interesting challenge. Modeling with AI-based approaches [419] [420] [421] [422] [423] is also an interesting challenge to improve the estimation accuracy. Current approaches are mostly oriented toward the stability lobe diagram prediction.

5. Compensation strategies

5.1. Compensation of quasi-static kinematic errors

5.1.1. Static compensation

Initially, a machine tool's accuracy is due to the quality of its components and their assembly [2] [1]. The errors are summarized in ISO 230–1 [16] and the compensation for their effect is in ISO/TR 16907 [357]. Reproducibility of these errors is the key to effective compensation. Accuracy variations may be due to wear and/or sag in the foundation (thermal and load effects will be treated in **Section 5.3 and 5**.4). A collision during use may also modify the alignment and dimensions of machine components.

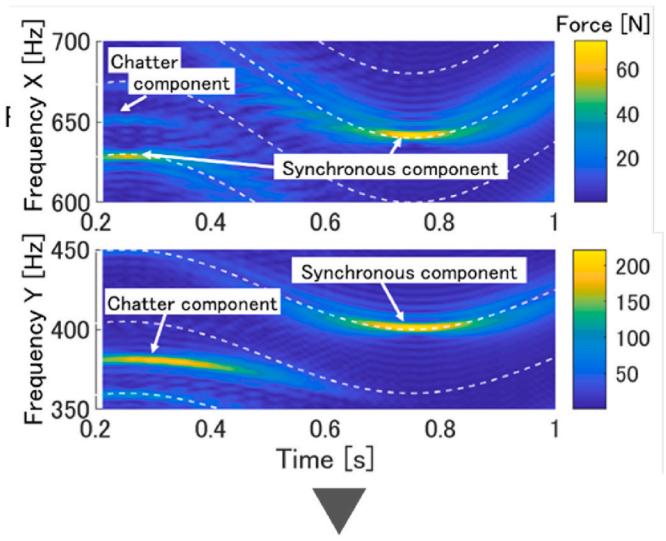

Identified model parameter values

Model parameters		Configured value	Identified value in SSV
Cutting process parameters	Specific cutting force MPa	1250	1233.2
	Edge force coefficient N/mm	10	10.29
	Tool eccentricity μm	10	19.7
Modal parameters	Mass kg	1.03	1.14
	Damping ratio	0.038	0.0334
	Natural frequency Hz	400	399.4

Fig. 47. Parameter identification method for a linear model of the milling process [341]. This example shows the concurrent identification of cutting process parameters and modal parameters from the disturbance forces measured during the transiently varying milling process by the spindle speed variation (SSV) method. The disturbance force includes both chatter and forced vibration components, as shown by the results of the short-time Fourier transform of the disturbance forces.

Table 13
Summary of modeling approaches for dynamic performance of machine tools. * low, *** high.

Methods	Modeling cost	Computational cost	Estimation accuracy	Cutting-edge technology
Time domain approach [394,397]	*	***	***	Modeling accuracy improvement [397,408,409, 417,418] Parameter identification improvement [341,342, 414–416] AI-based approach [419], [420] [421] [422] [423]
Frequency domain approach [400,401, 410]	***	*	*	
Semi discrete time domain approach [412]	**	**	**	

Compensation strategies to improve the workpiece quality can be classified into two classes: direct/indirect and model-based compensations. Both classes of compensations can be introduced, either in the controller setup of the machine tool or applied in the G-code part

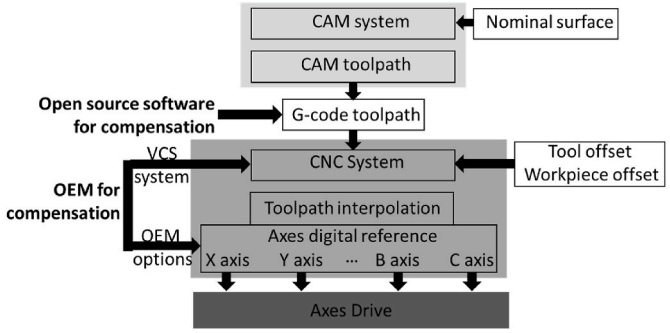

Fig. 48. Solutions for compensation: (I) Open-source software by modification of the G-code toolpath and (II) Original Equipment Manufacturer (OEM) using the OEM functionalities of the CNC system. The VCS system is a specific option added to CNC system, and the OEM options are directly implemented in the CNC system.

program to modify the toolpath (Fig. 48).

5.1.1.1. Direct/indirect static compensations using CNC function. Current CNC systems have numerous options to compensate major machine tool errors by applying direct corrections to the axis command. These are summarized in ISO Technical Report 16907 "Numerical Compensation of Machine Tools." The compensation will be said to be direct when the measured value is directly applied to the nominal position of the point to be corrected. Indirect compensation will use an equation to calculate the compensation from measured values.

I) Empirical backlash compensation: To compensate for backlash, the axis-specific value is corrected by the amount of backlash every time the axis changes direction. This quantity is introduced for each axis in the CNC machine tool data setup. Fig. 49a summarizes a procedure to determine the backlash value. The backlash of each axis can be determined easily using a dial indicator with a micrometer resolution.

II) Linear positioning errors of a linear axis (E_{XX}, E_{YY} or E_{ZZ}): The leadscrew and the measuring system errors can be compensated using a compensation table. This compensation assumes that the current position of the axis can be computed from the position of the drive actuator or directly by the measuring system. In the case of the encoder being mounted on the drive ball screw, the lead of the ball screw is assumed constant for the entire axis travel. The kinematic errors E_{XX}, E_{YY},and E_{ZZ}directly affect the accuracy of workpiece machining. Their compensation requires the relevant position-dependent compensation values. The compensation values are computed using measured error curves and entered in the form of compensation tables in the setup register of the CNC system. Fig. 49b shows the measurement of linear positioning errors using a laser interferometer. An interpolation procedure is used to derive the compensation value between two measured values. Classically, linear interpolation is employed for its simplicity. Other types of interpolations can be used, for example, B---Spline interpolation. The compensation value obtained after interpolation of the measured values is added by the CNC system to the current position value of the axis.

III) Sag and multi-axes compensation: The own weight of machine elements can cause deformations depending on their position. These deformations induce a displacement and an inclination change that modify the position and the orientation of the tool. Fig. 49c shows this situation in the case of a horizontal milling machine with a heavy *Y*-axis ram. The sag, or the straightness error motion induced by the moving mass, can be compensated using a compensation table where the difference between measured and nominal *Z* values are stored (see Fig. 49c). The compensation table describes the sag error in Z direction as a function of the nominal position of the Y-axis. The compensation value between two saved values in the compensation table is computed using an interpolation. Fig. 49d shows the compensation of sag in a foundation. This compensation can reduce the effect of structural deformations of the machine tool when its link with the foundation is static. The data for axis compensation are saved in the table with nominal axis position entries (for example *X* and *Y*) and the measured value of the compensation (for example *Z*). A more complete compensation makes it possible to deal with cases where the angular error is too great. In this case, an equation linking linear axis angular error motions and errors in the tool position can be used for the compensation of the sagging using a set of tables [424] (the quasi-static kinematic models, reviewed in **Section 4.1**, can be applied). These tables can be multiplied and/or added. This case is shown in Fig. 49d. This type of compensation can be extended to multi-axis compensation. The position of an axis can be the input quantity for several tables. This allows the derivation of the total compensation value of an axis from several compensation

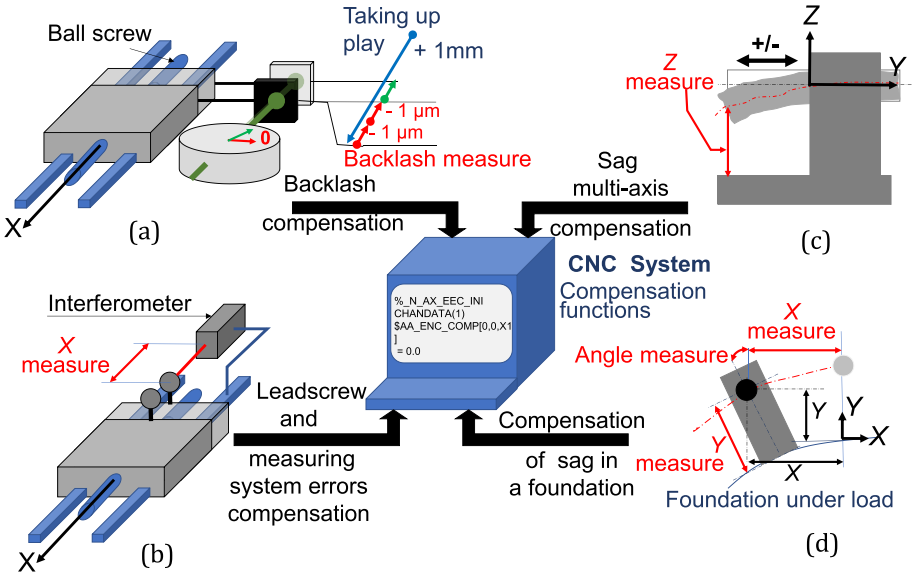

Fig. 49. Direct/indirect static compensations on CNC systems: (a) Backlash compensation option allows to take in account the clearance of ball-screws of the axes (except for the case of linear motors), (b) Leadscrew and measuring system errors compensation option permits to deal with linear positioning errors using compensation tables, (c) Multi-axis compensation allows to deal with machine errors merging by compensation tables (d) Compensation of sag in a foundation permits to balance structural deformations of the machine tool using compensation tables.

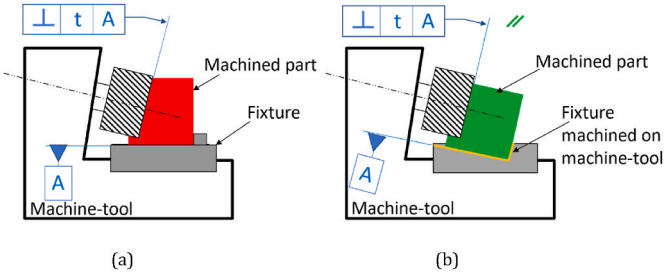

Fig. 50. Squareness error compensation for the case of a milling operation on a machine tool. The image on the left (a) shows the effect of the squareness error on the orientation error between reference A and the machined surface. In the right image (b), a physical compensation has been applied by machining the fixture on the machine-tool. In this case, the orientation between the reference A and the machined surface is not influenced by the squareness error of the machine tool.

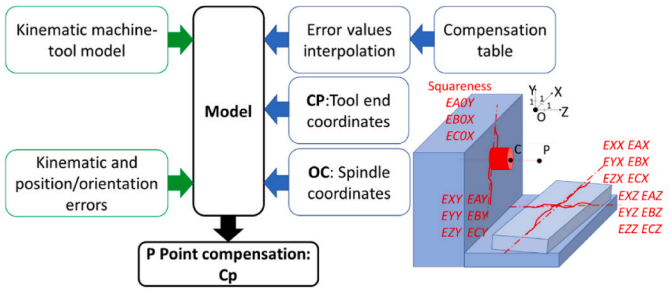

Fig. 51. Principle of VCS for a three-axis milling machine: The VCS software is based on the kinematics (18 errors) and position/orientation errors (3 errors). To compute the ***Cp*** compensation vector, the software needs to know the 21 machine errors (compensation table), and the ***CP*** and ***OC*** vectors. For each position of the points *C* and *P* during the machining, the VCS software calculates in real time the end point compensation that the CNC software must apply.

relationships (tables). Compensation that includes all position and angular errors can be performed using this approach. The eight inter-axis errors, two spindle lateral offsets, and the three linear axis scale errors of a five-axis machine tool were addressed using 40 compensation tables to derive compensation values for each axis (*X*, *Y*, *Z*, *A*, *C*) [425]. This work used symbolic variational forward and inverse kinematics approaches. The mean volumetric error was reduced by 79 %.

IV) Physical and empirical compensation of squareness error on a machine tool: A position compensation does not allow for the compensation of errors in tool orientation. Fig. 50 shows the effect of the parallelism error of the spindle axis to the worktable. Suppose that the bottom face of the workpiece is the datum surface. If it is fixed parallel to the machine table, the parallelism error of the spindle axis to the worktable can cause the perpendicularity error of the left side face to the bottom face, as shown in Fig. 50a. If the positioning surface of the fixture is machined on the machine tool by feeding the tool to the *Z*-direction, as shown in Fig. 50b, and if the parallelism error of the spindle axis to the *Z*-axis is sufficiently small, then the resulting perpendicularity error of the machined surface is not affected by this orientation error of the spindle axis to the worktable.

$$\mathrm{A}=\begin{pmatrix} 0 & -(ECX+ECOX) & EBX+EBY+EBOZ & \\ 0 & 0 & -(EAX+EAY+ECZ) & EXX+EXY+EXZ \\ 0 & EAX & 0 & EYX+EYY+EYZ \\ 0 & 0 & 0 & EZX+EAY+EAZ \end{pmatrix}$$

$$A_P=\begin{pmatrix} 0 & ECX+ECY+ECZ & (EBX+EBY+EBZ) & 0 \\ (ECX+ECY+ECZ) & 0 & -(EAX+EAY+EAZ) & 0 \\ -(EBX+EBY+EBZ)0 & (EAX+EAY+EAZ) & 0 & 0 \\ & 0 & 0 & 1 \end{pmatrix}$$

5.1.1.2. Static model-based compensation using CNC controller function. The volumetric error compensation of quasi-static kinematic errors is a direct application of compensation tables. Many OEMs of CNC systems have incorporated volumetric error compensation modules for three-axis machine tools, as is reviewed in ISO/TR 16907 [357]. This option is based on a static model and allows for the volumetric compensation of the TCP position (Fig. 51) of three axis milling machine tools.

Most volumetric error compensation modules available in commercial CNCs are based on the quasi-static kinematic model reviewed in **Section 4.1**.

$$C_p = A \times OC + Ap \times Cp$$

$$\mathrm{OC}=\begin{pmatrix} X \\ Y \\ Z \\ 1 \end{pmatrix} \text{ and } \mathrm{CP}=\begin{pmatrix} X_p \\ Y_p \\ Z_P \\ 1 \end{pmatrix} \tag{14}$$

In the CNC system setup, a set of compensation tables can be saved. If two or more tables are activated, the mean values of compensation table values are computed by the CNC system. This smoothens the effect of a newly added table. Each compensation table includes the measured values of each kinematic error expressed at each interval value (e.g., each 50 mm) along the considered axis. The estimation of the error value in the interval is derived using an interpolation. The measured squareness errors, E_{COX}, E_{BOZ}, and E_{COY}, are included at the end of the table. This is a typical volumetric error compensation, based on the quasi-static kinematic model reviewed in Section 4.1. Some commercial CNC systems offer compensation based on the representation of the volumetric error in a spatial error grid, which requires no kinematic model in the controller. ISO/TR 16907 [357] reviews various forms of volumetric error compensation.

5.1.1.3. Static model-based compensation using modified G-code. When the volumetric compensation is not available on the CNC controller, alternative methods have been used, such as modifying programmable application logic (PAL) software of CNC [426] or adding special

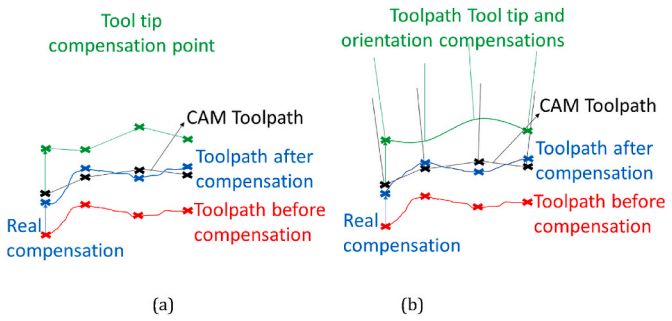

Fig. 52. Application of the compensation on the CAM toolpath. The compensation is limited by the degrees of freedom of the machine tool axes. In the case of three-axis machine tools (a) only translation compensations can be applied on tool tip point. In the case of five-axis machine tools (b) the compensations of tool tip position and the tool orientation can be applied by the CNC.

hardware devices to the drive feedback loops [427]. Due to significant increase in the amount of internal CNC memory over the years, the same compensation can now be performed by a modified G-code programs (Fig. 52a). The tool path generated by the computer aided manufacturing (CAM) system is modified to include the TCP at discrete positions, which are then compensated based on the modeled TCP errors [126] [428]. This compensation is applied in the workpiece coordinate system along the toolpath.

Over the past decade, the compensation of five-axis machine tools was the focus of numerous works. The five-axis machine tool structure has numerous kinematic errors (more than 40 errors) and has specific kinematic singularities and motion discontinuities along the curved tool paths. To avoid this impediment, the tool orientation vectors, and the movement of the tool tip were represented by a fifth degree B-spline curve in Ref. [371]. The use of polynomials allowed compensation of both tool tip position and tool orientation (Fig. 52b) [429]. Numerous applications for a set of five-axis machine tool structures were published in the last decade [430] [431] [432].

5.1.1.4. Efficiency and limitation of quasi-static error compensation. Quasi-static kinematic error compensation enables reducing the positioning deviation of the tool point around 60% or more [425] [156]. The TCP or direct/indirect method performance is directly linked with the repeatability of machine tool axes. The design of the machine components may impact the rigidity, the geometrical stability, and the repeatability of the machine tool movements, which remains the limit for a realistic error compensation. The installation quality of the machine on its foundation has much influence on the observed structural deformation, notably when the number of contact points is more than the minimal number to obtain an isostatic installation. This phenomenon can be observed for large machine tools. In three axes milling machine, the real orientation of the tool cannot be compensated numerically. This deviation has significant effects when the tool has a large size. In this case, angular error motions can have a larger influence on the TCP position. In the case of five axes milling machines, rotary axes can be used in most cases to align the normal vector of the machined surface with the tool axis. Finally, the quasi-static kinematic errors are correlated to the room temperature. A smooth gradient of the temperature can be compensated by changing the table as a function of the current room temperature. Quick temperature variations cannot be considered with a static compensation method.

The presented static compensation methods are summarized in Table 14. They are compared in terms of error type, direct or indirect application, complexity (* Easy-to-use method, ** Long and complicated method), cost (*Low cost, ** Expensive method), effect of compensation (Partial: some effects of errors are compensated; Complete: all effects of errors are compensated), and application domain. This classification brings to the fore that the compensation of machine tools with three-axis or less is overcame and routinely implemented in industry today (OEM facilities)

The most recent advances in static compensation for linear error motions, position and orientation errors have taken place in the field of multi-axis machines, in particular, to five-axis machine tool [430] [431] [126] [432] [428]. New research approaches are emerging to compensate machine errors, as described next. The use of artificial intelligence and machine learning is gaining momentum in the compensation of quasi-static kinematic errors [434]. Machine learning approaches have been tested to compensate volumetric errors in five-axis machine tool [435] and to predict the thermal error compensation [436].

5.1.2. Precise and high bandwidth compensation by using fast tool servo

Although quasi-static kinematic errors in a machine tool can be

Table 14
Summary of static compensation classes. * low, *** high.

Classes of static compensations	Methods for static compensation	Name	Error type	Direct or Indirect method	Complexity	Cost	Effect of compensation	Applications
Physical and empirical compensation	Physical compensation of squareness errors	Direct compensation of squareness errors	Orientation errors	Direct	*	*	Partial	All machine tools
Original Equipment Manufacturer (OEM) for compensation	Direct/indirect compensation using CNC functions	Empirical backlash compensation	Backlash	Direct	**	**	Partial	All machine tools with ball screws
		Linear positioning errors of a linear axis	Linear positioning errors	Direct	**	**	Partial	All machine tools
		Sag and multi-axis compensation	Kinematic and orientation/position errors	Indirect	*** to **** Difficulty to do the model and manage compensation tables in controller	***	Partial to complete	All machine tools
	Volumetric error compensation using CNC function	Matrix compensation and TCP compensation	21 errors: 18 kinematic and 3 orientation errors (more error components exist for 5-axis machines)	Indirect	* Model is implemented in controller. ** Setup management in controller	***	Complete	3 axis machine tools
Model-based compensation using modified G-code	Modified toolpath in G-code program	Machine tool model, matrix compensation and TCP compensation	Kinematic and orientation/position errors	Indirect	*** to **** Difficulty to do the complete model in multi-axis machine tools	****	Complete	All machine tools

compensated by moving slides, this is only possible for low frequency components of the quasi-static kinematic errors due to the low bandwidth of a slide that is typically limited to the order of 10 Hz [437]. The fast tool servo (FTS) technology, although limited in applications of diamond turning, was developed for the compensation of quasi-static kinematic errors over a wider bandwidth up to several hundreds of Hz [438] as well as for the fabrication of non-rotationally symmetric surfaces [439], large-area microstructured surfaces [440], and for cutting experiments in nanomachining instruments [441].

Kounno at NEC Cooperation and Patterson at Lawrence Livermore National Laboratory developed the first FTSs independently in the mid-1980s [442] [443]. In the FTS by Kounno, a linear variable differential transformer (LVDT) was employed as the displacement sensor for the feedback control of a piezo (PZT) actuator with a 10 nm resolution and a 6 μm range over a bandwidth 50 Hz [442]. The FTS by Patterson, which had a combination of a capacitance-type displacement sensor and a PZT actuator, could realize a dynamic repeatability of better than 1.3 nm over a bandwidth of 100 Hz [443]. The first application of FTS to the compensation of machine errors was made by Fawcett at North Carolina State University in 1989 [438]. To compensate for the vibration introduced by the *Z*-axis with an amplitude of 100 nm and a frequency of 67.5 Hz, an improved FTS shown in Fig. 53 was employed. The FTS, in which a capacitance-type displacement sensor and a PZT actuator were employed had a maximum stroke of 15 μm with a bandwidth over 1 kHz. The relative error motion of the workpiece with respect to the tool post, which was introduced by the *Z*-slide, was measured by a capacitance-type displacement sensor (A). The sensor output was used as the error signal to control the FTS. The expansion and contraction of the PZT actuator adjusts the tool position to compensate for the relative motion between the tool and the workpiece. The actual movement of the tool was monitored by a second capacitance-type displacement sensor (B) to verify that the tool motion corresponds to the measurement from sensor A. It can be seen that the periodic error component introduced by the *Z*-axis vibration error was removed. The peak-to-valley (PV) surface roughness was reduced from 50.1 nm to 34 nm.

When an FTS is employed on a diamond tuning machine (DTM) for further compensating the slide and the spindle errors, the integration of the FTS to the machine controller is a challenge since the FTS controller is independent of the machine CNC. In a specific diamond turning machine where the FTS was integrated [437], the spindle rotary position was measured by a rotary encoder, and the positions of the *X* and *Z* slides were measured by laser interferometers. The slide axes controller executes the correction algorithm at each controller cycle after the reference coordinates for each slide are calculated outside the feedback loop. The FTS feedback control loop is independent of the *X* and *Z* slide control. The interferometer data were made available to both the slide axes controller and the FTS feedback controller by connecting the two controllers directly to the interferometer interface output ports. An additional angular feedback interface, makes the FTS controller accessible to the spindle encoder with a maximum encoder resolution of 0.0015 radians per count. With this architecture, the *X*/*Z* and FTS control processes execute in parallel.

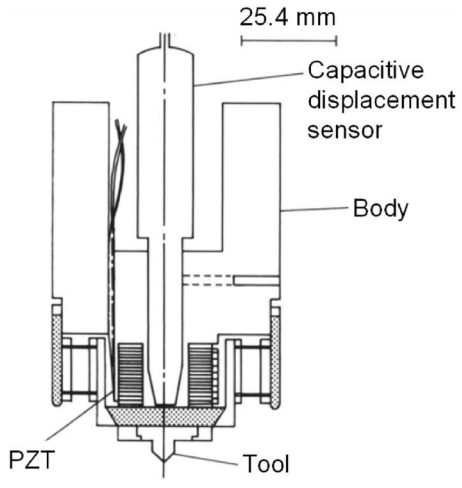

Fig. 53. An early FTS for compensating the *Z*-slide stability error [438]. The tool is actuated by a PZT actuator. The displacement of the tool is measured by a capacitive sensor (cap gauge) for full-close loop control.

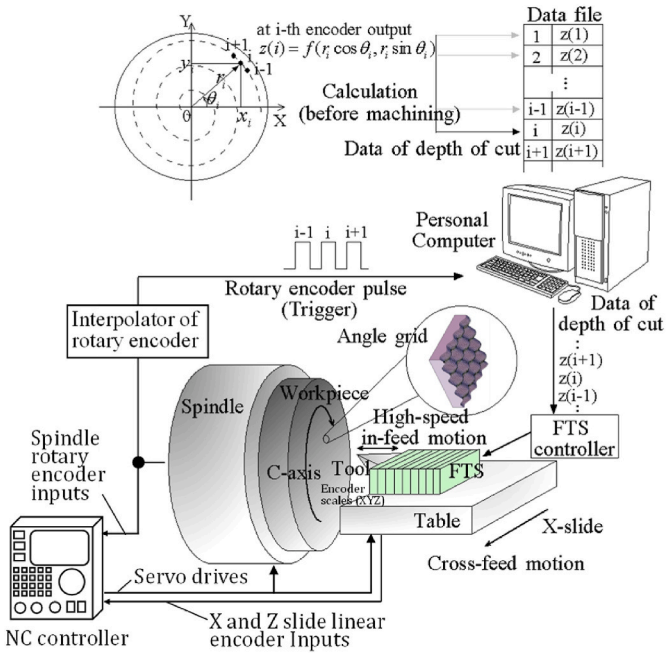

Fig. 54. An improved integration of FTS to an ultra-precision lathe (diamond turning machine) for fabrication of microstructured surfaces with compensation of machine errors [440]. The rotation of the spindle and the feed of the *X*-slide and/or the *Z*-slide is synchronized by the numerical controller (NC). When the fabrication starts, the depth of cut data stored in a personal computer are output to the NC one by one in responding to the output signals of spindle rotation positions from the NC.

Fig. 54 shows an improved integration of an FTS onto an ultra-precision lathe in which the position measurements of the slides were made by linear encoders [64] instead of laser interferometers [440]. Based on the spindle rotary encoder and the linear encoder outputs, the CNC provided servo drives to synchronize the rotation of the spindle and the feed of the *X*-slide and/or the *Z*-slide. Since the polar coordinates of the tool tip position in the *XY*-plane could be identified from the spindle rotary encoder output, a signal interpolator was added between the rotary encoder read head and the encoder serial interface of the CNC to receive the sinusoidal voltage output signals of the encoder. The sinusoidal voltage signals were then converted into pulsed output signals of the spindle rotational positions by the interpolator. A digital input/output (I/O) board was employed as the interface connecting the interpolator and the personal computer (PC). The data of depth of cut for compensating the slide and spindle errors as well as the data for fabricating the desired surface microstructures, are stored in a PC. The data stored on the hard disk of the PC are first transferred to the random-access memory (RAM) of the PC before fabrication. When the fabrication starts, the data in the RAM are then output to the CNC one by one through a 16-bit digital-to-analog (D/A) converter responding to the output signals of spindle rotation positions from the interpolator. High-speed data transfer from the memory to the FTS controller is carried out by using the function of direct memory access. Since the data

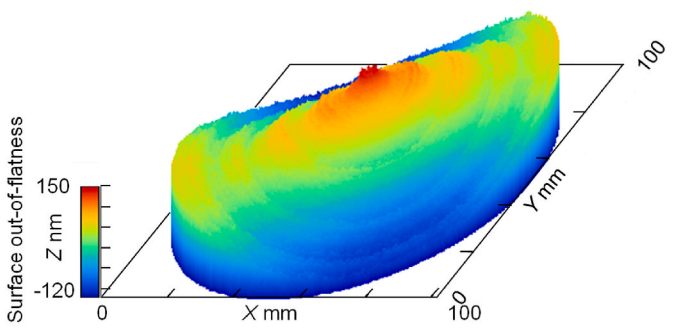

(a)

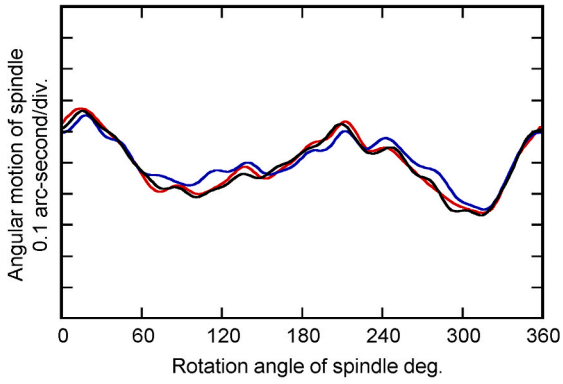

(b)

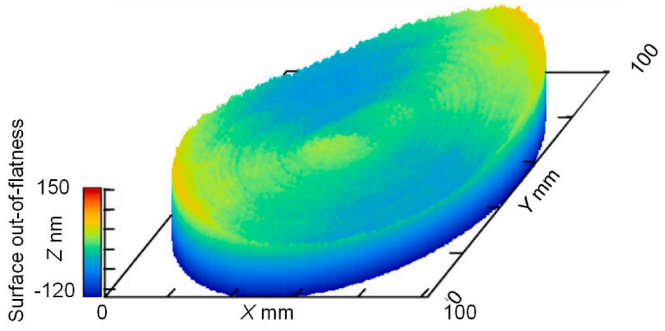

(c)

Fig. 55. Compensation on an ultra-precision lathe [232]. (a) The surface out-of-flatness of a facing-cut workpiece by the ultra-precision lathe without machine error compensation. The surface out-of-flatness with a peak-to-valley magnitude of 0.27 μm is composed of a periodic component along the radial direction of the workpiece surface with a pitch of approximately 11 mm and a 2 upr (undulations per revolution) component around the circular direction of the workpiece surface. (b) Measurement results of angular error motion $e_a(\theta)$ of spindle [232]. Three repeated measurement results are shown in the figure. $e_a(\theta)$ has a 2 upr component with a peak-to-valley amplitude of approximately 0.3 arcseconds. (c) The result of compensation cutting by FTS. The peak-to-valley (PV) value of the surface out-of-flatness was reduced to approximately 0.12 μm.

file is too large (approximately 3 GB) to be stored in the RAM at the same time, the RAM is divided into two parts. One updates the data from the hard disk, while the other transfers the data to the FTS controller. By using this technique, data exceeding the RAM capacity can also be output continuously.

Fig. 55a shows a facing cut result on an aluminum workpiece with a diameter of 150 mm by the ultra-precision lathe without machine error compensation by the FTS [232]. In the facing cut, the tool was moved by the *X*-slide against the workpiece being rotated by the spindle while the depth-of-cut of the tool was kept constant. As can be seen in the figure, the surface out-of-flatness was approximately 0.27 μm, which is composed of two major components: a periodic component along the radial direction of the workpiece surface with a pitch of approximately 11 mm and a 2 upr (undulations per revolution) component around the circular direction of the workpiece surface.

The specific error motions of the slide and spindle that could possibly cause the surface out-of-flatness were measured. The axial error motion $e_f(\theta)$ of the spindle was measured to be approximately 5 nm, which was too small to cause the surface out-of-flatness of the facing cut workpiece shown in Fig. 55a. On the other hand, as demonstrated in **Section 3.1.3**, the *X*-slide of the ultraprecision lathe had a straightness error motion $e_Z(x)$ of approximately 60 nm over the 80 mm travel. The peak-to-valley (PV) of the periodic component was approximately 20 nm with a pitch of 11 mm, which was corresponding to the diameter of the rollers used in the *V–V* shaped bearing of the *X*-slide. Obviously, the periodic component of the surface out-of-flatness of the facing cut workpiece was caused by $e_Z(x)$. The tilt error motion $e_a(\theta)$ of the spindle about the *Y*-axis was then measured. A photoelectric autocollimator was mounted on the *X*-slide for the measurement. An aluminum-coated glass disc with a thickness of 15 mm and a diameter of 100 mm, which was vacuum-chucked on the spindle, was employed as the reflector for the autocollimator. The surface out-of-flatness of the glass disc was approximately 10 nm. The large beam diameter of the autocollimator, which was 30 mm, acted as a filter to reduce the influence of the out-of-flatness of the glass disc.

Fig. 55b shows three repeated measurement results of $e_a(\theta)$. It can be seen that $e_a(\theta)$ was measured to be approximately 0.3 arcseconds, which corresponds to a 73 nm axial error motion in the *Z*-direction at an *x*-position of 50 mm relative to the spindle axis. Since $e_a(\theta)$ was dominated by a 2 upr component, it indicates that the 2 upr error component of the surface out-of-flatness of the facing cut workpiece along the circular direction shown in Fig. 55a was mainly caused by the angular error motion of the spindle. Fig. 55c shows the result of the compensation for face cutting by the FTS. The machine error components were compensated based on the measurement result of each machine error. The peak-to-valley (PV) value of the surface out-of-flatness of the face cut workpiece shown in Fig. 55c was approximately 0.12 μm, which was less than half the surface out-of-flatness before compensation by the FTS shown in Fig. 54. A comparison between the results before and after compensation by FTS reveals that the periodic out-of-flatness component with a radial pitch of 11 mm in the workpiece surface, which was caused by the straightness error motion $e_Z(x)$ of the *X*-slide, was removed. The 2 upr out-of-flatness component around the circular direction of the workpiece surface, which was caused by the tilt error motion $e_a(\theta)$ of the spindle, was also greatly reduced.

Recently, with the development of open controller architecture (Open CNC), it becomes easier for a PC-based FTS to access the CNC for obtaining machine axis positions and for uploading CNC data for FTS compensation [444]. Software interfaces such as application programing interfaces, and hardware interfaces such as Recommended Standard 232C (RS-232C), optical fiber, Universal Serial Bus (USB), and Ethernet network interface are now equipped in a CNC for communication with a PC. On the other hand, the performance of FTS has been improved with the advancement of sensor and actuator technologies [445]. FTS is now also commercially available [446] [447]. All of these developments will expand the flexibility and application range of FTS-based compensation for machine errors. In addition, a force sensor integrated FTS (FS-FTS) [448], has been developed for a nano-cutting instrument to conduct FTS diamond turning [449]. By using the FS-FTS, the diamond cutting tool, which has been conventionally only used for cutting operations, can be employed as a force-controlled measuring stylus for various measuring

operations [450] [451] [452], which is expected to expand the applications of FTS technology.

5.2. Compensation of thermally-induced errors

Since thermally-induced errors have significant influences on the positioning accuracy of machine tools, it is desired to reduce or compensate the thermal errors. Reduction of thermal errors is generally considered in the design phase of machine tools and includes reducing or isolating heat sources, cooling, or making the machine less sensitive to temperature variations. Examples are the use of materials with less friction like ceramic balls for bearing [453] or materials having a negative linear expansion coefficient like carbon fiber reinforced plastics (CFRP) [454] [455]. The optimization of lubrication is also a good way for the reduction of thermal errors [42]. [456] describes another effort to reduce the thermal deformation of machine tools by applying Coanda-effect cooling to spindle housing of a turning center. However, thermal reduction by using advanced materials might increase the cost of machine tools, and compensation of thermal errors may be a more cost-effective way to improve accuracy [3].

The compensation of thermally-induced errors normally relies on a predictive model that is built based on measurement of the machine temperature distribution typically by temperature sensors placed at critical points on the machine tools structure as well as measuring the thermal errors in tool position and orientation. The goal is an accurate model to predict the thermally-induced errors of machine tools for any specific temperature condition, based on which the necessary compensation values can be calculated and incorporated to the motion axes for compensation. Fig. 56 shows a common procedure for thermal error compensation. Moriwaki [274] summarizes the transfer functions between spindle speed and thermal deformation, as well as ambient temperature and thermal deformation. He then estimates and compensates thermal deformation through transfer function and convolution integral, reducing the machining error caused by spindle speed and ambient temperature to less than 15%. Gebhardt et al. [382] introduced a high-precision grey box model for predicting errors caused by internal heat sources such as drives or bearings. It is verified by experiments that 85% of the thermally-induced positioning errors can be corrected by this model.

Compensation strategies based on empirical models enable a data-based and efficient reduction of thermally-induced errors. However, the accuracy of the model depends on the characteristics of the training

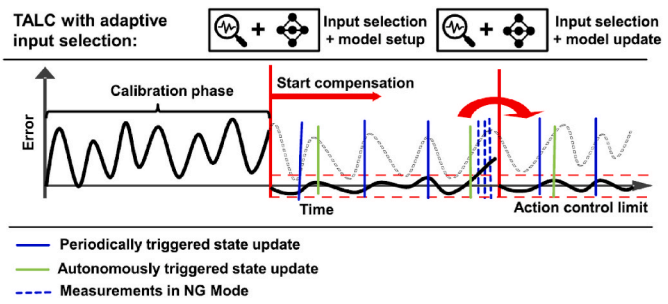

Fig. 57. Concept of the TALC with the adaptive input selection including the periodically and autonomously triggered on-machine measurements [384]. The purpose of the TALC method is to reduce the tool center point (TCP) deviation caused by the mark end error at the mark end and improve the long-term robustness of the phenomenological compensation model by combining the phenomenological compensation model with machine measurement. The input of the TALC method is static and predefined before starting the calibration phase.

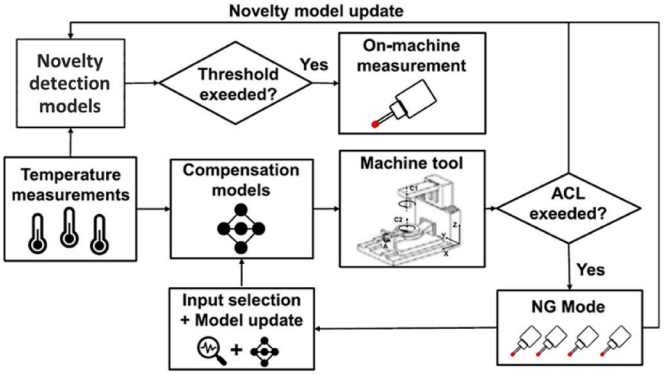

Fig. 58. Integration of the novelty detection model for on-demand triggered ST updates into the TALC [384]. An adaptive input selection iterative procedure is developed, including the main steps of creating a compensation model for each thermal error, and normalize the time series of the measured temperature and the time series of the thermal error considered to achieve a detailed comparison of the original time series with different scales.

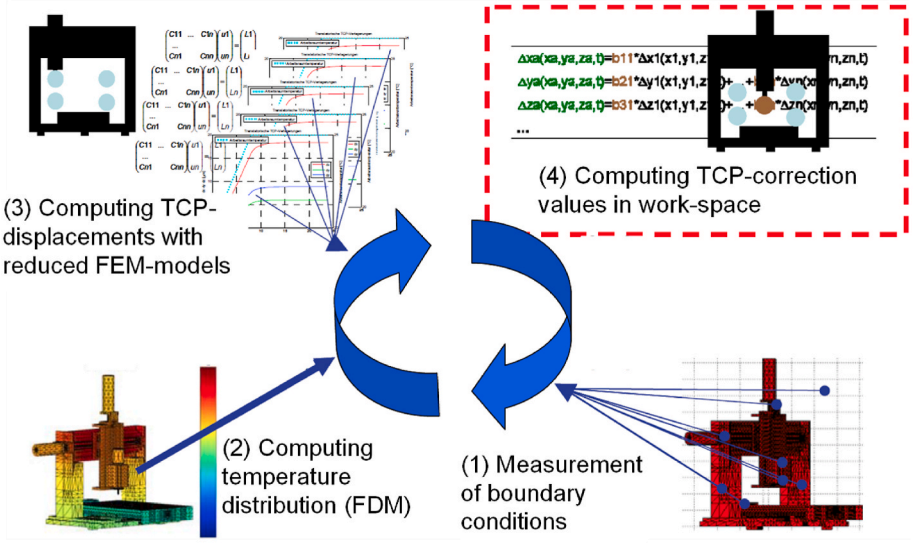

Fig. 56. Diagram of a thermally-induced error compensation procedure, (1) measuring boundary conditions, (2) computing the temperature distribution, (3) computing TCP displacements in the working envelope using reduced FEM models, (4) computing thermal locations and component errors for compensation [457].

data and the model does not have the ability to adapt or self-optimize. To deal with such problems, AI and ML based compensation methodologies are developed recently [434] [458] [459] [460] [461]. Zimmermann et al. [384] provide the foundation of self-learning compensation models for thermally-induced errors by developing the thermal adaptive learning control (TALC), which improves the long-term robustness of compensation results with respect to changing boundary conditions [462]. They developed a smart method for thermal adaptive learning to select the optimal input for the compensation model. Each input is automatically adjusted and the model is automatically calibrated after the initial model is built, without relying on detailed prior knowledge about thermal behavior (Fig. 57). This method significantly increases the self-optimization ability for compensation of thermally-induced errors by triggering on-machine measurement when an unknown thermal condition occurs (Fig. 58). TALC also increases the uptime and productivity of machine tools without reducing the precision of the compensation results. A thermal displacement compensation method using deep learning to change the compensation weight adaptively was developed by a commercial machine tool company [451]. By adjusting the compensation values based on the uncertainty, the method can prevent the deterioration of accuracy due to extreme prediction values caused by sensor failure [463]. A method of thermal error prediction and compensation for five-axis machine tools based on supervised online ML was proposed by researchers in Switzerland [454]. Based on the change and state of ambient temperature, load and boundary conditions, the thermal displacement of the tool center point is predicted and compensated to reduce most thermal errors [383]. Fabian Stoop proposed a cloud-based thermal error compensation method for cross-border federated learning of machine tools to compensate the thermal error of machine tools [424]. This method allows training of shared models locally derived by machine learning methods from a large number of distributed systems, the key thermal error of the machine tool is reduced by more than 80% under the best conditions [436]. Table 15 shows a summary of compensation methods for thermal errors.

5.3. Compensation of static load-induced deformation

A predictive compliance-based model for compensation in multi-pass milling by on-machine probing is introduced in Ref. [464]. In the presented method, a process-intermittent gauging by on-machine probing detects errors due to the cutting action such as system deflection, with a particular focus on milled thin wall parts. A general model is presented which relies solely on probing data from semi-finishing cuts to compensate the final cut. A variable cutting compliance coefficient relates the total system deflection to the depth of cut. The effect of both changes in the final depth of cut and the reduction in part compliance are anticipated by the model-based approach to more effectively compensate the final cut. Experimental validations for the milling of a straight thin wall and for a hole with variable wall thickness show that the compliance induced error is essentially eliminated using the proposed model compared to only 60% for a noncompliance-based approach.

To combine the quasi-static kinematic errors with spatial variation of static stiffness and resulting compliance deviations of machine tools a method describing synthesis of bottom-up and top-down model building approaches was proposed in Ref. [465]. The study introduces a characterization of the position- and direction-dependent static stiffness and presents the identification of the effects of the quasi-static machine tool behavior on the part accuracy.

[466] introduces a deformation compensation method for the case of machining large thin-walled parts. The compensation of cutting force induced deviations is performed with the adjustment of axial cutting depth and is built on the coupling effect of the axial cutting depth and the cutting force itself. The efficiency of the iterative method is dependent on reaching a sufficient convergence, which has to be reached within a short time period (real-time). The method is demonstrated for both first-order and higher-order convergence in both the simulation and the experiments for machining square pockets.

5.4. Compensation of dynamic errors

Dynamic errors due to the motion control and/or the structural vibration that occur during cutting are copied to the machined surface

Table 15
Summary of compensation methods for thermal errors.

Methods	Compensation steps	Characteristics	Effectiveness
Thermal Adaptive Learning Control methodology [384]	1. Calibration thermal error and setup the model 2. Adaptive input selection and start compensation 3. Update model and repeat compensation process	- Model input does not rely on detailed prior knowledge of thermal behavior	- The robustness of the compensation model is significantly improved. - The measurement time required by the method is reduced by 45%.
Compensation through grey box model [382]	1. Measuring the thermally induced displacement of shaft 2. Establish grey-box model of thermal displacement 3. Model-based compensation	- The model corrects the error of tool center point based on internal signal. - It can directly be implemented in machine tool controls or in a pre-processing CAM software.	- The model can correct the thermal positioning error of the machine tool up to 85%.
Method of using measured transfer function and convolution integral [274]	1. The transfer function of temperature and thermal deformation is obtained through experiments 2. Measure the heat change caused by the environment and the spindle rotation 3. Compensation for thermal deformation based on transfer function and heat change	- Does not need any sensor of the internal heat source in the processing process, but only uses the measured transfer function and a thermocouple to measure the ambient air temperature. - The transfer function depends on the rotational speed. This method needs to measure the transfer function at different rotational speeds.	- Reduce the processing error caused by the change of ambient temperature and the heat generated by the rotation of the main shaft to less than 15%.
Online machine learning based on process intermittent detection information [433]	1. Measure the thermal error and the current boundary and processing conditions to obtain the parameters of the thermal prediction model 2. Establish thermal error model 3. Compensate the thermal error by adaptive control	- By extending the weighted matrix of Least Squares estimation of system parameters, any sampling rate from any tool center point measurement can be processed. - It is feasible to dynamically adjust the action control limit to the expected accuracy of the machine compensation method.	- By continuously adjusting model parameters, the downtime of modeling is almost eliminated. - In a 88 h experimental study, the compensation reduced the error by more than 95%.

resulting in the deterioration of the machining quality. Therefore, counter measures to reduce dynamic errors are of interest to industrial researchers and engineers. When a machine tool with low damping and low stiffness is operated, its motion control must be designed to avoid excitation of the machine structure. This problem is particularly important in control of motion with high acceleration and deceleration.

A simple solution is filtering to avoid resonances. Low pass filters can be easily used for eliminating vibrations with high frequencies. However, in that case, the response bandwidth of the feed drive is limited by the first natural frequency. Thus, notch filters such as finite impulse response (FIR) and infinite impulse response (IIR) filters are used in commercial servo controllers to selectively attenuate vibrations for a preset frequency. The notch filter increases the phase delay in the servo response that can cause an oscillation in higher frequency ranges. IIR filters can be used to tune the notch depth and phase delay for avoiding such unexpected oscillation [467].

Modification of the motion command is also a popular approach to decrease the dynamic errors. As shown in Fig. 59, acceleration filtering with moving average filters is widely used to have vibration attenuation that is similar to the notch filters [468] [469]. Filtering is included in this review as a compensation technique to reduce dynamic errors for its easy implementation. The shortcoming of acceleration filtering is the increase of positioning time or delay when reduction of the low frequency vibration is targeted. To overcome this shortcoming, improved acceleration profiles were designed by optimizing the parameters of the spline function [470] and tuning the segmented acceleration time [471]. The input shaper that cancels the residual vibration by an impulse excitation with a delay of half the vibration period is also a popular approach [472] [473]. However, whereas these methods based on trajectory generation effectively suppress vibration in motion control without machining disturbance, they are not effective in the motion control with disturbance.

In contrast to software approaches, many mechanical and mechatronic devices have been proposed to reduce the dynamic errors by modifying the dynamic characteristic of the machine. Tuned mass damper (TMD) and active mass damper (AMD) are popular and practical approaches because an additional device can be attached without drastically modifying the entire machine structure [474] [475] [476]. Because its target frequency can be tuned, AMD can be used to adaptively compensate the dynamic errors that vary due to position

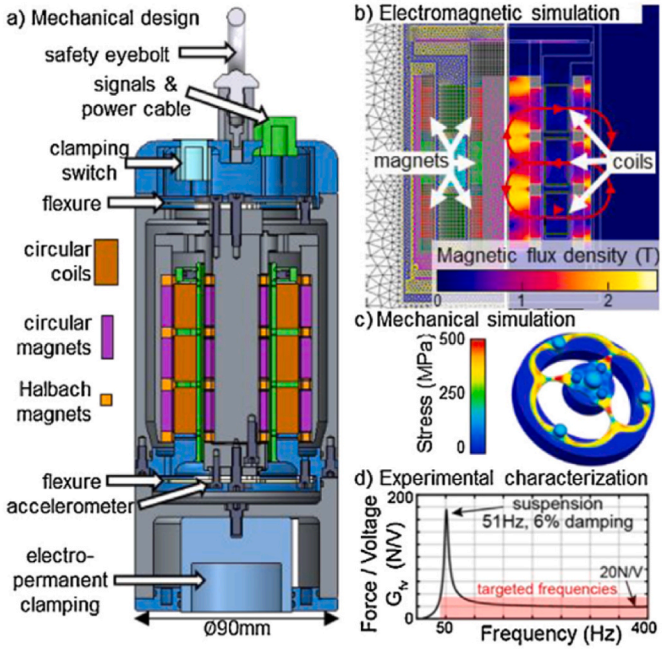

Fig. 60. Portable active mass damper (AMD) for machining flexible workpiece [477] (a) Mechanical design. (b) Electrical simulation. (c) Mechanical simulation. (d) Experimental characterization. The damper can be attached directly to the workpiece by the magnet.

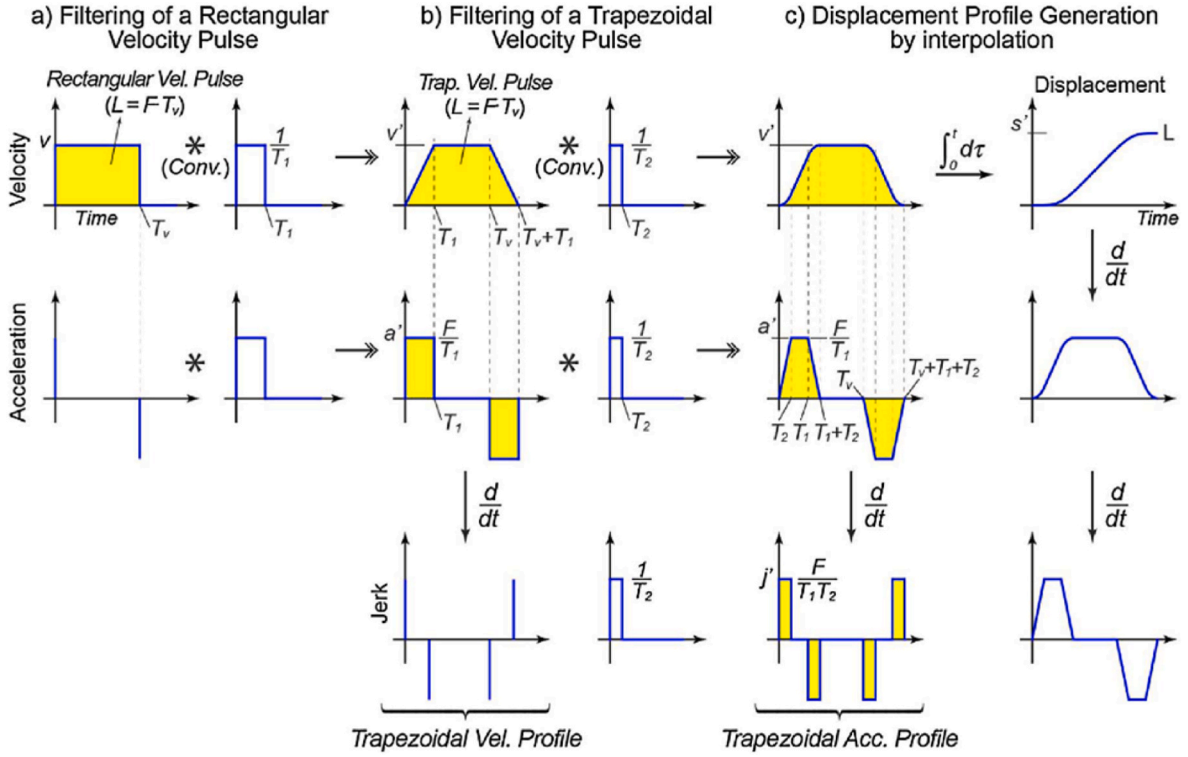

Fig. 59. Motion command generation using finite impulse response (FIR) filter [469]. (a) Filtering of a rectangular velocity pulse. (b) Filtering of a trapezoidal velocity pulse. (c) Displacement profile generation by interpolation. The FIR filter selectively attenuate vibrations for a preset frequency.

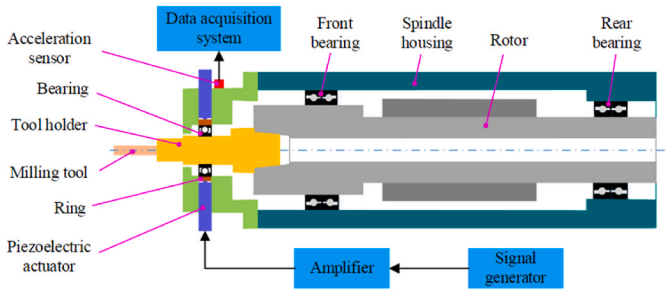

Fig. 61. Spindle equipped with stiffness tuning function using a piezoelectric actuator [487]. The stiffness of the front bearing is changed to achieve the anisotropic stiffness for reducing the vibration.

dependent dynamics and aging. Fig. 60 shows a recently developed small portable AMD that can be easily attached to the object by a magnet [477]. Application of various damping elements such as viscoelastic material [478] [476] [479] [480], high-damping interfaces [481] [482] [483], magneto–rheological fluids [484], air viscosity [474], and eddy current [485] were investigated.

An additional reinforcement beam was temporally attached to tune the workpiece stiffness [486] although this approach may not be practical when modification of the entire machine is targeted. Stiffness tuning of the machine component is possible using its preload dependency for bearings and contacted joints. As shown in Fig. 61, spindle stiffness [487] and support stiffness [61] were tuned by changing the preload. The dynamic error reduction by anisotropic stiffness has been studied based on such stiffness tuning methods [486] [487]. The dynamic error in one direction can be canceled by coupled vibration in the other direction in the anisotropic design [488].

To reduce dynamic errors caused by the machining process, the first thing to consider is the optimization of machining conditions. By carefully selecting the spindle speed and depth of cut, a highly efficient condition called "stable pocket" can be reached where chatter is avoided at relatively large depth of cuts. As shown in Fig. 62, methods using the Stability Lobe Diagrams (SLD) [6] or measurement signals during machining [489] have been proposed to identify these regions. On the other hand, in the stable pockets, forced vibration increases because the natural frequency of the system corresponds to the tooth passing frequency or its harmonic components. Therefore, comprehensive measures must be taken to prevent both chatter and forced vibration simultaneously [490].

The main mechanisms causing chatter vibration are regenerative effects and mode coupling. Only regenerative effects occur in turning operations, but in milling operations, regenerative effects and mode coupling usually occur simultaneously triggering chatter vibrations. Many advanced approaches have been proposed to mitigate each of

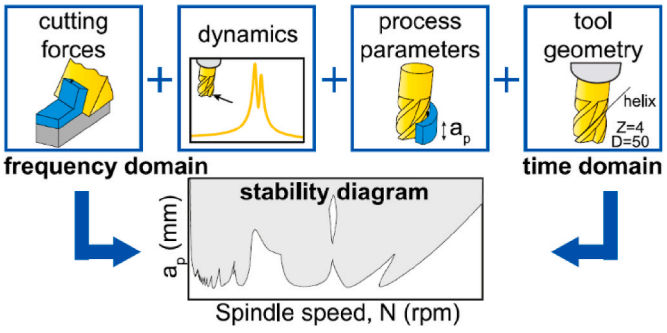

Fig. 62. Procedure to obtain stability lobe diagram [6]. This example demonstrates that frequency-domain and time-domain simulations from the machining process, dynamics, and various parameters can be used to estimate stable and unstable regions with respect to spindle speed and depth of cut.

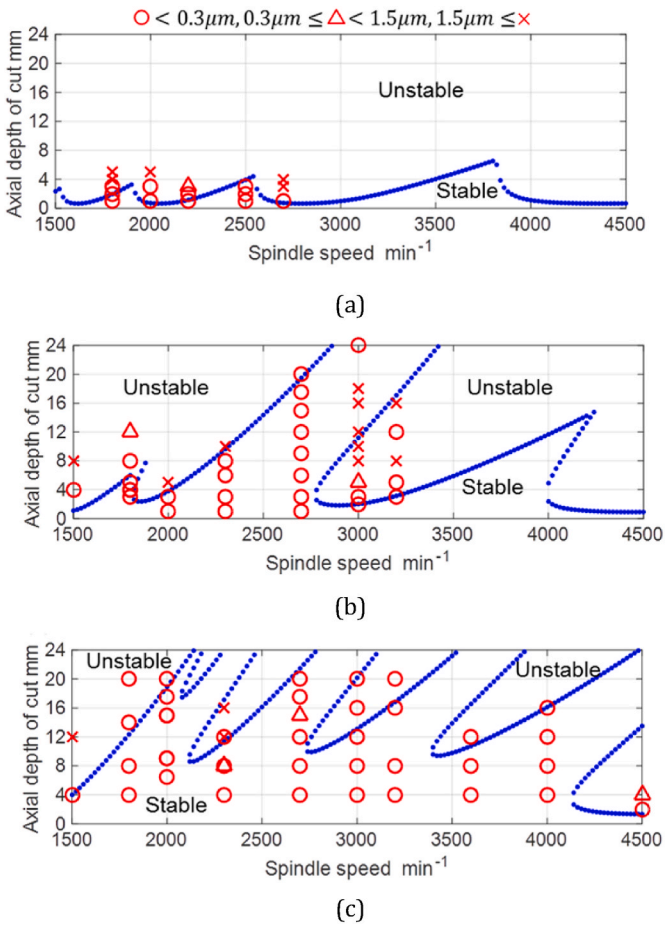

Fig. 63. Comparison of calculated stability lobe diagrams and experimental results with (a) regular pitch end mill (b) irregular pitch end mill with APV design (c) irregular pitch endmill with optimal design [493]. In this example, the irregular pitch endmill improved chatter stability by canceling out the regenerative effect. The dependence of chatter stability on spindle speed and depth of cut varies significantly depending on the pitch angle design, so optimal design is important.

these mechanisms. To suppress regenerative effects, irregular pitch and/or variable helix cutter designs are effective [491] [492], and an optimal design method that is robust for chatter frequency change has been proposed [493], as shown in Fig. 63. For mode coupling, effective measures are to provide anisotropy in dynamic stiffness to prevent interference between flexible modes, and selection of low immersion conditions with a small radial depth of cut. Optimization of the tool posture can be effective in suppressing chatter in terms of both structural dynamics [494] [495] and process force gain [496]. This approach is particularly advantageous in the processes that use multi-axis machine tools with flexible mechanical structures, such as robot machining.

Other methods have been proposed, such as varying the spindle rotation speed [497] [498] and actively using process damping [499]. In parallel turning and parallel milling, where multiple tools are used simultaneously, measures to slightly shift the tool position from a fully symmetrical arrangement [500] and the use of tool rotation speed difference [501] have also been proposed. Adaptive control strategy to mitigate regenerative chatter vibration utilizing machine tool feed drives [502] is an interesting challenge. Both measures have the effect of reducing the gain in the feedback loop consisting of the machining process and the machine dynamics. On the other hand, there is no broadly applicable, definitive solution, and appropriate methods must be selected according to the constraints of the machining process.

Table 16 summarizes the introduced compensation methods. The

Table 16
Summary of compensation methods for dynamic errors. * low, *** high.

Category	Methods	Installation cost	Effect	Cutting-edge technology
Software condition modification approach	Filtering [467]	***	*	Adaptive control strategy [502]
	Command modification [468–473]	*	*	
	Cutting condition modification [6,489,493,494–496]	*	***	
Hardware approach	Additional damper [478,474–476,479,480,484,485]	**	**	Wireless and portable device [477]
	Stiffness tuning [61,486–488]	***	**	

Table 17
Summary of the technological elements for calibration of machine tool errors.

Error sources	technological elements		
	Measuring methods	Modeling theories	Compensation strategies
Quasi-static kinematic errors	[Direct measurements] ■Described in ISO 230-1:2012. ■Artefact-based or optical. [Indirect measurements] ■dentification of individual kinematic error by "best-fitting" of kinematic model. ■Measurement of TCP positions: artefact-based or optical methods. For longer linear axes, the limited availability of artefact can be an issue. ■For rotary axes, single point tests are well established. Separation of rotary and linear axis kinematic errors can be an issue. ■Target kinematic errors to identify: intra-axis or inter-axis errors. ■Multi-axis coordinated motion trajectory" tests (e.g., circular tests). ■Self-calibration methods for ultra-precision and large-sized machines.	■Rigid-body kinematic models are well established. Various representations are available. ■Its extension to non-rigid body kinematic errors is possible. ■ML approaches can be applied for e.g., accuracy degradation and fault detection.	■Physical and empirical compensation of squareness errors. ■Original Equipment Manufacturer (OEM) for backlash compensation. ■OEM for linear positioning error compensation. ■OEM for Sag and multi-axis compensation. ■OEM volumetric error compensation (compensation based on multi-dimensional error tables and TCP compensation). ■Model-based compensation using modified G-code. ■Fast tool servo for precise and high-bandwidth compensation.
Thermal errors	[Direct measurements] ■Described in ISO 230-3:2020. ■Direct measurement of thermal deformation through sensors. ■Measurement performances only determined by those of the sensor. ■Interaction of multiple heat sources (composite thermal error) during machine operation and their effects in the full work volume can be improved with more clever measurement strategies or artifacts (sometimes based on the user specified machine operation regimes). [Indirect measurements] ■Indirect measurement by machining test artifacts described in ISO 10791-10:2022. ■Indirect measurements based on machine learning methods with effective prediction of thermal errors but requiring a large number of experimental data for establishing the ML tool.	[Temperature-based approaches] ■The heat source and thermal deformation are used as inputs and outputs respectively, the model is established through FEM, FDEM, the linear least square regression, etc.. ■The model based on temperature input could be used for calculating the static and dynamic machine characteristics. [Artificial intelligence and machine learning methods] ■AI and ML are adaptive to complex processing conditions, such as different feed rates, rotational speeds, and ambient temperatures. ■Modeling by AI and ML does not depend on massive and complete data information, making it the most promising modeling method.	[Compensation by advanced materials] ■Compensation by the use of materials and designs with less friction or materials having a negative linear expansion coefficient. [Compensation by models] ■Compensating for thermal errors through measured thermal deformation and established models can achieve compensation for all thermal errors of the machine tool. ■Compensation can directly be implemented in machine tool controls or in a pre-processing CAM software through ML and AI, and does not rely on detailed prior knowledge of thermal behavior. ■Compensation by online ML is adaptive to dynamically adjust the action control limit to the expected accuracy, the method could process sampling rate from any tool center point measurement.
Elastic deformation	[Stiffness measurements] ■Described in ISO 230-1: 2012 [224]. One axis loading device and displacement sensor is used. ■Devices for multi axes loading and displacement measurement were developed. [Motion trajectory measurements under loaded condition] ■Telescoping ball bar integrated with a loading device was developed.	■Stiffness model is developed for the component chain between tool and workpiece. ■Six-dimensional stiffness matrix at each tool center point in work space is modeled to consider its position dependency.	■Variable depth of cut for canceling deformation effect.
Dynamic errors	[Tracking error measurements] ■Measurements by integrated position detectors is possible in operational conditions. ■Errors at tool center point is mainly measured in offline state. [Frequency response measurements] ■Typically obtained by excitation and response measurements. ■Model based modal parameter identification in operational conditions is possible. ■ML is used to estimate the position dependent dynamic response variation.	■FEM or multi body models considering non-linear characteristics at mechanical interfaces. ■Modeling of process-machine-interaction to simulate dynamic errors triggered by forced vibration and/or self-excited vibration. ■ML is used to predict the stability lobe diagram.	■Trajectory generation with filtering to avoid resonance excitation in motion control. ■Modification of dynamic characteristic of the machine by tuning mass, damping, and stiffness. ■Optimization of machining conditions and tool geometry to avoid dynamic errors due to chatter vibration.

modification of cutting conditions is a current popular approach for machine tool users because of its low installation cost. However, the allowable machining condition is still limited by the dynamic response of the machining system. The hardware approach can be more effective in many cases because it improves the dynamic response. Wireless and downsized addon devices for decreasing the vibration can be expected as a near future solution.

6. Conclusion remarks, challenges and future opportunities

6.1. Conclusion remarks

1) General issues

Quasi-static kinematic error, thermal error, elastic deformation, and dynamic error have been described in this paper as the major error sources for machine tool calibration. Measuring instruments/methods, modeling theories and compensation strategies for each of the errors, which are summarized in Table 17, have been presented as the technological elements.

It should be noted that the roles and applicability of each of the technological elements may vary with the machine structure, number of axes, types of machine components, foundation, environmental temperature conditions, process forces, workpiece weight, feed rate, etc. This requires machine tool users to make a proper selection of the technological elements in the machine tool calibration. Table 18 shows some generalized indications on the roles and applicability of the technological elements from the viewpoint of machine tool types.

As shown in Table 18, machine tools can be categorized based on the size of machine work volume, with which the roles and applicability of the technological elements may change. Most small-sized machine tools with a size of the work volume in the order of 0.5 m or less, which are typically used to fabricate molds of small-sized optical or electronic devices, have light workpieces, moderate machining forces and repeatable machine motions while the influence of thermal errors is relatively small. All these make it effective to implement the measuring methods and compensation strategies while the modeling theories are less important, although the size of a typical commercial measuring instrument may be a limitation to fit in very small size machines and bring challenges to the measurement. On the other hand, when the size of a machine tool gets larger than 1.5 m, i.e., a large-sized machine, the measurement of kinematic errors gets difficult due to the limited availability of the measuring instruments and the reference artifacts, while the self-calibration techniques may provide a solution to this problem. The large mechanical loop from the tool to the workpiece results in a low machine stiffness. Complicated and difficult-to-predict machine deformations can result from the large masses of the workpiece and the machine axes. The influence of thermal errors is also large. Due to its relatively large volumetric errors, numerical compensation is often of more importance, although its precise kinematic modeling contains many technical challenges, related to larger work volume, long machining time, significant temperature changes, and complicated workpiece structures.

The normal-sized machine tools form the largest group of machine tools. A sub-categorization is further made in Table 18 based on the number of axes, which is often an indicator of the complexity of machine structure. As a two/three-axis machine tool, an ultraprecision lathe based on diamond turning has a simple machine structure with two or three linear axes, which does not require a complicated modeling theory. Diamond machinable materials are typically soft metals and the cutting force is generally small, resulting in small elastic deformation and dynamic errors. The cutting tool motion is transferred to the workpiece surface with a high accuracy associated with a material removing mechanism of single-point cutting with a diamond cutting tool. An ultraprecision lathe is often operated in a temperature-controlled environment and the error motions of the axes have a high repeatability. Due to these reasons, the most significant error source for an ultraprecision lathe is the kinematic errors of each machine axis, particularly the slide straightness error and the spindle axis of rotation error motion. The implementation of measurement technologies and compensation strategies of the kinematic errors thus plays an important role in calibration of an ultraprecision lathe. Meanwhile, for ultraprecision machines, the measurement uncertainties are much closer to machine precision/resolution, which brings challenges to the measurement. The self-calibration techniques are effective for addressing such challenges. The thermal errors will be significant when an ultraprecision lathe is employed to cut large-area 3D microstructures surfaces, which takes a long time. The dynamic errors can also be an issue when an ultraprecision lathe is employed to cut brittle materials. For a general-purpose two/three-axis cylindrical grinding machine or a surface grinding machine, the role of modeling theory is also weak due to the simple machine structure, which is similar to an ultraprecision lathe. Meanwhile, since a grinding machine is associated with a much larger machining force, the impact of elastic deformation, together with the thermal errors and dynamic errors, increase significantly. The material removing mechanism is also much more complicated compared with diamond turning. For these reasons, the implementation of measurement technologies and compensation strategies on a grinding machine tends to be more difficult.

As shown in Table 18, a machining center or a turning center can be a three-axis machine with linear axes only, or be a four/five-axis machine with one or two additional rotary axes. Due to the complicated machine structure, large depth-of-cut, severe machining environment, fast machining speeds, relatively long tools, the impact of thermal errors and dynamic errors are regarded as the most significant error sources in a machining center or a turning center. Kinematic errors, particularly position and orientation errors of rotary axes, can be a major source for workpiece geometric errors on four/five-axis machining centers or turning centers. On machines with rotary axis (axes), even under relatively simple thermal deformation, where only the linear positioning error of linear axes is thermally influenced, it changes the position and orientation errors of rotary axes with respect to linear axes, which can result in significant workpiece geometric errors. On three-axis machines, the linear positioning errors of linear axes typically cause workpiece dimensional errors only. Thermal errors can be more critical on five-axis machining centers or turning centers. Modeling theories play an important role especially for five-axis machining centers and turning centers. Model-based measurement and compensation strategies have also been well developed for machining turning centers or turning centers and are effective particularly for machines with rotary axes.

The information for four/five-axis laser or wire electro-discharge machines are also illustrated in Table 18. These machines have several linear and rotary axes that must be compensated to obtain an accurate cutting geometry on the workpiece. In such a machine, the machining force is negligible compared to the rigidity of the axes and the machine frame. Axis position/orientation errors are the largest compared to kinematic and structural deformation errors. The control of the workpiece geometry on these two processes is linked to the position/orientation control of laser beam or wire in the EDM and the wire/laser-material interaction. In addition, for laser cutting, the laser power, the feed rate, and the focal point are essential to control the laser-material interaction. The laser-material interaction can cause an increase in temperature of the cut part and influences the temperature of the machine structure. In consequence, the compensation of the quasi-static errors has been less developed in this type of machine and their measurement methods have been developed, principally, by the machine manufacturer. For EDM, the wire deformation under the action of electrical discharge must be considered for an efficient control of the machined geometry. The cutting process is made in deionized water or special dielectric oil. These liquids are filtered, and their temperature is regulated. In consequence, the axes and the structure of the machine are not influenced by the temperature due to cutting.

The information in Table 18 only provides readers a very rough picture about the roles of the elementary technologies for machine tool calibration. All the indications shown in the table may vary with a specific machine tool, the environment where the machine tool is operated, the sizes, geometries, masses and materials of the workpiece and tool, as well as the machining parameters, etc.

On the other hand, machine tool users are interested only in the machining performance for their specific machining applications. As

Table 18
Roles of technological elements for calibration of different types of machines. * weak, *** strong.

Type of machine			Technological element		
			Measuring methods	Modeling theories	Compensation strategies
Small-sized machine (work volume: 0.5 m or less)	Small-sized machining center or turning center, micro/nano-fabrication machine, small-sized laser cutting machine, T-base diamond turning machine, ultraprecision grinding machine, etc.		**	*	***
Normal-sized machine (work volume: 0.5 m–1.5 m)	Two/three-axis machine	Ultraprecision lathe (single-point cutting/small depth-of-cut/small machining force)	**	*	***
		General purpose cylindrical grinding machine and surface grinding machine (abrasive process/small depth-of-grinding/large machining force)	**	*	**
		Three-axis machining center or turning center with linear axes only (multi-point cutting/large depth-of-cut/medium machining force)	***	**	**
	Four/five-axis machine	Four/five-axis machining center or turning center with rotary axis (axes) (multi-point or single-point cutting/large depth-of-cut/medium machining force)	***	***	***
		Four/five-axis laser cutting machine (vaporization or melting process/no machining force)	**	*	**
		Four/five-axis wire electro-discharge machine (erosion process/no machining force)	*	*	*
Large-sized machine (work volume: 1.5 m or above)	Bridge-type milling machines, large-sized machining center or turning center, large-sized grinding machine, precision drum lathe, etc.		*	*	*

summarized in Fig. 64, this paper reviewed many potential source sources in a machine tool, and test methods to separately quantify them. It is important to note that the machining process, designed by a machine tool user, determines the relationship between error sources and the machining. Machine tool builders perform a subset of the accuracy tests in Fig. 64. Users want to know if it ensures the machining performance required for their specific machining applications. In our view, this is still an open, unsolved problem. To quantify the relationship between the accuracy tests, performed by machine tool builders or users, and the machining performance, quantitative analysis of the machining process is essential. The modeling of the machine and machining processes, reviewed in Section 4, plays an essential role in this analysis, but it should be tailored for individual machining applications, and more reliable modeling of machine-process interaction may be essential. Accuracy tests should be selected based on such an analysis of target machining applications.

Uncertainty is the most important parameter to evaluate the reliability of the results of machine tool calibration. In machine tool calibrations, the general rule of thumb is to carry out a warmup procedure to bring the machine tool to a "steady state" condition before initiating calibration measurements. The relevant standards assign the responsibility of providing such warmup procedures (along with the necessary environmental requirements, e.g., spatial and temporal environmental temperature gradients, for machine tool to operate within the provided specifications) to the machine tool builders in general. Machine tool user is responsible for providing the specified environment and carrying out required warmup procedures prior to any performance (calibration) measurements. However, during calibration measurements thermal conditions deviate from the steady state conditions, resulting in increased "test uncertainty", which includes the changes in machine

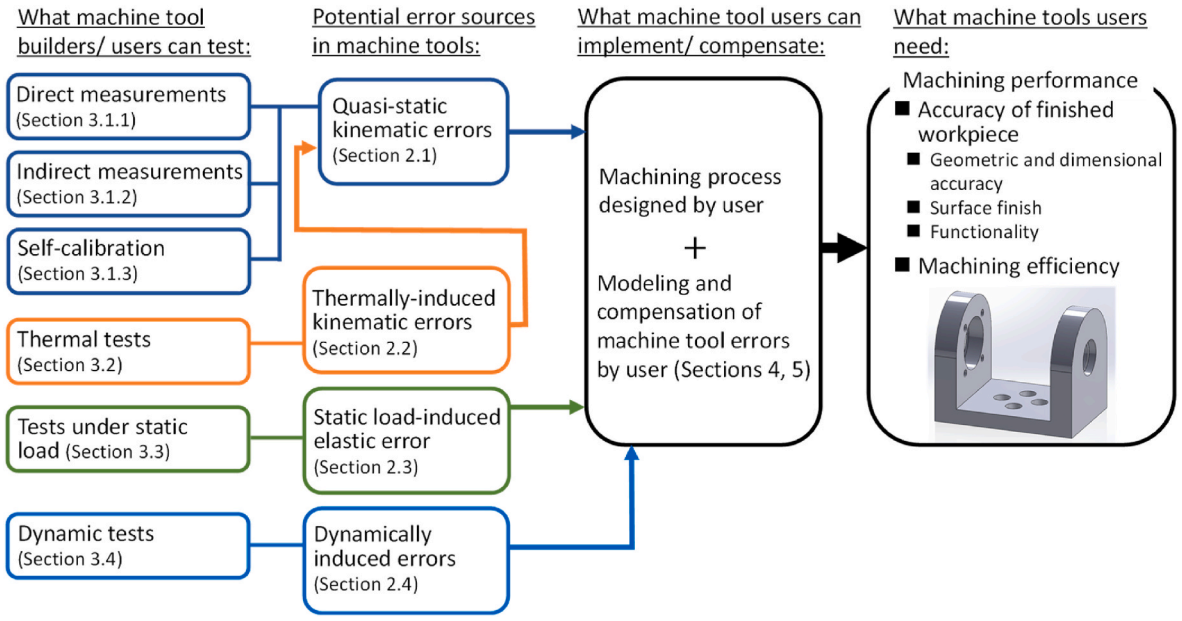

Fig. 64. Summary of potential error sources in machine tools, available tests, and the requirement from machine tool users.

2) Uncertainties in machine tool calibration

behavior during testing. In any case, test uncertainties always tend to dominate the limitation of the calibrations.

Assessment of measurement uncertainties for machine calibrations is provided in ISO/TR 230–9, with some practical examples. The influence of the measurement uncertainty has been discussed in many parts of the manuscript. Section 3.5 ("Error measurement result and uncertainty evaluation") has reviewed research works presenting the uncertainty assessment in machine tool calibration, particularly in direct measurement. Uncertainty in indirect measurements include additional contributors originating from the necessary computational steps. In indirect measurements, the propagation of the measurement uncertainty to the estimation of each error motion should be assessed, which is essential to design measurement conditions and procedures, as is discussed in Section 3.1.2.3. The self-calibration methods, reviewed in Section 3.1.3, are effective in practice to significantly reduce the propagation of the measurement uncertainties both in direct and indirect measurements. Measurement of thermally-induced errors at the tool/workpiece interface point is relatively straightforward utilizing linear displacement sensors against precision artifacts. Uncertainty of such measurements are assessed using well-known methods and are relatively small. On the other hand, estimating thermally-induced errors at any given time based on prior measurements (data-driven modeling) or based on physics-based models is limited by modeling uncertainties.

3) Machine tool errors and workpiece geometrical tolerances

One of the utmost motivations of machine tool calibration is to improve the workpiece geometrical tolerances. In the area of machine tool metrology, deterministic theory dictates that with adequate machine tool kinematic model supplemented with measured errors in 6 DOF, one should be able to reliably predict geometric errors of the machined part. Many studies in literature provided enough evidence about the validity of this theory. In addition, there are many well-established test procedures simulating the generation of various complex part geometries (using multi-axis contouring) that provide confidence in predicting the behavior of machine tool in actual cutting process. However, there are simplifying assumptions, such as rigid body behavior, as well as measurement setup limitations that prevent exact prediction of workpiece errors. One of the ultimate goals of machine tool calibration is to quantify a solid relationship of geometric tolerances of finished workpieces and machine tool and machining process models. For this purpose, quantitative analyses of the machining processes are essential where further research works are expected.

4) Applications of artificial intelligence (AI) and machine learning (ML) tools in machine tool calibration

Taking into consideration that the large number of influencing factors and variables in the manufacturing environment, AI and ML based tools are becoming increasingly important in modeling, compensation and optimization of machine tool errors. For these tools to be effective for real time analysis, availability of large datasets containing information about various categories of machine structures operating in various manufacturing environments, improved computational power and algorithms are required. Especially, as mentioned in **Sections 4.2** and **5.2,** in the field of thermal induced errors which are influenced by multiple varying and interacting internal and external heating and cooling conditions, AI and ML are promising to efficiently bridge the trade-off between precision and productivity. A number of ML methods for self-optimizing thermal error compensation, which improves the long-term robustness of compensation results with respect to changing boundary conditions have already been developed. AI and ML tools are desired to take more effect in future application of machine tool calibration with the aims of increasing of productivity, reduction of necessary sensors and people operations, self-adaption and self-optimizing dealing with varied working conditions.

Uncertainty assessment of measurements assisted by artificial intelligence (AI) and machine learning (ML) tools is an ongoing research area. In fact, there is an effort within the International Academy of Production Engineering (CIRP) to investigate the state-of-the-art in this area to be reported in 2026.

6.2. *Challenges and future opportunities*

Although machine tool performance modeling, calibration, and compensation methods have reached a significant level of maturity over the last decades, they still require high level of engineering and metrology expertise. Furthermore, machine tool calibrations, especially when requiring six-DOF error motion measurements for each machine tool axis, are time consuming and require expensive measuring instruments or special artifacts. In addition, wear, collisions, as well as changing machine loading conditions, manufacturing cycle times, and environmental conditions may require frequent updates to the machine calibrations. Such requirements create significant barriers for industrial applications. Therefore, a future goal in this area is to transition from the use of expensive measuring equipment operated by skilled engineers and technicians and implementing sophisticated models and algorithms developed by skilled engineers as add-on features to existing machine tools towards making these technologies transparent to machine tool users by embedding such capabilities through inexpensive sensors and intelligent self-optimized models and algorithms into machine tools and their control systems. This section summarizes some applications and the efforts towards this future goal.

In manufacturing, machine tools typically operate for more than ten years, likely in poorly controlled environmental conditions. To streamline production and address shortages of skilled labor, self-optimization and characterization of machine accuracy over, preferably, the machine's entire life, has a clear industrial demand. It can be an important part of self-optimization machining systems [434].

Self-optimization and characterization of machine accuracy can be achieved by implementing self-calibration methods. These methods generally rely on conducting multiple simple positioning measurements to form an overdetermined set of equations based on the machine tool kinematic models and solving them to quantify the error motions of individual machine tool axes (these are also covered in indirect methods of calibration section). The multilateration method described in Ref. [16] is the most common example of such calibration. Multilateration-based calibration using tracking interferometers is described in Ref. [126]. As with any measurement method, characterization of measurement uncertainty is important for machine calibrations [503]. In addition to the uncertainty associated with the laser tracker, the effect of environment temperature gradients and air turbulence results in uncertainties as high as 60 μm for typical machine workspaces [504]. To reduce environmental effects, Aguilar et al. developed a telescopic instrument to carry out multilateration measurements [505]. A similar commercial instrument is available [506]. Furthermore, to reduce numerical uncertainties associated with solving the system of equations, redundant measurements are needed, which increase the time and cost of the calibrations. Researchers have investigated how to optimize such measurements to reduce uncertainties by introducing weighted multilateration and different measurement strategies [507] [353] [156]. However, even with those improvements, the effects of thermal drift on measurements still cause concern and provide opportunities for further improvements.

As an alternative to laser interferometric multilateration, indoor GPS (iGPS) systems are attracting attention for potential future use in machine tool calibrations. iGPS systems are currently being proposed for the guidance of robots as shown in Fig. 65 [508]. iGPS uses multiple transmitters located around the workspace of the machine tool to determine the position of a single sensor located near the TCP. Multiple sensors can be located on different components of the machine tool to determine relative positions between those components. A

commercially available iGPS uses fanned lasers generated by a rotating head on transmitters acting as theodolites (see Fig. 66). The sensor detects the laser beams as they sweep past, determining the azimuth and elevation angles. Aangular data from at least two transmitters are used to determine the position of the sensor using triangulation. Redundancy achieved with multiple sensors located on the machine structure relaxes the line-of-sight requirement, enabling reconnecting to transmitters with relative ease [509]. A special touch probe system with three sensors attached to the probe body is described to calculate six-DOF pose measurement at a given position in space, which was applied to robot calibration [510].

There have been several research efforts investigating the performance and related measurement uncertainty of iGPS methods. Heiden and Porath compared the iGPS measurements of a specially designed artifact with the measurements obtained by a CMM, finding up to 500 μm difference between the two sets of measurements [511]. They reported repeatability of iGPS measurements ranging from 10 μm to 160 μm. Wang and Mastrogiacomo compared iGPS measurements with those of laser tracker with special emphasis on dynamic performance [512]. They observed a bias error when the iGPS sensor was moving at speeds above 0.1 m/s reaching a level of around 3 mm–4 mm at speeds of 1 m/s. Schmitt et al. conducted a detailed measurement uncertainty analysis for iGPS using Monte-Carlo simulations of the measurement process with different arrangements of the transmitters [513]. Their results indicated standard uncertainty levels ($k = 1$) of around 150 μm. It should be noted that this level of uncertainty is not acceptable for most precision machine tools. On the other hand, most recently, Nicksch et al. described a systematic approach to assess measurement uncertainties of iGPS systems following the Guide to the Expression of Uncertainty in Measurements (GUM) utilizing a virtual iGPS as a measurement model [514]. All these results point out that iGPS technology needs to improve to be feasible for machine tool calibrations. Further research is needed to reduce measurement uncertainties by optimizing transmitter designs and locations as well as designing new sensor nests.

Vision-based machine tool calibration has attracted interest from researchers and machine tool users due to rapid advances in the capabilities, cost, and size of camera systems. Vision-based measuring systems rely on capturing the target measurand information by a vision sensor, such as a visible-light camera, and processing it for the quantitative determination of the measurand, such as the coordinates of a target feature. Information processing consists of several steps, such as pre-processing of the raw image(s) to reduce noise, blurring, etc. and to normalize pixel intensity, image analysis, such as segmentation, edge detection, pattern recognition and pattern matching, and finally, the post-processing step, such as estimating feature positions or dimensions and applying calibration [515]. An example of using camera for calibration of positioning errors of a two-dimensional precision stage was described in Ref. [516]. In that study, an inexpensive imaging target consisting of a textured plane was used. The stage positioning errors were extracted from overlapping texture images utilizing a feature-matching algorithm (see Fig. 67). Compared against CMM measurements, a maximum measurement error of 3 μm over a measurement range of 100 mm was reported. Another example of machine calibration using a spindle mounted vision system was reported in Ref. [517].

As mentioned in **Section 3.4.1**, vision-based metrology can also be used in measuring machine tool vibrations achieving micrometer resolution at frame rates of 1000 fps [321]. A different application of vision-based positioning calibration was reported in Ref. [518]. In this application, an optical target grid plate was used as the dimensional reference artifact in combination with a camera located on the optical path of a two-dimensional scanning galvo system. Positioning errors of the scanner were determined from the series of images captured by the

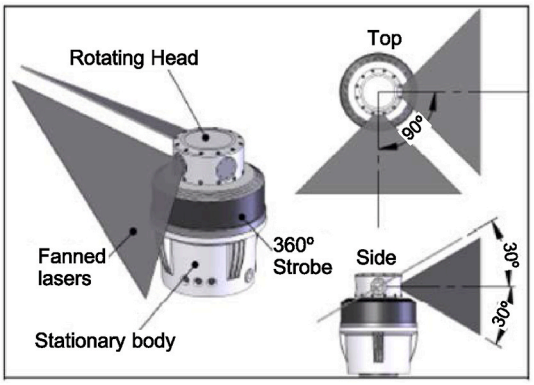

Fig. 66. Main components of iGPS transmitter [509]. A rotating head and fanned lasers acting as a theodolite are utilized.

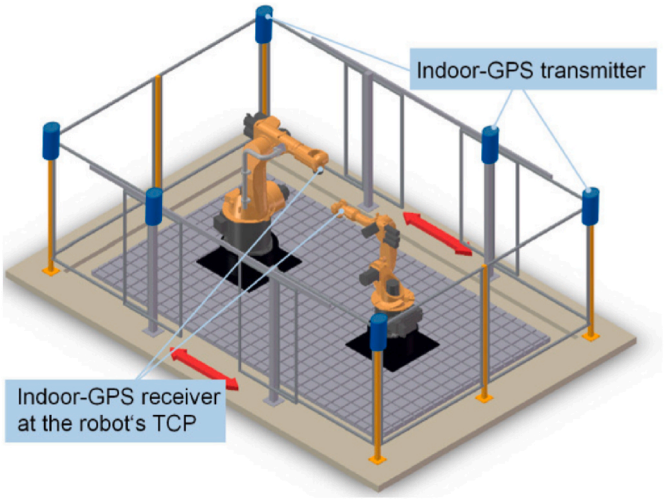

Fig. 65. Setup of the indoor GPS based robot cell [508]. Multiple transmitters located around the workspace are employed to determine the location of the receivers mounted on the end effectors of two robots.

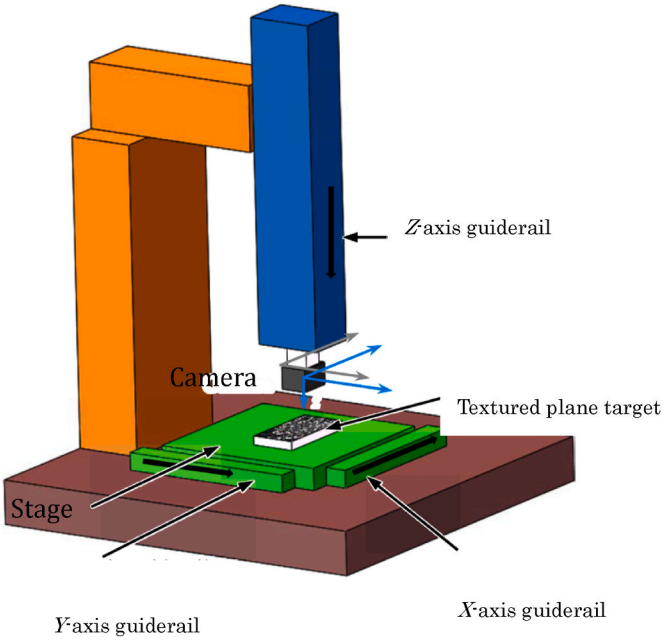

Fig. 67. Monocular vision-based measurement system [516]. A camera and a target with textured surface are included in the system to determine positioning errors of machine slides using a feature-matching algorithm.

camera while scanning the target artifact. Measured errors were compared to the more traditional "mark and measure" method with satisfactory results. However, none of these two application examples provide rigorous measurement uncertainty assessment. A general approach to uncertainty assessment of vision-based metrology was provided in Ref. [519]. Implementation of this approach or similar rigorous methods for use in machine tool calibrations are needed to enable reliable, fast, and inexpensive vision-based calibrations.

Image processing for optical metrology, which includes vision-based metrology, is a critical part of the measurement process. With advanced graphics processing units (GPUs) and large data sets, artificial intelligence (AI) and machine learning (ML) tools are becoming significant enablers to improve the capabilities of image processing algorithms. Zuo et al. provided a comprehensive review of the use of deep learning in optical metrology [520]. They correctly differentiate the deep learning in computer vision from the deep learning in optical metrology, the latter of which focuses on accuracy, repeatability, and traceability. To overcome such concerns, future directions were suggested for vision-based optical metrology, which include developing hybrid learning methods consisting of semi-supervised, unsupervised, and self-supervised learning, incorporating laws of physics into learning models to improve learning, and uncertainty quantification by integrating deep learning with Bayesian models. These approaches provide promising opportunities to improve machine tool calibrations by vision-based metrology.

Although individual kinematic, thermal, and dynamic machine tool error models were developed as separate research efforts as described in **Section 4**, a robust and unified machine tool performance model that includes all these machine tool characteristics is needed to predict the overall machine performance and the resulting workpiece accuracy under any relevant machining conditions. Such efforts should also address the deviations from rigid body assumptions as well as influence of machine foundations by including elastic deformation of machine structural components into the unified machine tool performance models [3]. Furthermore, to make the technology more transparent for users, numerical and information processing tools are needed to utilize available calibration data in combination with the machine tool structural configuration to automatically generate kinematic models supplemented with other measured errors, such as elastic deformations, servo coordination errors, etc. Fesperman et al. described such an approach and called it a "data driven virtual machine tool (DDVMT) in Ref. [521]. Further improvements are needed to make such tools commercially feasible, enabling performance-based digital twins of machine tools. A machine tool digital twin consists of multi-physics, multi-scale models incorporating calibration data and sensor updates to simulate the up-to-date realistic performance of its physical twin at any time. When available, these machine tool digital twins enable processing multiple "what if" scenarios to optimize machine tool utilization for given workpiece geometries with associated tolerance requirements. Considering the large number of influencing factors and variables in the manufacturing environment, AI and ML tools can be incorporated into such models to make the optimization more efficient based on prior performance results. For these tools to be effective for real time analysis, datasets containing information about various categories of machine structures operating in various manufacturing environments, environments need to be developed, as well as improved computational power and algorithms.

As mentioned in **Sections 4.2** and **5.3,** AI and ML tools are also good candidates to improve the prediction and compensation of thermally-induced errors of machine tools, which are influenced by multiple varying and interacting internal and external heating and cooling conditions. However, as mentioned earlier, a major challenge with the use of any AI and ML tools is the assessment of uncertainty in the predicted errors. More research is needed to establish robust and rigorous methods for uncertainty assessment and traceability of AI and ML tools used in estimating and compensating machine tool thermal deformations.

Changes in machine tool performance over time, due to inevitable wear and possible collisions of moving components, create the need for costly and time-consuming periodic checks and recalibration. Some of these checks are done relatively quickly with calibrated artifacts or telescoping ball bars. Nevertheless, such quick tests are still disruptive to ongoing machining operations. Therefore, they are often not conducted frequently enough, to detect performance degradations before their effects appear in inaccurate machined products. An approach to detect changes in machine tool performance in a timely fashion is to integrate multiple inexpensive non-intrusive sensors to track those changes. Vogl et al. used an inertial measurement unit (IMU), consisting of three accelerometers and triaxial rate gyroscope, mounted on a machine slide to measure its quasi-static kinematic errors (see Fig. 68) [522]. A similar approach was used to measure the squareness of two machine tool axes using inertial measurements [523]. Integration of such non-intrusive sensors enables continuous acquisition of real-time data that could be fed to machine models for updating compensation files in machine controllers. However, further research is needed to establish traceability of IMU-based quasi-static kinematic error measurements.

Except for specialized cases where real-time error measurement is feasible, error compensation is only possible for the average values of the measured errors (systematic component of the errors), repeatability of machine error motions creates a major limitation for implementing error compensation. The apparent non-repeatability of error motion is caused by multiple influencing factors, including play between components, typically caused by a lack of adequate preload, friction, and the interaction between moving non-ideal interface features, such as non-straight guideways and multiple trucks with recirculating balls carrying a machine slide. A recent research effort showed the effect of the periodicity of recirculating ball motion within the trucks of a linear slide to the measured positioning error of that slide [9]. This research identifies possibilities to improve error compensation by integrating inexpensive sensors to machine components to predict the systematic variations in positioning behavior that at first seem non-repeatable, and thus address the non-repeatability barrier to error compensation.

A challenge for error compensation of three-axis machine tools is that the orientation error of the cutting tool cannot be compensated by moving a machine axis, as mentioned in **Section 5.1.1.4**. More research is needed to develop and integrate active mounting or fixture designs into machine tools, similar to fast tool servos mentioned in **Section 5.1.2**, that manipulate workpiece or spindle orientation to compensate

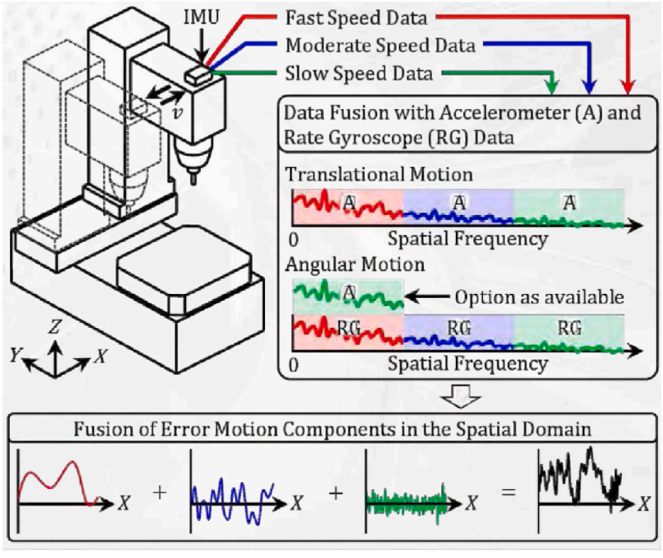

Fig. 68. IMU-based method for diagnostics of machine tool performance degradation [522]. IMU sensors are integrated with machine slides to continuously detect the changes in slide positioning errors.

for errors in the tool orientation errors (e.g., workpiece fixtures with piezo driven Stewart platforms), without compromising the static and dynamic stiffness of the machine tool structural loop.

Finally, implications of machine calibration, usage, and condition information in relation to Industry 4.0 need to be considered to take full advantage of the Industry 4.0 technologies. In the era of Industry 4.0 machine tools will have higher connectivity with each other and with the enterprise, in addition to higher degrees of adaptivity and autonomy. Liu et al. [524] recently stated that one of the ultimate goals of Industry 4.0 is digitization of manufacturing systems, including machine tools, in terms of data availability, accessibility, connectivity, communication, interoperability, as well as efficient data computation and storage. Achieving these goals will enable advanced data analytics, high-fidelity modeling and simulations, and intelligent decision making for optimized utilization of machine tools. Two categories of data exist in machine tools: data obtained by sensors and measuring systems attached to the machine and data generated and used by the machine control system. For efficient calibration of machines, both categories of data must be accessible. However, for the current generation of machine tools, accessing data from controllers is challenging. Various data communication protocols are being proposed by the machine tool community to enable such data acquisition. A conceptual framework is also needed to integrate data acquisition and processing technologies to generate and use next generation machine tool digital twins. Low-cost, reliable, accurate, multi-axis and easy-to-implement sensors and data acquisition devices, as well as unified, multi-dimensional, multi-scale machine tool digital twins, which include a virtual model, data model, a knowledge models and a service model, are among the other needs to achieve the full potential of Industry 4.0 [524].

Credit author statement

Wei Gao: Planning, Editing, Writing-error separation methods, compensation by FTS, Soichi Ibaraki: Planning, Writing-measurement of geometric errors, quasi-static kinematic models, M. Alkan Donmez: Reviewing, Writing-direct measurement of quasi-static error motions, conclusion remarks, challenges and future opportunities, Daisuke Kono: Writing: dynamic errors, René Mayer: Reviewing, Writing: classification of errors, Yuanliu Chen: Writing: thermal models and compensation, Károly Szipka: Writing: Error estimation and uncertainty, Static load-induced deformation models, Andreas Archenti: Writing: Static load-induced elastic deformation and compensation, Jean-Marc Linares, Aix-Marseille Université, France, Norikazu Suzuki: Writing: Dynamic models and compensation

Disclaimer

Certain commercial entities or products may be identified in this document, e.g., to describe concepts adequately. Such identification is not intended to imply recommendation or endorsement by the authors or their organizations, nor to imply that the entities or products are necessarily the best available for the purpose.

Declaration of competing interest

The authors declare that they have no known competing financial interests or personal relationships that could have appeared to influence the work reported in this paper.

Data availability

Data will be made available on request.

Acknowledgement

The authors would like to thank Dragos Axinte for his initiative and continuous support to this review paper. The suggestions from Beaucamp Anthony on the manuscript are appreciated. The authors thank Harald Bosse of PTB, Makoto Tano of JTEKT, Sadaji. Hayama of Hayama Professional Engineer Office, Masahide Katsuki and Makoto Sagara of Shibaura Machine, Yutaka Kondo of Renishaw, Noboru Shimizu of Heidenhain KK, Shigemasa Natsume of P&C for providing invaluable information. W. Gao thanks his students Kuangyi Li, Tao Liu, Yifan Hong, Jiahui Lin, Dong Wook Shin, Chenguang Yin and Zhiyang Zhang for their assistance in editing the manuscript. The invaluable review comments from IJMTM and NIST reviewers are also appreciated.

References

[1] H. Schwenke, W. Knapp, H. Haitjema, A. Weckenmann, R. Schmitt, F. Delbressine, Geometric error measurement and compensation of machines - an update, CIRP Ann. - Manuf. Technol. 57 (2) (2008) 660–675.
[2] S. Ibaraki, W. Knapp, Indirect measurement of volumetric accuracy for three-Axis and five-Axis machine tools: a review, Int. J. Autom. Technol. 6 (2) (2012) 110–124.
[3] R. Ramesh, M.A. Mannan, A.N. Poo, Error compensation in machine tools - a review Part II: thermal errors, Int. J. Mach. Tool Manufact. 40 (9) (2000) 1257–1284.
[4] R. Ramesh, M.A. Mannan, A.N. Poo, Thermal error measurement and modelling in machine tools Part I: influence of varying operating condition, Int. J. Mach. Tool Manufact. 43 (2003) 405–419.
[5] Y. Li, W.H. Zhao, S.H. Lan, J. Ni, W.W. Wu, B.H. Lu, A review on spindle thermal error compensation in machine Tools, Int. J. Mach. Tool Manufact. 95 (2015) 20–38.
[6] J. Munoa, X. Beudaert, Z. Dombovari, Y. Altintas, E. Budak, C. Brecher, G. Stepan, Chatter Suppression techniques in metal cutting, CIRP Ann. - Manuf. Technol. 65 (2) (2016) 785–808.
[7] JCGM 200, International vocabulary of metrology – Basic and general concepts and associated terms (VIM) (2012).
[8] L. Andolfatto, S. Lavernhe, J.R.R. Mayer, Evaluation of servo, geometric and dynamic error sources on five-axis high-speed machine tool, Int. J. Mach. Tool Manufact. 51 (10–11) (2011) 787–796.
[9] G.W. Vogl, K.F. Shreve, M.A. Donmez, Influence of bearing ball recirculation on error motions of linear axes, CIRP Ann. - Manuf. Technol. 70 (1) (2021) 345–348.
[10] P. Majda, Modeling of geometric errors of linear guideway and their influence on joint kinematic error in machine tools, Precis. Eng. 36 (3) (2012) 369–378.
[11] T.O. Ekinci, J.R.R. Mayer, G.M. Cloutier, Investigation of accuracy of aerostatic guideways, Int. J. Mach. Tool Manufact. 49 (2009) 478–487.
[12] J. Bryan, The Abbe principle revisited: an updated interpretation, Precis. Eng. 1 (1979) 129–132.
[13] T.O. Ekinci, J.R.R. Mayer, Relationships between straightness and angular kinematic errors in machines, Int. J. Mach. Tool Manufact. 47 (12–13) (2007) 1997–2004.
[14] S. Ibaraki, M. Sawada, A. Matsubara, T. Matsushita, Machining tests to identify kinematic errors on five-axis machine tools, Precis. Eng. 34 (2010) 387–398.
[15] M.M. Rahman, J.R.R. Mayer, Five axis machine tool volumetric error prediction through an indirect estimation of intra- and inter-axis error parameters by probing facets on a scale enriched uncalibrated indigenous artifact, Precis. Eng. 40 (2015) 94–105.
[16] Test code for machine tools — Part 1: Geometric accuracy of machines operating under no-load or quasi-static conditions, 2012.
[17] Y. Kakino, Y. Ihara, Y. Nakatsu, K. Okamura, The measurement of motion errors of NC machine tools and diagnosis of their origins by using telescoping magnetic ball bar method, CIRP Ann. - Manuf. Technol. 36 (1) (1987) 377–380.
[18] M. Weck, Handbook of Machine Tools, in: Metrological Analysis and Performance Tests, ume 4, John Wiley and Sons, 1984, ISBN 0471262250 (original publication in German in 1980).
[19] J.R.R. Mayer, Y. Abbaszaheh-Mir, C. Fortin, Calibration of a five-Axis machine tool for position independent geometric error parameters using a telescoping magnetic ball bar, in: D.R. Hayhurst, et al. (Eds.), Proceedings of the 33rd International MATADOR Conference, Springer, London, 2000.
[20] Y. Abbaszaheh-Mir, J.R.R. Mayer, G. Cloutier, C. Fortin, Theory and simulation for the identification of the link geometric errors for a five-axis machine tool using a telescoping magnetic ball-bar, Int. J. Prod. Res. 40 (18) (2002) 4781–4797.
[21] E.L.J. Bohez, B. Ariyajunya, C. Sinlapeecheewa, T.M.M. Shein, D.T. Lap, G. Belforte, Systematic geometric rigid body error identification of 5-axis milling machines, Comput. Aided Des. 39 (4) (2007) 229–244.
[22] B. Bringmann, W. Knapp, Model-based 'chase-the-ball' calibration of a 5-axes machining center, CIRP Ann. - Manuf. Technol. 55 (1) (2006) 531–534.
[23] ISO, 230-12, Test code for machine tools - Part 12: Accuracy of finished test pieces (2022).
[24] ISO, 230-7, Test code for machine tools — Part 7: Geometric accuracy of axes of rotation (2015).
[25] R. Schultschik, The components of volumetric accuracy, CIRP Ann. - Manuf. Technol. 26 (1) (1977) 223–226.
[26] E. Abbe, Messapparate für physiker, Zeitschrift für Instrumentenkunde 10 (12) (1890) 446–448.

[27] H. Tang, J.A. Duan, Q.C. Zhao, A systematic approach on analyzing the relationship between straightness & angular errors and guideway surface in precise linear stage, Int. J. Mach. Tool Manufact. 120 (2017) 12–19.
[28] M. Rahmani, F. Bleicher, Experimental and analytical investigations on normal and angular stiffness of linear guides in manufacturing systems, Procedia CIRP 41 (2016) 795–800.
[29] Y. Abbaszaheh-Mir, J.R.R. Mayer, C. Fortin, Tool path error prediction of a five-axis machine tool with geometric errors, Proc. IME B J. Eng. Manufact. 216 (5) (2002) 697–712.
[30] M. Tsutsumi, A. Saito, Identification and compensation of systematic deviations particular to 5-axis machining centers, Int. J. Mach. Tool Manufact. 43 (8) (2003) 771–780.
[31] C. Hong, S. Ibaraki, Matsubara, An Influence of position-dependent geometric errors of rotary axes on a machining test of cone frustum by five-axis machine tools, Precis. Eng. 35 (1) (2011) 1–11.
[32] Z.W. Tang, Y.S. Zhou, S.H. Wang, J. Zhu, J.Y. Tang, An innovative geometric error compensation of the multi-axis CNC machine tools with non-rotary cutters to the accurate worm grinding of spur face gears, Mech. Mach. Theor. 169 (2022), 104664.
[33] X.G. Jiang, Z.W. Cui, L. Wang, C. Liu, M.J. Li, J. Liu, Y. Du, Critical geometric errors identification of a five-axis machine tool based on global quantitative sensitivity analysis, Int. J. Adv. Manuf. Technol. 119 (2022) 3717–3727.
[34] R.J. Hocken, Technology of machine tools, Machine tool accuracy ume 5 (1980). No. UCRL-52960-5).
[35] J.R.R. Mayer, Five-axis machine tool calibration by probing a scale enriched reconfigurable uncalibrated master balls artifact, CIRP Ann. - Manuf. Technol. 61 (1) (2012) 515–518.
[36] ISO 10791-6, Test conditions for machining centres - Part 6: Accuracy of speeds and interpolations (2014).
[37] N.A. Duffie, S.M. Yang, J.G. Bollinger, Generation of parametric kinematic error-correction functions from volumetric error measurements, CIRP Ann. - Manuf. Technol. 34 (1) (1985) 435–438.
[38] W.J. Liu, S. Zhang, J.H. Lin, Y.H. Xia, J.X. Wang, Y.L. Sun, Advancements in accuracy decline mechanisms and accuracy retention approaches of CNC machine tools: a review, Int. J. Adv. Manuf. Technol. 121 (2022) 7087–7115.
[39] J. Mayr, J. Jedrzejewski, E. Uhlmann, A. Donmez, W. Knapp, F. Härtig, K. Wendt, T. Moriwaki, P. Shore, R. Schmitt, C. Brecher, T. Würz, K. Wegener, Thermal issues in machine tools, CIRP Ann. - Manuf. Technol. 61 (2) (2012) 771–791.
[40] J. Bryan, International status of thermal error research, CIRP Ann. - Manuf. Technol. 39 (2) (1990) 645–656.
[41] J. Bryan, International status of thermal error research, CIRP Ann. - Manuf. Technol. 16 (2) (1969) 203–215.
[42] M. Weck, P. Mckeown, R. Bonese, U. Herbst, Reduction, and compensation of thermal errors in machine tools, CIRP Ann. - Manuf. Technol. 44 (2) (1995) 589–598.
[43] W.S. Yun, S.K. Kim, D.W. Cho, Thermal error analysis for a CNC lathe feed drive system, Int. J. Mach. Tool Manufact. 39 (1999) 1088–1101.
[44] E. Creighton, A. Honegger, A. Tulsian, D. Mukhopadhyay, Analysis of thermal errors in a high-speed micro-milling spindle, Int. J. Mach. Tool Manufact. 50 (4) (2010) 386–393.
[45] S.N. Grama, A. Mathur, A.N. Badhe, A model-based cooling strategy for motorized spindle to reduce thermal errors, Int. J. Mach. Tool Manufact. 132 (2018) 3–16.
[46] L. Groos, C. Held, F. Keller, K. Wendt, M. Franke, N. Gerwien, Mapping and compensation of geometric errors of a machine tool at different constant ambient temperatures, Precis. Eng. 63 (2020) 10–17.
[47] J.G. Yang, J.X. Yuan, J. Ni, Thermal error mode analysis and robust modeling for error compensation on a CNC turning center, Int. J. Mach. Tool Manufact. 39 (9) (1999) 1367–1381.
[48] M. Weck, C. Brecher, Statisches verhalten von Werkzeugmaschinen, in: Werkzeugmaschinen 5. VDI-Buch, Springer Vieweg, Berlin, Heidelberg, 2006, https://doi.org/10.1007/978-3-540-32951-0_4: 163–177.
[49] X.C. Xi, A.N. Poo, G.S. Hong, Improving contouring accuracy by tuning gains for a bi-axial CNC machine, Int. J. Mach. Tool Manufact. 49 (5) (2009) 395–406.
[50] N. Tounsi, A. Otho, Identification of machine–tool–workpiece system dynamics, Int. J. Mach. Tool Manufact. 40 (9) (2000) 1367–1384.
[51] D. Kono, A. Matsubara, K. Nagaoka, K. Yamazaki, Analysis method for investigating the influence of mechanical components on dynamic mechanical error of machine tools, Precis. Eng. 36 (3) (2012) 477–484.
[52] D. Kono, F. Sakamoto, I. Yamaji, Linked ball bar for flexible motion error measurement for machine tools, Int. J. Autom. Technol. 11 (2) (2017) 188–196.
[53] D. Kono, S. Weikert, A. Matsubara, K. Yamazaki, Estimation of dynamic mechanical error for evaluation of machine tool structures, Int. J. Autom. Technol. 6 (2) (2012) 147–153.
[54] T. Fujita, A. Matsubara, K. Yamazaki, Experimental characterization of disturbance force in a linear drive system with high-precision rolling guideways, Int. J. Mach. Tool Manufact. 51 (2) (2011) 104–111.
[55] D. Kono, T. Osumi, Rolling resistance model for estimation of friction fluctuation in linear ball guideways, Precis. Eng. 75 (2022) 46–54.
[56] D.B. DeBra, Vibration isolation of precision machine tools and instruments, CIRP Ann. - Manuf. Technol. 41 (2) (1992) 711–718.
[57] B.W. Peukert, A. Archenti, A dynamic interaction between precision machine tools and their foundations, Int. J. Autom. Technol. (14) (2020) 386–398.
[58] K. Nagaoka, T. Sato, Feedforward controller for continuous path control of CNC machine tools, International Journal of Simulation 7 (8) (2006) 39–46.
[59] T. Iwasaki, T. Sato, A. Morita, A. Maruyama, Auto-tuning of two-degree-of-freedom motor control for high-accuracy trajectory motion, Control Eng. Pract. 4 (4) (1996) 537–544.
[60] D. Kono, T. Inagaki, A. Matsubara, I. Yamaji, Stiffness model of machine tool supports using contact stiffness, Precis. Eng. 37 (3) (2013) 650–657.
[61] D. Kono, S. Nishio, I. Yamaji, A. Matsubara, A method for stiffness tuning of machine tool supports considering contact stiffness, Int. J. Mach. Tool Manufact. (90) (2015) 50–59.
[62] C. Rebelein, M.F. Zaeh, Friction in feed drives of machine tools: investigation, modeling and validation, J. Inst. Eng. Prod. (10) (2016) 497–507.
[63] J. Lee, A study on the dynamic modelling of structures with bolted and bearing joints, CIRP Ann. - Manuf. Technol. (37) (1988) 343–346.
[64] W. Gao, S.W. Kim, H. Bosse, H. Haitjema, Y.L. Chen, X.D. Lu, W. Knapp, A. Weckenmann, W.T. Estler, H. Kunzmann, Measurement technologies for precision positioning, CIRP Ann. - Manuf. Technol. 64 (2) (2015) 773–796, 64(2).
[65] Renishaw plc, XL-80 laser system (2023).
[66] MÖLLER-WEDEL OPTICAL GmbH, Electronic autocollimator ELCOMAT 3000 (2023).
[67] BEWIS Sensing Technology LLC, High Accuracy Modbus Dual-axis Inclinometer BWS5700 (2023).
[68] Onishi Measurement Co. Ltd, Straight Edge OS-146B (2023).
[69] Sinto V-Cerax, LTD, Ceramics straight edge (2023).
[70] Zygo Corporation, Straight Edges (2023).
[71] Keyence Corporation, Contact-type displacement sensor AT2-52 (2023).
[72] Lion Precision, Capacitive sensor CPL490 (2023).
[73] Renishaw plc, XM-60 multi-axis calibrator (2023).
[74] X.G. Chen, Z. Tao, C. Chen, C. Wang, L. Wang, H. Jiang, D. Fan, Y. Ekinci, S. Y. Liu, All-dielectric metasurface-based roll-angle sensor, Sensor Actuator Phys. 279 (2018) 509–517.
[75] W. Gao, Y. Arai, A. Shibuya, S. Kiyono, C.H. Park, Measurement of multi-degree-of-freedom error motions of a precision linear air-bearing stage, Precis. Eng. 30 (2006) 96–103.
[76] Y. Shimizu, S.L. Tan, D. Murata, T. Maruyama, S. Ito, Y.L. Chen, W. Gao, Ultra-sensitive angle sensor based on laser autocollimation for measurement of stage tilt motions, Opt Express 24 (3) (2016) 2788–2805.
[77] W. Gao, Y. Saito, H. Muto, Y. Arai, Y. Shimizu, A three-axis autocollimator for detection of angular error motions of a precision stage, CIRP Ann. - Manuf. Technol. 60 (1) (2011) 515–518.
[78] Yuki Shimizu, S. Kataoka, W. Gao, High resolution clinometers for measurement of roll error motion of a precision linear slide, Chin. J. Mech. Eng. 31 (2018) 92, https://doi.org/10.1186/s10033-018-0294-6.
[79] Y. Shimizu, S. Kataoka, T. Ishikawa, Y.L. Chen, X.G. Chen, H. Matsukuma, W. Gao, A liquid-surface-based three-Axis inclination sensor for measurement of stage tilt motions, Sensors 18 (2) (2018) 398, https://doi.org/10.3390/s18020398.
[80] O. Borisov, O. Borisov, S. Fletcher, A. Longstaff, A. Myers, New low cost sensing head and taut wire method for automated straightness measurement of machine tool axes, Opt Laser. Eng. 51 (8) (2013) 978–985.
[81] W.T. Estler, Calibration and use of optical straightedges in the metrology of precision machines, Opt. Eng. 24 (3) (1985) 372–379.
[82] M.A.V. Chapman, Limitations of laser diagonal measurements, Precis. Eng. 27 (4) (2003) 401–406.
[83] M. Yamauchi, K. Matsuda, Interferometric straightness measurement system using holographic grating, Opt. Eng. 33 (4) (1994) 1078–1083.
[84] S.T. Lin, A laser interferometer for measuring straightness, Opt Laser. Technol. 33 (3) (2001) 195–199.
[85] C. Kuang, E. Hong, Q. Feng, B. Zhang, Z. Zhang, A novel method to enhance the sensitivity for two-degrees-of-freedom straightness measurement, Meas. Sci. Technol. 18 (12) (2007) 3795.
[86] M.A.V. Chapman, R. Fergusson-Kelly, W. Lee, Interferometric angle measurement and the hardware options available from Renishaw, Renishaw Technical White Paper: TE326 (2013).
[87] J. Yuan, X. Long, CCD-area-based autocollimator for precision small-angle measurement, Review of Scientific Instruments 74 (3) (2003) 1362–1365.
[88] S. Tang, Z. Wang, J. Gao, J. Guo, Measurement method for roll angular displacement with a high resolution by using diffraction gratings and a heterodyne interferometer, Review of Scientific Instruments 85 (4) (2014), 045110.
[89] F. Zheng, Q. Feng, B. Zhang, J. Li, A method for simultaneously measuring 6DOF geometric motion errors of linear and rotary axes using lasers, Sensors 19 (8) (2019) 1764, https://doi.org/10.3390/s19081764.
[90] J. Bryan, Spindle accuracy, American Machinist 111 (25) (1967) 149–164.
[91] S.E. Masry, Accuracy of rotation around an axis, Review of Scientific Instruments 39 (12) (1968) 1825–1828.
[92] P. Vanherck, J. Peters, An axis of rotation analyser, Proceedings of the 14th International Machine Tool Design and Research Conference (1974) 299–305.
[93] Lion Precision, Spindle Error Analyzer, 2023.
[94] Renishaw plc, XR20 Rotary axis Calibrator, 2023.
[95] HEIDENHAIN GmbH, Angle encoder ROD 880 (2023).
[96] Möller-Wedel Optical GmbH, Polygon mirror (2023).
[97] Z.F. Lou, X.P. Hao, Y.D. Cai, T.F. Lu, X.D. Wang, K.C. Fan, An embedded sensor system for real-time detecting 5-DOF error motions of rotary stages, Sensors 19 (13) (2019) 2855, https://doi.org/10.3390/s19132855.
[98] H.W. Wang, K. Peng, X.K. Liu, Z.C. Yu, Z.R. Chen, Design and realization of a compact high-precision capacitive absolute angular position sensor based on time grating, IEEE Transactions on Industrial Electronics 68 (4) (2021) 3548–3557.

[99] W. Gao, Precision Nanometrology: Sensors and Measuring Systems for Nanomanufacturing, Springer, 2010, ISBN 978-1849962544.
[100] W. Gao, S. Kiyono, E. Satoh, Precision measurement of multi-degree-of-freedom spindle errors using two-dimensional slope sensors, CIRP Annals - Manufacturing Technology 51 (1) (2002) 447–450.
[101] J. Chrzanowski, T. Sałaciński, P. Skiba, Spindle error movements and their measurement, Applied Sciences 11 (10) (2021) 4571, https://doi.org/10.3390/app11104571.
[102] X.K. Liu, K. Peng, Z.R. Chen, H.J. Pu, Z.C. Yu, A new capacitive displacement sensor with nanometer accuracy and long range, IEEE Sensors Journal 16 (8) (2016) 2306–2316.
[103] X.C. Fan, K. Peng, X.K. Liu, H.J. Pu, Z.C. Yu, A splicing technique and structure for long-range absolute-type capacitive displacement sensors, IEEE Transactions on Instrumentation & Measurement 71 (7) (2022) 1–10.
[104] M.A.V. Chapman, R. Fergusson-Kelly, W. Lee, Interferometric Calibration of Rotary Axes, Renishaw Technical White Paper, 2013, p. TE327.
[105] G.H.J. Florussen, F.L.M. Delbressine, M.J.G. Van De Molengraft, P.H. J. Schellekens, Assessing geometrical errors of multi-axis machines by three-dimensional length measurements. Measurement, Journal of the International Measurement Confederation 30 (4) (2001) 241–255, https://doi.org/10.1016/S0263-2241(01)00016-1.
[106] J. Bryan, A simple method for testing measuring machines and machine tools. Part 2: construction details, Precision Engineering 4 (3) (1982) 125–138.
[107] ISO, 230-4, Test code for machine tools - Part 4: Circular tests for numerically controlled machine tools (2005).
[108] A. Matsubara, K. Nagaoka, T. Fujita, Model-reference feedforward controller design for high-accuracy contouring control of machine tool axes, CIRP Annals - Manufacturing Technology 60 (1) (2011) 415–418.
[109] K.I. Lee, S.H. Yang, Accuracy evaluation of machine tools by modeling spherical deviation based on double ball-bar measurements, International Journal of Machine Tools and Manufacture 75 (2013) 46–54.
[110] W. Knapp, S. Hrovat, The Circular Test for Testing NC Machine Tools, S. Hrovat, Zurich, 1987.
[111] Y. Kakino, Y. Ihara, Shinohara, Accuracy Inspection of NC Machine Tools by Double Ball Bar Method, Hanser Publishers, 1993, ISBN 978-1569901601.
[112] ISO 10360-2, Geometrical product specifications (GPS) - Acceptance and reverification tests for coordinate measuring machines (CMM) - Part 2: CMMs used for measuring linear dimensions (2009).
[113] P. Cauchick-Miguel, CMM verification: a survey, Measurement 17 (1) (1996) 1–16.
[114] E. Trapet, J. Aguilarmartin, J. Yague, H. Spaan, V. Zeleny, Self-centering probes with parallel kinematics to verify machine tools, Precision Engineering 30 (2) (2006) 165–179.
[115] G. Florussen, K. Houben, H. Spaan, T. Spaan-Burke, Automating accuracy evaluation of 5-Axis machine tools, International Journal of Automation Technology 14 (3) (2020) 409–416.
[116] G.X. Zhang, Y.F. Zang, A method for machine geometry calibration using 1-D ball array, CIRP Annals - Manufacturing Technology 40 (1) (1991) 519–522.
[117] F. Viprey, H. Nouira, S. Lavernhe, C. Tournier, Novel multi-feature bar design for machine tools geometric errors identification, Precision Engineering 46 (2016) 323–338.
[118] E. Trapet, F. Wäldele, A reference object based method to determine the parametric error components of coordinate measuring machines and machine tools, Measurement 9 (1) (1991) 17–22.
[119] E.S. Lee, M. Burdekin, A hole-plate Artifact design for the volumetric error calibration of CMM, International Journal of Advanced Manufacturing Technology 17 (7) (2001) 508–515.
[120] B. Bringmann, A. Küng, W.A. Knapp, Measuring artifact for true 3D machine testing and calibration, CIRP Annals - Manufacturing Technology 54 (1) (2005) 471–474.
[121] T. Liebrich, B. Bringmann, W. Knapp, Calibration of a 3D-ball plate, Precision Engineering 33 (1) (2009) 1–6.
[122] A. Breitzke, H. Wolfgang, Workshop-suited geometric errors identification of three-axis machine tools using onmachine measurement for long term precision assurance, Precision Engineering 75 (2022) 235–247.
[123] J.P. Choi, B.K. Min, S.J. Lee, Reduction of machining errors of a three-axis machine tool by on-machine measurement and error compensation system, Journal of Materials Processing Technology 155–156 (30) (2004) 2056–2064.
[124] S. Carmignato, L. De Chiffre, H. Bosse, R.K. Leach, A. Balsamo, W.T. Estler, Dimensional artifacts to achieve metrological traceability in advanced manufacturing, CIRP Annals - Manufacturing Technology 69 (2) (2020) 693–716.
[125] HEIDENHAIN GmbH, KGM 200 Series Grid Encoders, 2021.
[126] H. Schwenke, M. Franke, J. Hannaford, H. Kunzmann, Error mapping of CMMs and machine tools by a single tracking interferometer, CIRP Annals - Manufacturing Technology 54 (1) (2005) 475–478.
[127] H. Schwenke, R. Schmitt, P. Jatzkowski, C. Warmann, On-the-fly calibration of linear and rotary axes of machine tools and CMMs using a tracking interferometer, CIRP Annals - Manufacturing Technology 58 (1) (2009) 477–480.
[128] www.etalonproducts.com/en/products/lasertracer/(accessed on March 2022).
[129] S. Ibaraki, M. Hiruya, A novel scheme to measure 2D error motions of linear axes by regulating the direction of a laser interferometer, Precision Engineering 67 (2021) 152–159.
[130] F.J. Brosed, J.J. Aguilar, R. Acero, J. Santolaria, S. Aguado, M. Pueo, Calibration and uncertainty budget analysis of a high precision telescopic instrument for simultaneous laser multilateration, Measurement 90 (2022), 110735.
[131] ISO/TR 230-11, Test code for machine tools - Part 11: Measuring instruments suitable for machine tool geometry tests (2018).
[132] S. Ibaraki, Y. Tanizawa, Vision-based measurement of two-dimensional positioning errors of machine tools, Journal of Advanced Mechanical Design, Systems, and Manufacturing 5 (4) (2011) 315–328.
[133] N. Irino, M. Shimoike, K. Mori, I. Yamaji, M. Mori, A vision-based machine accuracy measurement method, CIRP Annals - Manufacturing Technology 69 (1) (2020) 445–448.
[134] Q. Li, W. Wang, J. Zhang, R. Shen, H. Li, Z. Jiang, Measurement method for volumetric error of five-axis machine tool considering measurement point distribution and adaptive identification process, International Journal of Machine Tools and Manufacture 147 (2019), 103465.
[135] W. Liu, X. Li, Z. Jia, H. Yan, X. Ma, A three-dimensional triangular vision-based contouring error detection system and method for machine tools, Precision Engineering 50 (2017) 85–98.
[136] S. Ibaraki, W. Goto, A. Matsubara, T. Ochi, M. Hamamura, Self-calibration of a cross grid encoder, Journal of the Japan Society for Precision Engineering 72 (8) (2006) 1032–1037 (in Japanese).
[137] G. Zhang, R. Ouyang, B. Lu, R. Hocken, R. Veale, A. Donmez, A displacement method for machine geometry calibration, CIRP Annals - Manufacturing Technology 37 (1) (1988) 515–518.
[138] J.S. Chen, T.W. Kou, S.H. Chiou, Geometric error calibration of multi-axis machines using an auto-alignment laser interferometer, Precision Engineering 23 (4) (1999) 243–252, b.
[139] G. Chen, J. Yuan, J. Ni, A displacement measurement approach for machine geometric error assessment, International Journal of Machine Tools and Manufacture 41 (2001) 149–161.
[140] A. Balsamo, P. Pedone, E. Ricci, M. Verdi, Low-cost interferometric compensation of geometrical errors, CIRP Annals - Manufacturing Technology 58 (1) (2009) 459–462.
[141] ISO 230-6, Test code for machine tools - Part 6: Determination of positioning accuracy on body and face diagonals (Diagonal displacement tests) (2002).
[142] C. Wang, Laser vector measurement technique for the determination and compensation of volumetric positioning errors Part I: basic theory, Review of Scientific Instruments 71 (10) (2000) 3933–3937.
[143] L. Zhou, P. Vanherck, A method for squareness error verification on a coordinate measuring machine, International Journal of Advanced Manufacturing Technology 21 (2003) 874–878.
[144] S.H. Yang, H.H. Lee, K.I. Lee, Face- and body-diagonal length tests using a double ball-bar for squareness errors of machine tools, International Journal of Precision Engineering and Manufacturing 19 (2018) 1039–1045.
[145] H. Zhang, J. Yang, Y. Zhang, J. Shen, C. Wang, Measurement and compensation for volumetric positioning errors of CNC machine tools considering thermal effect, International Journal of Advanced Manufacturing Technology 55 (1/4) (2010) 275–283.
[146] C.B. Bui, J. Hwang, C.H. Lee, C.H. Park, Three-face step-diagonal measurement method for the estimation of volumetric positioning errors in a 3D workspace, International Journal of Machine Tools and Manufacture 60 (2012) 40–43.
[147] S. Ibaraki, T. Hata, A. Matsubara, A new formulation of laser step-diagonal measurement – two-dimensional case, Precision Engineering 33 (1) (2009) 56–64.
[148] S. Ibaraki, T. Hata, A new formulation of laser step diagonal measurement - three-dimensional case, Precision Engineering 34 (3) (2010) 516–525.
[149] H. Li, P. Zhang, M. Deng, S. Xiang, Z. Du, J. Yang, Volumetric error measurement and compensation of three-axis machine tools based on laser bidirectional sequential step diagonal measuring method, Measurement Science and Technology 31 (5) (2020), 055201.
[150] E.B. Hughes, A. Wilson, G.N. Peggs, Design of a high-accuracy CMM based on multi-lateration techniques, CIRP Annals - Manufacturing Technology 49 (1) (2000) 391–394.
[151] G.N. Peggs, Virtual technologies for advanced manufacturing and metrology, International Journal of Computer Integrated Manufacturing 16 (7/8) (2003) 485–490.
[152] S. Aguado, D. Samper, J. Santolaria, J.J. Aguilar, Identification strategy of error parameter in volumetric error compensation of machine tool based on laser tracker measurements, International Journal of Machine Tools and Manufacture 53 (1) (2012) 160–169.
[153] S. Ibaraki, T. Kudo, T. Yano, T. Takatsuji, S. Osawa, O. Sato, Estimation of three-dimensional volumetric errors of machining centers by a tracking interferometer, Precision Engineering 39 (2014) 179–186.
[154] S. Aguado, J. Santolaria, D. Samper, J.J. Aguilar, Influence of measurement noise and laser arrangement on measurement uncertainty of laser tracker multilateration in machine tool volumetric verification, Precision Engineering 37 (4) (2013) 929–943.
[155] H. Chen, B. Jiang, Z. Shi, Y. Sun, H. Song, L. Tang, Uncertainty modeling of the spatial coordinate error correction system of the CMM based on laser tracer multi-station measurement, Measurement Science and Technology 30 (2) (2019), 025007.
[156] J.M. Linares, J. Chaves-Jacob, H. Schwenke, A. Longstaff, S. Fletcher, J. Flore, E. Uhlmann, J. Wintering, Impact of measurement procedure when error mapping and compensating a small CNC machine using a multilateration laser interferometer, Precision Engineering 38 (3) (2014) 578–588.
[157] S. Ibaraki, K. Nagae, G. Sato, Proposal of 'open-loop' tracking interferometer for machine tool volumetric error measurement, CIRP Annals - Manufacturing Technology 63 (1) (2014) 501–503.

[158] S. Ibaraki, K. Tsuboi, Open-loop" tracking interferometer measurement using rotary axes of a five-axis machine tool, IEEE/ASME Transactions on Mechatronics 22 (5) (2017) 2342–2350.
[159] J.C. Ziegert, C.D. Mize, The laser ball bar: a new instrument for machine tool metrology, Precision Engineering 16 (4) (1994) 259–267.
[160] K.C. Fan, H. Wang, F.J. Shiou, C.W. Ke, Design analysis and applications of a 3D laser ball bar for accuracy calibration of multiaxis machines, Journal of Manufacturing Systems 23 (3) (2004) 194–203.
[161] B. Kauschinger, C. Friedrich, R. Zhou, S. Ihlenfeldt, Fast evaluation of volumetric motion accuracy of multi-axis machine tools using a Double-Ballbar, Journal of Machine Engineering 20 (3) (2020) 44–62.
[162] Y. Ihara, S. Matsushita, A study on tool position and posture measurement device by using parallel mechanism, International Journal of Automation Technology 3 (3) (2009) 271–276.
[163] T. Sun, W. Wang, Z. Chen, Y. Zhu, K. Xu, H. Wu, Z. Sang, K. Lu, H. Yang, Positioning errors measurement of CNC machine tools based on J-DBB method, Applied Sciences 11 (2021), 11770.
[164] H. Iwai, K. Mitsui, Development of a measuring method for motion accuracy of NC machine tools using links and rotary encoders, International Journal of Machine Tools and Manufacture 49 (1) (2009) 99–108.
[165] S. Ibaraki, M. Hiruya, Assessment of non-rigid body, direction- and velocity-dependent error motions and their cross-talk by two-dimensional digital scale measurements at multiple positions, Precision Engineering 66 (2020) 144–153.
[166] ISO 10360-12, Geometrical product specifications (GPS) - Acceptance and reverification tests for coordinate measuring systems (CMS) - Part 12: Articulated arm coordinate measurement machines (CMM) (2016).
[167] Y. Kakino, Y. Ihara, H. Sato, H. Otsubo, A Study on the motion accuracy of NC machine tools (7th report) -Measurement of motion accuracy of 5-axis machine by DBB tests, Journal of the Japan Society for Precision Engineering 60 (5) (1994) 718–723 (in Japanese).
[168] S. Sakamoto, I. Inasaki, H. Tsukamoto, T. Ichikizaki, Identification of alignment errors in five-axis machining centers using telescoping ballbar, Transaction of the Japan Society of Mechanical Engineers (C) 63 (605) (1997) 262–267 (in Japanese).
[169] R.M. Mahbubur, J. Heikkala, K. Lappalainen, J.A. Karjalainen, Positioning accuracy improvement in five-axis milling by post processing, International Journal of Machine Tools and Manufacture 37 (2) (1997) 223–236.
[170] H. Xia, W. Peng, X. Ouyang, X. Chen, S. Wang, X. Chen, Identification of geometric errors of rotary axis on multi-axis machine tool based on kinematic analysis method using double ball bar, International Journal of Machine Tools and Manufacture 122 (2017) 161–175.
[171] Y. Yao, Y. Itabashi, M. Tsutsumi, K. Nakamoto, Position error reduction of tool center point in multi-tasking machine tools through compensating influence of geometric deviations identified by ball bar measurements, Precision Engineering 72 (2021) 745–755.
[172] Z. Wang, D. Wang, S. Yu, X. Li, H. Dong, A reconfigurable mechanism model for error identification in the double ball bar tests of machine tools, International Journal of Machine Tools and Manufacture 165 (2021), 103737.
[173] W.T. Lei, Y.Y. Hsu, Accuracy test of five-axis CNC machine tool with 3D probe-ball. Part I: design and modeling, International Journal of Machine Tools and Manufacture 42 (10) (2002) 1153–1162.
[174] S. Weikert, R-test, a new device for accuracy measurements on five Axis machine tools, CIRP Annals - Manufacturing Technology 53 (1) (2004) 429–432.
[175] S.H.H. Zargarbashi, J.R.R. Mayer, Single setup estimation of a five axis machine tool eight link errors by programmed end point constraint and on the fly measurement with Capball sensors, International Journal of Machine Tools and Manufacture 49 (2009) 759–766.
[176] L. Jiang, B. Peng, G. Ding, S. Qin, J. Zhang, L. Yong, Optimization method for systematically improving non-contact R test accuracy, International Journal of Advanced Manufacturing Technology 107 (2020) 1697–1711.
[177] W.Y. Jywe, T.H. Hsu, C.H. Liu, Non-bar, an optical calibration system for five-axis CNC machine tools, International Journal of Machine Tools and Manufacture 59 (2012) 16–23.
[178] C. Hong, S. Ibaraki, Non-contact R-test with laser displacement sensors for error calibration of five-axis machine tools, Precision Engineering 37 (1) (2013) 159–171.
[179] Y. Guo, B. Song, X. Tang, X. Zhou, Z. Jiang, A calibration method of non-contact R-test for error measurement of industrial robots, Measurement 173 (2021), 108365.
[180] T. Erkan, J.R.R. Mayer, Y. Dupont, Volumetric distortion assessment of a five-axis machine by probing a 3D reconfigurable uncalibrated master ball artifact, Precision Engineering 35 (1) (2011) 116–125.
[181] S. Ibaraki, R. Okumura, A machining test to evaluate thermal influence on the kinematics of a five-axis machine tool, International Journal of Machine Tools and Manufacture 163 (2021), 103702.
[182] Test conditions for machining centres - Part 10: Evaluation of thermal distortions (2022).
[183] M. Wiessner, P. Blaser, S. Böhl, J. Mayr, W. Knapp, K. Wegener, Thermal test piece for 5-axis machine tools, Precision Engineering 52 (2018) 407–417.
[184] T. Matsushita, T. Oki, Identification of geometric errors in five-axis controlled machine tool with touch trigger probe, Proceedings of the 2010 JSPE Spring Annual Meeting (2010) 1105–1106 (in Japanese).
[185] Y.T. Chen, P. More, C.S. Liu, Identification and verification of location errors of rotary axes on five-axis machine tools by using a touch-trigger probe and a sphere, International Journal of Advanced Manufacturing Technology 100 (2019) 2653–2667.
[186] S. Ibaraki, C. Oyama, H. Otsubo, Construction of an error map of rotary axes on a five-axis machining center by static R-test, International Journal of Machine Tools and Manufacture 51 (3) (2011) 190–200.
[187] C. Hong, S. Ibaraki, Graphical presentation of error motions of rotary axes on a five-axis machine tool by static R-test with separating the influence of squareness errors of linear axes, International Journal of Machine Tools and Manufacture 59 (2012) 24–33.
[188] S. Ibaraki, Y. Nagai, H. Otsubo, Y. Sakai, S. Morimoto, Y. Miyazaki, R-test analysis software for error calibration of five-Axis machine tools –Application to a five-Axis machine tool with two rotary axes on the tool side–, International Journal of Automation Technology 9 (4) (2015) 387–395.
[189] S. Ibaraki, H. Inui, C. Hong, S. Nishikawa, M. Shimoike, On-machine identification of rotary axis location errors under thermal influence by spindle rotation, Precision Engineering 55 (2019) 42–47.
[190] S. Ibaraki, E. Yanai, Identification of rotary Axis location errors under spindle rotation by using a laser barrier tool measurement system - experimental comparison with R-test, Transactions of the Institute of Systems, Control and Information Engineers 34 (3) (2021) 81–88.
[191] S. Ibaraki, T. Iritani, T. Matsushita, Calibration of location errors of rotary axes on five-axis machine tools by on-the-machine measurement using a touch-trigger probe, International Journal of Machine Tools and Manufacture 58 (2012) 44–53.
[192] S. Ibaraki, Y. Ota, A machining test to calibrate rotary axis error motions of five-axis machine tools and its application to thermal deformation test, International Journal of Machine Tools and Manufacture 86 (2014) 81–88.
[193] Q. Bi, N. Huang, C. Sun, Y. Wang, L. Zhu, H. Ding, Identification and compensation of geometric errors of rotary axes on five-axis machine by on-machine measurement, International Journal of Machine Tools and Manufacture 89 (2015) 182–191.
[194] K. Xing, S. Achiche, J.R.R. Mayer, Five-axis machine tools accuracy condition monitoring based on volumetric errors and vector similarity measures, International Journal of Machine Tools and Manufacture 138 (2019) 80–93.
[195] Z. Jiang, B. Song, X. Zhou, X. Tang, S. Zheng, On-machine measurement of location errors on five-axis machine tools by machining tests and a laser displacement sensor, International Journal of Machine Tools and Manufacture 95 (2015) 1–12.
[196] S. Ibaraki, S. Tsujimoto, Y. Nagai, Y. Sakai, S. Morimoto, Y. Miyazaki, A pyramid-shaped machining test to identify rotary axis error motions on five-axis machine tools: software development and a case study, International Journal of Advanced Manufacturing Technology 94 (2017) 227–237.
[197] A. Velenosi, G. Campatelli, A. Scippa, Axis geometrical errors analysis through a performance test to evaluate kinematic error in a five axis tilting-rotary table machine tool, Precision Engineering 39 (2015) 224–233.
[198] Y. Morimoto, K. Nakato, M. Gontani, Accuracy evaluation of 5-Axis machining center based on measurements of machined workpiece - evaluation of accuracy of 5-Axis controlled machining center, International Journal of Automation Technology 6 (5) (2012) 675–680.
[199] S. Ibaraki, Y. Ibuki, T. Asano, A machining test to identify rotary axis geometric errors on a five-axis machine tool with a swiveling rotary table for turning operations, Precision Engineering 55 (2019) 22–32.
[200] M. Arizmendi, A. Jiménez, W.E. Cumbicus, M. Estrems, M. Artano, Modelling of elliptical dimples generated by five-axis milling for surface texturing, International Journal of Machine Tools and Manufacture 137 (2019) 79–95.
[201] N. Huang, Y. Zhang, L. Zhu, S. Ibaraki, Visually quantifiable test piece for five-Axis machine tools thermal effects, Trans. of the ASME, Journal of Manufacturing Science and Engineering 144 (5) (2022), 054501.
[202] ISO 10791-7, Test conditions for machining centres - Part 7: Accuracy of finished test pieces (2020).
[203] S. Bossoni, J. Cupic, Test piece for simultaneous 5-axis machining, Laser metrology and machine performance VIII (2007) 24–33.
[204] H. Chanal, E. Duc, A. Chevalier, Studying the influence of the machining process on the geometrical defects of the standardized S-shape test part, Precision Engineering 75 (2022) 193–209.
[205] W. Wang, Z. Jiang, Z. Jiang, W. Tao, A new test part to identify performance of five-axis machine tool–Part II validation of S part, International Journal of Advanced Manufacturing Technology 79 (5–8) (2015) 739–756.
[206] B. Bringmann, W. Knapp, Machine tool calibration: geometric test uncertainty depends on machine tool performance, Precision Engineering 33 (4) (2009) 524–529.
[207] B. Bringmann, J.P. Besuchet, L. Rohr, Systematic evaluation of calibration methods, CIRP Annals - Manufacturing Technology 57 (2008) 529–532.
[208] JCGM 101, Evaluation of measurement data - Supplement 1 to the "Guide to the expression of uncertainty in measurement" - Propagation of distributions using a Monte Carlo method (2008).
[209] ISO/FDIS, 10791-2, Test conditions for machining centres - Part 2: Geometric tests for machines with vertical spindle (vertical Z-axis) (2022).
[210] K.I. Lee, S.H. Yang, Measurement and verification of position-independent geometric errors of a five-axis machine tool using a double ball-bar, International Journal of Machine Tools and Manufacture 70 (2013) 45–52.
[211] T. Rooker, J. Stammers, K. Worden, G. Potts, K. Kerrigan, N. Dervilis, Error motion trajectory-driven diagnostics of kinematic and non-kinematic machine tool faults, Mechanical Systems and Signal Processing 164 (2022), 108271.
[212] K. Xing, X. Rimpault, J.R.R. Mayer, J. Chatelain, S. Achiche, Five-axis machine tool fault monitoring using volumetric errors fractal analysis, CIRP Annals 68 (1) (2019) 555–558.

[213] B. Schmidt, K. Gandhi, L. Wang, Diagnosis of machine tools: assessment based on double ball-bar measurements from a population of similar machines, Procedia CIRP 72 (2018) 1327–1332.
[214] S. Chen, S. Yang, C.F. Cheung, L.T. Ho, F. Zhang, Suppression strategy of micro-waviness error in ultra-precision parallel grinding, Nanomanufacturing and Metrology 5 (2022), https://doi.org/10.1007/s41871-022-00130-0.
[215] D.J. Whitehouse, Some theoretical aspects of error separation techniques in surface metrology, Journal of Physics E: Scientific Instruments 9 (1976) 531–536.
[216] C.J. Evans, R.J. Hocken, W.T. Estler, Self-calibration: reversal, redundancy, error separation, and absolute testing, CIRP Annals - Manufacturing Technology 45 (2) (1996) 617–634.
[217] M. Janssen, P. Schellekens, B. De Veer, Advanced spindle runout-roundness separation method, Adv Math Computational Tools Metrology (2001) 212–219, https://doi.org/10.1142/9789812811684_0024.
[218] R.R. Donaldson, A simple method for separating spindle error from test ball roundness error, CIRP Annals - Manufacturing Technology 21 (1) (1972) 125–126.
[219] R. Grejda, E. Marsh, R. Vallance, Techniques for calibrating spindles with nanometer error motion, Precision Engineering 29 (2005) 113–123.
[220] W.T. Estler, C.J. Evans, L.Z. Shao, Uncertainty estimation for multiposition form error metrology, Precision Engineering 21 (2/3) (1997) 72–82.
[221] Y. Aoki, S. Ozono, On a new method of roundness measurement based on the three points method, Journal of JSPE 32 (1966) 831–836 (in Japanese).
[222] D. Moore, Design considerations in multiprobe roundness measurement, Journal of Physics E: Scientific Instruments 9 (1989) 339–343.
[223] G.X. Zhang, R.K. Wang, Four-point method of roundness and spindle error measurements, CIRP Annals - Manufacturing Technology 42 (1) (1993) 593–596.
[224] W. Gao, S. Kiyono, T. Nomura, A new multiprobe method of roundness measurements, Precision Engineering 19 (1) (1996) 37–45.
[225] K. Endo, W. Gao, S. Kiyono, A new multi-probe arrangement for surface profile measurement of cylinders, JSME International Journal, Series C 46 (4) (2003) 1531–1537.
[226] W. Liu, J.S. Fu, B. Wang, S.L. Liu, Five-point cylindricity error separation technique, Measurement 145 (2019) 311–322.
[227] Y. Cai, B. Xie, S. Ling, K.C. Fan, On-line measurement method for diameter and roundness error of balls, Nanomanufacturing and Metrology 3 (2020) 218–227.
[228] J. Bai, Y. Wang, X. Wang, Q. Zhou, K. Ni, X.H. Li, Three-probe error separation with chromatic confocal sensors for roundness measurement, Nanomanufacturing and Metrology 4 (4) (2021) 247–255.
[229] W. Gao, Surface Metrology for Micro and Nanofabrication, Elsevier, 2020, ISBN 978-0128178508.
[230] S. Shi, H. Haitjema, Y. Wang, G. Jin, Uncertainty evaluation and reduction in three-probe roundness profile measurement based on the system transfer function, Precision Engineering 68 (2021) 139–157, https://doi.org/10.1016/j.precisioneng.2020.11.011.
[231] P. Huang, S. Shi, J. Xie, H. Haitjema, Z. Niu, Q. He, K. Lu, On-machine workpiece straightness profile measurement using a hybrid Fourier 3-sensor method, Precision Engineering 79 (2023) 190–199, https://doi.org/10.1016/j.precisioneng.2022.10.002.
[232] W. Gao, M. Tano, T. Araki, S. Kiyono, C.H. Park, Measurement and compensation of error motions of a diamond turning machine, Precision Engineering 31 (2007) 310–316.
[233] J.C. Lee, W. Gao, Y. Shimizu, J.H. Hwang, J.S. Oh, C.H. Park, Spindle error motion measurement of a large precision roll lathe, International Journal of Precision Engineering and Manufacturing 13 (6) (2012) 861–867.
[234] K. Mitsui, Development of a three-probe instrument for spindle accuracy measurement, Journal of the Japan Society of Mechanical Engineers 48 (1972) 115–123 (in Japanese).
[235] W. Gao, S. Kiyono, On-machine roundness measurement of cylindrical workpieces by the combined three-point method, Measurement 21 (4) (1997) 147–156.
[236] O. Horikawa, K. Sato, A. Shimokohbe, Roundness and absolute radial motion accuracy measurement by an improved reversal method, Journal of the Japanese Society for Precision Engineering 57 (12) (1991) 151–156.
[237] A. Wiegmann, M. Schulz, C. Elster, Improving the lateral resolution of a multi-sensor profile measurement method by non-equidistant sensor spacing, Optics Express 18 (15) (2010) 15807–15819.
[238] W. Gao, J. Yokoyama, H. Kojima, S. Kiyono, Precision measurement of cylinder straightness using a scanning multi-probe system, Precision Engineering 26 (3) (2002) 279–288.
[239] W. Gao, Nanometrology strategy (software)- Frontier of the precision nanometrology, Journal of the Japan Society for Abrasive Technology 48 (5) (2004) 245–248.
[240] S. Kiyono, W. Gao, Profile measurement of machined surface with combined method, Precision Engineering 16 (3) (1994) 212–218.
[241] W. Gao, S. Kiyono, High accuracy profile measurement of machined surface by the combined method, Measurement 19 (1) (1996) 55–64.
[242] X. Chen, K. Kotani, K. Takamasu, Study on spatial frequency domain 2-point method, Journal of JSPE 73 (6) (2007) 653–656 (in Japanese).
[243] S. Kiyono, Y. Asakawa, M. Inamoto, O. Kamada, A differential laser autocollimation probe for on-machine measurement, Precision Engineering 15 (2) (1993) 68–76.
[244] W. Gao, P.S. Huang, T. Yamada, S. Kiyono, A compact and sensitive two-dimensional angle probe for flatness measurement of large silicon wafers, Precision Engineering 26 (4) (2002) 396–404.
[245] W. Gao, S. Kiyono, Development of an optical probe for profile measurement of mirror surfaces, Optical Engineering 36 (12) (1997) 3360–3366.
[246] W. Gao, Y. Shimizu, Optical Metrology for Precision Engineering, De Gruyter, 2021, ISBN 978-3110541090.
[247] J.C. Lee, W. Gao, Y. Shimizu, J.H. Hwang, J.S. Oh, C.H. Park, Precision measurement of carrige slide motion error of a dram roll lathe, Precision Engineering 36 (2012) 244–251.
[248] Y.L. Chen, Z.Y. Niu, D. Matsuura, J.C. Lee, Y. Shimizu, W. Gao, J.S. Oh, C.H. Park, Implementation and verification of a four-probe motion error measurement system for a large-scale roll lathe used in hybrid manufacturing, Measurement Science and Technology 28 (2017), 105004.
[249] W. Gao, J.C. Lee, Y. Arai, Y.H. Noh, J.H. Hwang, C.H. Park, Measurement of slide error of an ultra-precision diamond turning machine by using a rotating cylinder workipece, International Journal of Machine Tools and Manufacture 50 (2010) 404–410.
[250] L. Tschirf, Testing of straightedges, parts I and II, Archiv für Technisches Messen (1941) 8224 (in German).
[251] Y. Shimizu, S. Goto, J.C. Lee, W. Gao, S. Adachi, K. Omiya, H. Sato, T. Saito, H. Kubota, Fabrication of large-size SiC mirror with precision aspheric profile for artificial satellite, Precision Engineering 37 (3) (2013) 640–649.
[252] I. Kamigaki, O. Yamakawa, O. Omori, T. Yamagiwa, H. Sakai, Roundness measurement and its uncertainty in an international comparison, Proceedings of IMEKO 2000 (2000) 139–144. Wien.
[253] H. Shinno, K. Mitsui, N. Tanaka, T. Omino, T. Tabata, A new method for evaluating error motion of ultra precision spindle, CIRP Annals - Manufacturing Technology 36 (1) (1987) 381–384.
[254] W. Gao, S. Kiyono, T. Sugawara, High accuracy roundness measurement by a new error separation method, Precision Engineering 21 (2/3) (1997) 123–133.
[255] J. Yamaguchi, Measurement of straight motion accuracy using the improved sequential three-point method, Journal of the Japan Society for Precision Engineering 59 (5) (1993) 773–778 (in Japanese).
[256] X.H. Li, W. Gao, H. Muto, Y. Shimizu, I. So, S.Y. Dian, A six-degree-of-freedom surface encoder for precision positioning of a planar motion stage, Precision Engineering 37 (3) (2013) 771–781.
[257] X.Y. Qiao, X. Chen, G. Ekberg, Q. Ding, X.Y. Cai, J.S. Wei, J.J. Wu, Self-calibration for the 2D stage based on weighted least squares, Measurement Science and Technology 30 (2019), 125015.
[258] X.Y. Qiao, C.J. Fan, X. Chen, G.Q. Ding, P. Cai, L. Shao, Uncertainty analysis of two-dimensional self-calibration with hybrid position using the GUM and MCM methods, Science and Technology Measurement Science and Technology 32 (11pp) (2021), 125012.
[259] K.N. Yu, J.H. Zhu, W.H. Yuan, Q. Zhou, G.P. Xue, G.H. Wu, X.H. Wang, X.H. Li, Two-channel six degrees of freedom grating-encoder for precision-positioning of sub-components in synthetic-aperture optics, Optics Express 29 (14) (2021) 21113–21128.
[260] W. Gao, A. Kimura, A fast evaluation method for pitch deviation and out-of-flatness of a planar scale grating, CIRP Annals - Manufacturing Technology 59 (2010) 505–508.
[261] X.G. Chen, Y. Shimizu, X. Xiong, Y.L. Chen, W. Gao, Self-calibration of Fizeau interferometer and planar scale gratings in Littrow setup, Optics Express 25 (18) (2017), 21567.
[262] X. Xiong, L. Quan, Y. Shimizu, H. Matsukuma, W. Gao, Self-calibration of a variable-line-spacing grating for an absolute optical encoder with a Fizeau interferometer, Measurement Science and Technology 32 (10pp) (2021), 064005.
[263] X. Xiong, C.G. Yin, L. Quan, R. Sato, H. Matsukuma, Y. Shimizu, H. Tamiya, W. Gao, Self-calibration of a large-scale variable-line-spacing grating for an absolute optical encoder by differencing spatially shifted phase maps from a Fizeau interferometer, Sensors 22 (2022) 9348.
[264] Y. Shimizu, R. Ishizuka, K. Mano, Y. Kanda, H. Matsukuma, W. Gao, An absolute surface encoder with a planar scale grating of variable periods Precision Engineering 67 (2021) 36–47.
[265] W.R. Moore, Foundations of Mechanical Accuracy, The Moore Special Tool Company, 1970.
[266] R.D. Geckeler, A. Link, M. Krause, C. Elster, Capabilities and limitations of the self-calibration of angle encoders, Meas. Sci. Technol. 25 (2014), 055003.
[267] R. Probst, Self-calibration of divided circles on the basis of a prime factor algorithm, Meas. Sci. Technol. 19 (2008), 015101.
[268] T. Watanabe, Self-calibration of rotary encoder, Journal of the Japan Society for Precision Engineering 82 (9) (2016) 792–796.
[269] X.D. Lu, D.L. Trumper, Self-Calibration of On-Axis Rotary Encoders CIRP Annals 56 (1) (2007) 499–504.
[270] N. Zimmermann, S. Ibaraki, Self-calibration of rotary axis and linear axes error motions by an automated on-machine probing test cycle, International Journal of Advanced Manufacturing Technology 107 (5–6) (2020) 2107–2120.
[271] S. Onishi, S. Ibaraki, T. Kato, M. Yamaguchi, T. Sugimoto, A self-calibration scheme to monitor long-term changes in linear and rotary axis geometric errors, Measurement 196 (2022), 111183.
[272] S. Onishi, S. Ibaraki, M. Yamaguchi, T. Sugimoto, A novel self-calibration scheme for on-machine measurement based on five-axis machine tool kinematic model, presented in the 2023 Spring JSPE Semiannual Meeting (2023) (in Japanese).
[273] J.H. Lee, J.H. Lee, S.H. Yang, Development of thermal error model with minimum number of variables using fuzzy logic strategy, KSME International Journal 15 (11) (2001) 1482–1489.
[274] T. Moriwaki, Development of an Intelligent Turning Machine Equipped with Open-Architecture CNC Controller to Compensate Thermal Deformation of Machine Tool, Proceedings of CIRP Sponsored International Seminar on Improving Machine Tool Performance, San Sebastian, 1998, pp. 317–325.

[275] Abhandlung, J. Mayr, Beurteilung und Kompensation des Temperaturgangs von Werkzeugmaschinen, Diss. ETH Zuric. (2010).
[276] T. Moriwaki, E. Shamoto, M. Kawano, Prediction of thermal deformation of machine tool with strain sensor, Proceedings of ASME International Mechanical Engineering Congress and Exposition 26782 (1997) 137–142.
[277] D. Biermann, R. Holtermann, A. Menzel, S. Schumann, Modelling and simulation of thermal effects in internal traverse grinding of hardened bearing steel, CIRP Annals - Manufacturing Technology 65 (1) (2016) 321–324.
[278] ISO 230-3, Test Code for Machine Tools - Part 3: Determination of Thermal Effects (2020).
[279] Q. Gao, P. Zhang, The errors recognition and compensation for the numerical control machine tools based on laser testing technology, Open Physics 17 (1) (2019) 857–862.
[280] O. Svoboda, P. Bach, G. Liotto, C. Wang, Machine tool 3D volumetric positioning error measurement under various thermal conditions, Proceedings of International Symposium on Precision Mechanical Measurements 6280 (2006) 377–383.
[281] H.S. Kim, Feed-forward control of fast tool servo for real-time correction of spindle error in diamond turning of flat surfaces, International Journal of Machine Tools and Manufacture 43 (12) (2003) 1177–1183.
[282] S.D. Ashok, G.L. Samuel, Modeling, measurement, and evaluation of spindle radial errors in a miniaturized machine tool, The International Journal of Advanced Manufacturing Technology 59 (5) (2012) 445–461.
[283] E. Gomez-Acedo, A. Olarra, L.N. Lopez de La Calle, A method for thermal characterization and modeling of large gantry-type machine tools, International Journal of Advanced Manufacturing Technology 62 (2012) 875–886.
[284] J. Feng, X. Tang, Y. Li, B. Song, Thermal error modelling of the spindle using neurofuzzy systems, Mathematical Problems in Engineering (2016), https://doi.org/10.1155/2016/828149.
[285] A.J. White, S.R. Postlethwaite, D.G. Ford, An identification and study of mechanisms causing thermal errors in CNC machine tools, Laser Metrology & Machine Performance IV (1970), https://doi.org/10.2495/LAMDAMAP990101.
[286] D.M.S. Blackshaw, Machine tool spindle error monitoring, Insight - Non-Destructive Testing and Condition Monitoring 40 (8) (1998) 561–563.
[287] M.H. Attia, L. Kops, Thermometric design considerations for temperature monitoring in machine tools and CMM structures, International Journal of Advanced Manufacturing Technology 8 (5) (1993) 311–319.
[288] C. Chen, J.F. Zhang, Z.J. Wu, P.F. Feng, Real-time measurement of machine tool temperature fields and their effect on machining errors, Mechanika 4 (2011) 413–417.
[289] D.X. Su, X. Cai, Y. Li, W.H. Zhao, H.J. Zhang, New approach to spindle thermal extension measuring based on machine vision for the vertical machine center, Metrology and Measurement Systems 28 (2) (2021) 357–370.
[290] Texas Instruments, Temperature sensor TMP117 (2023).
[291] Fluke, TiX1000 Infrared Camera (2023).
[292] Hexagon, ETALON LASERTRACER-NG (2023).
[293] Hans Turck GmbH & Co. KG, Inductive Sensor BI10U-M18-IOL6X2-H1141 (2023).
[294] S. Ibaraki, P. Blaser, M. Shimoike, N. Takayama, M. Nakaminami, Y. Ido, Measurement of thermal influence on a two-dimensional motion trajectory using a tracking interferometer, CIRP Annals - Manufacturing Technology 65 (1) (2016) 483–486.
[295] M. Mori, N. Irino, M. Shimoike, A new measurement method for machine tool thermal deformation on a two-dimensional trajectory using a tracking interferometer, CIRP Annals - Manufacturing Technology 68 (1) (2019) 551–554.
[296] E. Gomez-Acedo, A. Olarra, M. Zubieta, G. Kortaberria, E. Ariznabarreta, L. N. López de Lacalle, Method for measuring thermal distortion in large machine tools by means of laser multilateration, International Journal of Advanced Manufacturing Technology 80 (2015) 523–534.
[297] U. Mutilba, J.A. Yagüe-Fabra, E. Gomez-Acedo, G. Kortaberria, A. Olarra, Integrated multilateration for machine tool automatic verification, CIRP Annals - Manufacturing Technology 67 (1) (2018) 555–558.
[298] C. Brecher, R. Spierling, M. Fey, S. Neus, Direct measurement of thermo-elastic errors of a machine tool, CIRP Annals - Manufacturing Technology 70 (1) (2021) 333–336.
[299] C.H. Lo, J. Yuan, J. Ni, An application of real-time error compensation on a turning centre, International Journal of Machine Tools and Manufacture 35 (12) (1995) 1669–1682.
[300] Q. Cheng, Z. Qi, G.J. Zhang, Y.S. Zhao, B.W. Sun, P.H. Gu, Robust modelling and prediction of thermally induced positional error based on grey rough set theory and neural networks, Int J Adv Manuf Technol 83 (5–8) (2016) 753–764.
[301] M.R. Zhu, Y. Yang, X.B. Feng, Z.C. Du, J.G. Yang, Robust modeling method for thermal error of CNC machine tools based on random forest algorithm, Journal of Intelligent Manufacturing 1 (2022) 14.
[302] M. Mitsuishi, S. Warisawa, R. Hanayama, Development of an intelligent high-speed machining center, CIRP Annals 50 (1) (2001) 275–280.
[303] N. Ouerhani, B. Loehr, A. Rizzotti-Kaddouri, D. Santo De Pinho, A. Limat, P. Schinderholz, Data-Driven Thermal Deviation Prediction in Turning Machine-Tool - A Comparative Analysis of Machine Learning Algorithms, 3rd International Conference on Industry 4.0 and Smart Manufacturing (ISM) 200, 2022, pp. 185–193.
[304] N.S. Mian, S. Fletcher, A.P. Longstaff, A. Myers, Efficient estimation by FEA of machine tool distortion due to environmental temperature perturbations, Precision Engineering 37 (2) (2013) 372–379.
[305] J. Mayr, Comparing the thermo-mechanical behaviour of machine tool frame designs using a FDM – FEM simulation approach, Proceedings ASPE Annual Meeting (2007) 17–20.
[306] U. Heisel, Modelling of interaction processes in cutting, Proceedings of 2nd International Conference on Process Machine Interactions: 9780986633102 (2010).
[307] Y. Ito, Modular Design for Machine Tools, McGraw-Hill Education, 2008, ISBN 978-0071496605.
[308] E. Rivin, Handbook of Stiffness and Damping in Mechanical Design, ASME Press, 2010, ISBN 978-0791802939.
[309] A.H. Slocum, Precision Machine Design, Society of Manufacturing Engineers, 1992, ISBN 978-0872634923.
[310] A. Archenti, T. Laspas, Accuracy and performance analysis of machine tools, in: W. Gao (Ed.), Chapter 7 in Metrology, Springer, 2019, 978-981-10-4912-5_7-1.
[311] M.K. Gonzalez, N. Theissen, N. Agirre, J. Larrañaga, P. Hacala, A. Archenti, Influence of the velocity on quasi-static deflections of industrial articulated robots, Int J Adv Manuf Technol 125 (2023) (2023) 1429–1438, https://doi.org/10.1007/s00170-022-10661-x.
[312] A. Archenti, in: A Computational Framework for Control of Machining Systems Capability - from Formulation to Implementation, PhD thesis, KTH Royal Institute of Technology, Stockholm, Sweden, 2011, ISBN 978-91-7501-162-2.
[313] A. Archenti, M. Nicolescu, Accuracy analysis of machine tools using elastically linked systems, CIRP Annals - Manufacturing Technology 62 (1) (2013) 503–506.
[314] T. Laspas, N. Theissen, A. Archenti, Novel methodology for the measurement and identification for quasi-static stiffness of five-axis machine tools, Precision Engineering 65 (2020) 164–170.
[315] D. Kono, Y. Moriya, A. Matsubara, Influence of rotary axis on tool-workpiece loop compliance for five-axis machine tools, Precision Engineering 49 (2017) 278–286.
[316] N. Theissen, T. Laspas, S. Cedergren, A. Archenti, Measurement for the identification of static and quasi-static rotational stiffness, Precision Engineering 72 (2021) 215–223.
[317] J.F. Røsjordet, G. Hovland, Methods for experimentally determining stiffness of a multi-Axis machining centre, modeling, identification and control, A Norwegian Research Bulletin, Norwegian Society of Automatic Control 40 (2019) 11–25.
[318] P. Pawełko, D. Jastrzębski, A. Parus, J. Jastrzębska, A New Measurement System to Determine Stiffness Distribution in Machine Tool Workspace. Archives of Civil and Mechanical Engineering, Springer Science and Business Media LLC, 2021.
[319] C. Friedrich, B. Kauschinger, S. Ihlenfeldt, Stiffness evaluation of a hexapod machine tool with integrated force sensors, Journal of Machine Engineering 20 (1) (2020) 58–69.
[320] D. Kono, A. Matsubara, T. Shirai, K. Hhoshide, T. Miura, T. Togashi, Analysis of positional deviation caused by position-dependent disturbances in ball screw drive, Journal of the Japan Society for Precision Engineering 82 (6) (2016) 589–594.
[321] H. Huang, D. Kono, M. Toyoura, Vision-based vibration measurement of machine tool, Journal of Advanced Mechanical Design, Systems, and Manufacturing 16 (1) (2022) JAMDSM0014.
[322] M. Law, P. Gupta, S. Mukhopadhyay, Modal analysis of machine tools using visual vibrometry and output-only methods, CIRP Annals 69 (1) (2020) 357–360.
[323] M. Law, R. Lambora, P.A. Nuhman, S. Mukhopadhyay, Modal parameter recovery from temporally aliased video recordings of cutting tools, CIRP Annals 71 (1) (2022) 329–332.
[324] V.H. Brussel, J.W. Peters, Comparative assessment of harmonic, random, swept sine and shock excitation methods for the identification of machine tool structures with rotating spindles, CIRP Annals - Manufacturing Technology 24 (1) (1975) 291–296.
[325] T. Österlind, A. Archenti, L. Daghini, C.M. Nicolescu, Improvement of gear cutter dynamics by use of acoustic imaging and high damping interface, Procedia CIRP 4 (2012) 17–21.
[326] A. Kimura, W. Gao, W. Kim, K. Hosono, Y. Shimizu, L. Shi, L. Zeng, A sub-nanometric three-Axis surface encoder with short-period planar gratings for stage motion measurement, Precision Engineering 36 (5) (2012) 576–585.
[327] K. Nagaoka, M. Atsushi, F. Tomoya, S. Tomonori, Analysis method of motion accuracy using NC system with synchronized measurement of tool-tip position, International Journal of Automation Technology 3 (4) (2009) 394–400.
[328] A. Iglesias, J. Munoa, C. Ramírez, J. Ciurana, Z. Dombovari, FRF estimation through sweep milling force excitation (SMFE), Procedia CIRP 46 (2016) 504–507.
[329] K. Takasugi, T. Fukuda, R. Kito, N. Asakawa, Y. Morimoto, Fast swept sine cutting test for CNC lathes, Journal of Advanced Mechanical Design, Systems, and Manufacturing 14 (6) (2020) JAMDSM0092.
[330] A. Matsubara, S. Tsujimoto, D. Kono, Evaluation of dynamic stiffness of machine tool spindle by non-contact excitation tests, CIRP Annals - Manufacturing Technology 64 (1) (2015) 365–368.
[331] M. Rantatalo, J.O. Aidanpää, B. Göransson, P. Norman, Milling machine spindle analysis using FEM and non-contact spindle excitation and response measurement, International Journal of Machine Tools and Manufacture 47 (7–8) (2007) 1034–1045.
[332] C. Rabreau, D. Tlaolini, M. Ritou, S.L. Loch, B. Furet, Experimental Investigation of the Dynamic Behavior of High Speed Machining Spindles with an Electromagnetic Excitation Device, Proceedings of International Conference on Leading Edge Manufacturing in 21st century: LEM21, Session ID 202, 2015, pp. 1–6.
[333] J.J. Zulaika, F.J. Campa, L.N. Lopez de Lacalle, An integrated process–machine approach for designing productive and lightweight milling machines,

International Journal of Machine Tools and Manufacture 51 (7–8) (2011) 591–604.
[334] Z. Dombovari, J. Munoa, R. Kuske, G. Stepan, Milling stability for slowly varying parameters, Procedia CIRP 77 (2018) 110–113.
[335] M. Law, A.S. Phani, Y. Altintas, Position-dependent multibody dynamic modeling of machine tools based on improved reduced order models, ASME Journal of Manufacturing Science and Engineering 135 (2) (2013) 1–11, 21008.
[336] Y.P. Liu, Y. Altintas, Predicting the position-dependent dynamics of machine tools using progressive network, Precision Engineering (73) (2022) 409–422.
[337] A. Albrecht, S.S. Park, Y. Altintas, G. Pritschow, High frequency bandwidth cutting force measurement in milling using capacitance displacement sensors, International Journal of Machine Tools and Manufacture 45 (2005) 993–1008.
[338] D. Kono, T. Umezu, On-machine measurement method for dynamic stiffness of thin-walled workpieces, Precision Engineering 60 (2019) 299–305.
[339] C.P. Wang, K. Erkorkmaz, J. McPhee, S. Engin, In-process digital twin estimation for high-performance machine tools with coupled multibody dynamics, CIRP Annals - Manufacturing Technology 69 (1) (2020) 321–324.
[340] T. Fujita, T. Xi, R. Ikeda, S. Kehne, M. Fey, C. Brecher, Identification of a practical digital twin for simulation of machine tools, International Journal of Automation Technology 16 (3) (2022) 261–268.
[341] K. Takahei, S. Miwa, E. Shamoto, N. Suzuki, Parameter identification for linear model of the milling process using spindle speed variation, Precision Engineering 79 (2022) 16–33.
[342] K. Takahei, N. Suzuki, E. Shamoto, Identification of the model parameter for milling process simulation with sensor-integrated disturbance observer, Precision Engineering 78 (2022) 146–162.
[343] T. Umezu, D. Kono, Machining process for a thin-walled workpiece using on-machine measurement of the workpiece compliance, Int. J. Automation Technol 13 (5) (2019) 631–638.
[344] ISO/IEC GUIDE 98-3, Uncertainty of measurement - Part 3: Guide to the expression of uncertainty in measurement (GUM:1995) (2008).
[345] ISO 14253-2, Geometrical product specifications (GPS) - inspection by measurement of workpieces and measuring equipment - Part 2: guidance for the estimation of uncertainty in GPS measurement, in: Calibration of Measuring Equipment and in Product Verification, 2011.
[346] ISO/TR 230-9, Test code for machine tools - Part 9: Estimation of measurement uncertainty for machine tool tests according to series ISO 230, basic equations (2005).
[347] K. Szipka, T. Laspas, A. Archenti, Measurement Uncertainty Associated with the Performance of Machine Tool under Quasi-Static Loaded Test Condition, Proceedings of 12th International Conference on Laser Metrology and Machine Performance (Lamdamap), 2017.
[348] W. Knapp, Measurement uncertainty and machine tool testing, CIRP Annals - Manufacturing Technology 51 (1) (2002) 459–462.
[349] W. Knapp, B. Bringmann, Straightness measurements for long movements, Nanotechnology and Precision Engineering 3 (2005) 249–256.
[350] H.F.F. Castro, Uncertainty analysis of a laser calibration system for evaluating the positioning accuracy of a numerically controlled axis of coordinate measuring machines and machine tools, Precision Engineering 32 (2) (2008) 106–113.
[351] W.T. Estler, Uncertainty analysis for angle calibrations using circle closure, Journal of Research of the National Institute of Standards and Technology 103 (2) (1998) 141–151.
[352] K.I. Lee, S.H. Yang, Robust measurement method and uncertainty analysis for position-independent geometric errors of a rotary axis using a double ball-bar, International Journal of Precision Engineering and Manufacturing 14 (2013) 231–239.
[353] F. Ezedine, J.-M. Linares, J.-M. Sprauel, J. Julien Chaves-Jacob, Smart sequential multilateration measurement strategy for volumetric error compensation of an extra-small machine tool, Precision Engineering 43 (2016) 178–186.
[354] S. Ibaraki, C. Oyama, H. Otsubo, Construction of an error map of rotary axes on a five-axis machining center by static R-test, International Journal of Machine Tools and Manufacture 51 (3) (2011) 190–200.
[355] M.A. Donmez, D.S. Blomquist, R.J. Hocken, C.R. Liu, M. Barash, A general methodology for machine tool accuracy enhancement by error compensation, Precision Engineering 8 (4) (1986) 187–196.
[356] A.C. Okafor, Y.M. Ertekin, Derivation of machine tool error models and error compensation procedure for three axes vertical machining center using rigid body kinematics, International Journal of Machine Tools and Manufacture 40 (8) (2000) 1199–1213.
[357] ISO/TR 16907, Machine tools - Numerical compensation of geometric errors (2015).
[358] Y. Lin, Y. Shen, Modelling of five-Axis machine tool metrology models using the matrix summation approach, International Journal of Advanced Manufacturing Technology 21 (4) (2003) 243–248.
[359] S.H. Suh, E.S. Lee, S.Y. Jung, Error modelling and measurement for the rotary table of five-axis machine tools, The International Journal of Advanced Manufacturing Technology 14 (9) (1998) 656–663.
[360] M. Placid, C. Ferreira, R. Liu, An analytical quadratic model for the geometric error of a machine tool, Journal of Manufacturing Systems 5 (1) (1986) 51–63.
[361] D.N. Reshetov, V.T. Portman, Accuracy of Machine Tools, ASME Press, 1988, ISBN 978-0791800041.
[362] J. Denavit, R.S. Hartenberg, A kinematic notation for lower-pair mechanisms based on matrices, Journal of Applied Mechanics 22 (2) (1955) 215–221.
[363] J.J. Craig, Introduction to Robotics: Mechanics and Control, Prentice Hall, 2004, ISBN 978-0133489798.
[364] S. Ibaraki, N.A. Theissen, A. Archenti, M.M. Alam, Evaluation of kinematic and compliance calibration of serial articulated industrial manipulators, International Journal of Automation Technology 15 (5) (2022) 567–580.
[365] H. Zhuang, Z.S. Roth, Robot calibration using the CPC error model, Robotics and Computer-Integrated Manufacturing 9 (3) (1992) 227–237.
[366] K. Okamura, F.C. Park, Kinematic calibration using the product of exponentials formula, Robotica 14 (4) (1996) 415–421.
[367] B.V. Adorno, Robot Kinematic Modeling and Control Based on Dual Quaternion Algebra—Part I: Fundamentals. hal-01478225 (2017).
[368] G. Chen, L. Zhang, C. Wang, H. Xiang, G. Tong, D. Zhao, High-precision modeling of CNCs' spatial errors based on screw theory, SN Applied Sciences 4 (2) (2022) 1–15.
[369] S.K. Moon, Y.-M. Moon, S. Kota, R.G. Landers, Screw Theory Based Metrology for Design and Error Compensation of Machine Tools, Proceedings of ASME 2001 International Design Engineering Technical Conferences and Computers and Information in Engineering Conference, 2001, pp. 697–707.
[370] W. Tian, W. Gao, D. Zhang, T. Huang, A general approach for error modeling of machine tools, International Journal of Machine Tools and Manufacture 79 (2014) 17–23.
[371] J. Yang, Y. Altintas, Generalized kinematics of five-axis serial machines with non-singular tool path generation, International Journal of Machine Tools and Manufacture 75 (2013) 119–132.
[372] J. Yang, J.R.R. Mayer, Y. Altintas, A position independent geometric errors identification and correction method for five-axis serial machines based on screw theory, International Journal of Machine Tools and Manufacture 95 (2015) 52–66.
[373] Y. Zhao, T. Li, X. Tang, Geometric error modeling of machine tools based on screw theory, Procedia Engineering 24 (2011) 845–849.
[374] F.L.M. Delbressine, G.H.J. Florussen, L.A. Schijvenaars, P.H.J. Schellekens, Modelling thermomechanical behaviour of multi-axis machine tools, Precision Engineering 30 (1) (2006) 47–53, https://doi.org/10.1016/j.precisioneng.2005.05.005.
[375] R.J. Liang, W.H. Ye, H.Y.H. Zhang, Q.F. Yang, The thermal error optimization models for CNC machine tools, International journal of advanced manufacturing technology 63 (9) (2012) 1167–1176.
[376] J. Mayr, M. Ess, S. Weikert, K. Wegener, Compensation of Thermal Effects on Machine Tools Using a FDEM Simulation Approach, Proceedings of 9th international conference and exhibition on laser metrology, machine tool, CMM and robotic performance (Lamdamap), 2009.
[377] J. Mayr, M. Ess, S. Weikert, K. Wegener, Calculating thermal location and component errors on machine tools, Proceedings of 24th Annual Meeting of The American Society for Precision Engineering (2009) 128–131.
[378] Z. Winlarski, Z. Kowal, W. Kwasny, J.Y. Ha, Thermal model of the spindle drive structure, Journal of Machine Engineering 10 (4) (2010) 41–52.
[379] T. Holkup, H. Cao, P. Kolář, Y. Altintas, J. Zelený, Thermo-mechanical model of spindles, CIRP Annals - Manufacturing Technology 59 (1) (2010) 365–368.
[380] C. Brecher, P. Hirsch, M. Weck, Compensation of thermo-elastic machine tool deformation based on control internal data, CIRP Annals - Manufacturing Technology 53 (1) (2004) 299–304.
[381] J. Mayr, M. Egeter, S. Weikert, K. Wegener, Thermal error compensation of rotary axes and main spindles using cooling power as input parameter, Journal of Manufacturing Systems 37 (2) (2015) 542–549.
[382] M. Gebhardt, J. Mayr, N. Furrer, T. Widmer, S. Weikert, W. Knapp, High precision grey-box model for compensation of thermal errors on five-axis machines, CIRP Annals-Manufacturing Technology 63 (1) (2014) 509–512.
[383] P. Blaser, J. Mayr, K. Wegener, Long-term thermal compensation of 5-axis machine tools due to thermal adaptive learning control, MM Science Journal 4 (2019) 3164–3171.
[384] N. Zimmermann, S. Lang, P. Blaser, J. Mayr, Adaptive input selection for thermal error compensation models, CIRP Annals - Manufacturing Technology 69 (1) (2020) 485–488.
[385] X.J. Shi, W.K. Wang, Y.J. Mu, X. Yang, Thermal characteristics testing and thermal error modeling on a worm gear grinding machine considering cutting fluid thermal effect, International Journal of Advanced Manufacturing Technology 103 (9–12) (2019) 4317–4329.
[386] M. Mares, O. Horejs, Modelling of cutting process impact on machine tool thermal behaviour based on experimental data, 16TH CIRP CONFERENCE ON MODELLING OF MACHINING OPERATIONS (16TH CIRP CMMO) 58 (2017) 152–157.
[387] N. Zimmermann, M. Breu, J. Mayr, K. Wegener, Autonomously triggered model updates for self-learning thermal error compensation, CIRP Annals - Manufacturing Technology 70 (1) (2021) 431–434.
[388] B. Li, X.T. Tian, M. Zhang, Thermal error modeling of machine tool spindle based on the improved algorithm optimized BP neural network, International Journal of Advanced Manufacturing Technology 105 (1–4) (2019) 1497–1505.
[389] Y.C. Chiu, P.H. Wang, Y.C. Hu, The thermal error estimation of the machine tool spindle based on machine learning, Machines 9 (9) (2021) 184.
[390] B. Beglarzadeh, J.R.R. Mayer, A. Archenti, Modelling and indirect measurement of machine tool equivalent joint compliances, CIRP Journal of Manufacturing Science and Technology 35 (2021) 882–895.
[391] X. Gao, B. Li, J. Hong, J. Guo, Stiffness modeling of machine tools based on machining space analysis, International Journal of Advanced Manufacturing Technology 86 (5) (2016) 2093–2106.
[392] M. Zaeh, D. Siedl, A new method for simulation of machining performance by integrating finite element and multi-body simulation for machine tools, CIRP Annals - Manufacturing Technology 56 (1) (2007) 383–386.

[393] H.N. Huynh, Y. Altintas, Multibody dynamic modeling of five-axis machine tool vibrations and controller, CIRP Annals - Manufacturing Technology 71 (2022) 325–328.
[394] R. Sato, S. Noguchi, T. Hokazono, I. Nishida, K. Shirase, Time domain coupled simulation of machine tool dynamics and cutting forces considering the influences of nonlinear friction characteristics and process damping, Precision Engineering 61 (2020) 103–109.
[395] R. Sato, G. Tashiro, K. Shirase, Analysis of the coupled vibration between feed drive systems and machine tool structure, International Journal of Automation Technology 9 (6) (2015) 689–697.
[396] T. Ohashi, H. Shibata, S. Futami, H. Kishi, R. Sato, Influence of linear ball guide preloads and retainers on the microscopic motions of a feed-drive system, Journal of Advanced Mechanical Design, Systems, and Manufacturing 12 (5) (2018) JAMDSM0099.
[397] N. Irino, Y. Imabeppu, Y. Higuchi, Y. Shinba, K. Kawai, N. Suzuki, J. Kaneko, Y. Kakinuma, M. Mori, Vibration analysis and cutting simulation of structural nonlinearity for machine tool, CIRP Annals - Manufacturing Technology 70 (1) (2021) 317–320.
[398] O. Özşahin, E. Budak, H.N. Özgüven, Identification of bearing dynamics under operational conditions for chatter stability prediction in high speed machining operations, Precision Engineering 42 (2015) 53–65.
[399] C. Guo, L. Chen, J. Ding, A novel dynamics model of ball-screw feed drives based on theoretical derivations and deep learning, Mechanism and Machine Theory 141 (2019) 196–212.
[400] M. Eynian, Y. Altintas, Chatter stability of general turning operations with process damping, Journal of Manufacturing Science and Engineering 131 (4) (2009), 041005.
[401] Y. Sun, S. Jiang, Predictive modeling of chatter stability considering force-induced deformation effect in milling thin-walled parts, International Journal of Machine Tools and Manufacture 135 (2018) 38–52.
[402] K. Mori, D. Kono, I. Yamaji, A. Matsubara, Support placement for machine tools using stiffness model, International Journal of Automation Technology 9 (6) (2015) 680–688.
[403] D. Kono, K. Mori, On-site estimation of floor stiffness for modelling machine tool supports, Procedia CIRP 77 (2018) 38–41.
[404] D.M.G. Mori, Digital Twin Test Cut Now Powered by Japanese Supercomputer 'Fugaku', Press release of DMG MORI, 2023.
[405] Y. Altintas, P. Kersting, D. Biermann, E. Budak, B. Denkena, I. Lazoglu, Virtual process systems for part machining operation, CIRP Annals - Manufacturing Technology 63 (2) (2014) 585–605.
[406] G. Quintana, J. Ciurana, Chatter in machining processes: a review, International Journal of Machine Tools and Manufacture 51 (5) (2011) 363–376.
[407] E. Budak, A. Matsubara, A. Donmez, J. Munoa, Mechanical interfaces in machine tools, CIRP Annals - Manufacturing Technology 71 (2) (2022) 647–670.
[408] Y. Altintas, M. Eynian, H. Onozuka, Identification of dynamic cutting force coefficients and chatter stability with process damping, CIRP Annals - Manufacturing Technology 57 (1) (2008) 371–374.
[409] O. Tuysuz, Y. Altintas, Analytical modeling of process damping in machining, Journal of Manufacturing Science and Engineering 141 (6) (2019), 061006.
[410] Y. Altintas, E. Budak, Analytical prediction of stability lobes in milling, CIRP Annals - Manufacturing Technology 44 (1) (1995) 357–362.
[411] M.A. Davies, J.R. Pratt, B.S. Dutterer, T.J. Burns, The stability of low radial immersion milling, CIRP Annals - Manufacturing Technology 49 (1) (2000) 37–40.
[412] E. Goverkar, J. Gradisek, M. Kalveram, T. Insperger, K. Weinert, G. Stepan, I. Grabec, On stability and dynamics of milling at small radial immersion, CIRP Annals - Manufacturing Technology 54 (1) (2005) 357–362.
[413] N. Suzuki, Chatter vibration in cutting, Part 1, Journal of the Japanese Society for Precision Engineering 76 (2010) 280–284 (in Japanese).
[414] Q. Yao, M. Luo, D. Zhang, B. Wu, Identification of cutting force coefficients in machining process considering cutter vibration, Mechanical Systems and Signal Processing 103 (2018) 39–59.
[415] M. Eynian, In-process identification of modal parameters using dimensionless relationships in milling chatter, International Journal of Machine Tools and Manufacture 143 (2019) 49–62.
[416] N. Suzuki, Y. Kurata, T. Kato, R. Hino, E. Shamoto, Identification of transfer function by inverse analysis of self-excited chatter vibration in milling operations, Precision Engineering 36 (4) (2012) 568–575.
[417] S. Shekhar, B. Bediz, O.B. Ozdoganlar, Tool-tip dynamics in micromachining with arbitrary tool geometries and the effect of spindle speed, International Journal of Machine Tools and Manufacture 185 (2022), 103981.
[418] O. Franco, X. Beudaert, K. Erkorkmaz, J. Munoa, Influence of guideway friction on the cutting point receptance in machine tools, CIRP Annals – Manufacturing Technology 71 (1) (2022) 361–364.
[419] T. Schmitz, A. Cornelius, J. Karandikar, C. Tyler, S. Smith, Receptance coupling substructure analysis and chatter frequency-informed machine learning for milling stability, CIRP Annals – Manufacturing Technology 71 (1) (2022) 321–324.
[420] G. Chen, Y. Li, X. Liu, B. Yang, Physics-informed Bayesian inference for milling stability analysis, International Journal of Machine Tools and Manufacture 167 (2021), 103767.
[421] M. Postel, B. Bugdayci, K. Wegener, Ensemble transfer learning for refining stability predictions in milling using experimental stability states, Int J Adv Manuf Technol 107 (2020) 4123–4139.
[422] J. Friedrich, J. Torzewski, A. Verl, Online learning of stability lobe diagrams in milling, Procedia CIRP 67 (2018) 278–283.
[423] B. Denkena, B. Bergmann, S. Reimer, Analysis of different machine learning algorithms to learn stability lobe diagrams, Procedia CIRP 88 (2020) 282–287.
[424] Siemens Controller, SINUMERIK 840d/840Di/810d extended functions, 6FC5397-1BP10-1BA0 (2006).
[425] S.M. Esmaeili, J.R.R. Mayer, CNC table-based compensation of inter-axis and linear axis scale gain errors for a five-axis machine tool from symbolic variational kinematics, CIRP Annals - Manufacturing Technology 70 (1) (2021) 439–442.
[426] M.A. Donmez, K. Lee, R. Liu, M. Barash, A real-time error compensation system for a CNC turning center, Proceedings of the 1986 IEEE International Robotics and Automation Conference 3 (1986) 172–176.
[427] K.W. Yee, Alternative Designs of a Real-Time Error Corrector for Machine Tools with Encoder Position Feedback, NIST Internal Report (NISTIR) 4832, 1992. https://nvlpubs.nist.gov/nistpubs/Legacy/IR/nistir4832.pdf.
[428] S.W. Zhu, G.F. Ding, S.F. Qin, J. Lei, L. Zhuang, K.Y. Yan, Integrated geometric error modeling, identification and compensation of CNC machine tools, International journal of Machine Tools and Manufacture 52 (1) (2012) 24–29.
[429] S. Xiang, Y. Altintas, Modeling and compensation of volumetric errors for five-axis machine tools, International Journal of Machine Tools and Manufacture 101 (2016) 65–78.
[430] S. Ding, X.D. Huang, C.J. Yu, W. Wang, Actual inverse kinematics for position-independent and position-dependent geometric error compensation of five-axis machine tools, International Journal of Machine Tools and Manufacture 111 (2016) 55–62.
[431] M. Givi, J.R.R. Mayer, Optimized volumetric error compensation for five-axis machine tools considering relevance and compensability, CIRP Journal of Manufacturing Science and Technology 12 (2016) 44–55.
[432] M.S. Uddin, S. Ibaraki, A. Matsubara, T. Matsushita, Prediction and compensation of machining geometric errors of five-axis machining centers with kinematic errors, Precision Engineering 33 (2) (2009) 194–201.
[433] J. Mayr, P. Blaser, A. Ryser, Hernandez-Becerro, An adaptive self-learning compensation approach for thermal errors on 5-axis machine tools handling an arbitrary set of sample rates, CIRP Annals 67 (1) (2018) 551–554.
[434] H.C. Möhring, P. Wiederkehr, K. Erkorkmaz, Y. Kakinuma, Self-optimizing machining systems, CIRP Annals - Manufacturing Technology 69 (2020) 740–763.
[435] V.H. Nguyen, T.T. Le, H.S. Truong, H.T. Duong, M.V. Le, Predicting volumetric error compensation for five-axis machine tool using machine learning, International Journal of Computer Integrated Manufacturing (2023), https://doi.org/10.1080/0951192X.2022.2163295.
[436] F. Stoop, J. May, C. Sulz, P. Kaftan, F. Bleicher, K. Yamazaki, K. Wegener, Cloud-based thermal error compensation with a federated learning approach, Precision Engineering 79 (2023) 135–145.
[437] M.H. Miller, K.P. Garrard, T.A. Dow, L.W. Taylor, A controller architecture for integrating a fast tool servo into a diamond turning machine, Precision Engineering 16 (1) (1994) 42–48.
[438] S.C. Fawcett, Small amplitude vibration compensation for precision diamond turning, Precision Engineering 12 (2) (1990) 91–96.
[439] T.A. Dow, M.H. Miller, P.J. Falter, Application of a fast tool servo for diamond turning of nonrotationally symmetric surfaces, Precision Engineering 13 (4) (1991) 233–250.
[440] W. Gao, T. Araki, S. Kiyono, Y. Okazaki, M. Yamanaka, Precision nano-fabrication and evaluation of a large area sinusoidal grid surface for a surface encoder, Precision Engineering 27 (3) (2003) 289–298.
[441] W. Gao, R.J. Hocken, J.A. Patten, J. Lovingood, Experiments using a nano-machining instrument for nano-cutting brittle materials, CIRP Annals - Manufacturing Technology 49 (1) (2000) 439–442.
[442] K. Kouno, A fast response piezoelectric actuator for servo correction of systematic errors in precision machining, CIRP Annals - Manufacturing Technology 33 (1) (1984) 369–372.
[443] S.R. Patterson, E.B. Magrab, Design and testing of a fast tool servo for diamond turning, Precision Engineering 7 (3) (1985) 123–128.
[444] W. Gao, H. Haitjema, F.Z. Fang, R.K. Leach, C.F. Cheung, E. Savio, J.M. Linares, On-machine and in-process surface metrology for precision manufacturing, CIRP Annals - Manufacturing Technology 68 (2) (2019) 843–866.
[445] W. Gao, M. Tano, S. Sato, S. Kiyono, On-machine measurement of a cylindrical surface with sinusoidal micro-structures by an optical slope sensor, Precision Engineering 30 (3) (2006) 274–279.
[446] C.F. Cheung, K. Hua, X.Q. Jiang, L.B. Kong, Characterization of surface defects in fast tool servo machining of microlens array using a pattern recognition and analysis method, Measurement 43 (9) (2010) 1240–1249.
[447] Z.X. Li, F.Z. Fang, J.J. Chen, X.D. Zhang, Machining approach of freeform optics on infrared materials via ultra-precision turning, Optics Express 25 (3) (2017) 2051–2062.
[448] Y.J. Noh, Y. Arai, M. Tano, W. Gao, Fabrication of large-area micro-lens arrays with fast tool control, International Journal of Precision Engineering and Manufacturing 9 (4) (2008) 32–38.
[449] W. Gao, R.J. Hocken, J.A. Patten, J. Lovingood, D.A. Lucca, Construction and testing of a nanomachining instruments, Precision Engineering 24 (4) (2000) 320–328.
[450] Y.L. Chen, Y.D. Cai, Y. Shimizu, S. Ito, W. Gao, B.F. Ju, On-machine measurement of microtool wear and cutting edge chipping by using a diamond edge artifact, Precision Engineering 43 (2016) 462–467.
[451] Y.L. Chen, S. Wang, Y. Shimizu, S. Ito, W. Gao, B.F. Ju, An in-process measurement method for repair of defective microstructures by using a fast tool servo with a force sensor, Precision Engineering 39 (2015) 134–142.

[452] W. Gao, Y.L. Chen, K.W. Lee, Y.J. Noh, Y. Shimizu, S. Ito, Precision tool setting for fabrication of a microstructure array, CIRP Annals - Manufacturing Technology 62 (1) (2013) 523–526.
[453] K.P. Anandan, O.B. Ozdoganlar, Analysis of error motions of ultra-high-speed (UHS) micromachining spindles, International Journal of Machine Tools & Manufacture 70 (2013) 1–14.
[454] E. Uhlmann, P. Marcks, Adaptronic Compensation of Thermal Strain at Machine Tool Spindles Using CRP-Bandages, Proceedings of 2nd Manufacturing Engineering Society International Conference, Madrid, Spain, 2007.
[455] E. Uhlmann, P. Marcks, C. Mense, Milling Machine Evolution in Area of Conflict between Efficiency Accuracy and Social Ecology, Proceedings of 12th International Seminar on High Technology UNIMEP, 2007.
[456] M.A. Donmez, M.H. Hahn, J.A. Soons, A novel cooling system to reduce thermally-induced errors of machine tools, CIRP Annals – Manufacturing Technology 56 (1) (2007) 521–524.
[457] J. Mayr, Beurteilung und Kompensation des Temperaturgangs von Werkzeugmaschinen, Doctoral Thesis ETH No, 2009, 18677.
[458] X.P. Yao, T. Hu, G.F. Yin, C.H. Cheng, Thermal error modeling and prediction analysis based on OM algorithm for machine tool's spindle, International Journal of Advanced Manufacturing Technology 106 (7–8) (2020) 3345–3356.
[459] M.H. Lei, J. Yang, S. Wang, L. Zhao, P. Xia, G.D. Jiang, X.S. Mei, Semi-supervised modeling and compensation for the thermal error of precision feed axes, International Journal of Advanced Manufacturing Technology 104 (9–12) (2019) 4629–4640.
[460] S. Yang, J. Yuan, J. Ni, The improvement of thermal error modeling and compensation on machine tools by CMAC neural network, International Journal of Machine Tools & Manufacture 36 (4) (1996) 527–537.
[461] Y. Kang, C.W. Chang, Y.R. Huang, C.L. Hsu, I.F. Nieh, Modification of a neural network utilizing hybrid filters for the compensation of thermal deformation in machine tools, International Journal of Machine Tools & Manufacture 47 (2) (2007) 376–387.
[462] J. Deutsch, T. Albrecht, M. Riedel, L. Penter, H. Wiemer, J. Müller, S. Ihlenfeldt, Thermo-elastic structural analysis of a machine tool using a multi-channel absolute laser interferometer, Journal of Machine Engineering 20 (3) (2020) 63–75.
[463] M. Fujishima, K. Narimatsu, N. Irino, M. Mori, S. Ibaraki, Adaptive thermal displacement compensation method based on deep learning, CIRP Journal of Manufacturing Science and Technology 25 (2019) 22–25.
[464] R. Guiassa, J.R.R. Mayer, Predictive compliance based model for compensation in multi-pass milling by on-machine probing, CIRP Annals - Manufacturing Technology 60 (1) (2011) 391–394.
[465] X.Z. Wang, Z.L. Li, Q.Z. Bi, L.M. Zhu, H. Ding, An accelerated convergence approach for real-time deformation compensation in large thin-walled parts machining, International Journal of Machine Tools and Manufacture 142 (2019) 98–106.
[466] K. Szipka, T. Laspas, A. Archenti, Measurement and analysis of machine tool errors under quasi-static and loaded conditions, Precision Engineering 51 (2017) 59–67.
[467] C.C. Liu, M.S. Tsai, M.Q. Hong, P.Y. Tang, Development of a novel tuning approach of the notch filter of the servo feed drive system, Journal of Manufacturing and Materials Processing 4 (1) (2020) 21.
[468] C.S. Chen, A.C. Lee, Design of acceleration/deceleration profiles in motion control based on digital FIR filters, International Journal of Machine Tools and Manufacture 38 (7) (1998) 799–825.
[469] S. Tajima, B. Sencer, E. Shamoto, Accurate interpolation of machining tool-paths based on FIR filtering, Precision Engineering 52 (2018) 332–344.
[470] B. Sencer, S. Tajima, Frequency optimal feed motion planning in computer numerical controlled machine tools for vibration avoidance, ASME Journal of Manufacturing Science and Engineering 139 (1) (2016), 011006.
[471] R. Sato, K. Shirase, Analytical time constant design for jerk-limited acceleration profiles to minimize residual vibration after positioning operation in NC machine tools, Precision Engineering 71 (2021) 47–56.
[472] Y. Altintas, M.R. Khoshdarregi, Contour error control of CNC machine tools with vibration avoidance, CIRP Annals - Manufacturing Technology 61 (1) (2012) 335–338.
[473] W.E. Singhose, W.P. Searing, N.C. Singer, Improving repeatability of coordinate measuring machines with shaped command signals, Precision Engineering 18 (2–3) (1996) 138–146.
[474] G. Gubanov, Broadband pneumatic mass damper for the elimination of workpiece vibrations, CIRP Journal of Manufacturing Science and Technology 30 (2020) 184–194.
[475] I. Mancisidor, X. Beudaert, G. Aguirre, R. Barcena, J. Munoa, Development of an active damping system for structural chatter suppression in machining centers, International Journal of Automation Technology 12 (5) (2018) 642–649.
[476] A. Rashid, C.M. Nicolescu, Design and implementation of tuned viscoelastic dampers for vibration control in milling, International Journal of Machine Tools and Manufacture 48 (9) (2008) 1036–1053.
[477] X. Beudaert, K. Erkorkmaz, J. Munoa, Portable damping system for chatter suppression on flexible workpieces, CIRP Annals - Manufacturing Technology 68 (1) (2019) 423–426.
[478] K. Mori, D. Kono, I. Yamaji, A. Matsubara, Modelling of viscoelastic damper support for reduction in low frequency residual vibration in machine tools, Precision Engineering 50 (2017) 313–319.
[479] L. Daghini, C.M. Nicolescu, Influence of the Join System Turret-Boring Bar on Machining Performance of the Cutting Process, Proceedings of CIRP 2nd International Conference on Process Machine Interactions, Vancouver, Canada, 2010.
[480] L. Daghini, A. Archenti, T. Osterlind, Extending stability limits by designed-in damping, Journal of Machine Engineering 13 (1) (2013) 37–48.
[481] Q. Fu, A. Rashid, Constraining the shear strain in viscoelastic materials and utlization of the "incompressible" properties for damping treatment in hybrid joint interface module to improve their effect for vibration control in machining, Int J Adv Manuf Technol 83 (2016) 1079–1097.
[482] M.U. Rashid, A. Archenti, Manufacturing and characterization of a carbon-based amorphous (a-CNX) coating, Material. Nanomanufacturing and Metrology 1 (2018) 156–170.
[483] M.U. Rashid, R. Tomkowski, A. Archenti, Effect of surface pre-treatment on the adhesion between HiPIMS thick Cu:CuCNx coating and WC-Co shim, Coatings 12 (10) (2022) 1484.
[484] A. Milecki, Investigation and control of magneto–rheological fluid dampers, International Journal of Machine Tools and Manufacture 41 (3) (2001) 379–391.
[485] M.A. Butt, Y. Yang, X. Pei, Q. Liu, Five-axis milling vibration attenuation of freeform thin-walled part by eddy current damping, Precision Engineering 51 (2018) 682–690.
[486] T. Hashimoto, D. Kono, M. Furusawa, A. Matsubara, Novel method for changing dynamic characteristics balance of machining system, International Journal of the Japan Society for Precision Engineering 88 (2022) 589–596.
[487] D.H. Li, H.R. Cao, J.X. Liu, X.W. Zhang, X.F. Chen, Milling chatter control based on asymmetric stiffness, International Journal of Machine Tools and Manufacture 147 (2019), 103458.
[488] N. Suzuki, K. Nishimura, R. Watanabe, T. Kato, E. Shamoto, Development of novel anisotropic boring tool for chatter suppression, Procedia CIRP 1 (2012) 56–59.
[489] N. Dijk, E. Doppenberg, R. Faassen, N. Wouw, J. Oosterling, H. Nijmeijer, Automatic in-process chatter avoidance in the high-speed milling process, ASME Journal of Dynamic Systems Measurement and Control 132 (3) (2010), 031006.
[490] N. Suzuki, T. Ikada, R. Hino, R. Shamoto, Comprehensive study on milling conditions to avoid forced/self-excited chatter vibration, Journal of the Japanese Society for Precision Engineering 75 (2009) 908–914 (in Japanese).
[491] Y. Altintas, S. Engin, E. Budak, Analytical stability prediction & design for variable pitch cutters, J Manuf Sci Eng 121 (2) (1999) 173–178.
[492] R.S. Hahn, Metal-cutting chatter & its elimination, Transactions of ASME 75 (6) (1952) 1073–1078.
[493] N. Suzuki, R. Ishiguro, T. Kojima, Design of irregular pitch end mills to attain robust suppression of regenerative chatter, CIRP Annals - Manufacturing Technology 65 (1) (2016) 129–132.
[494] V. Nguyen, J. Johnson, S. Melkote, Active vibration suppression in robotic milling using optimal control, International Journal of Machine Tools and Manufacture 152 (2020), 103541.
[495] S. Xin, F. Peng, X. Tang, R. Yan, Z. Li, J. Wu, Research on the influence of robot structural mode on regenerative chatter in milling and analysis of stability boundary improvement domain, International Journal of Machine Tools and Manufacture 1779 (2022), 103918.
[496] E. Shamoto, S. Fujimaki, B. Sencer, N. Suzuki, T. Kato, R. Hino, A novel tool path/posture optimization concept to avoid chatter vibration in machining – proposed concept and its verification in turning, CIRP Annals - Manufacturing Technology 66 (1) (2012) 331–334.
[497] S. Nam, T. Hayasaka, H. Jung, E. Shamoto, Proposal of novel spindle speed variation profile with constant acceleration rate for improvement of chatter stability, Precision Engineering 68 (2021) 218–234.
[498] S. Yamato, T. Ito, H. Matsuzaki, J. Fujita, Y. Kakinuma, Self-acting optimal design of spindle speed variation for regenerative chatter suppression based on novel analysis of internal process energy behavior, International Journal of Machine Tools and Manufacture159 (2020), 103639.
[499] N. Suzuki, W. Takahashi, H. Igeta, T. Nakanomiya, Flank face texture design to suppress chatter vibration in cutting, CIRP Annals - Manufacturing Technology 69 (1) (2020) 93–96.
[500] S. Yamato, Y. Yamada, K. Nakanishi, N. Suzuki, H. Yoshioka, Y. Kakinuma, Integrated in-process chatter monitoring and automatic suppression with adaptive pitch control in parallel turning, Advances in Manufacturing 6 (3) (2018) 291–300.
[501] E. Shamoto, T. Mori, B. Sencer, N. Suzuki, R. Hino, Suppression of regenerative chatter vibration in multiple milling utilizing speed difference method – analysis of double-sided milling and its generalization to multiple milling operations, Precision Engineering 37 (3) (2013) 580–589.
[502] A. Dumanli, B. Sencer, Active control of high frequency chatter with machine tool feed drives in turning, CIRP Annals - Manufacturing Technology 70 (1) (2021) 309–312.
[503] J. Guillory, D. Truong, J.P. Wallerand, Uncertainty assessment of a prototype multilateration coordinate measurement system, Precision Engineering 66 (2020) 496–506.
[504] P.P. Munoz, J.A.A. Garcia, J.S. Mazo, Analysis of the initial thermal stabilization and air turbulences effects on laser tracker measurements, Journal of Manufacturing Systems 41 (2016) 277–286.
[505] J.J. Aguilar, R. Raquel Acero, F.J. Brosed, J. Santolaria, Development of a high precision telescopic instrument based on simultaneous laser multilateration for machine tool volumetric verification, Sensors 20 (13) (2020) 3798.
[506] Etalon X-AX LASERBAR, Accessed: March 2022, https://www.etalonproducts.com/en/products/x-ax_laserbar/, 2021.
[507] S. Aguado, J. Santolaria, D. Samper, J. Velázquez, C. Javierre, Fernández Á, Adequacy of technical and commercial alternatives applied to machine tool verification using laser tracker, Applied Sciences 6 (2016) 1–16.

[508] R. Schmitt, A. Schoenberg, B. Damm, Indoor-GPS Based Robots as a Key Technology for Versatile Production, Proceedings of 41st International Symposium on Robotics (ISR 2010) and 6th German Conference on Robotics (ROBOTIK 2010), 2010.
[509] J.E. Muelaner, P. Maropoulos, Large Scale Metrology in Aerospace Assembly, Proceedings of 5th International Conference on Digital Enterprise Technology, Nantes, France, 2008.
[510] S.H. Kang, D. Tesar, Indoor GPS metrology system with 3D probe for precision applications, Proceedings of ASME IMECE 2004 International Mechanical Engineering Congress and RD&D Expo (2004).
[511] G. Heiden, MdC. Porath, Metrological performance of indoor-GPS in a simulated measurement assisted assembly process, Journal of Physics: Conference Series 733 (2015) 1–6.
[512] Z. Wang, L. Mastrogiacomo, Experimental comparison of dynamic tracking performance of iGPS and laser tracker, International Journal of Advanced Manufacturing Technology 56 (2011) 205–213.
[513] R. Schmitt, S. Nisch, A. Schonberg, F. Demeester, S. Renders, Performance evaluation of iGPS for industrial applications, Proceedings of 2010 International Conference on Indoor Positioning and Indoor Navigation (IPIN) (2010).
[514] C. Nicksch, M. Sabzehi, R.H. Schmitt, Virtual indoor-GPS for measurement uncertainty determination in reconfigurable environments, Production Engineering 16 (2022) 545–560.
[515] S. Shirmohammadi, A. Ferrero, Camera as the instrument: the rising trend of vision based measurement, IEEE Instrumentation and Measurement Magazine 17 (2014) 41–47.
[516] J. Wang, W. Zhao, R. Leach, L. Xu, W. Lu, X. Liu, Positioning error calibration for two-dimensional precision stages via globally optimized image registration, Measurement 186 (2021) 1–9.
[517] A. Mendikute, I. Leizea, J.A. Yague-Fabra, M. Zatarin, Self-calibration technique for on-machine spindle-mounted vision systems, Measurement 113 (2018) 71–81.
[518] H. Yeung, B.M. Lane, M.A. Donmez, S. Moylan, In-situ calibration of laser/galvo scanning system using dimensional reference artifacts, CIRP Annals – Manufacturing Technology 69 (1) (2020) 441–444.
[519] M. Brandner, Bayesian uncertainty evaluation in vision-based metrology. www.intechopen.com, 2010.
[520] C. Zuo, J.M. Qian, S.J. Feng, W. Yin, Y.X. Li, P.F. Fan, J. Han, K.M. Qian, Q. Chen, Deep learning in optical metrology: a review, Light: Science & Applications 11 (2022) 39.
[521] R.R. Fesperman, S.P. Moylan, G.W. Vogl, M.A. Donmez, Reconfigurable data driven virtual machine tool: geometric error modeling and evaluation, CIRP Journal of Manufacturing Science and Technology 10 (2015) 120–130.
[522] G.W. Vogl, M.A. Donmez, A. Archenti, Diagnostics for geometric performance of machine tool linear axes, CIRP Annals – Manufacturing Technology 65 (1) (2016) 377–380.
[523] K. Szipka, A. Archenti, G.W. Vogl, M.A. Donmez, Identification of machine tool squareness errors via inertial measurements, CIRP Annals – Manufacturing Technology 68 (1) (2019) 547–550.
[524] C. Liu, P. Zheng, X. Xu, Digitalization and servitization of machine tools in the era of Industry 4.0: a review, International Journal of Production Research (2021), https://doi.org/10.1080/00207543.2021.1969462.